Finite element methods for the Onsager–Stefan–Maxwell equations

and their formulations in thermodiffusion and electrochemistry

Alexander J. Van-Brunt

Merton College

University of Oxford

A thesis submitted for the degree of

Doctor of Philosophy

Trinity 2022

Acknowledgements

I would like to thank my supervisors Patrick E. Farrell and Charles W. Monroe. It was only due to a rare combination of their knowledge, support and faith that this thesis was possible. Most importantly, they shared my vision from day one.

I would like to thank my parents Anne and Bruce and my wife Rutvika for the gems of advice they have given me over the past few years and for always being at my side. I would also like to thank Jyoti and Nandan for the immense kindness they have shown me. I would like to acknowledge my colleagues in the mathematical institute and engineering department who have provided me with much valuable insight and discussion.

Finally I would like to thank Merton college and the directors of the centre for doctoral training in partial differential equations, which I was enrolled in. They made these past four years both possible and enjoyable.

Abstract

This thesis lays the foundation for the computation of transport of mass, momentum and heat in multicomponent flows, systems which involve the transport of two or more chemical species in a common thermodynamic phase. Although commonplace in nature, problems of this type remain relatively unstudied in the numerical literature.

The transport problems considered in this thesis are formulated in terms of the Onsager–Stefan–Maxwell equations, which describe multi-species molecular diffusion in fluids, and the Navier–Stokes equations, which account for convection. Under some mild assumptions, we prove existence and uniqueness for some linearized systems. Effective numerical methods using finite elements are then obtained and analyzed to provide a general methodology for simulation.

The scope of the thesis is broader than numerical analysis. It also makes original contributions to formulations of transport problems within the framework of linear irreversible thermodynamics. The theory of fluid thermodiffusion is consolidated and cast into a new form, which allows for straightforward simulation of heat transfer alongside molecular diffusion. In addition we provide original and substantial detail on how to extend the framework to encompass transport in electrolytic materials under the assumption of electroneutrality, which generalizes some of the equations arising in porous electrode theory.

The power of the framework developed is illustrated throughout the thesis. We employ it to simulate a diverse range of examples, such as oxygen diffusion in the lungs, the mixing of flowing hydrocarbons streams, thermal separation of gases and transport in electrolytes.

Contents

List of Figures

Chapter 1

Introduction

1.1 Overview

Many fluids consist of mixtures; for example, air is a mixture of nitrogen, oxygen, carbon dioxide, and other species. In many situations, it is not necessary to resolve the motions of the individual species, such as when modelling the flow of air over an aircraft. However, in other contexts, detailed knowledge of the transport of individual species is required. We describe this situation as a *multicomponent flow*, where a fluid is composed of $2 \leq n \in \mathbb{N}_+$ distinct chemical species in a common thermodynamic phase. Examples include biological applications, where one may be interested in the transport of oxygen and carbon dioxide in blood, in chemical engineering, where one may be interested in separating or combining the constituents of petroleum, or in electrochemistry, where the performance of a battery is often limited by the transport of ions within an electrolyte.

Modelling transport in multicomponent flow necessitates effective numerical methods to solve the governing equations. These equations consider two distinct types of variables. The first are *thermodynamic state variables*, which are quantities that describe the macroscopic state of a system, such as its pressure, temperature or chemical composition. The other types of variables are *velocities* or *fluxes*, which describe the magnitude and direction of flow of a substance or property.

The equations arising in transport theory may also be placed into two distinct categories: *balance equations*, which derive from conservation laws; and *constitutive equations*, which postulate material-specific relationships between the gradients of thermodynamic state variables and the fluxes. The transport phenomena studied in this

thesis are restricted to mass, heat and momentum transfer, occurring via diffusion and convection. The common three constitutive laws to describe these transport phenomena are Fick's law of molecular diffusion, Fourier's law of heat conduction, and Newton's law of viscosity.

A general constitutive relationship for transport phenomena was proposed by Onsager [120, 121]. Given a system whose state is described by the independent thermodynamic state variables $\{x_i\}_{i=1}^m$, with associated velocities or fluxes, denoted by $\{J_i\}_{i=1}^m$, it was postulated that *in situations not too far from thermodynamic equilibrium*[1]

$$F_i = \sum_{j=1}^{m} \Lambda_{ij} J_i. \tag{1.1}$$

The terms F_i are known as the thermodynamic forces, which depend primarily on the gradients of state variables x_i. The terms Λ_{ij} are transport or phenomenological coefficients.

The law (1.1) places the constitutive laws of Newton, Fourier and Fick under a common framework. If one identifies the thermodynamic driving forces as the infinitesimal strain, the temperature gradient, and the concentration gradient, the transport matrix as the inverse of viscosity, thermal conductivity and diffusivity, and the flux as the viscous stress, heat flux, and molar flux, the elementary constitutive laws of Newton, Fourier and Fick.

There exists a substantial body of literature for each law considered separately, including the development of effective finite element methods for each of the corresponding partial differential equations. However, a rigorous unified numerical method coupling these transport phenomena in multicomponent systems is lacking. The need for such a method arises naturally in many applications.

The objective of this thesis is twofold. First, we aim to develop rigorous finite element methods to solve these transport phenomena simultaneously, thus assisting in rendering a broad and fertile area of engineering tractable to numerical simulation. Second, we set out to make original reformulations of the constitutive laws for both thermodiffusion and electrochemical transport, and demonstrate the utility of such reformulations. This works hand in hand with the first objective, as the primary benefit of these reformulations is to allow for an extension of the finite element methods developed in Chapter 2 and Chapter 3 to anisothermal, charged fluids. It also carries

[1] In this thesis, we understand 'not too far from equilibrium' to mean that the forces F_i are sufficiently small so that any non-linear relation between the forces F_i and fluxes J_i, can be neglected.

a distinct motivation that exceeds numerical analysis, in that a general consolidation of the underlying theory of the constitutive laws is achieved.

1.2 Thermodynamic fundamentals

When modelling transport equations, one must take into account thermodynamic principles. We detail these in this section as they pertain to mass, heat and momentum transport.

1.2.1 Summary of thermodynamics

State variables are *extensive* if they are proportional to the size of the system, such as the number of moles of each species $\{n_i\}_{i=1}^n$ and the volume of the system V. Conversely, state variables are *intensive* if they are independent of the size of the system. Examples include the pressure, denoted by $p > 0$ and the temperature $T > 0$.

The free energy of the system is expressed by the Gibbs free energy function $G(\{n_i\}_{i=1}^n, p, T)$, measured in joules. G has the fundamental property of extensivity; for any $\lambda \geq 0$

$$G(\{\lambda n_i\}_{i=1}^n, p, T) = \lambda G(\{n_i\}_{i=1}^n, p, T). \tag{1.2}$$

The first law of thermodynamics may be formulated as

$$dG = -SdT + Vdp + \sum_{i=1}^{n} \mu_i dn_i, \tag{1.3}$$

where S is the entropy. The term dG is common notation in thermodynamics used to denote a differential, infinitesimal or otherwise. For our purposes, the practical value of this differential is that it can be replaced with a differential operator. For a more mathematically rigorous treatment of thermodynamics, we refer the reader to [66]. The chemical potential of the ith species is defined as

$$\mu_i := \Big(\frac{\partial G}{\partial n_i}\Big)_{n_{j\neq i}, p, T}. \tag{1.4}$$

The volume V and entropy S are additional properties of the system, which satisfy

$$V := \Big(\frac{\partial G}{\partial p}\Big)_{\{n_i\}_{i=1}^n, T} \quad \text{and} \quad S := -\Big(\frac{\partial G}{\partial T}\Big)_{\{n_i\}_{i=1}^n, p}. \tag{1.5}$$

Because of how they appear in (1.5), V and S are referred to as being conjugate to p and T respectively, and each μ_i conjugate to the corresponding molar content n_i. Note that various alternative parameterisations of energy are possible in thermodynamics; for example, one could exchange the Gibbs energy $G(\{n_i\}_{i=1}^n, p, T)$ for the Helmholtz energy $A(\{n_i\}_{i=1}^n, V, T)$. Since various parameterisations that exchange extensive (intensive) variables for their intensive (extensive) conjugate variables are possible, it is conventional in thermodynamics to notate the intended parameterisation with subscripts when taking partial derivatives.

It can be shown that the Gibbs free energy satisfies

$$G = \sum_{i=1}^{n} \mu_i n_i \tag{1.6}$$

as a direct consequence of the definition of the chemical potential and Euler's theorem for homogeneous functions. Combining equations (1.3) and (1.6) we can derive

$$\sum_{i=1}^{n} n_i d\mu_i = -S dT + V dp \tag{1.7}$$

which is known as the Gibbs–Duhem equation. It will be convenient to use concentrations within the system rather than molar contents. Dividing through (1.7) by V and replacing the differential with a gradient, we deduce that

$$\sum_{i=1}^{n} c_i \vec{\nabla} \mu_i = -\overline{S} \vec{\nabla} T + \vec{\nabla} p \tag{1.8}$$

where $c_i = n_i/V$ is the concentration of species i and $\overline{S} = S/V$ the molar entropy. The total molar concentration of the phase, will be denoted as c_{T} and is defined by

$$c_{\mathrm{T}} = \sum_{i=1}^{n} c_i. \tag{1.9}$$

Similarly, we may use $n_{\mathrm{T}} = \sum_{i=1}^{n} n_i$ to indicate the total number of moles in the system. In terms of concentrations, (1.3) may be written as

$$\vec{\nabla} \tilde{G} = -\overline{S} \vec{\nabla} T + \vec{\nabla} p + \sum_{i=1}^{n} \mu_i \vec{\nabla} c_i, \tag{1.10}$$

where $\tilde{G} = G/V$ is the Gibbs free energy per volume.

Further useful properties are the *partial molar volumes*, $\{\overline{V}_i\}_{i=1}^n$ and *partial molar entropies* $\{\overline{S}_i\}_{i=1}^n$, which may be defined as

$$\overline{V}_i = \left(\frac{\partial \mu_i}{\partial p}\right)_{\{n_j\}_{j\neq i}, T} \quad \text{and} \quad \overline{S}_i = -\left(\frac{\partial \mu_i}{\partial T}\right)_{\{n_j\}_{j\neq i}, p}. \tag{1.11}$$

Differentiation of equation (1.6) with respect to pressure or temperature and the use of the relations (1.5) yields the respective equations

$$V = \sum_{i=1}^{n} \overline{V}_i n_i \tag{1.12a}$$

$$S = \sum_{i=1}^{n} \overline{S}_i n_i. \tag{1.12b}$$

Dividing equation (1.12a) through by V, we can alternatively express this as

$$1 = \sum_{i=1}^{n} \overline{V}_i c_i \tag{1.13}$$

which will lead us to the equation of state in the next subsection.

There are two further properties of liquids and gases that will be useful when analyzing the transport problem. The first of these properties is the isothermal bulk modulus K, defined by

$$\frac{1}{K} = -\frac{1}{V}\Big(\frac{\partial V}{\partial p}\Big)_{\{n_i\}_{i=1}^n, T}. \tag{1.14}$$

This measures the resistance of a change in volume of the phase to a change in pressure. The incompressible limit occurs when $K \to \infty$. By the relation (1.12a) we can derive that incompressiblity occurs whenever the partial molar volumes are assumed constant with pressure.

The second property is the volumetric coefficient of thermal expansion, α_V

$$\alpha_V = \frac{1}{V}\Big(\frac{\partial V}{\partial T}\Big)_{\{n_i\}_{i=1}^n, p}. \tag{1.15}$$

This measures the change in volume of the phase given a change in the temperature, an important material property to utilize when we consider the anisothermal case.

1.2.1.1 Setting and notation

Having now introduced the thermodynamic quantities, we may cast the setting for all equations as a bounded Lipschitz domain Ω. The *intensive* variables we have introduced, $\{\mu_i\}_{i=1}^n$, p, $\{c_i\}_{i=1}^n$, T, and which are used throughout this thesis, are functions $\Omega :\to \mathbb{R}$. Indeed, with the important exception of the *extensive* variables, such as V, S, n_i, each quantity in this thesis henceforth will be a function $\Omega \to \mathbb{R}^k$ where $k = 1, d$, depending on if the vector is scalar-valued or vector-valued respectively, or $\Omega \to \mathbb{R}^{d\times d}_{\text{sym}}$ if the variable is symmetric-tensor-valued. Vector-valued functions will be distinguished by $\vec{\cdot}$ and symmetric-tensor-valued functions by $\overrightarrow{\overrightarrow{\cdot}}$.

1.2.1.2 The chemical potential and equation of state

Generally each species concentration c_i can be inferred from $\{\mu_i\}_{i=1}^n$ and p given constitutive laws for the chemical potential and an equation of state which relates c_{T} to temperature, pressure and composition. Within an isothermal ideal gas, this relation is simply

$$c_i = \frac{p^{\ominus}}{RT} \exp\left(\frac{\mu_i - \mu_i^{\ominus}}{RT}\right), \tag{1.16}$$

for some known reference pressure $p^{\ominus}$ and a set of reference chemical potentials $\{\mu_i^{\ominus}\}_{i=1}^n$. Here R is the gas constant. In non-ideal solutions, the reference potentials $\mu_i^{\ominus}$ generally depend on the temperature and pressure [8, 76]; they determine the value of the molar Gibbs free energy of pure species i at the T and p values of interest. A general relation for non-ideal systems is

$$\mu_i = \mu_i^{\ominus} + RT \ln(\gamma_i y_i), \tag{1.17}$$

where $y_i \coloneqq c_i/c_{\mathrm{T}}$ is the *mole fraction*, and γ_i the *activity coefficient*, of species i. (Within a system made up of n species, specifying $n-1$ mole fractions determines the *composition* referred to earlier.) Activity coefficients generally depend on temperature, pressure, and composition; the definition of the reference state further requires that they approach unity at infinite dilution, i.e. $\lim_{y_i\to 0} \gamma_i = 1$. Constitutive laws like (1.17) suffice to determine the mole fractions (but not concentrations) within non-ideal solutions. To obtain the concentrations, an additional equation of state for the system as a whole is required. A straightforward rearrangement of (1.13) leads us to

$$c_{\mathrm{T}} = \frac{1}{\sum_i \overline{V}_i y_i}. \tag{1.18}$$

The importance of these relations will be apparent in Chapter 3, where our algorithm is designed so that calculation of the concentrations occurs only as a postprocessing step. Consequently our analysis of the linearized system may be completely separated from the calculation of the concentrations. The advantage of this will be borne out in Chapter 3 where our analysis may cover all systems, regardless of nonideality.

1.2.2 Example: ideal gas

The equation of state for an ideal gas mixture may be written as

$$p = c_{\mathrm{T}} RT. \tag{1.19}$$

The chemical potential of an ideal gas mixture, with constant molar heat capacities of the pure components, $\{\overline{C}_{p,i}\}_{i=1}^{n}$, is known to be (for example see, [80, pp. 77])

$$\mu_i = \mu^{\ominus} + \left(RT \ln \frac{p}{p^{\ominus}} + RT \ln \frac{n_i}{n_{\mathrm{T}}} + \overline{C}_{p,i} \Big[T - T \ln \frac{T}{T^{\ominus}} \Big] \right) \tag{1.20}$$

for a chosen reference pressure $p^{\ominus}$ and reference temperature $T^{\ominus}$.

For an ideal gas, we may invert (1.21) use (1.19) to generalize the relation (1.16) to

$$c_i = \frac{p^{\ominus}}{RT} \exp \left(\frac{\mu_i - \mu_i^{\ominus}}{RT} + \overline{C}_{p,i} \Big[T - T \ln \frac{T}{T^{\ominus}} \Big] \right). \tag{1.21}$$

For an ideal gas, the bulk modulus is $K = p = c_{\mathrm{T}} RT$ and the thermal expansion coefficient is $\alpha_V = T$. The partial molar volume is

$$\overline{V}_i = \frac{RT}{p} \tag{1.22}$$

for each i. With this definition we can recover (1.18) from (1.19) after some rearrangement.

1.3 Convection-diffusion and balance equations

Transport phenomena are not described by constitutive equations or thermodynamics alone, but must be augmented with balance equations. In this section we detail the balance equations arising for mass and momentum transport and discuss their differences in the dilute and concentrated regimes. In Chapter 4 we will extend this to include the thermal balance equation. It is possible to derive other balance equations, such as one for internal energy or pressure [69], but they will not be utilized here. Fluid flow is governed by a momentum balance, typically expressed in the form of the Cauchy equation

$$\frac{\partial(\rho\vec{v})}{\partial t} = -\vec{\nabla}p + \operatorname{div}\left(\vec{\vec{\tau}}\right) + \operatorname{div}\left(\rho\vec{v}\otimes\vec{v}\right) + \rho\vec{f}, \tag{1.23}$$

where ρ is the fluid density, $\vec{v}$ is the flow velocity (the velocity of the medium as a bulk), $\vec{\vec{\tau}}$ is the dissipative (viscous) stress tensor, and $\vec{f}$ is the body acceleration induced within Ω by the action of external fields. In a fluid comprising two or more distinct chemical species, mass transport within Ω is governed by a set of material balances, usually expressed as the species continuity equations

$$\frac{\partial c_i}{\partial t} = -\operatorname{div}\left(c_i\vec{v}_i\right) + r_i, \quad i = 1, \ldots, n. \tag{1.24}$$

For each species i, $\vec{v}_i$ denotes the species velocity. The given function r_i quantifies the volumetric rate at which species i is generated or depleted by homogeneous chemical reactions.

In fluid mechanics, Cauchy's equation (1.23) is usually closed by stating a second governing equation to describe mass continuity and adopting a material-specific constitutive law that relates viscous stress with velocity gradients. Incorporating Newton's law of viscosity leads to the well-known Navier–Stokes equations, a governing system that generally determines the distribution of the flow velocity $\vec{v}$. In the mass transport literature, material balance equations (1.24) are closed by postulating constitutive laws that relate the species fluxes (and hence gradients) to concentration gradients and the flow velocity, leading to a governing system that determines the distributions of all the concentrations c_i.

The portion of species flux $c_i\vec{v}_i$ driven by the flow velocity, $c_i\vec{v}$, is called *convection*, and the excess flux $\vec{J}_i = c_i(\vec{v}_i - \vec{v})$ is said to arise from mass diffusion. Many elementary examples in physical chemistry and engineering consider *simple diffusion*, in which the flow is taken to be stationary, such that $\vec{v} = 0$ uniformly. The *convective diffusion* problem describes diffusion within a generally nonzero flow field [93].

Despite the fact that models for fluid flow and simple diffusion are well established, it is not always clear how the standard modelling approaches should be combined to simulate convective diffusion. An issue stems from the fact that species concentrations determine a fluid's density, through the definition

$$\rho = \sum_{i=1}^{n} \overline{m}_i c_i, \tag{1.25}$$

in which $\overline{m}_i$ represents the molar mass of species i. This linkage between density and composition affects mass continuity, because even within a stationary fluid, a transient composition change will generally induce a density change. Moreover, the connection affects momentum continuity, because even when a fluid moves at constant velocity, a transient composition change will generally change the momentum density $\rho\vec{v}$ associated with the bulk flow.

1.3.1 The dilute and concentrated regimes

When applicable, a dilute-solution approximation decouples the flow problem from the mass transport problem. This approximation is nearly universally used throughout the convective diffusion literature. In a *dilute solution*, a single species called the *solvent* (conventionally assigned index $i = n$) is taken to have a concentration very far in excess of the remaining species ($i < n$), which are called *solutes*. Thus the fluid density varies negligibly with solute content in a dilute solution and approximately coincides with the mass density of the pure solvent. At moderate pressure this density is relatively constant in the same way that it would be for a single-component fluid, so that the incompressibility condition

$$\operatorname{div} \vec{v} = 0 \quad \text{(dilute solution)} \tag{1.26}$$

expresses mass continuity. Also, on the statistical grounds that each solute in a dilute solution interacts at a molecular level almost solely with solvent molecules, the excess solute fluxes can each be modelled by Fick's law [61],

$$\vec{J}_i = -D_i \vec{\nabla} c_i \quad \text{(dilute solution)} \tag{1.27}$$

for $i = 1, \ldots, n-1$, in which $D_i > 0$ is the Fickian diffusivity of solute i in the solvent. To model convective diffusion under the dilute-solution approximation, one

solves the incompressible Navier–Stokes equations for the distributions of flow velocity and pressure without any reference to the composition of solutes. Given the flow velocity, one then uses Fick's law within material balance equations (1.24) to solve for the solute concentrations. This strategy provides a theory of convective diffusion with a vast array of applications [16, 41, 93].

While the dilute-solution approximation has been applied to great effect, it fails starkly when no single species is present in great excess—the so-called *concentrated solution* regime. Several problems arise when attempting to relax the dilute-solution approximation and formulate models for concentrated solutions.

In concentrated solutions, the very notion of the 'flow velocity' appearing in the momentum equation (1.23) becomes ambiguous, because it is no longer coincident with a particular species velocity. One can still identify a natural composition-dependent definition of $\vec{v}$ in the concentrated case, however. Time differentiation of (1.25), followed by elimination of the concentration derivatives with species-continuity equations (1.24), yields

$$\frac{\partial \rho}{\partial t} = \sum_{i=1}^{n} \overline{m}_i \left[r_i - \operatorname{div}\left(c_i \vec{v}_i\right) \right] = \sum_{i=1}^{n} \overline{m}_i r_i - \operatorname{div}\left(\sum_{i=1}^{n} \overline{m}_i c_i \vec{v}_i \right). \tag{1.28}$$

Equation (1.28) is consistent with the common understanding of mass continuity if the flow velocity $\vec{v}$ within a multicomponent fluid is identified as the so-called *mass-average velocity*, defined as [83, p. 454]

$$\vec{v} = \sum_{i=1}^{n} \omega_i \vec{v}_i, \tag{1.29}$$

where

$$\omega_i = \frac{\overline{m}_i c_i}{\rho} \tag{1.30}$$

defines the *mass fraction* of species i. Indeed, bringing in the mass-average velocity reduces (1.28) to

$$\frac{\partial \rho}{\partial t} = -\operatorname{div}(\rho \vec{v}), \tag{1.31}$$

thereby recovering the mass continuity equation familiar from fluid mechanics.

When concentrated solutions comprise more than two species, the constitutive laws for mass transport become incomplete because Fick's law (1.27) fails to take into account all possible species–species interactions. Even in the case of simple diffusion, excess flux of a given species can generally be driven by a concentration gradient of any other species in the solution — a phenomenon known as *cross diffusion*. One can include cross diffusion with a generalized Fickian model [16, 20, 92]. This extends

(1.27) as

$$\vec{J}_i = -\sum_{j=1}^{n} D_{ij}\vec{\nabla}c_j, \quad i = 1, \ldots, n, \tag{1.32}$$

a form that includes double-indexed Fickian diffusivities D_{ij} to account for the diffusion of species i through species j. The generalized form of Fick's law can account for most phenomena observed in isothermal simple diffusion systems. A particular feature it captures is 'uphill diffusion' [92], where the excess flux of species i aligns with its concentration gradient, contradicting the Fickian ansatz (1.27).

Although the generalized Fick's law (1.32) allows for cross diffusion, the formulation lacks practical utility because no clearly defined structure underpins the set of double-indexed Fickian diffusivities. Little can be said about their spectral characteristics, or the minimal number of independently specifiable coefficients D_{ij}. It is not clear whether constitutive laws (1.32) preserve fundamental thermodynamic relations such as the volumetric equation of state (1.18) or the Gibbs–Duhem equation (1.8), or how the formulation maintains the distinction between diffusion and convection. The theory of irreversible thermodynamics, pioneered by Onsager [120–122], may be applied to relax the assumptions of dilute solution theory. Onsager's principles enable the statement of thermodynamically consistent, stable constitutive relations for species excess fluxes and stress. Importantly, the framework yields transport-coefficient matrices with clear spectral structure, providing a useful tool for developing numerical methods.

1.4 Linear irreversible thermodynamics and the Onsager–Stefan–Maxwell equations

1.4.1 Irreversible thermodynamics

Transport laws based on irreversible thermodynamics derive from the local entropy balance. Following the derivation of Jaumann [87], one begins with the entropy continuity equation

$$\frac{\partial \rho \hat{S}}{\partial t} = -\vec{\nabla} \cdot \vec{N}_S + \dot{s}, \tag{1.33}$$

where $\hat{S}$ is the specific entropy, $\vec{N}_S$ the total entropy flux, and $\dot{s}$ the volumetric rate of entropy production. Through a lengthy thermodynamic analysis involving the first law (1.3), the volumetric equation of state (1.18), Euler's extensivity theorem, and the Gibbs–Duhem equation (1.7), as well as various Legendre transformations and Maxwell

relations[2] [69, 83], entropy continuity transforms into an expression that describes the instantaneous energy dissipation. Within an isothermal fluid, the dissipation function quantifying entropy generation due to diffusion and viscous dissipation is given as [69, 83]

$$T\dot{s} = \sum_{i=1}^{n} \vec{d}_i \cdot \vec{v}_i + \overrightarrow{\overrightarrow{\tau}} : \dot{\overrightarrow{\overrightarrow{\varepsilon}}}. \tag{1.34}$$

Here $\vec{d}_i$ and $\dot{\overrightarrow{\overrightarrow{\varepsilon}}}$ are the thermodynamic force driving diffusion of species i and the linearized strain rate, respectively. They are identified as[3]

$$\vec{d}_i = -c_i \vec{\nabla} \mu_i + \omega_i \vec{\nabla} p \tag{1.35a}$$

$$\dot{\overrightarrow{\overrightarrow{\varepsilon}}} = \frac{1}{2} \left(\vec{\nabla} \vec{v} + \vec{\nabla} \vec{v} \right). \tag{1.35b}$$

In general, other phenomena such as chemical reactions [20, 47] or heat transport may contribute to the dissipation, but these will be neglected to simplify the present discussion[4].

The second law of thermodynamics demands that for any change that occurs in a closed system, the entropy either increases or remains constant. Equilibrium thermodynamics only concerns stationary states, and makes no reference to time. Irreversible thermodynamics associates the second law with the passage of time by demanding that the energy dissipation is non-negative, $T\dot{s} \geq 0$ everywhere, with equality holding only in an equilibrium state.

Onsager leveraged the dissipation function (1.34) to bring thermodynamic rigour to cross-diffusion modelling. He first postulated that the constitutive laws for transport can be expressed in the form of a linear operator, which maps the set of all fluxes that contribute to the dissipation into all of their conjugate forces [120, 121]. Further physical considerations impose additional structure on this constitutive operator, such as Curie's principle, which disallows coupling between quantities whose tensor order differs by one [126], and the principle that convection is non-dissipative, which imposes a null space within the constitutive laws for mass transport [122]. Thus, Onsager's framework asserts the existence of two distinct constitutive relationships applicable to

[2]Maxwell relations in thermodynamics refers to a set of equalities derived from the symmetry of the Hessian of a (sufficiently smooth) thermodynamic potential, such as the Gibbs free energy.

[3]The term $\omega_i \vec{\nabla} p$ in (1.35a) gives rise to the *pressure diffusion* phenomenon, where pressure gradients drive species diffusion according to their mass fraction.

[4]The inclusion of heat transport is extensively detailed in Chapter 4.

isothermal convective diffusion systems, with force-explicit forms

$$\vec{d}_i = \sum_{j=1}^{n} \mathbf{M}_{ij} \vec{v}_j, \quad i = 1, \ldots, n, \tag{1.36a}$$

$$\dot{\overrightarrow{\overrightarrow{\varepsilon}}} = \mathcal{A} \overrightarrow{\overrightarrow{\tau}}. \tag{1.36b}$$

In these relationships $\mathbf{M}$ is a matrix of Onsager drag coefficients, second-order tensors that quantify how diffusion driving forces transform into excess fluxes, and $\mathcal{A}$ is the fourth-order compliance tensor, which quantifies how the linearized rate-of-strain tensor (the 'force') that drives dissipative flow relates to viscous stress (the conjugate 'flux'). Over a Cartesian basis, the vector–tensor products $\mathbf{M}_{ij}\vec{v}$ are defined component wise as

$$(\mathbf{M}_{ij}\vec{v})^k = \sum_{l=1}^{d} M_{ijkl} v^l \tag{1.37}$$

for any i and j between 1 and n, where scalars v^i refer to individual spatial components of vector $\vec{v}$ (a superscript is used for spatial components of $\vec{v}$ to avoid confusion with the species index subscript). It should be borne in mind that the first two indices of scalar component M_{ijkl} refer to the n-dimensional space of species, whereas the second two refer to spatial directions.

The tensor contraction operations $\mathcal{A}\overrightarrow{\overrightarrow{\sigma}}$ are defined componentwise as

$$(\mathcal{A}\overrightarrow{\overrightarrow{\tau}})^{ij} = \sum_{k,l=1}^{d} \mathcal{A}_{ijkl} \tau_{kl} \tag{1.38}$$

in which all four indices of the scalar component $\mathcal{A}_{ijkl}$ refer to directions in space.

Substituting constitutive laws (1.36) into entropy-generation equation (1.34) yields

$$T\dot{s} = \sum_{i,j=1}^{n} \vec{v}_i \cdot \mathbf{M}_{ij} \vec{v}_j + \overrightarrow{\overrightarrow{\tau}} : \mathcal{A} \overrightarrow{\overrightarrow{\tau}}, \tag{1.39}$$

revealing that the dissipation is a quadratic form in the fluxes. Since the second law requires that energy dissipation is positive in every nonequilibrium situation, the transport-coefficient tensors $\mathcal{A}$ and $\mathbf{M}$ both must also be positive semidefinite, in the sense that the two individual terms appearing on the right hand side of equation (1.39) must be non-negative for any choice of $\{\vec{v}_i\}_{i=1}^n$ and $\overrightarrow{\overrightarrow{\tau}}$.

Onsager used microscopic arguments to identify further structure within trans-

port constitutive laws. Using statistical mechanics, he demonstrated fundamental relationships among the time correlations between fluctuations within systems at equilibrium, and observed that similar relationships could be derived from macroscopic transport models in which the constitutive operators are self-adjoint [120, 121]. This self-adjointness of the positive semidefinite constitutive tensors expresses what is known as the *Onsager reciprocal relation* among transport coefficients.

Onsager reciprocity requires $\mathbf{M}$ to be self-adjoint in the sense that

$$\sum_{l=1}^{n}\left[\left(\sum_{k=1}^{n}\mathbf{M}_{lk}\vec{u}_k\right)\cdot\vec{v}_l\right]=\sum_{l=1}^{n}\left[\vec{u}_l\cdot\left(\sum_{k=1}^{n}\mathbf{M}_{lk}\vec{v}_k\right)\right] \tag{1.40}$$

for all n-tuples of species velocities $\vec{u}_i$ and $\vec{v}_i$. This implies symmetry of the second-order tensors that make up $\mathbf{M}$, such that $\mathbf{M}_{ij}=\mathbf{M}_{ij}^{\top}$ for all $i,j=1,...,n$ [120], but also symmetry in the indices of $\mathbf{M}$ corresponding to species, such that $\mathbf{M}_{ij}=\mathbf{M}_{ji}$ [121].

Since the Frobenius operation ':' is an inner product on the space of symmetric tensors, $\mathcal{A}$ is self-adjoint in the sense that [31, 90]

$$\left(\mathcal{A}\overset{\rightrightarrows}{\tau}\right):\overset{\rightrightarrows}{\sigma}=\overset{\rightrightarrows}{\tau}:\left(\mathcal{A}\overset{\rightrightarrows}{\sigma}\right)\qquad\forall\ \sigma,\overset{\rightrightarrows}{\tau}\in\mathbb{R}^{d\times d}_{\mathrm{sym}}. \tag{1.41}$$

In this way the commonly assumed major symmetry of the compliance tensor, written in terms of its Cartesian components as $\mathcal{A}_{ijkl}=\mathcal{A}_{klij}$, is seen to be an Onsager reciprocal relation [83].

Some additional structure of the transport matrix is specific to multicomponent mass diffusion. Importantly, the theory must guarantee that diffusional motion, driven by thermodynamic property gradients, remains distinct from species convection, a non-dissipative process driven by bulk flow. This distinction is made by requiring that $\mathbf{M}$ be invariant to a shift of every species velocity by a vector field $\vec{u}$, i.e. the equation (1.36a) remains unchanged when each v_i is replaced by $(v_i-\vec{u})$. The essential physical distinction between diffusion and convection consequently requires that

$$\sum_{j=1}^{n}\mathbf{M}_{ij}=0, \tag{1.42}$$

as noted by Onsager [122] and Helfand [79]. Hence $\mathbf{M}$ has a null eigenvalue corresponding to the eigenvector $\mathbf{1}^{\top}=(1,1,\ldots,1)^{\top}$. From (1.36a), one can use the symmetry of

$\mathbf{M}$ combined with the nullspace (1.42) to show that

$$\sum_{i=1}^{n} \vec{d}_i = \sum_{i=1}^{n} \left(-c_i \vec{\nabla} \mu_i + \omega_i \vec{\nabla} p \right) = 0, \tag{1.43}$$

an expression of the (isothermal) Gibbs–Duhem equation (1.8). A further consequence of the nullspace (1.42) is the velocities of every species, and hence a complete description of the transport problem, cannot be ascertained from the diffusion driving forces alone; one must also solve the Cauchy momentum equation (1.23) in the compressible regime to determine the flow velocity. This in turn requires use of the Newtonian constitutive law (1.36b), so the coupling between the flow and mass-transport problems is strong.

A final simplification of the transport-coefficient tensors is achieved by asserting that the material being modelled is isotropic, which will be assumed henceforth. For mass transport, isotropy requires rotational invariance of $\mathbf{M}_{ij}$, namely that given any orthonormal tensor $\overset{\Rightarrow}{Q}$, $\overset{\Rightarrow}{Q} \cdot \mathbf{M}_{ij} \cdot \overset{\Rightarrow}{Q}^{\top} = \mathbf{M}_{ij}$ for all $i, j = 1, ..., n$, implying that the tensor entries that make up matrix $\mathbf{M}$ must all be proportional to the identity tensor $\mathbb{I}$. Hence $\mathbf{M}$ can be considered as a matrix of scalar quantities, for which the reciprocal relation is a simple symmetry, $\mathbf{M} = \mathbf{M}^{\top}$. Taken together, the physical arguments require that $\mathbf{M}$ is symmetric positive semidefinite $n \times n$ matrix, and that its eigenvalues, $\{\lambda_{i=1}^{\mathbf{M}}\}_{i=1}^{n}$, may be ordered as

$$0 = \lambda_1^{\mathbf{M}} < \lambda_2^{\mathbf{M}} \leq \cdots \leq \lambda_n^{\mathbf{M}}, \tag{1.44}$$

a spectral structure that will be used throughout this thesis. This implies that at positive concentrations, energy dissipation $T\dot{s} > 0$ occurs whenever there is relative species motion.

One must take care to note that $\mathbf{M}$ may afford additional nullspaces beyond (1.42) if any of the species concentrations vanishes. Consequently, in order to phrase the Stefan–Maxwell equations in terms of Onsager's transport laws (1.36) with a transport matrix $\mathbf{M}$ that possesses the spectral structure (1.44), it will be necessary to assume that $c_i > 0$ almost everywhere for each $i = 1, 2, \ldots n$. We make this assumption henceforth.

In the case of the viscous constitutive law, isotropy is ensured by demanding that the deformation stress and rate-of-strain tensors commute (as a matrix product) [3]. The number of free parameters in (1.36b) reduces to just two, leaving Newton's law of viscosity,

$$\overset{\Rightarrow}{\tau} = 2\eta \left(\dot{\overset{\Rightarrow}{\varepsilon}} - \frac{\operatorname{tr}(\dot{\overset{\Rightarrow}{\varepsilon}})}{d} \mathbb{I} \right) + \zeta \operatorname{tr}(\dot{\overset{\Rightarrow}{\varepsilon}}) \mathbb{I}, \tag{1.45}$$

in which $\eta > 0$ represents the (Newtonian shear) viscosity and $\zeta > 0$ the bulk viscosity. Equivalently, inverted to the force-explicit form (1.36b), this becomes

$$\varepsilon(v) = \frac{1}{2\eta}\tau + \left(\frac{1}{d^2\zeta} - \frac{1}{2\eta d}\right)(\operatorname{tr}\tau)\mathbb{I} =: \mathcal{A}\tau, \tag{1.46}$$

which will be used in Chapter 3.

1.4.2 Navier–Stokes–Onsager–Stefan–Maxwell equations

Historically, flux laws (1.36a) were preceded by the Stefan–Maxwell theory of diffusion in gas mixtures. In an isobaric isothermal ideal gas, the driving forces (1.35a) simplify to

$$\vec{d}_i = -RT\vec{\nabla}c_i, \quad i = 1, \dots, n. \tag{1.47}$$

Maxwell [103] and Stefan [135] related these concentration gradients to the product of a matrix of binary diffusivities and species velocities. The resulting equations are

$$-RT\vec{\nabla}c_i = \sum_{\substack{j=1 \\ i\neq j}}^{n} \frac{RTc_ic_j}{\mathscr{D}_{ij}c_{\mathrm{T}}}(\vec{v}_i - \vec{v}_j), \quad i = 1, \dots, n. \tag{1.48}$$

Here $\mathscr{D}_{ij} \in \mathbb{R}$ represents the Stefan–Maxwell diffusivity of species i through species j. The Stefan–Maxwell diffusivities are symmetric in the species indices, $\mathscr{D}_{ij} = \mathscr{D}_{ji}$, and coefficients $\mathscr{D}_{ii}$ are not defined.

Lightfoot et al. [94] noted that the Stefan–Maxwell equations can be reconciled with the isotropic Onsager equations (1.36a) by identifying the entries of the isotropic transport matrix $\mathbf{M}$ as

$$\mathbf{M}_{ij} = \begin{cases} -\frac{RTc_ic_j}{\mathscr{D}_{ij}c_{\mathrm{T}}} & \text{if } i \neq j, \\ \sum_{k=1,k\neq i}^{n} \frac{RTc_ic_k}{\mathscr{D}_{ik}c_{\mathrm{T}}} & \text{if } i = j. \end{cases} \tag{1.49}$$

Observe that symmetry of Onsager's $\mathbf{M}$ is equivalent to the Stefan–Maxwell hypothesis $\mathscr{D}_{ij} = \mathscr{D}_{ji}$. Moreover, the nullspace of $\mathbf{M}$ demanded by (1.42) is naturally built in into the Stefan–Maxwell system because $\vec{v}_i - \vec{v}_j = (\vec{v}_i - \vec{u}) - (\vec{v}_j - \vec{u})$ for any choice of vector field $\vec{u}$.

The Onsager–Stefan–Maxwell (OSM) framework embodied by the identification of

$\mathbf{M}$ as (1.49) extends readily to isothermal but nonisobaric simple diffusion, and can also be applied to non-gaseous isotropic phases [83, 92]. In this case the nonisobaric diffusion driving forces extend to expression (1.35a). Both Darken [43] and Lightfoot et al. [94] used the isobaric version of the driving forces in equation (1.35a) to describe simple diffusion within condensed phases—the former for solids and the latter for viscous liquids.

One may derive a more explicit and illuminating form for entropy production. Using the equation (1.34) combined with the constitutive laws (1.45), (1.36), (1.49), allows us to derive

$$T\dot{s} = \frac{1}{2}\sum_{i\neq j}\frac{RTc_ic_j}{\mathscr{D}_{ij}c_{\mathrm{T}}}|\vec{v}_i - \vec{v}_j|^2 + 2\eta\left|\dot{\vec{\vec{\varepsilon}}} - \frac{1}{d}(\vec{\nabla}\cdot\vec{v})\mathbb{I}\right|^2 + \zeta\left(\vec{\nabla}\cdot\vec{v}\right)^2. \tag{1.50}$$

These are known formulas for entropy generation due to diffusion and viscous dissipation, which can be found for example in references [83, equation (11.2-44)], [134, equation (34)] or [68, Lemma 7.7.1].

Equation (1.50) shows that that if coefficients $\mathscr{D}_{ij}$ are positive, then $\mathbf{M}$ is symmetric positive semidefinite. In the case of ideal-gas mixtures, it can be assumed that the Stefan–Maxwell diffusion coefficients $\mathscr{D}_{ij}$ are given constants, which places even stronger restrictions on their values. Whenever the concentrations satisfy $c_i \geq \kappa > 0$ for each $i = 1, 2, \ldots, n$ and any positive constant κ, then $\lambda_\kappa \leq \lambda_2^{\mathbf{M}}$ for a positive constant λ_κ which depends only on κ, a fact that will be used throughout this thesis. From the expression (1.50), one can show that the positivity of $\mathscr{D}_{ij}$ is also a necessary condition for (1.44) to be true for all positive concentrations [134]. It must be stressed, however, that the Stefan–Maxwell diffusion coefficients in many physical systems depend strongly on the concentrations of the species, in which case negative Stefan–Maxwell diffusion coefficients are not only possible, but are observed and of practical interest [91, 148]. Therefore in order to present a general framework for multispecies diffusion, the results in this thesis only use the spectral structure (1.44), not the positivity of the Stefan–Maxwell diffusion coefficients.

On the other hand, one can see from the formula (1.50) that both the shear and bulk viscosities must be nonnegative to ensure consistency with the second law.

We reserve the term *Stefan–Maxwell equations* for the equations (1.48), which are restricted to an isothermal isobaric ideal gas with a prescribed convection component. The general non-ideal fluids coupled with the momentum equation (1.23) and the constitutive law (1.46) via the mass-average velocity constraint (1.29) we will call the *Navier–Stokes–Onsager–Stefan–Maxwell* (NSOSM) equations. A regime that will be

of particular interest to us will be a creeping flow appropriate for low Reynolds number flow, for which the momentum balance equation reduces to the Stokes equation

$$\operatorname{div} \vec{\vec{\tau}} - \vec{\nabla} p = \rho \vec{f}. \tag{1.51}$$

With this simplification, we call the corresponding equations the *Stokes–Onsager–Stefan–Maxwell* (SOSM) equations.

1.5 Literature summary

1.5.1 Historical overview of constitutive laws

The earliest constitutive law was proposed by Robert Hooke [84] in 1678, who stated that the extension of a spring was proportional to the force through a material-dependent constant. Shortly thereafter Newton postulated in 1687 that the stress in a fluid was proportional to the gradient of the fluid velocity [117], stated in modern notation as (1.45).

In addition to the constitutive law relating stress and strain, Newton also derived a law stating that the transfer of heat between two systems was proportional to the difference in temperature between them, the so-called Newton law of cooling. In 1822 Fourier [64] greatly extended this for continuum materials and derived a law for heat conduction relating the heat flux $\vec{q}$ to the temperature gradient $\vec{\nabla} T$, via the thermal conductivity $k > 0$:

$$\vec{q} = -k \vec{\nabla} T. \tag{1.52}$$

In 1855 Fick [61] proposed the law (1.27) for diffusive mass transport, by analogy Fourier's law. Maxwell [103] applied kinetic theory to deduce Fick's law for binary isothermal ideal gas diffusion, showing that D relates to a material property. Stefan [135] extended Maxwell's analysis to multicomponent gases, expressing the gradient of each species concentration in terms of a matrix of binary diffusivities (1.48).

Around a similar time the coupling of mass diffusion with thermal diffusion were discovered, at first by Ludwig in 1856 [97]. Primarily this coupling refers to the process by which a temperature gradient drives diffusion, known as the Soret effect [133], and the converse process, by which a concentration gradient drives an irreversible heat flux, called the Dufour effect [52]. We use the term thermodiffusion to indicate coupled thermal and mass diffusion.

Nernst [112] and later Planck [124] posed an extension of the Fickian model (1.27) to account for the effect of an electric field on charged particles

$$\vec{J_i} = -D_i \vec{\nabla} c_i + F z_i c_i \vec{\nabla} \Phi. \tag{1.53}$$

Here F is Faraday's constant and z_i is the charge of the ith species and Φ is taken to be the electric potential.

A seminal theoretical breakthrough was laid by the kinetic theory [35] developed independently by Chapman and Enskog in the years 1916-1917. The Chapman–Enskog theory gave a framework for which transport equations could be derived from the kinetic theory of gases, and was used by Chapman and Enskog to derive Fourier's law of heat conduction, Fick's law of diffusion and Newton's law of viscosity. Importantly the kinetic theory provided a method to calculate the relevant transport properties from intermolecular potentials. Development of this theory also allowed for the prediction of the thermodiffusion effect in gases, and the constitutive laws that couple heat transfer with diffusion. The extension to thermodiffusion was developed later by Hirschfelder et al. [83], who derive what are sometimes called the generalized Stefan–Maxwell equations for an ideal gas:

$$-c_{\mathrm{T}} R T \vec{\nabla} y_i + (\omega_i - y_i) \vec{\nabla} p - \sum_{j=1}^{n} \frac{R T c_i c_j}{\mathscr{D}_{ij} c_{\mathrm{T}}} \left(\frac{D_i^T}{\rho_i} - \frac{D_j^T}{\rho_j} \right) \vec{\nabla} \ln T = \sum_{j=1}^{n} \frac{R T c_i c_j}{\mathscr{D}_{ij} c_{\mathrm{T}}} \left(\vec{v}_i - \vec{v}_j \right). \tag{1.54}$$

Independently, another far reaching breakthrough was achieved by Onsager in a series of papers [120–122], which laid the foundations of linear irreversible thermodynamics — a primary topic of this thesis. The structure of this linear irreversible thermodynamics as it pertains to convection and thermodiffusion has been detailed in the preceding section. Lightfoot, Cussler and Rettig's observation that Onsager's transport matrix, which applied to condensed phases as well as gases, can be cast in terms of Stefan–Maxwell diffusivities extended the Stefan–Maxwell theory to cover molecular diffusion processes in fluids [94]. Newman et al. [114] brought the generalization further, accounting for materials containing charged solutes, thereby completing the development of the contemporary theory. Modern expositions of the theory can be found in [68, 92, 134] and [44].

Finally it is worth recalling that the Onsager ansatz (1.1) rests on an assumption of the system being close to equilibrium. This is not always adequate to describe situations of interest. For example chemical reactions often occur far from equilibrium

and many fluids are non-Newtonian, in the sense that they are not described by equations of the form (1.45). Extending constitutive laws beyond the purview of linear relationships in a thermodynamically consistent way, has been a topic of extensive research over the past few decades. Some notable works in this direction include the GENERIC framework of Öttinger [123], the work of Rajagopal et al. on implicitly constituted fluids and solids [127, 128] and the recent wealth of research extending multicomponent flow models [20, 26]. This thesis emphatically only deals with linear irreversible thermodynamics, which is adequate to describe a vast array of practical problems and for which many numerical issues remain. Doubtless, numerical analysis of linear irreversible thermodynamics will be a useful guide for further extensions far from equilibrium.

1.5.2 Survey on numerical literature

Although to our knowledge there is no general numerical technique developed for transport theory in the broad regime we have detailed above, there is a vast literature, numerical and otherwise, analysing certain subcomponents of the equations we have presented. In this section we attempt to provide the reader with an overview of the existing literature on transport and detail its connection with the Onsager–Stefan–Maxwell equations we have presented.

1.5.2.1 Thermodiffusion

For a dilute solution in a stationary medium (that is $\vec{v} = 0$), one can use Fick's law for mass diffusion and the continuity equation to derive a parabolic equation

$$\frac{\partial c}{\partial t} = -\vec{\nabla} \cdot (D\vec{\nabla} c). \tag{1.55}$$

Similarly in an isobaric medium where one does not need to take into account mass transfer ($\vec{v}_i = 0$), but wishes to compute heat transfer, Fourier's law may be applied with the thermal balance equation to derive

$$\rho \hat{C}_p \frac{\partial T}{\partial t} = -\vec{\nabla} \cdot (k\vec{\nabla} T) \tag{1.56}$$

where $\hat{C}_p$ is the specific heat capacity. Numerical methods for such parabolic equations is a mature field. For both transient and the steady-state simulations there is a wealth

of choices utilising finite difference, finite volume and finite element methods. A comprehensive survey of such methods is beyond the scope of the thesis, however we direct the reader to [85, 142] and the references contained therein for further details.

Less widely spread yet of specific interest to us are numerical methods for solving the Stefan–Maxwell equations. For ideal gases with no pressure gradients or momentum, i.e. the purely diffusional aspect of the problem — considerable recent attention has been has been given to numerical methods, such as the finite element method proposed by McLeod and Bourgault [105], the finite volume method of Cancès et al. [28] and a finite difference scheme by Bondesan et al. [19].

Traditionally such techniques rely on specifying a reference velocity, such as the mass-average velocity, and using this to invert the Stefan–Maxwell equations into a flux explicit form,

$$\vec{N}_i = \sum_{j=1}^{n} c_i \mathbf{L}_{ij} \vec{d}_j, \tag{1.57}$$

where $\vec{N}_i = c_i \vec{v}_i$ is the molar flux and $\mathbf{L}$ is also a singular matrix. The details of this process are explained in depth in Chapter 4. Expanding the $\vec{d}_i$ first in terms of chemical potential (neglecting the pressure diffusion term in equation (4.6)), and then in terms of concentration gradients, one can derive a generalized Fickian law. Further details of the inversion process and its expansion in terms of composition gradients are contained in [92] and Chapter 4 and the appendix in the present work.

1.5.2.2 Convection

Many effective numerical methods have been developed to solve the Navier–Stokes equations. We do not attempt any systematic review of this field but cite the work of [56] as a general reference in the area. Effective numerical methods for the Navier–Stokes equations remains an active topic of research, particularly in the regimes of high Reynolds or Mach numbers.

A key point of divergence between this work and other work in the literature is the treatment of compressibility. The typical assumption for incompressiblity in fluid mechanics takes the form of (1.26). For a single component system, this is equivalent to our definition that $1/K = 0$, or $K \to \infty$. However for a multicomponent system undergoing mass transfer, there is little reason why density should be constant, regardless of the value of the bulk modulus K. Indeed by the definition of ρ (1.25) one can see that whenever there are significant concentration gradients, there should be corresponding density gradients. For example, consider a chamber of carbon dioxide diffusing into a chamber of hydrogen. As a consequence of the sharp difference in molar masses, in the

transient there will be a significant difference in density between the two chambers, despite the fact that there is no forced convection. Hence there is no reason why one should expect (1.26) to hold. Rather than (1.26), we will be applying the surrogate equation

$$\vec{\nabla} \cdot \vec{v} = \vec{\nabla} \cdot \Big(\sum_{j=1}^{n} \omega_j \vec{v}_j \Big). \tag{1.58}$$

The fact that density may not be considered constant in the concentrated solution regime is arguably is greatest challenge confronted in this thesis as it means that the vast arsenal of numerical methods available to incompressible fluid mechanics, cannot readily be applied.

Although significantly more challenging, extensive literature on the compressible Navier–Stokes equations also exists and the practitioner may select from various carefully engineered finite difference, finite element or finite volume schemes. For a historical overview of numerical solvers for the compressible Navier-Stokes equations, we may refer the reader to reference [33]. Mostly this literature is confined to ideal gases.

In principle our equations encompass fluid dynamics in the compressible and incompressible cases. In the case $n = 1$, the transport matrix (1.36) disappears and we are left only with the Gibbs–Duhem equation

$$c\vec{\nabla}\mu = \vec{\nabla}p. \tag{1.59}$$

The equation of state (1.18) also reduces to

$$\overline{V}c = 1. \tag{1.60}$$

With these two reductions, the assumption of constant density may be recovered when the volume is assumed independent of composition, pressure and temperature. On the other hand, gas laws relating pressure to density, as used in compressible fluid dynamics may also be derived when the volume is allowed to vary with these terms: one way of phrasing the ideal gas equation of state is to assert that $\overline{V}_i = RT/p$ for each species i.

Although nominally our equations include the compressible Navier–Stokes equations, our solvers are not yet designed to work at high Reynolds, Péclet or Mach numbers. We hope that in the future, sophisticated methods may be built on the foundation we lay in this thesis to effectively include turbulence, shock waves and other hydrodynamic instabilities for multicomponent transport. For example, effective numerical methods based on finite difference schemes for multicomponent transport were

successfully applied to model shock waves in a hydrogen air mixture [15].

The most significant numerical works on the full NSOSM equations are those by Ern, Giovangigli, and coauthors, which include a monograph [58] and a series of other papers [15, 27, 57, 59, 68] that apply multicomponent transport to combustion modelling for an ideal gas. These schemes use sophisticated finite difference methods, with the important exception of [27] which uses a finite element method with additional least squares terms to stabilize the formulation.

1.5.2.3 Dilute solution theory and convection–diffusion equations

In the dilute solution regime, equations (1.23) and (1.46) reduce to the incompressible Navier–Stokes equations, diffusion described by Fick's law (1.27), and a set of convection-diffusion equations. Each of these equations has been studied for many decades, with many effective numerical techniques available. We do not attempt any systematic review of these fields, but mention the works of [56, 85, 137, 142] as general references in these areas. In this regime, the momentum solve and the equation for the transport of concentration are decoupled using incompressibility.

Analogously, if one is interested in coupling thermal transport to convection, then a common technique is to use the approximation due to Oberbeck and Boussinesq [24, 119]. This approximation assumes that density varies linearly with temperature and thus in lieu of the equation of state (1.18), we have

$$\rho = \rho_0 - \alpha(T - T_0) \tag{1.61}$$

where α is a coefficient of thermal expansion, and ρ_0 and T_0 denote the reference density and temperature states. In the single component case, or the dilute regime, one may use the thermal balance equation

$$\rho \hat{C}_p \Big(\frac{\partial T}{\partial t} + v \cdot \vec{\nabla} T \Big) = -\vec{\nabla} \cdot \vec{q}' + \overset{\rightrightarrows}{\tau} : \dot{\overset{\rightrightarrows}{\varepsilon}}. \tag{1.62}$$

The equations (1.61), (1.62) coupled with Fourier's law and the Navier–Stokes equations, are generally referred to as the Boussinesq equations, again a well understood problem for which effective numerical methods have been constructed [56]. We note that equation (1.62) has a similar form to the convection-diffusion equations.

Analysis of the Nernst–Planck equation (1.53) may also be found in abundance, [23, 82, 95, 132]. In part this is on account of its tractability and it part due to it being the most canonical model used for electrolyte transport. As with Fick's law (1.27),

often it is supplemented with a constant density assumption and extrapolated beyond the dilute solution regime.

These convection–diffusion equations can be challenging to solve, particularly at high Péclet numbers where diffusive transport is dominated by convective transport. There is, however, a large body of literature dedicated to precisely solving such equations [137]. We therefore see that solving the transport equations we have laid out in the dilute solution regime is a well developed field. For our problems of interest, the concentrated solution regime where the solvents and solutes are in comparable proportions, the importation of these techniques is not straightforward.

1.6 Scope and contributions of this Thesis

Chapters 2 and 3 are concerned with the first objective, the development of finite element methods for coupled multicomponent transport phenomena in the concentrated solution regime. Chapter 2 analyzes the Stefan–Maxwell equations, where the convective velocity is regarded as a prescribed quantity. Although limited in its scope of realistic applications, this provides a useful pedagogical stepping stone. This chapter presents a variational formulation and proves well-posedness of the linearized system. A finite element method arising from this formulation is then analyzed and error estimates obtained. The error estimates are then numerically verified and a simulation modeling diffusion in the lungs is performed. The research in this chapter has been published in the IMA journal of Numerical Analysis [146].

Chapter 3 extends the analysis of the second chapter, with some modifications, to study the system of momentum coupled to diffusion, solving the Onsager–Stefan–Maxwell system for non-ideal fluids. Using the structure of irreversible thermodynamics, we analyze and illustrate a family of finite element solvers for the associated equations. We prove well-posedness and error estimates of the discrete and continuous system under an isothermal and vanishing Reynolds number assumption. A key construction is a novel function space representing the space of thermodynamic forces. A finite element method arising from this formulation is then analyzed and error estimates obtained. As in Chapter 2, our error estimates are numerically verified, and are applied to simulate the mixing of hydrocarbons. This research was done in collaboration with another DPhil student, Francis R. Aznaran and formed a paper currently in submission.

Chapters 4 and 5 address the second objective of this thesis, original reformulations of the constitutive laws for both thermodiffusion and electrochemical transport.

In Chapter 4 the equations of multicomponent diffusion are novelly extended to cover the anisothermal case. The main contribution of this chapter is the generalization of the isothermal transport matrix $\mathbf{M}$ to include the Soret and Dufour effects in multicomponent fluids. The equations are presented in novel force explicit form and the spectral structure of the resulting anisothermal transport matrix, which we label as $\widetilde{\mathbf{M}}$, is studied. The framework is then deployed to perform numerical simulations of steady three-dimensional thermodiffusion in a ternary gas. The research in this chapter has been published in the AIChE journal [145].

In Chapter 5 the important case of transport in liquid electrolytes is analyzed. The fundamental question of how to incorporate electroneutrality, voltage, and current whilst preserving the structure of linear irreversible thermodynamics is resolved. This allows one to essentially port the numerical techniques developed in the previous chapters over with minimal alteration to model transport of charged species. A further pleasant consequence is that it allows one to recover and generalize some of the equations that arise in the widely used porous electrode theory.

Chapter 2

The Stefan–Maxwell equations

The basis of this chapter is the original paper [146].

As a first step to discretizing the general problem, we will analyze in detail the diffusional aspect of a isothermal, isobaric ideal gas mixture. To do this, we effectively decouple the problem from its convection component. This will be done by assuming that the mass-flux, $\vec{\mathfrak{J}} = \rho\vec{v}$, is given data, and we are to enforce the constraint

$$\vec{\mathfrak{J}} = \sum_{i=1}^{n} \overline{m}_i c_i \vec{v}_i \tag{2.1}$$

whilst solving the equations

$$-RT\vec{\nabla}c_i = \sum_{\substack{j=1 \\ i\neq j}}^{n} \frac{RTc_i c_j}{\mathscr{D}_{ij} c_{\mathrm{T}}}(\vec{v}_i - \vec{v}_j), \quad i = 1, \ldots, n. \tag{2.2}$$

$$\vec{\nabla} \cdot (c_i \vec{v}_i) = r_i \tag{2.3}$$

which we label the steady-state Stefan–Maxwell equations.

This chapter is similar in scope to the work of [105], but with several key differences and extensions some of which will also be carried forth in future chapters.

First, our approach does not need any rearrangement of (2.1) to eliminate one species, but rather incorporates the constraint via an augmented formulation. The choice of species to eliminate in [105] is somewhat arbitrary, and with the augmentation we propose, is no longer necessary. Augmentation also exploits the symmetric positive semidefinite structure of the transport matrix and preserves permutational symmetry

of the system. This will be particularly pertinent for future chapters where we study more complex driving forces, e.g. of the form (1.35a).

Second, the symmetric positive definite structure of the augmented transport matrix yields straightforward proofs of the coercivity of bilinear forms on appropriate function spaces. As a consequence, we will prove that the linearized system is well-posed in the continuous and discrete setting and derive error bounds for its discretization in the general case of n species. An aspect of our formulation different from [105] is that we formulate $c_i \in H^1(\Omega)$ and $\vec{v}_i \in L^2(\Omega)^d$, whereas they formulate $c_i \in L^2(\Omega)$ and $\vec{N}_i \in H(\mathrm{div}, \Omega)$. This has its consequent advantages and disadvantages. In addition we also solve for the velocity $\vec{v}_i$ instead of the molar flux $\vec{N}_i = c_i \vec{v}_i$.

Finally we are able to design the discrete formulation in a structure-preserving way so that the Gibbs–Duhem equation is satisfied up to machine precision, independent of mesh size.

2.0.1 Augmentation of the transport matrix

An initial obstacle is that in systems with more than one spatial dimension, the existence of the nullspace (1.42) on $\mathbf{M}$ means that the one cannot recover the species velocities given only the driving forces, but must find a tractable way to incorporate the additional information provided by the mass-average velocity constraint (2.1).

A central idea of this thesis is to incorporate the mass-average velocity constraint (2.1) by augmenting (2.2), in a manner inspired by the augmented Lagrangian approach [17, 63]. Given $\gamma > 0$, for each i we multiply both sides of (2.1) by $\gamma RT\omega_i$ and add the resulting term to the i^{th} equation of (2.2) to deduce that

$$\vec{d}_i + \frac{\gamma RT\overline{m}_i c_i}{\rho}\vec{\mathfrak{J}} = \sum_{j\neq i}^{n} \frac{RTc_i c_j}{\mathscr{D}_{ij} c_{\mathrm{T}}}\big(\vec{v}_i - \vec{v}_j\big) + \frac{\gamma RT\overline{m}_i c_i}{\rho}\sum_{j=1}^{n}\overline{m}_i c_j \vec{v}_j = \sum_{j=1}^{n}\mathbf{M}_{ij}^{\gamma}\vec{v}_j \tag{2.4}$$

for $i = 1, 2, \ldots, n$, where $\mathbf{M}_{ij}^{\gamma}$ is the augmented transport matrix

$$\mathbf{M}_{ij}^{\gamma} = \mathbf{M}_{ij} + \gamma\mathcal{L}_{ij}, \tag{2.5}$$

in which

$$\mathcal{L}_{ij} := RT\overline{m}_i\overline{m}_i c_i c_j/\rho. \tag{2.6}$$

Our particular choice of the entries of $\mathcal{L}$ allows us to compute

$$\sum_{i,j=1}^{n} \vec{v}_i \cdot \mathbf{M}_{ij}^{\gamma} \vec{v}_j = \frac{1}{2} \sum_{i=1}^{n} \sum_{j \neq i}^{n} \frac{c_i c_j RT}{\mathscr{D}_{ij} c_{\mathrm{T}}} \|\vec{v}_j - \vec{v}_i\|^2 + \frac{\gamma RT}{\rho} \Big\| \sum_{j=1}^{n} \overline{m}_i c_j \vec{v}_j \Big\|^2 \tag{2.7}$$

to show that the augmented transport matrix is symmetric positive definite.

The first appearance of this augmentation seems to be from Helfand [79] and was subsequently remarked upon by Giovangigli [67]. Its utility is greatly extended in this work. Specifically, we show that the positive-definiteness achieved by this augmentation will cause the associated bilinear forms in the variational formulation to be coercive, greatly facilitating the analysis.

The chapter is organized as follows. Section 2 3 we derives a suitable weak formulation for the problem. In section 3 we prove well-posedness of a linearized system of (2.2)-(2.3). In section 4 we show stability of a discretization of this linearized system and prove error estimates for the linearisation. Finally, in section 5 we verify our error estimates with a manufactured solution and illustrate our method by simulating the interdiffusion of oxygen, carbon dioxide, water vapour, and nitrogen in the lungs.

2.1 Problem formulation

We proceed to cast the problem (2.2)-(2.3) into variational form. Note that both sides of equation (2.4) are proportional to RT and hence without loss of generality we assume that $RT = 1$. Our idealized assumption on the driving forces then becomes

$$\vec{d}_i := -\vec{\nabla} c_i, \quad i = 1, 2, \ldots n. \tag{2.8}$$

In this case the Gibbs–Duhem equation (1.43) reduces to

$$\vec{\nabla} c_{\mathrm{T}} = 0, \tag{2.9}$$

i.e. that total concentration is constant. This is also important as the constancy of c_{T} is required to be consistent with the ideal gas equation of state (1.19), which is distinct from the Gibbs–Duhem equation. We assume that $\vec{\mathfrak{J}} \in H^1(\Omega)^d$ and $r_i \in L^2(\Omega), \quad i =$

$1, 2, \ldots, n$, and consider the boundary conditions

$$N_i \cdot \hat{n} = c_i \vec{v}_i \cdot \hat{n} = g_i \ \in H^{-1/2}(\Gamma_N) \ \text{ on } \ \Gamma_N, \quad i = 1, 2, \ldots, n, \tag{2.10}$$

$$c_i = f_i > 0 \ \in H^{1/2}(\Gamma_D) \ \text{ on } \ \Gamma_D, \quad i = 1, 2, \ldots, n, \tag{2.11}$$

where $\hat{n}$ is the outward facing unit normal vector and Γ_N, Γ_D partition $\partial\Omega$. The equalities in (2.10)-(2.11) are to be understood in the sense of traces [60]. It is necessary to assume that f_i is positive for each $i = 1, 2, \ldots, n$ to avoid $\mathbf{M}$ acquiring another nullspace at the boundary. Either one of Γ_N and Γ_D may be empty. This boundary data is assumed to satisfy

$$\sum_{i=1}^{n} g_i \overline{m}_i = \vec{\mathfrak{J}} \cdot \hat{n} \ \text{ on } \ \Gamma_N, \tag{2.12}$$

$$\sum_{i=1}^{n} f_i = C_{\mathrm{T}} \ \text{ on } \ \Gamma_D, \tag{2.13}$$

where $C_{\mathrm{T}} > 0$ is a constant that we will show is equal to the total concentration (1.9). These assumptions are necessary to be consistent with the Gibbs–Duhem equation (2.9) and the mass-flux constraint (2.1). In the steady state, the mass continuity equation (1.31) implies that

$$\sum_{i=1}^{n} r_i \overline{m}_i = \vec{\nabla} \cdot \vec{\mathfrak{J}} \text{ in } \Omega \tag{2.14}$$

which imposes a further constraint on the reaction rates r_i. We assume (2.14) henceforth[1].

We define the function space

$$H^1_{\Gamma_D}(\Omega) = \{w_i \in H^1(\Omega) \ : \ w_i|_{\Gamma_D} = 0\}, \tag{2.15}$$

and the affine function space

$$H^1_{f_i}(\Omega) = \{w_i \in H^1(\Omega) \ : \ w_i|_{\Gamma_D} = f_i\}. \tag{2.16}$$

We can now derive the weak formulation for (2.2)-(2.3). We test (2.4) with $\vec{u}_i \in$

[1] According to mass conservation, physically this term should be zero for a single phase. However we relax this condition in this chapter to allow for full generality.

$L^2(\Omega)^d$ and integrate over Ω to derive for all $i = 1, 2, \ldots, n$,

$$\int_\Omega \Big(- \vec{\nabla} c_i + \frac{\gamma \overline{m}_i c_i}{\rho} \vec{\mathfrak{J}} \Big) \cdot \vec{u}_i = \int_\Omega \Big(\sum_{j \neq i}^n \frac{c_i c_j}{\mathscr{D}_{ij} c_{\mathrm{T}}} \big(\vec{v}_i - \vec{v}_j \big) + \frac{\gamma \overline{m}_i c_i}{\rho} \sum_{j=1}^n \overline{m}_i c_j \vec{v}_j \Big) \cdot \vec{u}_i \quad (2.17)$$

for all $\vec{u}_i \in L^2(\Omega)^d$.

For a given $w_i \in H^1_{\Gamma_D}(\Omega)$ we multiply both sides of (2.3) by $-w_i$ and integrate by parts to yield that for all $i = 1, 2, \ldots, n$,

$$\int_\Omega c_i \vec{v}_i \cdot \vec{\nabla} w_i - \int_{\Gamma_N} g_i w_i = - \int_\Omega r_i w_i \quad (2.18)$$

for all $w_i \in H^1_{\Gamma_D}(\Omega)$. We therefore seek $\vec{v}_i \in L^2(\Omega)^d$ and $c_i \in H^1_{f_i}(\Omega)$ such that (2.17) and (2.18) hold for every $\vec{u}_i \in L^2(Q)^d$ and $w_i \in H^1_{\Gamma_D}(\Omega)$, for each $i = 1, 2, \ldots, n$.

Remark 1. *In the case of one dimension,* (2.3) *and the boundary data* (2.10)-(2.11) *allow us to recover $c_i \vec{v}_i$ completely. Consequently no augmentation is necessary. In higher dimensions we require $\gamma > 0$.*

We will now show that such a weak solution satisfies both the Gibbs–Duhem equation (2.9) and the mass-flux constraint (2.1). Choosing $\vec{u}_i = \vec{u} \in L^2(\Omega)^d$ for every $i = 1, 2, \ldots, n$ and summing over i in (2.17) yields

$$\sum_{i=1}^n \int_\Omega \Big(- \vec{\nabla} c_i + \frac{\gamma \overline{m}_i c_i}{\rho} \vec{\mathfrak{J}} \Big) \cdot \vec{u}_i = \sum_{i=1}^n \int_\Omega \Big(\sum_{j \neq i}^n \frac{c_i c_j}{\mathscr{D}_{ij} c_{\mathrm{T}}} \big(\vec{v}_i - \vec{v}_j \big) + \frac{\gamma \overline{m}_i c_i}{\rho} \sum_{j=1}^n \overline{m}_i c_j \vec{v}_j \Big) \cdot \vec{u}. \quad (2.19)$$

Here we can use the nullspace (1.42) and symmetry of $\mathbf{M}$ to deduce

$$\sum_{i=1}^n \sum_{j \neq i}^n \frac{c_i c_j}{\mathscr{D}_{ij} c_{\mathrm{T}}} \big(\vec{v}_i - \vec{v}_j \big) = \sum_{i,j=1}^n \mathbf{M}_{ij} \vec{v}_j = 0, \quad (2.20)$$

and further exploiting the definition of density (5.85), we obtain that

$$\sum_{j=1}^n \int_\Omega \gamma \overline{m}_i c_j \vec{v}_j \cdot \vec{u}_i - \int_\Omega \gamma \vec{\mathfrak{J}} \cdot \vec{u} + \int_\Omega \vec{\nabla} c_{\mathrm{T}} \cdot \vec{u} = 0 \quad (2.21)$$

for all $\vec{u} \in L^2(\Omega)^d$. Considering the first and second terms with the choice $\vec{u} = \vec{\nabla} w$ for

some $w \in H^1_{\Gamma_D}(\Omega)$, and using (2.18),

$$\sum_{j=1}^{n} \int_\Omega \gamma \overline{m}_i c_j \vec{v}_j \cdot \vec{\nabla} w - \int_\Omega \gamma \vec{\mathfrak{J}} \cdot \vec{\nabla} w = \sum_{j=1}^{n} \gamma \Big(- \int_\Omega \overline{m}_i r_j w + \int_{\Gamma_N} \overline{m}_i g_j w \Big) - \int_\Omega \gamma \vec{\mathfrak{J}} \cdot \vec{\nabla} w \tag{2.22}$$

$$= - \int_\Omega \gamma w \vec{\nabla} \cdot \vec{\mathfrak{J}} + \int_{\Gamma_N} \gamma w \vec{\mathfrak{J}} \cdot \hat{n} - \int_\Omega \gamma \vec{\mathfrak{J}} \cdot \vec{\nabla} w \quad \text{(by (2.12) and (2.14))}$$

$$= 0,$$

the final equality following from integration by parts. In light of this, (2.21) becomes

$$\int_\Omega \vec{\nabla} c_{\mathrm{T}} \cdot \vec{\nabla} w = 0 \tag{2.23}$$

for every $w \in H^1_{\Gamma_D}(\Omega)$. In particular, as c_{T} is constant on Γ_D by (2.13), there exists a $w \in H^1_{\Gamma_D}(\Omega)$ such that $\vec{\nabla} w = \vec{\nabla} c_{\mathrm{T}}$. For this choice of w, (2.23) becomes

$$\int_\Omega \left\| \vec{\nabla} c_{\mathrm{T}} \right\|^2 = 0. \tag{2.24}$$

Hence $\vec{\nabla} c_{\mathrm{T}} = 0$ almost everywhere, which equivalent to the Gibbs–Duhem equation (2.9). The constraint on the Dirichlet data (2.13) ensures that $c_{\mathrm{T}} = C_{\mathrm{T}}$. Equation (2.21) then simplifies to

$$\int_\Omega \Big(\sum_{j=1}^{n} \overline{m}_i c_j \vec{v}_j \Big) \cdot \vec{u} = \int_\Omega \vec{\mathfrak{J}} \cdot \vec{u} \qquad \forall \ \vec{u} \in L^2(\Omega)^d, \tag{2.25}$$

a variational statement of the mass-flux constraint (2.1).

Remark 2. *With pure Neumann boundary data ($\Gamma_D = \emptyset$), the system* (2.17)-(2.18) *is not in general well-posed. For example, consider the case where a solution is given by $\vec{v}_i = v \in L^2(\Omega)^d$ for each i and $c_i = C$ for a constant $C > 0$. This is possible for $r_i = R$ and $g_i = G$ with $R \in L^2(\Omega)$ and $G \in H^{-1/2}(\Gamma_N)$ independent of i. Observe that the variables $\hat{c}_i = \alpha c_i = \alpha C$ and $\hat{v}_i = \alpha^{-1} \vec{v}_i = \alpha^{-1} v$ are also solutions for any $\alpha > 0$.*

In particular, due to (1.42)*, the weak form of the Stefan–Maxwell equations reduces to*

$$\frac{\gamma}{\alpha}\int_\Omega \frac{\overline{m}_i c_i}{\rho}\vec{\mathfrak{J}}\cdot\vec{u}_i = \frac{\gamma}{\alpha}\int_\Omega \Big(\frac{\overline{m}_i c_i}{\rho}\sum_{j=1}^{n}\overline{m}_i c_j\vec{v}_j\Big)\cdot\vec{u}_i, \tag{2.26}$$

which holds for each $\vec{u}_i \in L^2(\Omega)$ *in light of* (2.25)*.*
In order to make the problem well-posed we introduce the auxiliary conditions

$$\int_\Omega c_i = \bar{C}_i, \quad i = 1, 2, \ldots, n, \tag{2.27}$$

for known constants $\bar{C}_i$*. The physical interpretation of this constraint is clear. In the transient dynamics we have the continuity equations*

$$\frac{\partial c_i}{\partial t} = -\vec{\nabla}\cdot(c_i\vec{v}_i) + r_i. \tag{2.28}$$

Integrating over Ω *and using the divergence theorem, we deduce that*

$$\frac{d}{dt}\int_\Omega c_i = -\int_\Omega g_i + \int_\Omega r_i. \tag{2.29}$$

For a steady-state solution to exist, it is necessary that the right hand side of this equation vanishes. Therefore, for all time t*,*

$$\frac{d}{dt}\int_\Omega c_i = 0. \tag{2.30}$$

Hence (2.27) *must hold. This will lead to our linearization, considered in the next section, to be well-posed in the case of pure Neumann data. In the case of mixed Dirichlet–Neumann data this assumption is not needed and the linearized system will be well posed.*

2.2 Linearization and well-posedness

We consider a linearization of Picard type. The general approach is that whenever a velocity is multiplied by a concentration, we replace the concentration with our current guess. An exception to this is explained in Remark 3 below. Let us define the function

spaces $X = H^1(\Omega)^n$, $X_{\Gamma_D} = H^1_{\Gamma_D}(\Omega)^n$, $Q = (L^2(\Omega)^d)^n$ as well as the affine function space $X_{\tilde{f}} = (H^1_{f_1}(\Omega), \ldots, H^1_{f_n}(\Omega))$. We endow X_{Γ_D} with the norm $\|\cdot\|_{X_{\Gamma_D}} = |\cdot|_{1,\Omega}$. Throughout the rest of this chapter we will frequently use the notation $\tilde{q} = (q_1, \ldots, q_n)$ to denote an n-tuple in one of these linear/affine function spaces as well as their discrete subspaces.

Given a previous guess for the concentration $\tilde{c}^k = (c_1^k, \ldots, c_n^k)$, we define a bilinear form $a_{\tilde{c}^k}(\cdot,\cdot) : Q \times Q \to \mathbb{R}$ given by

$$a_{\tilde{c}^k}(\tilde{v}, \tilde{u}) = \sum_{i=1}^{n} \int_\Omega \Big(\sum_{j \neq i}^{n} \frac{c_i^k c_j^k}{\mathscr{D}_{ij} c_{\mathrm{T}}} (\vec{v}_i - \vec{v}_j) + \frac{\gamma \overline{m}_i c_i^k}{\rho^k} \sum_{j=1}^{n} \overline{m}_i c_j^k \vec{v}_j \Big) \cdot \vec{u}_i = \sum_{i,j}^{n} \int_\Omega \mathbf{M}_{ij}^{\gamma,k} \vec{v}_j \cdot \vec{u}_i \tag{2.31}$$

for $\tilde{u}, \tilde{v} \in Q$. Here $\mathbf{M}^{\gamma,k}$ denotes the augmented transport matrix, the i,j entries being defined by using the current guess for the concentration $\tilde{c}^k$ in equations (5.2) and (2.5). Similarly, ρ^k is the density evaluated using $\tilde{c}^k$ in (5.85).

For the current guess $\tilde{c}^k$ we also define the bilinear form $b_{\tilde{c}^k} : Q \times X \to \mathbb{R}$,

$$b_{\tilde{c}^k}(\tilde{u}, \tilde{w}) = \sum_{i=1}^{n} \int_\Omega c_i^k \vec{u}_i \cdot \vec{\nabla} w_i \tag{2.32}$$

for $(\tilde{u}, \tilde{w}) \in Q \times X$ and the bilinear form $b : Q \times X \to \mathbb{R}$,

$$b(\tilde{u}, \tilde{w}) = \sum_{i=1}^{n} \int_\Omega \vec{u}_i \cdot \vec{\nabla} w_i. \tag{2.33}$$

For $\tilde{u} \in Q$ the linear functional $l_{\tilde{c}^k}(\cdot) : Q \to \mathbb{R}$ is defined as

$$l_{\tilde{c}^k}(\tilde{u}) = \gamma \sum_{i=1}^{n} \int_\Omega \frac{c_i^k \overline{m}_i}{\rho^k} \vec{u}_i \cdot \vec{\mathfrak{J}}. \tag{2.34}$$

The non-linear iteration scheme is as follows. We take an initial guess $(\tilde{v}^0, \tilde{c}^0) \in Q \times X_{\tilde{f}}$, which satisfies the Dirichlet boundary data (2.11) and

$$\sum_{i=1}^{n} c_i^0 = c_{\mathrm{T}} \tag{2.35}$$

almost everywhere for a given constant c_{T}, determined by either (2.13) or (2.27). For $k = 0, 1, 2, \ldots$ the next iterate of the sequence is computed as the solution to the

following generalized saddle point problem: find $(\tilde{v}^{k+1}, \tilde{c}^{k+1}) \in Q \times X_{\tilde{f}}$ such that

$$a_{\tilde{c}^k}(\tilde{v}^{k+1}, \tilde{u}) + b(\tilde{u}, \tilde{c}^{k+1}) = l_{\tilde{c}^k}(\tilde{u}), \quad \forall\, \tilde{u} \in Q, \tag{2.36}$$

$$b_{\tilde{c}^k}(\tilde{v}^{k+1}, \tilde{w}) = -(\tilde{r}, \tilde{w})_{L^2(\Omega)^n} + (\tilde{g}, \tilde{w})_{L^2(\Gamma_N)^n}, \quad \forall\, \tilde{w} \in X_{\Gamma_D}, \tag{2.37}$$

subject to the Dirichlet conditions (2.11). This is repeated until

$$\|\tilde{c}^{k+1} - \tilde{c}^k\|_X + \|\tilde{v}^{k+1} - \tilde{v}^k\|_Q \leq \varepsilon, \tag{2.38}$$

for a set tolerance $\varepsilon > 0$.

Note that $(\tilde{v}^k, \tilde{c}^k)$ is a weak solution to the non-linear problem (2.17)-(2.18) if and only if it is a fixed point of this iteration scheme. Indeed if $(\tilde{v}^k, \tilde{c}^k)$ is a weak solution to the non-linear problem (2.17)-(2.18) then the solution $(\tilde{v}^{k+1}, \tilde{c}^{k+1})$ to the equations (2.36)-(2.37) remains $(\tilde{v}^k, \tilde{c}^k)$. Conversely if $(\tilde{v}^{k+1}, \tilde{c}^{k+1}) = (\tilde{v}^k, \tilde{c}^k)$ then, converting (2.36)-(2.37) to a non-linear system by replacing $\tilde{c}^k$ with $\tilde{c}^{k+1}$, we recover the non-linear problem (2.17)-(2.18) and observe it is solved with $(\tilde{v}^{k+1}, \tilde{c}^{k+1})$.

We proceed to prove well-posedness of the variational problem (2.36)-(2.37) by applying either Theorem 2.1 in [36] or Theorem 3.1 in [118]. To invoke these theorems we shall prove the following conditions.

Condition 1: There exists a constant $\alpha > 0$ such that

$$a_{\tilde{c}^k}(\tilde{v}, \tilde{v}) \geq \alpha \|\tilde{v}\|_Q^2 \tag{2.39}$$

for all $\tilde{v} \in Q$.

Condition 2: There exist constants $\beta_i > 0$, $i = 1, 2$ such that for all $\tilde{w} \in X$,

$$\begin{aligned} \sup_{\tilde{u} \in Q} \frac{b(\tilde{u}, \tilde{w})}{\|\tilde{u}\|_Q} &\geq \beta_1 \|\tilde{w}\|_X, \\ \sup_{\tilde{u} \in Q} \frac{b_{\tilde{c}^k}(\tilde{u}, \tilde{w})}{\|\tilde{u}\|_Q} &\geq \beta_2 \|\tilde{w}\|_X. \end{aligned} \tag{2.40}$$

Remark 3. *An alternative to our definition of the linear functional* (2.34) *would be to replace* $\tilde{c}^k$ *with* $\tilde{c}^{k+1}$ *and therefore include the term as part of the bilinear functional* $b(\cdot, \cdot)$ *instead. However, the current formulation* (2.36)-(2.37) *ensures that we can*

derive the equivalent of (2.21) *for the linearized system*

$$\sum_{i=1}^{n} \int_{\Omega} \gamma \overline{m}_i c_i^k \vec{v}_i \cdot \vec{u} - \int_{\Omega} \gamma \vec{\mathfrak{J}} \cdot \vec{u} + \int_{\Omega} \sum_{i=1}^{n} \vec{\nabla} c_i^{k+1} \cdot \vec{u} = 0. \tag{2.41}$$

Then, following an argument identical to that presented in section 3, we deduce that for each k, the iterates satisfy

$$\sum_{i=1}^{n} c_i^{k+1} = c_T \tag{2.42}$$

almost everywhere. When combined with the assumption that the concentrations are positive almost everywhere, this implies that $a_{\tilde{c}^k}(\cdot,\cdot), b(\cdot,\cdot), b_{\tilde{c}^k}(\cdot,\cdot)$ are all bounded bilinear functionals on their respective function spaces.

In order to prove (2.39) it will be useful to write the bilinear form, $a_{\tilde{c}^k}(\cdot,\cdot)$ as the integral of a quadratic form. Denoting the Kronecker product by $\otimes$, we define the matrix

$$\mathcal{M}^{\gamma,k} = \mathbf{M}^{\gamma,k} \otimes \mathbb{I} \tag{2.43}$$

where $\mathbb{I}$ is the $d \times d$ identity matrix. We can then write the bilinear form as

$$a_{\tilde{c}^k}(\tilde{v}, \tilde{u}) = \int_{\Omega} \tilde{u} \cdot \mathcal{M}^{\gamma,k} \tilde{v}. \tag{2.44}$$

To show the coercivity condition (2.39) we must show for some $\alpha > 0$

$$a_{\tilde{c}^k}(\tilde{v}, \tilde{v}) = \int_{\Omega} \tilde{v} \cdot \mathcal{M}^{\gamma,k} \tilde{v} \geq \int_{\Omega} \alpha \|\tilde{v}\|^2. \tag{2.45}$$

Hence (2.39) will be satisfied if and only if $\mathcal{M}^{\gamma,k}$ is uniformly positive definite over Ω almost everywhere. Either by direct calculation, or by using a standard property of the Kronecker product, one can verify that $\mathcal{M}^{\gamma,k}$ will have the same eigenvalues as $\mathbf{M}^{\gamma,k}$, each with geometric multiplicity of d. Therefore coercivity of the bilinear form $a_{\tilde{c}^k}(\cdot,\cdot)$ is equivalent to showing that $\mathbf{M}^{\gamma,k}$ is symmetric positive definite almost everywhere in Ω. We prove this in the following lemma, which will be used throughout the thesis.

Lemma 1. *If $c_i^k \geq \kappa > 0$ a.e. for each $i = 1, 2, \ldots, n$ and a positive constant κ, then for any $\gamma > 0$, the matrix $\boldsymbol{M}^{\gamma,k}$ is symmetric positive definite almost everywhere.*

Proof. For almost every $x \in \Omega$, $\mathbf{M}^k$ is symmetric positive semidefinite. We proceed with the following argument pointwise. The normalized eigenvectors $\{\vartheta_1^{\mathbf{M}}, \ldots, \vartheta_n^{\mathbf{M}}\}$

form an orthonormal basis. By hypothesis the associated eigenvalues $\{\lambda_1^{\mathbf{M}}, \ldots, \lambda_n^{\mathbf{M}}\}$ can be ordered such that

$$0 = \lambda_1^{\mathbf{M}} < \lambda_2^{\mathbf{M}} \leq \cdots \leq \lambda_n^{\mathbf{M}}. \tag{2.46}$$

The nullspace of $\mathbf{M}^k$ then consists of the space spanned by the vector $\vartheta_1^{\mathbf{M}} = n^{-1/2}(1, 1, \ldots, 1) \in \mathbb{R}^n$. Furthermore,

$$\lambda_2^{\mathbf{M}} \geq \lambda_\kappa > 0 \tag{2.47}$$

for a λ_κ that depends only on κ.

The matrix $\mathcal{L}^k$ defined in (2.6) is also symmetric positive semidefinite, explicitly for $\tilde{\vartheta} = (\vartheta_1, \ldots, \vartheta_n) \in \mathbb{R}^n$

$$\tilde{\vartheta} \cdot \mathcal{L}^k \tilde{\vartheta} = \frac{1}{\rho^k} \Big\| \sum_{j=1}^n \overline{m}_i c_j^k \vartheta_j \Big\|^2. \tag{2.48}$$

In particular for the vector $\vartheta_1^{\mathbf{M}}$ we have that

$$\vartheta_1^{\mathbf{M}} \cdot \mathcal{L}^k \vartheta_1^{\mathbf{M}} = \frac{1}{n\rho^k} \Big(\sum_{j=1}^n \overline{m}_i c_j^k \Big)^2 = \frac{\rho^k}{n}. \tag{2.49}$$

Given any $\tilde{\vartheta} \in \mathbb{R}^n$ we can expand it in terms of the basis $\{\vartheta_1^{\mathbf{M}}, \ldots, \vartheta_n^{\mathbf{M}}\}$ as

$$\tilde{\vartheta} = \sum_{i=1}^n \alpha_i \vartheta_i^{\mathbf{M}} \tag{2.50}$$

for basis coefficients $\{\alpha_i\}_{i=1}^n$. Furthermore, by orthonormality,

$$\tilde{\vartheta} \cdot \mathbf{M}^k \tilde{\vartheta} = \sum_{i=1}^n \lambda_i^{\mathbf{M}} |\alpha_i|^2. \tag{2.51}$$

We combine this to get a bound on $\mathbf{M}^{\gamma,k}$

$$\tilde{\vartheta} \cdot \mathbf{M}^{\gamma,k} \tilde{\vartheta} = \tilde{\vartheta} \cdot \mathbf{M}^k \tilde{\vartheta} + \gamma \tilde{\vartheta} \cdot \mathcal{L}^k \tilde{\vartheta} \geq \gamma \frac{\rho^k}{n} |\alpha_1|^2 + \sum_{i=2}^n \lambda_i^{\mathbf{M}} |\alpha_i|^2. \tag{2.52}$$

Therefore $\mathbf{M}^{\gamma,k}$ is positive definite at x. This argument can be repeated for every $x \in \Omega$ except perhaps on a set of measure zero. Therefore $\mathbf{M}^{\gamma,k}$ is symmetric positive definite almost everywhere. □

Remark 4. *It is useful to understand how λ_κ scales with κ. This can be achieved by the following scaling argument. Suppose that whenever $c_i^k \geq 1$ for each $i = 1, 2, \ldots, n$ we have the lower bound on the eigenvalues, as in* (2.47)*, of $\lambda_{\kappa=1}$. Now suppose that for any $\kappa > 0$ we have $c_i^k \geq \kappa$ for each $i = 1, 2, \ldots, n$. We can then define the new variables $\kappa_i = c_i^k/\kappa$. We then see that $\kappa_i \geq 1$ for each i. Define the $\boldsymbol{M}_\kappa$ as the transport matrix with these new variables κ_i replacing c_i. By direct calculation we can check that*

$$\boldsymbol{M}_\kappa = \frac{1}{\kappa}\boldsymbol{M}. \tag{2.53}$$

By construction we have that $\lambda_2^{\boldsymbol{M}_\kappa} \geq \lambda_{\kappa=1}$. It follows from (2.53) *that $\lambda_2^{\boldsymbol{M}} = \kappa\lambda_2^{\boldsymbol{M}_\kappa} \geq \kappa\lambda_{\kappa=1}$. Hence we see that $\lambda_\kappa = \mathrm{O}(\kappa)$.*

Lemma 2. *Assume that $c_i^k \geq \kappa > 0$ a.e. for each $i = 1, 2, \ldots, n$ and $\gamma > 0$. Then the bilinear forms $a(\cdot,\cdot), b(\cdot,\cdot)$ and $b_{\tilde{c}^k}(\cdot,\cdot)$ satisfy the conditions* (2.39) *and* (2.40) *for some constants α, β_1, β_2 respectively, which depend only on κ, Ω.*

Proof. From Lemma (1) we have that

$$a_{\tilde{c}^k}(\tilde{v}, \tilde{v}) = \int_\Omega \tilde{u} \cdot \mathcal{M}^{\gamma,k}\tilde{v} = \sum_{i,j} \int_\Omega \vec{v}_j \cdot \mathbf{M}_{ij}^{\gamma,k}\vec{v}_i \geq \alpha\|\tilde{v}\|_Q^2, \tag{2.54}$$

where

$$\alpha = \min\{n^{-1}\gamma\rho^k, \lambda_\kappa\}, \tag{2.55}$$

and λ_κ is as in equation (2.47). This proves condition (2.39).

For conditions (2.40), given a $\tilde{w} \in X$, we can choose $\tilde{u} = \vec{\nabla}\tilde{w}$ which then yields

$$b(\vec{\nabla}\tilde{w}, \tilde{w}) = \sum_{i=1}^n \int_\Omega \|\vec{\nabla}w_i\|^2 = \|\tilde{w}\|_{X_{\Gamma_D}}^2. \tag{2.56}$$

Similarly for $b_{\tilde{c}^k}$ we have

$$b_{\tilde{c}^k}(\vec{\nabla}\tilde{w}, \tilde{w}) \geq \kappa\|\tilde{w}\|_{X_{\Gamma_D}}^2. \tag{2.57}$$

The final step is that we use either $\Gamma_D \neq \emptyset$ or the condition (2.27) to deduce a Poincaré inequality of the form

$$C_p\|\tilde{w}\|_{X_{\Gamma_D}} \geq \|\tilde{w}\|_X \text{ for all } \tilde{w} \in X \tag{2.58}$$

for some constant $C_p > 0$ depending only on Ω. Hence

$$b(\vec{\nabla}\tilde{w}, \tilde{w}) \geq C_p^{-1} \|\tilde{w}\|_X^2 \tag{2.59}$$

$$b_{\tilde{c}^k}(\vec{\nabla}\tilde{w}, \tilde{w}) \geq \kappa C_p^{-1} \|\tilde{w}\|_X^2. \tag{2.60}$$

□

Theorem 1. *Assume $\gamma > 0$ and the current guess $\tilde{c}^k$ satisfies $c_i^k \geq \kappa > 0$ a.e. for each $i = 1, 2, \ldots, n$ and a positive constant κ. Then, under the condition $\Gamma_D \neq \emptyset$ or (2.27), there exists a unique $(\tilde{v}^{k+1}, \tilde{c}^{k+1}) \in Q \times X_{\tilde{f}}$ that solves the system (2.36)-(2.37).*

Proof. Our remaining obstacle for the proof is that $X_{\tilde{f}}$ is not a Hilbert space. If we use the ansatz $\tilde{c}^{k+1} = \widehat{c}_0^{k+1} + \tilde{c}^0$, where $\widehat{c}_0^{k+1} \in X_{\Gamma_D}$ and $\tilde{c}^0 \in X_{\tilde{f}}$ was our initial guess, then we can recast the saddle point problem (2.36)-(2.37) as: find $(\tilde{v}^{k+1}, \widehat{c}_0^{k+1}) \in Q \times X_{\Gamma_D}$ such that

$$a_{\tilde{c}^k}(\tilde{v}^{k+1}, \tilde{u}) + b(\tilde{u}, \widehat{c}_0^{k+1}) = l_{\tilde{c}^k}(\tilde{u}) - b(\tilde{u}, \tilde{c}^0) \quad \forall\, \tilde{u} \in Q, \tag{2.61}$$

$$b_{\tilde{c}^k}(\tilde{v}^{k+1}, \tilde{w}) = -(\tilde{r}, \tilde{w})_{L^2(\Omega)^n} + (\tilde{g}, \tilde{w})_{L^2(\Gamma_N)^n} \quad \forall\, \tilde{w} \in X_{\Gamma_D}. \tag{2.62}$$

By [36, Theorem 2.1] or [118, Theorem 3.1] there exists a unique $(\tilde{v}^{k+1}, \widehat{c}_0^{k+1}) \in Q \times X_{\Gamma_D}$ solution to this system. The proof concludes by observing that if $\tilde{c}^{k+1} = \widehat{c}_0^{k+1} + \tilde{c}^0$ then $\tilde{c}^{k+1} \in X_{\tilde{f}}$ and satisfies the system (2.36)-(2.37). □

2.3 Discretization and error estimates

Here we discretize the generalized saddle point problem (2.36)-(2.37) and prove error estimates. Let $\mathcal{T}_h$ be a regular simplicial triangulation of Ω with maximum diameter h. For $m \geq 1$ we define the finite dimensional subspaces,

$$Q_h = \{\tilde{u}_h \in Q \mid \vec{u}_{h,i}|_K \in [P^{m-1}(K)]^d \ \forall\, K \in \mathcal{T}_h,\ i = 1, 2, \ldots, n\}, \tag{2.63}$$

$$X_h = \{\tilde{w}_h \in X \mid w_{h,i}|_K \in P^m(K) \ \forall\, K \in \mathcal{T}_h,\ i = 1, 2, \ldots, n\}, \tag{2.64}$$

$$X_{\Gamma_D,h} = \{\tilde{w}_h \in X_{\Gamma_D} \mid w_{h,i}|_K \in P^m(K) \ \forall\, K \in \mathcal{T}_h,\ i = 1, 2, \ldots, n\}. \tag{2.65}$$

Here $P^m(K)$ denotes the set of m^{th} order polynomials on the cell $K \in \mathcal{T}_h$.

We will require linear interpolation operators on the spaces X and Q, see [18, pp 72].

Proposition 1. *There exist linear interpolation operators $\Pi_h : X \to X_h$ and $\Lambda_h : Q \to Q_h$ and constants C_1, C_2 such that, for any $\tilde{c} \in X$, $\tilde{v} \in Q$ sufficiently regular,*

$$\|\tilde{c} - \Pi_h \tilde{c}\|_{X_{\Gamma_D}} \leq \|\tilde{c} - \Pi_h \tilde{c}\|_X \leq C_1 h^m |\tilde{c}|_{m+1,\Omega},$$

$$\|\tilde{v} - \Lambda_h \tilde{v}\|_Q \leq C_2 h^m |\tilde{v}|_{m,\Omega}.$$

Our non-linear iteration scheme in the discrete case is as follows; we take an initial guess $\tilde{c}^0 \in X_{\tilde{f}}$ that satisfies (2.35) and then construct $\tilde{c}_h^0 := \Pi_h \tilde{c}^0 \in X_h$. The Dirichlet boundary conditions (2.11) are typically only satisfied approximately; however we note that, due to the linearity of the interpolation operator and equation (2.35),

$$\sum_{i=1}^{n} c_{h,i}^0 = \sum_{i=1}^{n} \Pi_h c_i^0 = \Pi_h c_{\mathrm{T}} = c_{\mathrm{T}}, \tag{2.66}$$

and therefore condition (2.13) remains enforced.

For $k = 0, 1, 2, \ldots$ the next iterate of the sequence $(\tilde{v}_h^{k+1}, \tilde{c}_h^{k+1})$ is computed by solving the following linear system: find $(\tilde{v}_h^{k+1}, \hat{c}_{0,h}^{k+1}) \in Q_h \times X_{\Gamma_D,h}$ such that

$$a_{\tilde{c}_h^k}(\tilde{v}_h^{k+1}, \tilde{u}_h) + b(\tilde{u}_h, \hat{c}_{0,h}^{k+1}) = l_{\tilde{c}_h^k}(\tilde{u}_h) - b(\tilde{u}_h, \tilde{c}_h^0) \quad \forall\, \tilde{u}_h \in Q_h, \tag{2.67}$$

$$b_{\tilde{c}_h^k}(\tilde{v}_h^{k+1}, \tilde{w}_h) = -(\tilde{r}, \tilde{w}_h)_{L^2(\Omega)^n} + (\tilde{g}, \tilde{w}_h)_{L^2(\Gamma_N)^n} \quad \forall\, \tilde{w}_h \in X_{\Gamma_D,h}. \tag{2.68}$$

We then set $\tilde{c}_h^{k+1} = \hat{c}_{0,h}^{k+1} + \tilde{c}_h^0$ and repeat this until $\|\tilde{c}_h^{k+1} - \tilde{c}_h^k\|_X + \|\tilde{v}_h^{k+1} - \tilde{v}_h^k\|_Q \leq \varepsilon$ for our tolerance $\varepsilon > 0$.

A distinct advantage of our formulation is that the coercivity condition (2.39) and the inf-sup conditions (2.40) are automatically satisfied with the same (state-dependent) constants α, β_1, β_2. This follows from the fact that the choice of discrete function spaces preserves a crucial structure:

$$\text{for any } \tilde{w}_h \in X_h,\ \vec{\nabla} \tilde{w}_h \in Q_h, \tag{2.69}$$

which in particular allows us to repeat the proofs of (2.39) and (2.40) in the discrete setting in exactly the same manner. We thus have the following.

Theorem 2. *Assume $\gamma > 0$ and that $\tilde{c}_h^k$ satisfies $c_{h,i}^k \geq \kappa > 0$ a.e. for each $i = 1, 2, \ldots, n$ and a positive constant κ. Then, under the condition $\Gamma_D \neq \emptyset$ or (2.27), there exists a unique $(\tilde{v}_h^{k+1}, \hat{c}_{0,h}^{k+1}) \in Q_h \times X_{\Gamma_D,h}$ which solves the system (2.67)-(2.68).*

Given the well-posedness of the discretized system, we proceed to obtain error estimates. The proof strategy is to invoke Theorem 4.1 of [118], which we restate here for convenience.

Theorem 3 ([118])**.** *For $V_h \subset V$ and $X_h \subset X$ let $(\tilde{v}, \tilde{c}) \in Q \times X$ and $(\tilde{v}_h, \tilde{c}_h) \in Q_h \times X_h$ be solutions to the respective continuous and discrete generalized saddle point systems*

$$a(\tilde{v}, \tilde{u}) + b_1(\tilde{u}, \tilde{c}) = l(\tilde{u}) \quad \forall\, \tilde{u} \in Q \tag{2.70}$$

$$b_2(\tilde{u}, \tilde{w}) = R(\tilde{w}) \quad \forall\, \tilde{w} \in X \tag{2.71}$$

and

$$a(\tilde{v}_h, \tilde{u}_h) + b_1(\tilde{u}_h, \tilde{c}_h) = l(\tilde{u}_h) \quad \forall\, \tilde{u}_h \in Q_h \tag{2.72}$$

$$b_2(\tilde{u}_h, \tilde{w}_h) = R(\tilde{w}_h) \quad \forall\, \tilde{w}_h \in X_h. \tag{2.73}$$

Here a, b_1, b_2 are continuous bilinear forms and l, R are continuous linear functionals. Further assume that each of the bilinear forms satisfy the respective conditions (2.39) and (2.40) for coefficients α, β_1 and β_2. Then there exists constants L_1, L_2, depending on α, β_1 and β_2 such that

$$\|\tilde{c} - \tilde{c}_h\|_X \leq L_1 \Big(\inf_{\tilde{w}_h \in X_h} \|\tilde{c} - \tilde{w}_h\|_X + \inf_{\tilde{u}_h \in Q_h} \|\tilde{v} - \tilde{u}_h\|_Q \Big), \tag{2.74}$$

$$\|\tilde{v} - \tilde{v}_h\|_Q \leq L_2 \Big(\inf_{\tilde{w}_h \in X_h} \|\tilde{c} - \tilde{w}_h\|_X + \inf_{\tilde{u}_h \in Q_h} \|\tilde{v} - \tilde{u}_h\|_Q \Big). \tag{2.75}$$

We now deduce the main result of this section.

Theorem 4. *There exist constants $\bar{C}_{1,k}$ and $\bar{C}_{2,k}$ such that*

$$\|\tilde{c}^{k+1} - \tilde{c}_h^{k+1}\|_X \leq \bar{C}_{1,k} h^m \Big(|\tilde{c}^0|_{m+1,\Omega} + |\hat{c}_0^{k+1}|_{m+1,\Omega} + |\tilde{v}^{k+1}|_{m,\Omega} + \|\tilde{v}_h^{k+1}\|_{L^\infty(\Omega)} + \|\vec{\mathfrak{J}}\|_{L^\infty(\Omega)^d} \Big), \tag{2.76}$$

$$\|\tilde{v}^{k+1} - \tilde{v}_h^{k+1}\|_Q \leq \bar{C}_{2,k} h^m \Big(|\hat{c}_0^{k+1}|_{m+1,\Omega} + |\tilde{v}^{k+1}|_{m,\Omega} + \|\tilde{v}_h^{k+1}\|_{L^\infty(\Omega)} + \|\vec{\mathfrak{J}}\|_{L^\infty(\Omega)^d} \Big). \tag{2.77}$$

Proof. Given that the conditions (2.39)-(2.40) are satisfied for the spaces Q_h and X_h, we can almost use Theorem 3 to deduce an error estimate. An obstacle to this is that we are committing a variational crime: the continuous and discrete bilinear forms are in general different, that is $a_{\tilde{c}^k}(\cdot,\cdot) \neq a_{\tilde{c}_h^k}(\cdot,\cdot)$ etc.

Hence to apply Theorem 3, we must consider a new pair $(\mathring{v}_h^{k+1}, \mathring{c}_{0,h}^{k+1}) \in Q_h \times X_{\Gamma_D,h}$ as the unique solution to the following 'intermediate' saddle point system

$$a_{\tilde{c}^k}(\mathring{v}_h^{k+1}, \tilde{u}_h) + b(\tilde{u}_h, \mathring{c}_{0,h}^{k+1}) = l_{\tilde{c}^k}(\tilde{u}_h) - b(\tilde{u}_h, \tilde{c}_h^0) \quad \forall\, \tilde{u}_h \in Q_h, \tag{2.78}$$

$$b_{\tilde{c}^k}(\mathring{v}_h^{k+1}, \tilde{w}_h) = -(\tilde{r}, \tilde{w}_h)_{L^2(\Omega)^n} + (\tilde{g}, \tilde{w}_h)_{L^2(\Gamma_N)^n} \quad \forall\, \tilde{w}_h \in X_{\Gamma_D,h}, \tag{2.79}$$

where the forms are evaluated at the infinite-dimensional iterate $\tilde{c}^k$ rather than its discrete approximation $\tilde{c}_h^k$.

We then estimate

$$\|\tilde{c}^{k+1} - \tilde{c}_h^{k+1}\|_X \leq \|\widehat{c}_0^{k+1} - \mathring{c}_{0,h}^{k+1}\|_X + \|\tilde{c}^0 - \tilde{c}_h^0\|_X + \|\widehat{c}_{0,h}^{k+1} - \mathring{c}_{0,h}^{k+1}\|_X \tag{2.80}$$

$$\|\tilde{v}^{k+1} - \tilde{v}_h^{k+1}\|_Q \leq \|\tilde{v}^{k+1} - \mathring{v}_h^{k+1}\|_Q + \|\tilde{v}_h^{k+1} - \mathring{v}_h^{k+1}\|_Q. \tag{2.81}$$

Our strategy will be to show that each of the terms on the right-hand side of the inequalities (2.80)-(2.81) satisfy the estimates (2.76)-(2.77). For the first terms on the right-hand side in (2.80) and (2.81) we can directly apply Theorem 3 and deduce that there exist constants L_1, L_2 depending on α, β_1, β_2 such that

$$\|\widehat{c}_0^{k+1} - \mathring{c}_{0,h}^{k+1}\|_{X_{\Gamma_D}} \leq L_1\Big(\inf_{\tilde{w}_h \in X_{\Gamma_D,h}} \|\widehat{c}_0^{k+1} - \tilde{w}_h\|_{X_{\Gamma_D}} + \inf_{\tilde{u}_h \in Q_h} \|\tilde{v}^{k+1} - \tilde{u}_h\|_Q\Big), \tag{2.82}$$

$$\|\tilde{v}^{k+1} - \mathring{v}_h^{k+1}\|_Q \leq L_2\Big(\inf_{\tilde{w}_h \in X_{\Gamma_D,h}} \|\widehat{c}_0^{k+1} - \tilde{w}_h\|_{X_{\Gamma_D}} + \inf_{\tilde{u}_h \in Q_h} \|\tilde{v}^{k+1} - \tilde{u}_h\|_Q\Big). \tag{2.83}$$

The Poincaré inequality (2.58) allows us to replace the $\|\cdot\|_{X_{\Gamma_D}}$ norm with $\|\cdot\|_X$:

$$\|\widehat{c}_0^{k+1} - \widehat{c}_{0,h}^{k+1}\|_X \leq C_p^{-1} \|\widehat{c}_0^{k+1} - \widehat{c}_{0,h}^{k+1}\|_{X_{\Gamma_D}}. \tag{2.84}$$

Proposition (1) yields that for some constants C_1, C_2

$$\|\hat{c}_0^{k+1} - \mathring{c}_{0,h}^{k+1}\|_X \leq L_1 C_1 h^m \Big(|\hat{c}_0^{k+1}|_{m+1,\Omega} + |\tilde{v}^{k+1}|_{m,\Omega} \Big), \tag{2.85}$$

$$\|\tilde{v}^{k+1} - \mathring{v}_h^{k+1}\|_Q \leq L_2 C_2 h^m \Big(|\hat{c}_0^{k+1}|_{m+1,\Omega} + |\tilde{v}^{k+1}|_{m,\Omega} \Big). \tag{2.86}$$

This concludes the estimate on the first term on the right-hand side of (2.80)-(2.81). The second term of (2.80) satisfies (2.76)-(2.77) directly by the definition of $\tilde{c}_h^0$ and Proposition 1. It remains to obtain an estimate for the final term of (2.80)-(2.81).

The difference $\delta\hat{c}_{0,h}^{k+1} := \widehat{c}_{0,h}^{k+1} - \mathring{c}_{0,h}^{k+1}$ and $\delta\tilde{v}_h^{k+1} := \tilde{v}_h^{k+1} - \mathring{v}_h^{k+1}$, which belong in $X_{\Gamma_D,h}$ and Q_h respectively, satisfy the system

$$a_{\tilde{c}^k}(\delta\tilde{v}_h^{k+1}, \tilde{u}_h) + b(\tilde{u}_h, \delta\hat{c}_{0,h}^{k+1}) = l_{\tilde{c}_h^k}(\tilde{u}_h) - l_{\tilde{c}^k}(\tilde{u}_h) + a_{\tilde{c}^k}(\tilde{v}_h^{k+1}, \tilde{u}_h) - a_{\tilde{c}_h^k}(\tilde{v}_h^{k+1}, \tilde{u}_h) \quad \forall\, \tilde{u}_h \in Q_h, \tag{2.87}$$

$$b_{\tilde{c}^k}(\delta\tilde{v}_h^{k+1}, \tilde{w}_h) = b_{\tilde{c}^k}(\tilde{v}_h^{k+1}, \tilde{w}_h) - b_{\tilde{c}_h^k}(\tilde{v}_h^{k+1}, \tilde{w}_h) \quad \forall\, \tilde{w}_h \in X_{\Gamma_D,h}. \tag{2.88}$$

Note that, in this system, the bilinear forms on the right hand side have one argument fixed and therefore become linear functionals. Intuitively we expect that the right hand side of (2.87)-(2.88) is small, and consequently so is the solution. This is verified by, for example, using [36, Theorem 2.1] to deduce for some constant C

$$\|\delta\tilde{c}_h^{k+1}\|_{X_{\Gamma_D}} + \|\delta\tilde{v}_h^{k+1}\|_Q \leq \tag{2.89}$$

$$C\Big(\|b_{\tilde{c}^k}(\tilde{v}_h^{k+1}, \cdot) - b_{\tilde{c}_h^k}(\tilde{v}_h^{k+1}, \cdot)\| + \|a_{\tilde{c}^k}(\tilde{v}_h^{k+1}, \cdot) - a_{\tilde{c}_h^k}(\tilde{v}_h^{k+1}, \cdot)\| + \|l_{\tilde{c}^k} - l_{\tilde{c}_h^k}\| \Big). \tag{2.90}$$

Hence the proof will be complete upon obtaining a bound for the difference of each of these linear functionals of the form (2.76)-(2.77). First, applying Hölder's inequality

yields

$$|a_{\tilde{c}^k}(\tilde{v}_h^{k+1},\tilde{u})-a_{\tilde{c}_h^k}(\tilde{v}_h^{k+1},\tilde{u})| \le \sum_{i,j=1}^{n}\Big|\int_\Omega \vec{v}_{h,i}^{k+1}\big(\mathbf{M}_{ij}^{\gamma,\tilde{c}^k}-\mathbf{M}_{ij}^{\gamma,\tilde{c}_h^k}\big)\cdot\vec{u}_j\Big| \tag{2.91}$$

$$\le \sum_{i,j=1}^{n}\Big(\int_\Omega \big(\mathbf{M}_{ij}^{\gamma,\tilde{c}^k}-\mathbf{M}_{ij}^{\gamma,\tilde{c}_h^k}\big)^2\|\vec{v}_{h,i}^{k+1}\|^2\Big)^{\frac{1}{2}}\Big(\int_\Omega\|\vec{u}_j\|^2\Big)^{\frac{1}{2}} \tag{2.92}$$

$$\le \sum_{i,j=1}^{n}\Big(\int_\Omega \big(\mathbf{M}_{ij}^{\gamma,\tilde{c}^k}-\mathbf{M}_{ij}^{\gamma,\tilde{c}_h^k}\big)^2\Big)^{1/2}\|\tilde{v}_h^{k+1}\|_{(L^\infty(\Omega)^d)^n}\|\tilde{u}\|_Q. \tag{2.93}$$

The values of the matrix $\mathbf{M}^\gamma$ are smooth (C^∞) functions with respect to the concentrations. Such functions are locally Lipschitz. Since the concentrations lie within the compact domain $0 \le c_i^k, c_{h,i}^k \le c_{\mathrm{T}}$ for each $1 \le i \le n$, we can find a global Lipschitz constant $C_{\mathbf{M}}$:

$$|a_{\tilde{c}^k}(\tilde{v}_h^{k+1},\tilde{u})-a_{\tilde{c}_h^k}(\tilde{v}_h^{k+1},\tilde{u})| \le C_{\mathbf{M}}\|\tilde{c}^k-\tilde{c}_h^k\|_{L^2(\Omega)^n}\|\tilde{v}_h^{k+1}\|_{(L^\infty(\Omega)^d)^n}\|\tilde{u}\|_Q. \tag{2.94}$$

For example, explicitly we can take the constant $C_{\mathbf{M}}$ as

$$C_{\mathbf{M}} = \frac{4n}{\min_{i,j}\mathscr{D}_{ij}} + 4\gamma n\max_i \overline{m}_i + 2\gamma n^2\frac{\max_i(\overline{m}_i)^2}{\min_i \overline{m}_i}. \tag{2.95}$$

Note that the density ρ is uniformly bounded below by $(\min_i \overline{m}_i)c_T$.

As $\tilde{u}_h$ was arbitrary, we have thus shown that

$$\|a_{\tilde{c}^k}(\tilde{v}_h^{k+1},\cdot)-a_{\tilde{c}_h^k}(\tilde{v}_h^{k+1},\cdot)\| \le C_{\mathbf{M}}\|\tilde{c}^k-\tilde{c}_h^k\|_{L^2(\Omega)^n}\|\tilde{v}_h^{k+1}\|_{(L^\infty(\Omega)^d)^n}. \tag{2.96}$$

The estimates on the remaining linear functionals are deduced in a similar manner and we obtain

$$\|l_{\tilde{c}^k}-l_{\tilde{c}_h^k}\| \le C_l\|\tilde{c}^k-\tilde{c}_h^k\|_{L^2(\Omega)^n}\|\vec{\mathfrak{J}}\|_{L^\infty(\Omega)^d} \tag{2.97}$$

$$\|b_{\tilde{c}^k}(\tilde{v}_h^{k+1},\cdot)-b_{\tilde{c}_h^k}(\tilde{v}_h^{k+1},\cdot)\| \le \|\tilde{c}^k-\tilde{c}_h^k\|_{L^2(\Omega)^n}\|\tilde{v}_h^{k+1}\|_{(L^\infty(\Omega)^d)^n}. \tag{2.98}$$

Using these estimates we then deduce from (2.89)

$$\|\delta\tilde{c}_h^{k+1}\|_{X_{\Gamma_D}} + \|\delta\tilde{v}_h^{k+1}\|_Q \leq C\|\tilde{c}^k - \tilde{c}_h^k\|_{L^2(\Omega)^n}\Big((C_{\mathbf{M}}+1)\|\tilde{v}_h^{k+1}\|_{(L^\infty(\Omega)^d)^n} + C_l\|\vec{\mathfrak{J}}\|_{L^\infty(\Omega)^d}\Big). \tag{2.99}$$

Therefore, the consistency error is bounded in terms of $\|\tilde{c}^k - \tilde{c}_h^k\|_{L^2(\Omega)^n}$. In particular suppose that $\|\tilde{c}^k - \tilde{c}_h^k\|_{L^2(\Omega)^n} \leq C_k h^m$ for some constant C_k. This holds if Theorem 4 holds for the kth iterate. Then we have that

$$\|\delta\tilde{c}_h^{k+1}\|_{X_{\Gamma_D}} + \|\delta\tilde{v}_h^{k+1}\|_Q \leq CC_k h^m\Big((C_{\mathbf{M}}+1)\|\tilde{v}_h^{k+1}\|_{(L^\infty(\Omega)^d)^n} + C_l\|\vec{\mathfrak{J}}\|_{L^\infty(\Omega)^d}\Big). \tag{2.100}$$

Using (2.85)-(2.86), the definition of $\tilde{c}_h^0$, and (2.100) respectively on the terms in (2.80)-(2.81) this implies (after a regrouping of constants)

$$\|\tilde{c}^{k+1} - \tilde{c}_h^{k+1}\|_X \leq \bar{C}_{1,k}h^m\Big(|\tilde{c}^0|_{m+1,\Omega} + |\hat{c}_0^{k+1}|_{m+1,\Omega} + |\tilde{v}^{k+1}|_{m,\Omega} + \|\tilde{v}_h^{k+1}\|_{L^\infty(\Omega)} + \|\vec{\mathfrak{J}}\|_{L^\infty(\Omega)^d}\Big), \tag{2.101}$$

$$\|\tilde{v}^{k+1} - \tilde{v}_h^{k+1}\|_Q \leq \bar{C}_{2,k}h^m\Big(|\hat{c}_0^{k+1}|_{m+1,\Omega} + |\tilde{v}^{k+1}|_{m,\Omega} + \|\tilde{v}_h^{k+1}\|_{L^\infty(\Omega)} + \|\vec{\mathfrak{J}}\|_{L^\infty(\Omega)^d}\Big). \tag{2.102}$$

Consequently we have verified Theorem 4 is valid for the $(k+1)$th iterate, provided we can suitably estimate $\|\tilde{c}^k - \tilde{c}_h^k\|_{L^2(\Omega)^n}$. The argument concludes by induction as we note that the base case, $k = 1$, satisfies the required error estimate as we have $\|\tilde{c}^0 - \tilde{c}_h^0\|_{L^2(\Omega)^n} \leq C_1 h^m |\tilde{c}^0|_{m+1,\Omega}$ by Proposition 1.

□

For example, our analysis implies if we choose $m = 1$ then we have

$$\|\tilde{v}^{k+1} - \tilde{v}_h^{k+1}\|_Q + \|\tilde{c}^{k+1} - \tilde{c}_h^{k+1}\|_X = \mathrm{O}(h). \tag{2.103}$$

Remark 5. *One apparent drawback of Theorem 4 is that the constants $\bar{C}_{1,k}$ and $\bar{C}_{2,k}$ may compound in size as $k \to \infty$. Indeed, iterating* (2.99) *over k we may in general*

deduce an estimate of the following form:

$$\|\delta\tilde{c}_h^{k+1}\|_{X_{\Gamma_D}} + \|\delta\tilde{v}_h^{k+1}\|_Q \leq h^m \prod_{s=1}^{k} \widetilde{C}_s \tag{2.104}$$

where the constants $\widetilde{C}_s$ *involve products of the term* $(C_{\boldsymbol{M}}+1)\|\tilde{v}_h^{s+1}\|_{(L^\infty(\Omega)^d)^n}+C_l\|\vec{\mathfrak{J}}\|_{L^\infty(\Omega)^d}$. *A natural concern is that the consistency errors will degrade as* $k \to \infty$, *except in the cases where the right-hand side data is small. Before addressing this in further detail, we emphasize that this possible degradation on the control in the consistency errors should not be confused with degradation of the stability of the discretized system* (2.67)-(2.68), *whose stability is guaranteed by the continuous dependence on the data as stated in [36, Theorem 2.1] or [118, Theorem 3.1].*

In practice, the degradation of the consistency errors is not observed, for which there is a natural explanation. Let us now suppose that $\tilde{c}$ *is a fixed point of the discrete system* (2.67)-(2.68). *Then we remove the* k *dependence in* (2.99) *to write*

$$\|\delta\tilde{c}_h\|_{X_{\Gamma_D}} + \|\delta\tilde{v}_h\|_Q \leq C\|\tilde{c}-\tilde{c}_h\|_{L^2(\Omega)^n}\Big(\ (C_{\boldsymbol{M}}+1)\|\tilde{v}_h\|_{(L^\infty(\Omega)^d)^n} + C_l\|\vec{\mathfrak{J}}\|_{L^\infty(\Omega)^d}\Big). \tag{2.105}$$

Using (2.80), *the estimates* (2.85) *and our bound on* $\|\tilde{c}^0-\tilde{c}_h^0\|_X$, *we may write this as (redefining constants as necessary)*

$$\|\delta\tilde{c}_h\|_{X_{\Gamma_D}} + \|\delta\tilde{v}_h\|_Q \leq C\Big(h^m + \|\delta\tilde{c}_h\|_{X_{\Gamma_D}}\Big)\Big(\ (C_{\boldsymbol{M}}+1)\|\tilde{v}_h\|_{(L^\infty(\Omega)^d)^n} + C_l\|\vec{\mathfrak{J}}\|_{L^\infty(\Omega)^d}\Big) \tag{2.106}$$

It can be immediately observed that if the data on the right hand side is sufficiently small, then $\|\delta\tilde{c}_h\|_{X_{\Gamma_D}} = \mathrm{O}(h^m)$. *However, rather than relying on this, let us conjecture that an estimate of the following form holds:*

$$\|\tilde{c}-\tilde{c}_h\|_{L^2(\Omega)^n} \leq Ch\|\tilde{c}-\tilde{c}_h\|_X, \tag{2.107}$$

where C *is independent of* h. *Such estimates are obtained in the theory of saddle point approximation using the Aubin–Nitsche duality technique (for example see [18, Theorem 5.5.6]), but have not yet been developed for the generalized saddle point problem* (2.36)–(2.37). *For our system we will experimentally observe in the following section that* $\|\tilde{c}-\tilde{c}_h\|_{L^2(\Omega)^n} = \mathrm{O}(h^{m+1})$. *This is consistent with the duality estimate* (2.107) *combined with Theorem 4.*

With the conjecture (2.107) *we may instead derive the alternate bound*

$$\|\delta\tilde{c}_h\|_{X_{\Gamma_D}} + \|\delta\tilde{v}_h\|_Q \leq Ch\Big(Ch^m + \|\delta\tilde{c}_h\|_{X_{\Gamma_D}}\Big)\Big((C_{\boldsymbol{M}}+1)\|\tilde{v}_h\|_{(L^\infty(\Omega)^d)^n} + C_l\|\vec{\mathfrak{J}}\|_{L^\infty(\Omega)^d}\Big). \tag{2.108}$$

Provided that h is taken small enough, we will immediately have a bound on $\|\delta\tilde{c}_h\|$ of order $\mathrm{O}(h^{m+1})$. Hence this analysis implies in practice that if we compute a fixed point of our iteration scheme on a sufficiently fine mesh, then the consistency errors will be well controlled.

This argument is very similar to existing analyzes of quasilinear elliptic systems such as by [48], and especially [7], in which duality techniques are leveraged to obtain error estimates subject to the condition that h be of a sufficiently small size. An important future goal is the development of Aubin–Nitsche duality estimates for generalized saddle point systems, to provide a rigorous foundation to the argument above.

Remark 6. *The Gibbs–Duhem equation is preserved up to machine-precision as can observed by the following argument. Replacing c_T with $c_{T,h}$ we can reproduce the argument of section* 3 *and derive the equivalent of equation* (2.24)*;*

$$\int_\Omega \|\vec{\nabla} c_{T,h}\|^2 = 0. \tag{2.109}$$

Combining this with (2.66) *we see that $c_{T,h} = C_T$, where C_T is determined by either* (2.13) *or* (2.27)*. This calculation does not use any approximation based on the mesh size.*

2.4 Numerical results

Several numerical simulations were implemented with our method. The discretization was implemented using the Firedrake software [129] and PETSc [12, 13, 42, 81]. The arising linear systems were solved using MUMPS [1, 2].

2.4.1 Numerical example one: Manufactured solution

For $n = 4$ we first consider a test case on $\Omega = (0,1)^2$ for which the solution is analytically known in order to validate the error estimates of section 5.

The family of manufactured solutions is constructed as follows. For $j = 1, 2$ let $k_j(\cdot) : \Omega \to \mathbb{R}$ be a differentiable function with a strict bound $\|k_j\|_{L^\infty(\Omega)} < K$ for a

positive constant K. We set

$$c_1 = k_1 + K, \quad c_2 = -k_1 + K,$$
$$c_3 = k_2 + K, \quad c_4 = -k_2 + K.$$

We further assume that

$$\mathscr{D}_{13} = \mathscr{D}_{31} = \mathscr{D}_{14} = \mathscr{D}_{41} = \mathscr{D}_{24} = \mathscr{D}_{42} = \mathscr{D}_{23} = \mathscr{D}_{32}, \tag{2.110}$$

and that $RT = 1$.

Then for any given mass-flux $\vec{\mathfrak{J}} \in L^2(\Omega)^d$ an exact solution is given when

$$\vec{v}_1 = -\frac{2}{RT}\Big(\frac{K}{\mathscr{D}_{12}} + \frac{K}{\mathscr{D}_{13}}\Big)^{-1}\vec{\nabla}\ln c_1 + \frac{\vec{\mathfrak{J}}}{c_{\mathrm{T}}}, \quad \vec{v}_2 = -\frac{2}{RT}\Big(\frac{K}{\mathscr{D}_{12}} + \frac{K}{\mathscr{D}_{13}}\Big)^{-1}\vec{\nabla}\ln c_2 + \frac{\vec{\mathfrak{J}}}{c_{\mathrm{T}}},$$
$$\vec{v}_3 = -\frac{2}{RT}\Big(\frac{K}{\mathscr{D}_{34}} + \frac{K}{\mathscr{D}_{31}}\Big)^{-1}\vec{\nabla}\ln c_3 + \frac{\vec{\mathfrak{J}}}{c_{\mathrm{T}}}, \quad \vec{v}_4 = -\frac{2}{RT}\Big(\frac{K}{\mathscr{D}_{34}} + \frac{K}{\mathscr{D}_{31}}\Big)^{-1}\vec{\nabla}\ln c_4 + \frac{\vec{\mathfrak{J}}}{c_{\mathrm{T}}},$$

and, for $i = 1, 2, 3, 4$,

$$r_i = \mathrm{div}\big(c_i\vec{v}_i\big). \tag{2.111}$$

We then choose $\overline{m}_i = 1$ for $i = 1, 2, 3, 4$ so that the mass-flux constraint (2.1) is satisfied.

For this numerical experiment we take

$$k_1(x, y) = \frac{1}{2}\exp(8xy(1-y)(1-x)), \quad k_2(x, y) = \frac{1}{2}\sin(\pi x)\sin(\pi y); \tag{2.112}$$

we can then take $K = 1$. We then have $c_{\mathrm{T}} = 4$. For $i = 1, 2, 3, 4$ we pose the Dirichlet boundary conditions

$$c_1 = \frac{3}{2}, \quad c_2 = \frac{1}{2}, \quad c_3 = c_4 = 1, \qquad \text{on } \partial\Omega, \tag{2.113}$$

and set the mass-flux $\vec{\mathfrak{J}} = (0, 1)^\top$.

The diffusion coefficients are chosen as $\mathscr{D}_{12} = \mathscr{D}_{21} = 2$, $\mathscr{D}_{34} = \mathscr{D}_{43} = 3$ and all other diffusion coefficients set to 1. For our initial guess we choose $c_i^0 = c_{h,i}^0 = 1$ for $i = 1, 2, 3, 4$. We then proceed with the iteration detailed in section 5 and compute the

sequence $(\tilde{v}_h^{k+1}, \tilde{c}_h^{k+1})$ until

$$\|\tilde{c}_h^{k+1} - \tilde{c}_h^k\|_X + \|\tilde{v}_h^{k+1} - \tilde{v}_h^k\|_Q \leq \varepsilon, \tag{2.114}$$

and for this k we set $(\tilde{v}, \tilde{c}) = (\tilde{v}^{k+1}, \tilde{c}^{k+1})$. In this experiment we set $\varepsilon = 10^{-13}$. The parameter γ was set to 1, with the rationale being that we want to choose γ sufficiently large so that the coercivity parameter α appearing in (2.55) depends only on λ_κ. Although in practice λ_k cannot be calculated, our argument from Remark 4 ensures that $\lambda_k = \mathrm{O}(\kappa)$. For this example, $\kappa = 1$ and consequently $\gamma = 1$ is a reasonable choice. The effect of varying γ is explored in the discussion below.

To analyze the rate of convergence we define the three errors

$$E_1 = \Big(\sum_{j=1}^{n} \|c_j - c_{j,h}\|^2_{L^2(\Omega)} \Big)^{\frac{1}{2}}, \tag{2.115}$$

$$E_2 = \Big(\sum_{j=1}^{n} \|\vec{\nabla} c_j - \vec{\nabla} c_{j,h}\|^2_{L^2(\Omega)^d} \Big)^{\frac{1}{2}}, \tag{2.116}$$

$$E_3 = \Big(\sum_{j=1}^{n} \|\vec{v}_j - \vec{v}_{j,h}\|^2_{L^2(\Omega)^d} \Big)^{\frac{1}{2}}, \tag{2.117}$$

and the error in the mass-flux

$$E_4 = \Big\| \sum_{j=1}^{n} \overline{m}_i c_j \vec{v}_j - \vec{\mathfrak{J}} \Big\|_{L^2(\Omega)^d}. \tag{2.118}$$

According to Proposition 1, $E_j = \mathrm{O}(h^m)$ for $j = 1, 2, 3$. These estimates are verified for $m = 1, 2$ on the log-log error plot displayed in Figure 2.1. We also observe that $E_4 = \mathrm{O}(h^m)$. Note that $E_1 = \mathrm{O}(h^{m+1})$, supporting our duality-based error estimate hypothesis (2.107) for the system (2.67)-(2.68).

Other important solver characteristics are tabulated for the case $m = 1$ in Table 2.1. In particular we observe that the number of fixed point iterations is independent of the mesh size. It was also confirmed that our discretization preserves the Gibbs–Duhem equation up to machine precision — in each of our simulations we observed that $\|\vec{\nabla} c_{\mathrm{T}}\| \leq 10^{-14}$.

We also consider the effect of varying the parameter γ in Table 2.2. We plot solver characteristics varying γ for the case $m = 1$ on the 64×64 mesh. Across four orders of magnitude for γ, the iteration converges with only a minor change in the number of

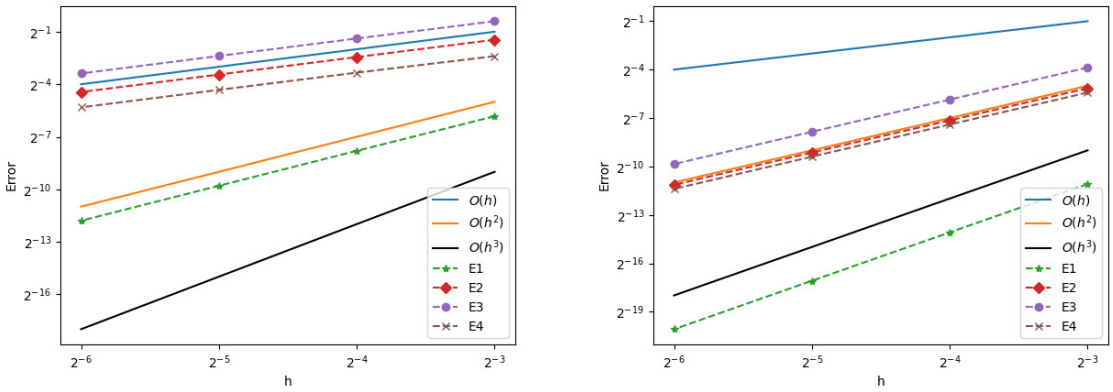

Figure 2.1: Log-Log error plots with $m = 1$ (left) and $m = 2$ (right).

Mesh size	Non-linear iterations	dof	Average linear solve time (s)
8×8	11	1348	0.22
16×16	11	5252	0.30
32×32	11	20740	0.63
64×64	11	82436	1.99

Table 2.1: Table showing the dependence of the solver characteristics on the mesh size for $m = 1$.

non-linear iterations. Taking $\gamma = 10^3$, the non-linear solver diverged; taking $\gamma = 10^{-3}$, the tolerance threshold of $\varepsilon = 10^{-13}$ was not reached. This indicates that, although

γ	Non-linear iterations	Average linear solve time (s)
10^{-2}	11	2.59
1	11	1.88
10^2	12	1.89

Table 2.2: Table showing the dependence of the solver characteristics as γ is varied.

the solver is generally robust for different values of γ, the solver does break down at extremes. It also suggests that γ should be chosen large enough such that the bound (2.55) depends only on λ_κ, but not larger, as it may cause the non-linear iteration scheme to fail to converge.

Much of the analysis we performed rested on the assumption that $c_i^k \geq \kappa$. It is then of interest to analyze the performance of the solver at extremely low concentrations.

For this purpose we define the function

$$f(x,y;\alpha) = x^\alpha + y^\alpha + (1-x)^\alpha + (1-y)^\alpha - x^\alpha y^\alpha - (1-x)^\alpha(1-y)^\alpha - x^\alpha(1-y)^\alpha - y^\alpha(1-x)^\alpha \tag{2.119}$$

for some $\alpha \geq 1$. Observe that this function is 1 on $\partial\Omega$ for every α but rapidly approaches 0 in the interior for large α. Furthermore at $\alpha = 1$, we have that $f(x,y;\alpha) = 1$.

We then take the following initial guesses for the concentrations as

$$c_1^0 = f(x,y;\alpha), \quad c_2^0 = 2 - f(x,y;\alpha) \tag{2.120}$$

and $c_3^0 = c_4^0 = 1$. These initial guesses satisfy $c_\mathrm{T} = 4$. We solve the system with the interpolants of these initial guesses on a 64×64 uniform mesh for various values of α. The results are tabulated in Table 2.3.

α	Non-linear iterations	Average linear solve time (s)
$\alpha = 2$	12	1.97
$\alpha = 16$	12	1.87
$\alpha = 64$	14	1.93

Table 2.3: Table showing the dependence of the solver characteristics on α.

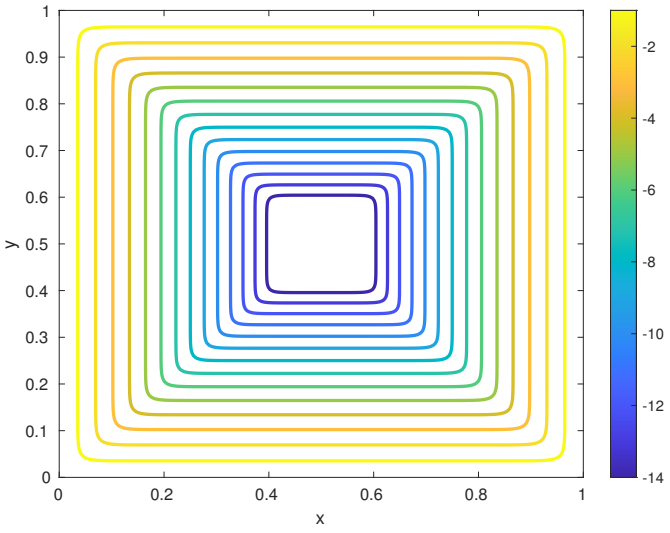

Figure 2.2: Contour plot of $\log_{10}(c_1) = \log_{10}(f(x,y;\alpha))$ for $\alpha = 64$.

The initial guess for c_1 for $\alpha = 64$ is plotted on a logarithmic scale in figure (2.2). Note that within the innermost contour, corresponding to the region $2/5 \leq x, y \leq 3/5$,

we have that $c_3 \approx 10^{-14}$. This is of the order of machine precision. This suggests that, although our analysis relies on the concentrations being uniformly bounded away from zero, in practice this is less of a restriction, as we can achieve convergence at extremely low concentrations for a similar number of non-linear iterations. The solver finally fails when $\alpha \geq 80$, due to the matrix becoming singular.

2.4.2 Numerical example two: Diffusion of oxygen and effusion of carbon dioxide in the lungs

If treated as a steady diffusion process, mass transport in the bronchi within the lungs involves simultaneous ingress of oxygen and egress of carbon dioxide. Moreover, the air through which these species diffuse also contains nitrogen and water vapour. For most modelling purposes, it is not necessary to distinguish among the various constituents of air, but in lung modelling we are interested in the distributions of both the oxygen consumed and carbon dioxide produced by the body, as well as the relative humidity along their diffusion paths. The concentrations of these compounds throughout the lungs has been modelled using the Stefan–Maxwell equations in [22] and [34]. For this example we solve for the mole fraction $y_i = c_i/c_{\mathrm{T}}$. Mathematically this is the same as normalising the total concentration to 1. As c_{T} is a constant in this setting, this does not change the weak formulation or the algorithm. We take the mass-flux, $\vec{\mathfrak{J}}$, as zero, and thus consider purely diffusional forces. For a realistic lung model it would be necessary to model the transient dynamics as well as the convective forces and pressure-driven elastic expansion, but this example suffices to illustrate the time-averaged multispecies transport physics.

This simulation was computed on the mesh shown in Figure 2.3. The surface mesh was provided by C. Geuzaine and J. F. Remacle [100, 130], and from this the 3D mesh was constructed using the software MeshMixer [131] and Gmsh [65]. The mesh consisted of 115609 vertices and 404174 elements.

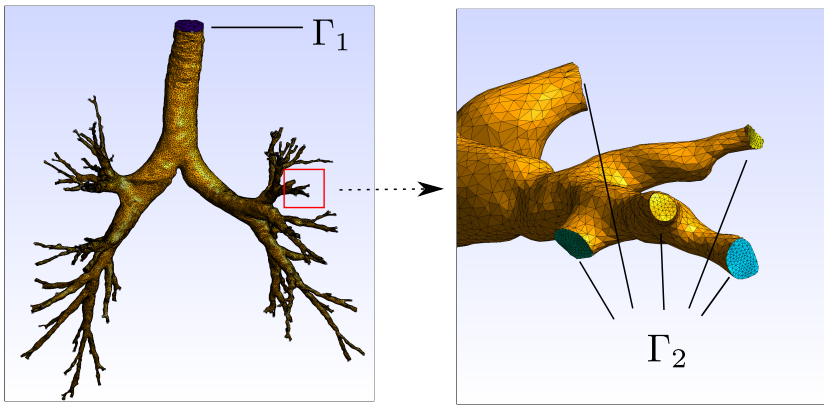

Figure 2.3: Mesh of the void space within the lungs at ambient pressure. The surface Γ_1 denotes the inlet at the trachea; the surface Γ_2 is a grouping of all the surfaces at the end of the tertiary bronchi.

Following the two-dimensional numerical experiments performed in [22], we take mixed Neumann-Dirichlet boundary conditions. At the inlet of the trachea, Γ_1, and at the end of the tertiary bronchi, Γ_2, we set the Dirichlet boundary data to the compositions of humidified air and alveolar air respectively. For the remaining boundary region we set homogeneous Neumann (no-flux) conditions. The Stefan–Maxwell coefficients and the boundary data for this experiment, both taken from [22], are tabulated in Tables 2.4 and 2.5.

Table 2.4: Values of the Stefan–Maxwell diffusion coefficients $\mathscr{D}_{ij}$ between species ($\mathrm{mm}^2\,\mathrm{s}^{-1}$)

Species	N_2	O_2	CO_2	H_2O
N_2		21.87	16.63	23.15
O_2	21.87		16.40	22.85
CO_2	16.63	16.40		16.02
H_2O	23.15	22.85	16.02	

As there are no reactions among the species in the lung, we have $r_i = 0$ for each $i = 1, 2, 3, 4$. The solving parameters were set as $\varepsilon = 10^{-11}$ and $\gamma = 0.0004$. As discussed in the previous example, we wish to take γ such that $\gamma n^{-1}\rho = \mathrm{O}(\lambda_\kappa) = \mathrm{O}(\kappa)$. Here $\rho \approx 28$ and hence this suggests a reasonable choice is $\gamma = \kappa = 0.0004$. (Strictly speaking, ρ in this case is not the density as we are using mole fractions, but this does not affect the mathematical argument regarding the choice of γ.)

Table 2.5: Dirichlet boundary data at the entrance of the trachea (Γ_1) and the end of the tertiary bronchi (Γ_2). These values can be found in [77]. Note that the air is humidified such that the water vapour mole fraction is equal at both Γ_1 and Γ_2.

	N_2	O_2	CO_2	H_2O
Mole fraction at Γ_1	0.7409	0.1967	0.0004	0.0620
Mole fraction at Γ_2	0.7490	0.1360	0.0530	0.0620

Following our algorithm from section 5, convergence was achieved in 9 non-linear iterations. Each linear system had $5,312,524$ degrees of freedom and was solved on 12 cores. We remark that despite the very low concentration of carbon dioxide at Γ_1, convergence was achieved in few iterations, and the mole fraction remained positive across all iterations.

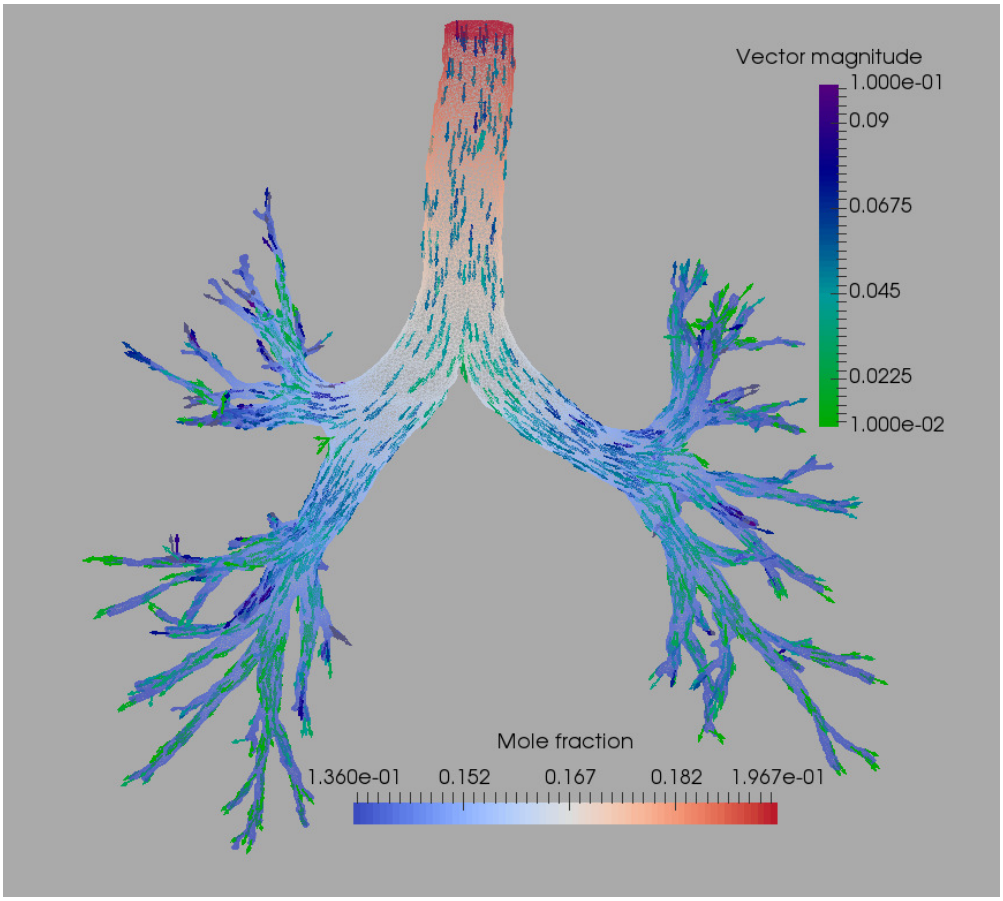

Figure 2.4: A plot of the distribution of oxygen in the lungs with its velocity vector field ($\mathrm{mm\,s^{-1}}$).

Interesting physical effects are revealed by the diffusional drag forces in the water vapour. Since the mole fractions for water vapour on the boundaries Γ_1 and Γ_2 are

the same, any concentration gradient of water vapour is a consequence of diffusional interactions with the other species.

Figure 2.5 shows modest uphill diffusion of water vapour at the trachea, where the velocity points in the same direction as the mole-fraction gradient. This can be explained as follows. The difference in the mole fractions of oxygen and carbon dioxide between the trachea and the tertiary bronchi creates a strong mole-fraction gradient, which in turn drives the velocity fields of the respective species in opposing directions. These velocity fields interact with the water vapour and attempt to drag the water vapour along with them, but the diffusional drag force exerted by CO_2 on H_2O exceeds the drag by O_2 on H_2O. Consequently, the water vapour tends to be dragged along with the carbon dioxide — the H_2O velocity flows up the trachea.

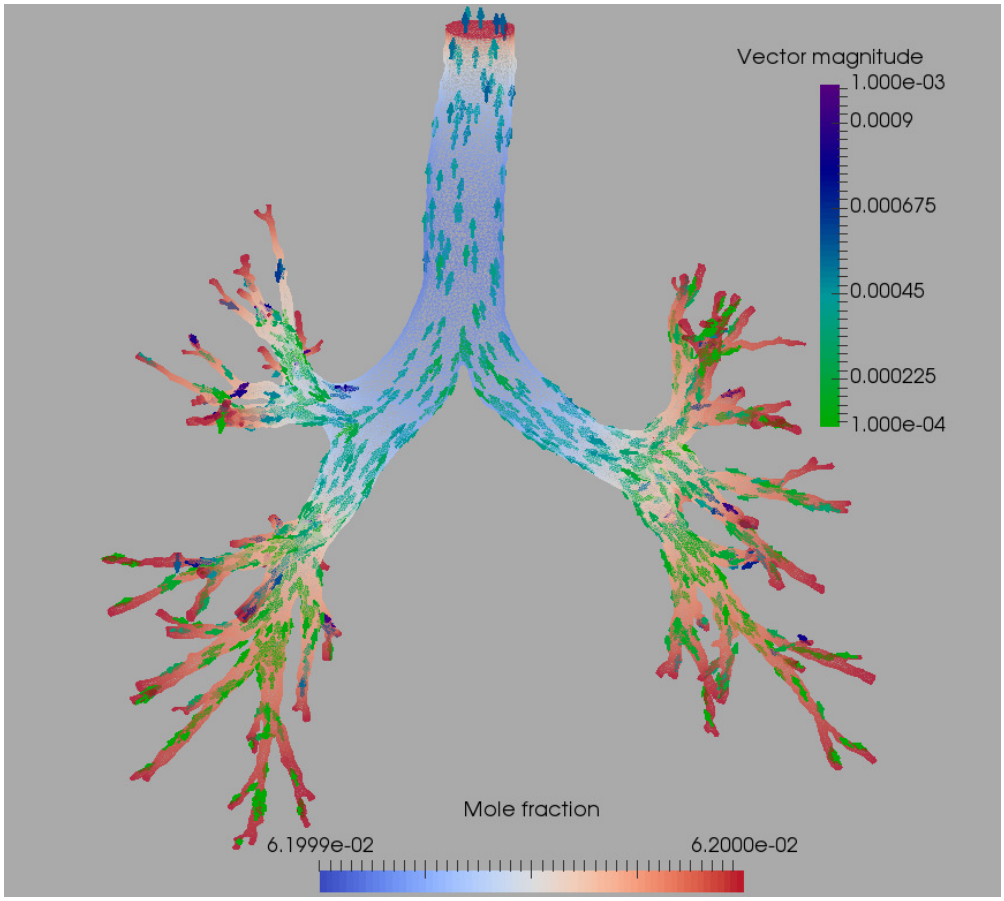

Figure 2.5: A plot of the distribution of water vapour in the lungs with its velocity vector field ($\mathrm{mm\,s^{-1}}$).

2.4.3 Code availability

For reproducibility, the exact software versions used to produce the results in this chaper, along with instructions for installation, has been archived on Zenodo [157].

The exact scripts used to produce each numerical experiment can be found at `https://bitbucket.org/AlexanderVanBrunt/maxwell-stefan-diffusion-equations-repository` along with the mesh used for the lungs.

2.5 Conclusion

In this chapter we derived a structure-preserving discretization of the steady-state Stefan–Maxwell diffusion problem based on an augmented saddle point formulation. The inf-sup conditions for the linearized continuous and discrete systems fundamentally rely on the symmetric positive definite structure of an augmented transport matrix, which follows from thermodynamical principles and the construction of the augmentation involving the mass-flux. Error estimates for the general case of n species were then deduced, which were confirmed with numerical experiments.

This work has been limited to an ideal setting and does not consider the full coupling between momentum and diffusion — a dubious assumption. Despite this, the work presented here lays an important cornerstone for considering the full Navier–Stokes–Onsager–Stefan–Maxwell framework. In particular the analysis of the augmented transport matrix (yielding coercive bilinear forms) is general in scope and will be applied to fully couple momentum and diffusion in the next chapter. We will also apply this idea to non-ideal fluids.

Given that our analysis depended highly on positivity of the concentrations, it would be highly desirable to prove that, at each non-linear iteration, the concentrations remain positive in both the continuous setting and its discrete approximation. A strategy pursued in the next chapter is to reformulate the problem using the chemical potential μ_i, in which non-negative concentrations emerge as a post-processing step.

Similarly one can formulate the problem in terms of molar fluxes rather than velocities, which has the advantage that the continuity equations do not need to be linearized. However, a disadvantage is that the resulting bilinear form $a(\cdot,\cdot)$ is no longer symmetric or coercive, which would add significant difficulty to the analysis. One way to circumvent this is to divide both sides of (2.2) by c_i, which would ensure symmetry and coercivity. The drawback of this approach is that it would introduce additional non-linearity in the diffusion driving forces, unless one uses the chemical potential, as pursued in the next chapter.

Regardless, although this chapter solved for the concentrations and velocities, this is not the only viable choice. This choice will be changed throughout the thesis as the context evolves. For example, in Chapter (3) we use chemical potentials, in Chapter 4

we use mole fractions (which essentially correspond to the concentrations in this chapter, as c_{T} was constant), in Chapter 5, the advantageous choice is found to be chemical potentials and fluxes. Rather than advocate for one particular choice, this chapter is meant to demonstrate how the structure of thermodynamics and the augmentation can be used to derive robust numerical algorithms.

Chapter 3

The Stokes–Onsager–Stefan–Maxwell equations

3.1 Introduction

The basis of this chapter formed an original paper, currently in submission. The preprint is available on ArXiv. This work was done in collaboration with another DPhil student, Francis Aznaran.

Although the previous chapter developed an effective solver, its scope of physical applicability is limited. This chapter extends this scope greatly by incorporating momentum, pressure and non-ideality into our formulation. We pose the problem at low Reynolds number and prove well-posedness and error estimates for a class of finite elements.

This imposes some key differences which require a shift in thinking. Firstly we must solve for both mass-average velocity, and pressure. This done by solving the Stokes equation,

$$\operatorname{div} \vec{\vec{\tau}} - \vec{\nabla} p = -\rho \vec{f}, \tag{3.1}$$

which derives from the momentum balance (1.23) at low Reynolds number.

To solve (3.1) we write the Newtonian constitutive equation in the form (1.46) which expresses the thermodynamic force (the linearized strain rate) in terms of the corresponding flux (the viscous stress) [83]. Consequently, we do not eliminate the viscous stress, but include it as an implicit variable to be solved for. This is at odds with most works in computational fluid dynamics, in which a flux-explicit formulation such as (1.46) is used to eliminate the viscous stress in the first instance.

While including the viscous stress as an unknown variable increases the computational cost, it has substantial benefits; the viscous stress plays a fundamental role in the calculation of local entropy production, but more significantly, it is key to developing a symmetric perturbed saddle point-like system, which is conducive to both theoretical analysis and (we anticipate) efficient linear solvers.

On the other hand, in solid mechanics, mixed methods which include $\overrightarrow{\overrightarrow{\tau}}$ as a variable to be solved for have become well-founded. The seminal paper of Arnold and Winther [6] introduced a new family of symmetric stress finite elements which could be used to model linear elasticity in a stress-displacement formulation. More particular to us is the recent paper by Carstensen et al. [30], which applied these families of finite elements to discretize the incompressible Stokes equations. A key quantity in their formulation was the Cauchy stress, or total stress,

$$\overrightarrow{\overrightarrow{\sigma}} := \overrightarrow{\overrightarrow{\tau}} - p\mathbb{I}. \tag{3.2}$$

Similarly the Cauchy stress, $\overrightarrow{\overrightarrow{\sigma}}$, will also be central to the analysis of this chapter.

Second the incorporation of the mass-average velocity must be rethought — indeed as $\vec{v}$ is now one of the variables we are solving for, it cannot be hoped that the mass-average velocity constraint (1.29) will be achieved only through consistency conditions on the boundary data such as (2.12), (2.13) which were posed in the previous chapter.

The augmentation introduced in the previous chapter modified the OSM equations, which induced coercivity of a bilinear form. Much of the results of the analysis of this chapter will be based on a similar deployment of this augmentation, albeit with a different scaling and now with more complex driving forces of the form (1.35a) on account of non-ideality and pressure diffusion. However it will be seen that augmenting only the OSM equations as before will come at the cost of symmetry. To enforce symmetry, we add a 'dual' augmentation to the Stokes equation (3.1)

$$\operatorname{div} \overrightarrow{\overrightarrow{\tau}} - \vec{\nabla} p = -\rho \vec{f} + \gamma \sum_j \omega_j (\vec{v} - \vec{v}_j). \tag{3.3}$$

With these two augmentations, an important bilinear form defined later in (3.31a) will be both symmetric and coercive on an appropriate kernel. The two augmentations (2.4) and (3.3) greatly aid the proofs of well-posedness for the continuous and discrete problems, as we demonstrate in (3.3.2) and (3.4.1).

Perhaps the biggest shift from the last chapter though is that we will now be solving for the chemical potential. This will carry several advantages. After the introduction of pressure, the OSM equations take the form

$$-c_i\vec{\nabla}\mu_i + \omega_i\vec{\nabla}p = \sum_{i=1}^{n}\mathbf{M}_{ij}\vec{v}_i. \tag{3.4}$$

From (3.4), we see using the chemical potential allows for a general statement of the OSM equations (specifically the diffusion driving forces) independent of the materials considered. If we were to make the (perhaps more obvious) choice of solving for concentrations or mole fraction as the primary variables instead, the form of the diffusion driving forces would change in a material-dependent manner. Second, our choice allows for a decoupling in the linearization we employ: the primary mixed system to solve only depends on the material via the diffusion coefficients and viscosities, with any non-ideality confined to the computation of concentrations and density postprocessed at every iteration the using material-dependent thermodynamic constitutive relations discussed in subsection 1.2.1.2. This decoupling is another key ingredient to formulate the equations with a symmetric perturbed saddle point-like structure, which will considerably simplify the analysis.

The price one has to pay for this, is that it cannot be said to be structure preserving — the Gibbs–Duhem equation will not hold up to machine precision and the transient balance equations are more intricate.

3.1.1 Coupled problem statement

The goal of this chapter is to find and analyze a variational formulation and finite element discretization of the following problem: given data f and $\{r_i\}_{i=1}^n$, find chemical potentials $\{\mu_i\}_{i=1}^n$, viscous stress $\vec{\vec{\tau}}$, pressure p, species velocities $\{\vec{v}_i\}_{i=1}^n$, and convective

velocity $\vec{v}$ satisfying

$$-c_i\vec{\nabla}\mu_i + \omega_i\vec{\nabla}p + \gamma\omega_i\vec{v} = \sum_j \mathbf{M}_{ij}^{\gamma}\vec{v}_j \ \forall i, \qquad \text{(augmented OSM equations)} \tag{3.5a}$$

$$\vec{\vec{\varepsilon}}(v) = \mathcal{A}\vec{\vec{\tau}}, \qquad \text{(stress constitutive law)} \tag{3.5b}$$

$$\operatorname{div}\vec{\vec{\tau}} - \vec{\nabla}p - \gamma\sum_j \omega_j(\vec{v} - \vec{v}_j) = -\rho\vec{f}, \qquad \text{(augmented Stokes equation)} \tag{3.5c}$$

$$-\operatorname{div}(c_i\vec{v}_i) = r_i \ \forall i, \qquad \text{(species continuity equation)} \tag{3.5d}$$

$$\operatorname{div}(\vec{v}) = \operatorname{div}\left(\sum_j \omega_j\vec{v}_j\right), \qquad \text{(mass-average velocity constraint)} \tag{3.5e}$$

for an augmentation parameter $\gamma \geq 0$, where $\{c_i, \omega_i\}_{i=1}^n, \rho$ are functions of the unknowns via chemical potential constitutive laws such as (1.17) and (1.18), and algebraic relations (1.25), (1.30). Furthermore in this chapter we understand the augmented transport matrix $\mathbf{M}^{\gamma}$ to mean

$$\mathbf{M}_{ij}^{\gamma} = \mathbf{M} + \gamma\omega_i\omega_j \tag{3.6}$$

which is a mildly different scaling than Chapter 2. Principally this done as it is more commensurate with the mass-average constraint (3.5e) enforced in this section. We call the system (3.5) the (augmented) *Stokes–Onsager–Stefan–Maxwell* (SOSM) system. When the convection term $\operatorname{div}(\rho\vec{v}\otimes\vec{v})$ is incorporated into (3.5c), we call this the *Navier–Stokes–Onsager–Stefan–Maxwell* (NSOSM) system. Appropriate boundary conditions will be introduced in (3.2.2).

Note in the system we only directly enforce the *divergence* of the mass-average velocity constraint (3.5e), which may be interpreted as the compressible generalization of the standard divergence constraint (1.26); this choice gives rise to a saddle point-like structure, as we show in the next section. Nevertheless, the full constraint (1.29) is incorporated via the augmentations (3.5a) and (3.5c), as discussed further in Remark 8.

Remark 7. *Many cross-diffusion systems, such as those describing multiagent systems in mathematical biology [29], arise from a gradient flow of an associated entropy functional. Unfortunately, although the OSM system admits an associated thermodynamic energy—the Gibbs free energy—we are not able to show equivalence of the (S)OSM system to the Euler–Lagrange stationarity condition of any energy or Lagrangian functional, and hence cannot exploit any gradient flow structure. Instead, our mathematical line of attack will be to exploit the positive definiteness of the augmented transport matrix* $\mathbf{M}^\gamma$*. With our augmentations of the equations, the Picard scheme we propose below in Section 3.3 nevertheless gives rise to symmetric linearized problems to solve at each nonlinear iteration.*

The remainder of this chapter is organized as follows. In Section 3.2, derives a novel variational formulation of the fully coupled nonlinear SOSM problem, incorporating boundary conditions and augmentation terms, as a nonlinear perturbed saddle point-like system, using a novel solution-dependent test space relating to the thermodynamic driving force; our principal discovery is the duality between the diffusion driving forces, and the combination of species continuity equations with the divergence of the mass-average velocity constraint. Section 3.3 proposes a Picard-like linearization, which is proven to be well-posed under physically reasonable assumptions. Section 3.4 identifies appropriate finite element spaces, and the structural relations which should hold between them, for a well-posed and convergent discretization of this linearization. We then validate our convergence results numerically. Finally, we illustrate our method by simulating the steady mixing of liquid benzene and cyclohexane in a two-dimensional microfluidic laminar-flow device.

3.2 Variational formulation

In this chapter, we employ standard notation for the Sobolev space $H^k(\Omega;\mathbb{X})$ (or $L^2(\Omega;\mathbb{X})$ when $k=0$) with domain $\Omega\subset\mathbb{R}^d$ and codomain $\mathbb{X}$, and associated norm $\|\cdot\|_k$ and seminorm $|\cdot|_k$. We denote by $\mathbb{S}=\mathbb{R}^{d\times d}_{\mathrm{sym}}$ the space of $d\times d$ symmetric tensors. The symbol $\lesssim$ denotes inequality up to a constant which may depend on mesh regularity but not mesh spacing h. Let $L^2_0(\Omega)\coloneqq\{z\in L^2(\Omega)\mid \fint_\Omega z\,\mathrm{d}x=0\}$. As in Chapter 2, we use the notation $\tilde{q}=(q_1,\dots,q_n)$ to denote an n-tuple of functions. Let $\Gamma=\partial\Omega$ and let $\langle\cdot,\cdot\rangle_\Gamma$ denote the $(H^{-1/2}\times H^{1/2})(\Gamma;\mathbb{R}\text{ or }\mathbb{R}^d)$ dual pairing.

3.2.1 Integrability of pressure gradients

In a variational formulation of the nonisobaric case, one would like to integrate the pressure gradient term in our diffusion driving forces (1.35a) by parts, to reduce the regularity requirement on p. However, it is not obvious how to do so, since the mass fractions ω_i are spatially varying. In order to rigorously incorporate the effect of pressure-driven diffusion, we are therefore led to consider the somewhat unorthodox possibility of formulating the Stokes subproblem with pressure lying in $H^1(\Omega)$. Typically, the condition that $p \in H^1(\Omega)$ may be provided by elliptic regularity results for the pressure field, but to the author's knowledge, the *a priori* square-integrability of pressure gradients (i.e. for which, we emphasize, pressure is *defined* to lie in $H^1(\Omega)$) has not been considered for the Stokes system, except at the discrete level for the incompressible case in [136]. This condition is also suggested by the case of pure Stefan–Maxwell diffusion for nonisobaric ideal gases. Here the driving forces are

$$\vec{d}_i = -RT\vec{\nabla}c_i + \omega_i\vec{\nabla}p, \tag{3.7}$$

which suggests considering each c_i (and hence c_T) to lie in $H^1(\Omega)$, which forces the pressure to lie in the same space due to the ideal equation of state $p = c_\mathrm{T}RT$.

In general, one must distinguish between the *thermodynamic* pressure p, which we use throughout this thesis, and the *mechanical* pressure $p_\mathrm{m} \coloneqq -\operatorname{tr}\sigma/d$. The mechanical pressure is related to the spherical Cauchy stress by $\operatorname{sph}\sigma \coloneqq \frac{\operatorname{tr}\sigma}{d}\mathbb{I} = -p_\mathrm{m}\mathbb{I}$, and to p by

$$p = p_\mathrm{m} + \zeta \operatorname{div}\vec{v}. \tag{3.8}$$

In the context of multicomponent flow, this decomposition is discussed in further detail by Bothe & Dreyer [20]. Even in the simpler incompressible limit where $\operatorname{div}\vec{v} = 0$ so that $p = p_\mathrm{m}$, we cannot expect extra regularity of $\vec{\nabla}p = -\operatorname{div}(\operatorname{sph}\sigma)$ because $H(\operatorname{div};\mathbb{S})$, the natural space for σ, is not closed under taking spherical parts.[1] Consequently, we do not take $p \in H^1(\Omega)$, but as a compromise consider a weaker condition defined by the combined viscous stress-pressure space

$$\mathbb{T} = \{(\vec{\vec{\tau}}, p) \in L^2(\Omega;\mathbb{S}) \times L^2(\Omega) \mid \operatorname{div}\vec{\vec{\tau}} - \vec{\nabla}p \in L^2(\Omega;\mathbb{R}^d)\} \left(\supsetneq H(\operatorname{div};\mathbb{S}) \times H^1(\Omega)\right), \tag{3.9}$$

[1] We also remark that, viewing the pressure as a component of the full Cauchy stress, appealing to the Hodge decomposition of the stress space $H(\operatorname{div};\mathbb{S})$ [4, Theorem 4.5] does not endow that component with any extra regularity.

and assign to it the weaker norm $\|\overrightarrow{\overrightarrow{\tau}}\|_0^2 + \|p\|_0^2 + \|\operatorname{div}\overrightarrow{\overrightarrow{\tau}} - \vec{\nabla}p\|_0^2$. This space and norm were previously employed by Manouzi & Farhloul in an analysis of a non-Newtonian incompressible Stokes flow [99] where $\overrightarrow{\overrightarrow{\tau}}$ was taken to be the deviatoric shear stress. Membership of the space $\mathbb{T}$ is naturally interpretable as the square-integrability of the divergence of the full Cauchy stress, i.e. that $\sigma = \overrightarrow{\overrightarrow{\tau}} - p\mathbb{I} \in H(\operatorname{div};\mathbb{S})$. Together with an analogous condition for the chemical potential gradient to be detailed in the next section (3.2.2), this weaker condition will account for the pressure gradient in the driving forces.

3.2.2 Fully coupled variational formulation

In this subsection, we derive a variational formulation for the stationary problem as a nonlinear perturbed saddle point-like system. We have found the following statement of the problem to be a feasible tradeoff between the (competing) goals of: physical relevance of variables and boundary data, regularity assumptions, numerical implementability and effectiveness, analytic tractability, enforcement of fundamental thermodynamic relations, and extensibility to the transient, anisothermal, and non-ideal settings.

For boundary data, we prescribe mass flux and molar fluxes:

$$\rho\vec{v} = g_{\mathrm{v}} \in H^{1/2}(\Gamma;\mathbb{R}^d) \text{ on } \Gamma, \tag{3.10a}$$

$$c_i\vec{v}_i \cdot \mathbf{n} = g_i \in H^{-1/2}(\Gamma) \quad \text{ on } \Gamma, \quad i = 1,\dots,n. \tag{3.10b}$$

For consistency with the mass-average velocity constraint (1.29), we require

$$\sum_i \overline{m}_i g_i = g_{\mathrm{v}} \cdot \mathbf{n}, \tag{3.11}$$

with equality in $H^{-1/2}(\Gamma)$. We further impose conditions

$$\int_\Omega p \,\mathrm{d}x = \int_\Omega \mu_i \,\mathrm{d}x = 0, \quad i = 1,\dots,n, \tag{3.12}$$

on the pressure and chemical potentials. Typically, the equation of state will require or imply strict positivity of p everywhere, in which case this condition should be understood as $\fint_\Omega p \,\mathrm{d}x = p^{\ominus} > 0$ and that p be shifted by the known value $p^{\ominus}$ as a postprocessing step.

Let $Q = L^2(\Omega;\mathbb{R}^d)^n \times L^2(\Omega;\mathbb{R}^d)$. For formal derivation of the weak form, we assume the solution tuple $(\tilde{\mu}, \vec{\vec{\tau}}, p, \tilde{v}, \vec{v})$ to be smooth on $\overline{\Omega}$, and consider choosing $(\tilde{w}, \vec{\vec{s}}, q)$ from the solution-dependent potential-stress-pressure test space

$$\Theta := \left\{ \left(\tilde{w}, \vec{\vec{s}}, q\right) \in L^2_0(\Omega)^n \times L^2(\Omega;\mathbb{S}) \times L^2_0(\Omega) \;\middle|\; \begin{array}{c} \operatorname{div} \vec{\vec{s}} - \vec{\nabla} q \in L^2(\Omega;\mathbb{R}^d), \\ -c_i \vec{\nabla} w_i + \omega_i \vec{\nabla} q \in L^2(\Omega;\mathbb{R}^d)\ \forall i \end{array} \right\}. \tag{3.13}$$

Here it is understood that the $\{c_i, \omega_i\}_i$ are computed from the solution tuple. Multiplying the i^{th} continuity equation (3.5d) by w_i, the divergence of the mass-average velocity constraint (3.5e) by q, and contracting the stress constitutive law (3.5b) with $\vec{\vec{s}}$, we obtain

$$\sum_i \left(\operatorname{div}(c_i \vec{v}_i) - r_i\right) w_i + \operatorname{div}\left(\vec{v} - \sum_i \omega_i \vec{v}_i\right) q + (\mathcal{A}\vec{\vec{\tau}} - \varepsilon(v)) : \vec{\vec{s}} = 0, \tag{3.14}$$

and hence

$$\int_\Omega \sum_i (\operatorname{div}(c_i \vec{v}_i) w_i - \operatorname{div}(\omega_i \vec{v}_i) q) + \mathcal{A}\vec{\vec{\tau}} : \vec{\vec{s}} - (\vec{\vec{s}} - q\mathbb{I}) : \varepsilon(v)\ \mathrm{d}x = \int_\Omega \sum_i r_i w_i\ \mathrm{d}x. \tag{3.15}$$

Integrating by parts yields

$$\begin{aligned} &\int_\Omega \mathcal{A}\vec{\vec{\tau}} : \vec{\vec{s}} + \sum_i (-c_i \vec{\nabla} w_i + \omega_i \vec{\nabla} q) \cdot \vec{v}_i + (\operatorname{div} \vec{\vec{s}} - \vec{\nabla} q) \cdot v\ \mathrm{d}x \\ &\quad = \left\langle (\vec{\vec{s}} - q\mathbb{I})\mathbf{n}, \vec{v} \right\rangle_\Gamma + \sum_i \left\langle c_i \vec{v}_i \cdot \mathbf{n}, -w_i + \frac{\omega_i}{c_i} q \right\rangle_\Gamma + \int_\Omega \tilde{r} \cdot \tilde{w}\ \mathrm{d}x \\ &\quad = \left\langle (\vec{\vec{s}} - q\mathbb{I})\mathbf{n}, \frac{g_{\mathrm{v}}}{\rho} \right\rangle_\Gamma + \sum_i \left\langle g_i, -w_i + \frac{M_i}{\rho} q \right\rangle_\Gamma + \int_\Omega \tilde{r} \cdot \tilde{w}\ \mathrm{d}x. \end{aligned} \tag{3.16}$$

Now for each $i = 1, \ldots, n$, we take the scalar product of $u_i \in L^2(\Omega;\mathbb{R}^d)$ with the augmented OSM equation (3.5a) and integrate over Ω to obtain

$$\int_\Omega \left(-c_i \vec{\nabla} \mu_i + \omega_i \vec{\nabla} p\right) \cdot \vec{u}_i - \vec{u}_i \cdot \sum_j \mathbf{M}_{ij} \vec{v}_j - \gamma \omega_i \sum_j \omega_j (\vec{v}_j - \vec{v}) \cdot \vec{u}_i\ \mathrm{d}x = 0. \tag{3.17}$$

Taking the inner product of the augmented Cauchy momentum balance (3.5c) with

$u \in L^2(\Omega;\mathbb{R}^d)$ yields

$$\int_\Omega (\operatorname{div} \vec{\vec{\tau}} - \vec{\nabla} p) \cdot \vec{u} - \gamma \left(\sum_j \omega_j (\vec{v} - \vec{v}_j) \right) \cdot \vec{u} \, \mathrm{d}x = - \int_\Omega \rho \vec{f} \cdot \vec{u} \, \mathrm{d}x. \tag{3.18}$$

We sum (3.17) over i and add (3.18) to derive

$$\begin{aligned} &\int_\Omega \sum_i \left(-c_i \vec{\nabla} \mu_i + \omega_i \vec{\nabla} p \right) \cdot \vec{u}_i + \left(\operatorname{div} \vec{\vec{\tau}} - \vec{\nabla} p \right) \cdot \vec{u} \\ &- \sum_{i,j} \vec{u}_i \cdot \mathbf{M}_{ij} \vec{v}_j - \gamma \left(\sum_i \omega_i (\vec{v}_i - \vec{v}) \right) \cdot \left(\sum_j \omega_j (\vec{u}_j - \vec{u}) \right) \, \mathrm{d}x = \int_\Omega - \rho \vec{f} \cdot \vec{u} \, \mathrm{d}x. \end{aligned} \tag{3.19}$$

Note that both augmentations (3.5a) and (3.5c) were involved in deriving this expression.

Finally, we observe that by definition, we have $\omega_i \in L^\infty(\Omega)$ with $\|\omega_i\|_{L^\infty(\Omega)} \leq 1$. Moreover, we make the physically reasonable assumptions that the concentrations associated with the solution are uniformly bounded, $c_i \in L^\infty(\Omega)$, with $c_i \geq \kappa > 0$ a.e. (almost everywhere), as in [146] (which in turn implies $\mathbf{M}_{ij}^\gamma, \rho \in L^\infty(\Omega)$, and $\rho \geq \kappa \sum_i M_i > 0$ a.e.), and that the density gradient is uniformly bounded, $\vec{\nabla}\rho \in L^\infty(\Omega;\mathbb{R}^d)$.[2]

Definition 1. *We define a* weak solution to the augmented Stokes–Onsager–Stefan–Maxwell system *to be a* $(2n+3)$*-tuple*

$$(\{\mu_i\}_{i=1}^n, \vec{\vec{\tau}}, p, \{\vec{v}_i\}_{i=1}^n, \vec{v}) \in L_0^2(\Omega)^n \times L^2(\Omega;\mathbb{S}) \times L_0^2(\Omega) \times \underbrace{L^2(\Omega;\mathbb{R}^d)^n \times L^2(\Omega;\mathbb{R}^d)}_{Q} \tag{3.20}$$

inducing concentrations $\{c_i\}_{i=1}^n$ *through a constitutive law (such as* (1.16)*) implicitly*

[2] A comparable condition, that $\rho \in (H^1 \cap W^{1,\infty})(\Omega)$ is bounded below with $\frac{\vec{\nabla}\rho}{\rho} \in L^\infty(\Omega;\mathbb{R}^d)$, was used to analyze a compressible Stokes flow in [32].

defining $c_i = c_i(\{\mu_i\}_{i=1}^n, p) \geq \kappa > 0$ *a.e. for* $i = 1, \ldots, n$*, such that*

$$\|c_i\|_{L^\infty(\Omega)} < \infty, \ i = 1, \ldots, n, \tag{3.21a}$$

$$\|\vec{\nabla}\rho\|_{L^\infty(\Omega;\mathbb{R}^d)} < \infty, \tag{3.21b}$$

$$\|\operatorname{div} \vec{\vec{\tau}} - \vec{\nabla}p\|_0^2 < \infty, \tag{3.21c}$$

$$\| - c_i\vec{\nabla}\mu_i + \omega_i\vec{\nabla}p\|_0^2 < \infty, \ i = 1, \ldots, n, \tag{3.21d}$$

and satisfying (3.16), (3.19) *for all test tuples* $(\{w_i\}_{i=1}^n, \vec{\vec{s}}, q, \{\vec{u}_i\}_{i=1}^n, \vec{u}) \in \Theta \times Q$*, where* Θ *is defined in* (3.13)*.*

Observe that the solution tuple does not reside in any standard Sobolev space, but that the regularity assumptions placed on the solution tuple and test spaces ensure that the surface terms in (3.16) are well-defined. Recall that condition (3.21c) is the square-integrability of the Cauchy stress σ (as in [99]). The nonlinear integrability condition (3.21d) is to our knowledge a novel requirement, but also has a natural interpretation, namely the square-integrability of the diffusion driving forces:[3]

$$\vec{d}_i \in L^2(\Omega;\mathbb{R}^d). \tag{3.22}$$

Moreover, we emphasize that this unorthodox formulation allows the rigorous incorporation of pressure diffusion via the pressure gradient on the left side of (3.5a), despite the fact that the pressure field is not *a priori* H^1-regular in the Stokes subsystem. Later in (3.4.4) we observe convergence of the diffusion driving forces in L^2 and of the pressure in H^1, but otherwise leave this consideration, and further investigation into the optimal nonlinear formulation of the SOSM system, as intriguing open questions.

Remark 8. *In the derivation of* (3.14)*, we used* (3.5e) *which ignores the* curl *component in the Helmholtz decomposition of the mass-average velocity relationship* (1.29)*. The full constraint is weakly incorporated, however, via the augmentations* (3.5a) *and* (3.3)*. A proof that this is sufficient to preserve in the Gibbs-Duhem equation was given in the case of an ideal isobaric isothermal gas in Section 2.1. Here we show that this is true in general, providing that the constitutive laws for the chemical potential are such that they derive from a Gibbs free energy. Choosing* $\vec{u}_i = \vec{u}$ *for every* $\vec{u}$

[3]We conjecture that one could alternatively derive a formulation of the SOSM system dual to ours which takes $\vec{d}_i$ as a primary unknown in a space to be identified. We also conjecture that the integrability assumptions in Definition 1 could potentially be relaxed.

and summing over i we have

$$\int \sum_{i=1}^{n} \Big(- c_i \vec{\nabla} \mu_i + \omega_i \vec{\nabla} p \Big) \cdot \vec{u} + \gamma \vec{v} \cdot \vec{u} = \gamma \sum_{i=1}^{n} \omega_i \vec{v}_i \cdot \vec{u}. \tag{3.23}$$

Choosing $\vec{u} = \vec{\nabla} q \in H^1(\Omega)$ and noting (3.5e) *we derive that*

$$\int \sum_{i=1}^{n} \Big(- c_i \vec{\nabla} \mu_i + \omega_i \vec{\nabla} p \Big) \cdot \vec{\nabla} q = 0 \tag{3.24}$$

for each $q \in H^1(\Omega)$. Further rearrangement of the integrand yields

$$\sum_{j=1}^{n} \Big(-c_i \vec{\nabla} \mu_i + \omega_i \vec{\nabla} p \Big) = \sum_{i=1}^{n} -\vec{\nabla} \left(c_i \mu_i \right) + \vec{\nabla} p + \sum_{i=1}^{n} \mu_i \vec{\nabla} c_i \tag{3.25}$$

$$= \vec{\nabla} \left(c_i \mu_i \right) + \vec{\nabla} \tilde{G} \tag{3.26}$$

where we have used the first law as in form (1.10)*. However then we see that the integrand* (3.24)*, is it fact itself a gradient so* (3.24) *implies it is zero. That is, choosing $\vec{\nabla} q = \vec{\nabla}(c_i \mu_i) + \vec{\nabla} \tilde{G}$ we derive*

$$\int \left(\sum_{i=1}^{n} -c_i \vec{\nabla} \mu_i + \omega_i \vec{\nabla} p \right)^2 = 0. \tag{3.27}$$

Then (3.23) *reduces to*

$$\vec{v} \cdot \vec{u} = \sum_{i=1}^{n} \omega_i \vec{v}_i \cdot \vec{u} \tag{3.28}$$

showing the enforcement of the mass-average velocity. Although this shows the preservation of the Gibbs–Duhem and mass-average velocity in the nonlinear infinite dimensional case, it is significantly harder in the non-ideal case to enforce this exactly in the linearized discretization as was achieved for an ideal gas in Chapter 2. This is a price we pay for solving for the chemical potential.

3.3 Linearization and well-posedness

3.3.1 Variational formulation of a generalized Picard scheme

In this section we derive a variational formulation of a generalized Picard linearization. Given a previous estimate for the potentials $\tilde{\mu}^k$ and pressure p^k for $k \geq 0$, we regard these as fixed quantities which determine the concentrations $\tilde{c}^k$ via chemical potential constitutive laws and an appropriate equation of state such as (1.16). This in turn determines the density ρ^k, mass fractions $\tilde{\omega}^k$, total concentration c_{T}^k, and transport matrix $\mathbf{M}^k$ defined via (1.25), (1.30), (1.9), and (1.49), respectively. We then construct a linear system to solve for the next iterate $((\tilde{\mu}^{k+1}, \vec{\vec{\tau}}^{\,k+1}, p^{k+1}), (\tilde{u}^{k+1}, \vec{u}^{k+1}))$. This update strategy is expected to be effective because the gradients of chemical potential, pressure, and mass-average velocity primarily drive the dynamics of multicomponent flow; the role of the species concentrations is mostly confined to the effect of altering the drag coefficients in the transport matrix. We make the following physically reasonable assumptions about each iterate, in analogy to Definition 1.

Assumption 1. *For each $k \geq 0$, we assume $c_i^k \in L^\infty(\Omega), \rho^k \in W^{1,\infty}(\Omega)$, and that $c_i^k \geq \kappa > 0$ a.e. for each i.*

This again implies $\rho^k \geq \kappa \sum_i M_i > 0$ a.e. We also assume henceforth that $\gamma > 0$.

Given $\tilde{c}^k$ and the corresponding $\tilde{\omega}^k$, we define the iteration-dependent weighted function space

$$\Theta^k := \left\{ (\tilde{w}, \vec{\vec{s}}, q) \in L_0^2(\Omega)^n \times L^2(\Omega; \mathbb{S}) \times L_0^2(\Omega) \;\middle|\; \begin{array}{rl} \operatorname{div} \vec{\vec{s}} - \vec{\nabla} q & \in L^2(\Omega; \mathbb{R}^d), \\ -c_i^k \vec{\nabla} w_i + \omega_i^k \vec{\nabla} q & \in L^2(\Omega; \mathbb{R}^d) \ \forall i \end{array} \right\}, \tag{3.29}$$

whose defining conditions linearize those in (3.13). This mixed space is Hilbertian with graph norm

$$\|(\tilde{w}, \vec{\vec{s}}, q)\|_{\Theta^k}^2 := \|\vec{\vec{s}}\|_0^2 + \|q\|_0^2 + \|\operatorname{div} \vec{\vec{s}} - \vec{\nabla} q\|_0^2 + \sum_i \left(\|w_i\|_0^2 + \| - c_i^k \vec{\nabla} w_i + \omega_i^k \vec{\nabla} q\|_0^2 \right). \tag{3.30}$$

We now formulate our linearized problem as a symmetric perturbed saddle point prob-

lem. Define $A_k : Q \to Q^*, \Lambda : \Theta^k \to (\Theta^k)^*, B_k : \Theta^k \to Q^*$ by

$$A_k(\tilde{v}, \vec{v}; \tilde{u}, \vec{u}) \coloneqq \int_\Omega \sum_{i,j} \vec{v}_i \cdot \mathbf{M}^k_{ij} \vec{u}_j \mathrm{d}x + \gamma \int_\Omega \left(\sum_i \omega^k_i (\vec{v}_i - \vec{v}) \right) \cdot \left(\sum_j \omega^k_j (\vec{u}_j - \vec{u}) \right) \mathrm{d}x, \tag{3.31a}$$

$$\Lambda(\tilde{\mu}, \vec{\vec{\tau}}, p; \tilde{w}, \vec{\vec{s}}, q) \coloneqq \int_\Omega \mathcal{A} \vec{\vec{\tau}} : \vec{\vec{s}} \ \mathrm{d}x, \tag{3.31b}$$

$$B_k(\tilde{\mu}, \vec{\vec{\tau}}, p; \tilde{u}, \vec{u}) \coloneqq \int_\Omega \sum_i (-c^k_i \vec{\nabla} \mu_i + \omega^k_i \vec{\nabla} p) \cdot \vec{u}_i + (\mathrm{div}\, \vec{\vec{\tau}} - \vec{\nabla} p) \cdot \vec{u} \ \mathrm{d}x, \tag{3.31c}$$

and the functionals

$$\begin{aligned} \ell^1_k(\tilde{w}, \vec{\vec{s}}, q) &\coloneqq \left\langle (s - q\mathbb{I})\mathbf{n}, \frac{g_\mathrm{v}}{\rho^k} \right\rangle_\Gamma + \sum_i \left\langle g_i, -w_i + \frac{M_i}{\rho^k} q \right\rangle_\Gamma + \int_\Omega \tilde{r} \cdot \tilde{w} \ \mathrm{d}x, \\ \ell^2_k(\tilde{u}, \vec{u}) &\coloneqq - \int_\Omega \rho^k f \cdot \vec{u} \ \mathrm{d}x. \end{aligned} \tag{3.32}$$

Note that under Assumption 1, each of the bilinear functionals is continuous; we will denote their norms as $\|A_k\|$, $\|\Lambda\|$, and $\|B_k\|$, respectively. Our linearized problem is posed as follows: find $((\tilde{\mu}^{k+1}, \vec{\vec{\tau}}^{k+1}, p^{k+1}), (\tilde{v}^{k+1}, v^{k+1})) \in \Theta^k \times Q$ such that

$$\begin{aligned} \Lambda(\tilde{\mu}^{k+1}, \vec{\vec{\tau}}^{k+1}, p^{k+1}; \tilde{w}, \vec{\vec{s}}, q) + B_k(\tilde{w}, \vec{\vec{s}}, q; \tilde{v}^{k+1}, \vec{v}^{k+1}) &= \ell^1_k(\tilde{w}, \vec{\vec{s}}, q) \quad \forall\ (\tilde{w}, \vec{\vec{s}}, q) \in \Theta^k, \\ B_k(\tilde{\mu}^{k+1}, \vec{\vec{\tau}}^{k+1}, p^{k+1}; \tilde{u}, \vec{u}) - A_k(\tilde{v}^{k+1}, \vec{v}^{k+1}; \tilde{u}, \vec{u}) &= \ell^2_k(\tilde{u}, \vec{u}) \qquad \forall\ (\tilde{u}, \vec{u}) \in Q, \end{aligned} \tag{3.33}$$

We note that the variational terms involving chemical potential and pressure gradients are precisely of the same variational form as the species continuity equations and the divergence of the mass-average velocity constraint, which can be seen by inspecting (3.16) and (3.19). This key insight is what leads to a symmetric system.

Our nonlinear iteration scheme is as follows: for an initial estimate of the concentrations $\tilde{c}^0$, we solve the system (3.33) for the updated variables $((\tilde{\mu}^{k+1}, \vec{\vec{\tau}}^{k+1}, p^{k+1}), (\tilde{v}^{k+1}, v^{k+1})) \in \Theta^k \times Q$, for $k = 0, 1, 2, \ldots$. By the relations detailed in (1.2.1.2), these variables are used to calculate the updated concentrations $\tilde{c}^{k+1}$. This is iterated until for some set tolerance $\varepsilon > 0$,

$$\left(\|(\tilde{\mu}^{k+1}, \vec{\vec{\tau}}^{k+1}, p^{k+1}) - (\tilde{\mu}^k, \vec{\vec{\tau}}^k, p^k)\|^2_{\Theta^k} + \|(\tilde{v}^{k+1}, \vec{v}^{k+1}) - (\tilde{v}^k, \vec{v}^k)\|^2_Q \right)^{1/2} \leq \varepsilon. \tag{3.34}$$

3.3.2 Well-posedness of the linearized system

We will now prove that the saddle point system (3.33) is well-posed under Assumption 1. This will require a Poincaré-type inequality for the following seminorm on Θ^k:

$$|(\tilde{w}, \vec{\vec{s}}, q)|^2_{\Theta^k} := \|\vec{\vec{s}}\|_0^2 + \|\operatorname{div} \vec{\vec{s}} - \vec{\nabla} q\|_0^2 + \sum_i \| - c_i^k \vec{\nabla} w_i + \omega_i^k \vec{\nabla} q\|_0^2. \tag{3.35}$$

Lemma 3. *Let Ω be a Lipschitz domain. Under Assumption 1, there exists $K > 0$ such that for each $(\tilde{\mu}, \vec{\vec{\tau}}, p) \in \Theta^k$,*

$$\|(\tilde{\mu}, \vec{\vec{\tau}}, p)\|_{\Theta^k} \leq K |(\tilde{\mu}, \vec{\vec{\tau}}, p)|_{\Theta^k}. \tag{3.36}$$

This lemma will allow us to control the chemical potential and pressure in terms of the (linearized) driving forces, divergence of total stress, and the viscous stress. It should be thought of as the generalization to the OSM framework of [99, Lemma 4].

Proof of Lemma 3. The first stage of the proof is to show that

$$\|p\|_0 \lesssim \|\vec{\vec{\tau}}\|_0 + \|\operatorname{div} \vec{\vec{\tau}} - \vec{\nabla} p\|_0, \tag{3.37}$$

following and mildly generalizing [99, Lemma 4]. Set $\theta = \vec{\vec{\tau}} - p\mathbb{I} - r\mathbb{I}$ where $r = \frac{1}{d|\Omega|} \int_\Omega \operatorname{tr} \vec{\vec{\tau}} \, \mathrm{d}x$. Then

$$\|\vec{\vec{\tau}} - p\mathbb{I}\|_0 \leq \|\theta\|_0 + \|r\mathbb{I}\|_0. \tag{3.38}$$

As $\int_\Omega \operatorname{tr} \theta \, \mathrm{d}x = 0$, we can use [18, Proposition 9.1.1] to derive

$$\begin{aligned} \|\vec{\vec{\tau}} - p\mathbb{I}\|_0 &\lesssim \|\operatorname{dev} \theta\|_0 + \|\operatorname{div} \theta\|_0 + \|r\mathbb{I}\|_0 \\ &\lesssim \|\vec{\vec{\tau}}\|_0 + \|\operatorname{div} \vec{\vec{\tau}} - \vec{\nabla} p\|_0, \end{aligned} \tag{3.39}$$

where the deviator is defined as $\operatorname{dev} \theta \coloneqq \theta - \frac{\operatorname{tr} \theta}{d} \mathbb{I} = \operatorname{dev} \vec{\vec{\tau}}$. Now using

$$\sqrt{d} \|p\|_0 \leq \|\vec{\vec{\tau}} - p\mathbb{I}\|_0 + \|\vec{\vec{\tau}}\|_0, \tag{3.40}$$

the result (3.37) follows. For the second stage of the proof, we will show that

$$\|\mu_i\|_0 \lesssim \|p\|_0 + \| - c_i^k \vec{\nabla} \mu_i + \omega_i^k \vec{\nabla} p\|_0. \tag{3.41}$$

This combined with (3.37) gives (3.36). To prove this second inequality, for each i we take the unique $\vec{z}_i \in H_0^1(\Omega;\mathbb{R}^d)/\ker(\operatorname{div})$ such that $\operatorname{div}\vec{z}_i = \mu_i$. Then $\vec{u}_i \coloneqq \vec{z}_i/c_i^k \in L^2(\Omega;\mathbb{R}^d)$ with $\operatorname{div}(c_i^k\vec{u}_i) = \mu_i$. With integration by parts we deduce

$$\int_\Omega (-c_i^k\vec{\nabla}\mu_i + \omega_i^k\vec{\nabla}p)\cdot\vec{u}_i \,\mathrm{d}x = \int_\Omega |\mu_i|^2 - M_i p\left(\frac{\mu_i}{\rho^k} - \frac{\vec{\nabla}\rho^k}{(\rho^k)^2}\cdot c_i^k\vec{u}_i\right)\mathrm{d}x. \tag{3.42}$$

Upon rearrangement, we can derive the inequality

$$\begin{aligned}\|\mu_i\|_0^2 &\le M_i\|p\|_0\left(\frac{\|\mu_i\|_0}{\kappa\sum_j M_j} + \|\vec{u}_i\|_0\|c_i^k\|_0\left\|\frac{\vec{\nabla}\rho^k}{(\rho^k)^2}\right\|_{L^\infty(\Omega;\mathbb{R}^d)}\right) + \|-c_i^k\vec{\nabla}\mu_i + \omega_i\vec{\nabla}p\|_0\|\vec{u}_i\|_0\\ &\le \kappa^{-1}\|p\|_0\left(\|\mu_i\|_0 + \|\vec{u}_i\|_0\|c_i^k\|_{L^\infty(\Omega)}\|\vec{\nabla}\ln\rho^k\|_{L^\infty(\Omega;\mathbb{R}^d)}\right) + \|-c_i^k\vec{\nabla}\mu_i + \omega_i\vec{\nabla}p\|_0\|\vec{u}_i\|_0.\end{aligned} \tag{3.43}$$

By the bounded inverse theorem, div admits a bounded left inverse, so $\|\vec{z}_i\|_1 \lesssim \|\mu_i\|_0$ and thus

$$\|\vec{u}_i\|_0 \le \kappa^{-1}\|z_i\|_0 \lesssim \kappa^{-1}\|\mu_i\|_0. \tag{3.44}$$

Combining this with (3.43), we can divide through by $\|\mu_i\|_0$ to derive

$$\|\mu_i\|_0 \lesssim \kappa^{-1}\|p\|_0\left(1 + \kappa^{-1}\|c_i^k\|_{L^\infty(\Omega)}\|\vec{\nabla}\ln\rho^k\|_{L^\infty(\Omega)}\right) + \kappa^{-1}\|-c_i^k\vec{\nabla}\mu_i + \omega_i^k\vec{\nabla}p\|_0. \tag{3.45}$$

This concludes our proof. □

Remark 9. *The constants appearing in* (3.36) *depend on two factors; the relative variation of the density and* κ*. Provided these two quantities are well-behaved across iterations, so will be the resulting constants.*

A further intermediate lemma we need to prove well-posedness is the following. Let $\|(\tilde{v},\vec{v})\|_Q^2 \coloneqq \|\tilde{v}\|_0^2 + \|\vec{v}\|_0^2$.

Lemma 4. *Under Assumption 1 there exists* $\lambda_\kappa^\gamma > 0$ *depending on* κ *and* γ *such that for all* $(\tilde{v},\vec{v}) \in Q$*,*

$$\left(\frac{n+1}{2}\right)\lambda_\kappa^\gamma\|\vec{v}\|_0^2 + A_k(\tilde{v},\vec{v};\tilde{v},\vec{v}) \ge \frac{\lambda_\kappa^\gamma}{2}\|(\tilde{v},\vec{v})\|_Q^2. \tag{3.46}$$

Proof. Let us define $\vec{\delta}_i = \vec{v}_i - \vec{v}$ for each i. Then we can explicitly compute

$$A_k(\tilde{v}, \vec{v}; \tilde{v}, \vec{v}) = \int_\Omega \sum_{i,j} \vec{\delta}_i \cdot \mathbf{M}_{ij}^{k,\gamma} \vec{\delta}_j \, \mathrm{d}x, \tag{3.47}$$

where $\mathbf{M}^{k,\gamma}$ is defined using $\tilde{c}^k$ via (2.5). It follows from Lemma 1 that this is a coercive bilinear form in $\tilde{\delta}$: for some λ_κ^γ,

$$A_k(\tilde{v}, \vec{v}; \tilde{v}, \vec{v}) \geq \frac{\lambda_\kappa^\gamma}{2} \sum_i \|\vec{\delta}_i\|_0^2 = \frac{\lambda_\kappa^\gamma}{2} \sum_i \|\vec{v}_i - \vec{v}\|_0^2, \tag{3.48}$$

hence

$$\begin{aligned} \left(\frac{n+1}{2}\right) \lambda_\kappa^\gamma \|\vec{v}\|_0^2 + A_k(\tilde{v}, \vec{v}; \tilde{v}, \vec{v}) &\geq \frac{\lambda_\kappa^\gamma}{2} \sum_i (\|\vec{v}_i - \vec{v}\|_0^2 + \|\vec{v}\|_0^2) + \frac{\lambda_\kappa^\gamma}{2} \|\vec{v}\|_0^2 \\ &\geq \frac{\lambda_\kappa^\gamma}{2} \sum_i \|\vec{v}_i\|_0^2 + \frac{\lambda_\kappa^\gamma}{2} \|\vec{v}\|_0^2 = \frac{\lambda_\kappa^\gamma}{2} \|(\tilde{v}, \vec{v})\|_Q^2. \end{aligned} \tag{3.49}$$

□

We now invoke standard Babuška theory for well-posedness [10].

Theorem 5. *Under Assumption 1, there exists a unique solution to the perturbed saddle point system* (3.33).

Proof. For a given $(\mathfrak{p}, \mathfrak{q}) := \left((\tilde{\mu}, p, \vec{\vec{\tau}}), (\tilde{v}, \vec{v})\right) \in \Theta^k \times Q$ and $(\mathfrak{s}, \mathfrak{u}) := \left((\tilde{w}, \vec{\vec{s}}, q), (\tilde{u}, \vec{u})\right) \in \Theta^k \times Q$ we will define the bounded bilinear form $\mathcal{G} : (\Theta^k \times Q) \times (\Theta^k \times Q) \to \mathbb{R}$ as

$$\mathcal{G}(\mathfrak{p}, \mathfrak{q}; \mathfrak{s}, \mathfrak{u}) := \Lambda(\mathfrak{p}; \mathfrak{s}) + B_k(\mathfrak{s}; \mathfrak{q}) + B_k(\mathfrak{p}; \mathfrak{u}) - A_k(\mathfrak{q}; \mathfrak{u}). \tag{3.50}$$

We will prove Babuška's inf-sup condition, namely that there exists a constant $c > 0$ such that for each $(\mathfrak{p}, \mathfrak{q}) \in \Theta^k \times Q$ there is $(\mathfrak{s}, \mathfrak{u}) \in \Theta^k \times Q$ such that

$$\frac{\mathcal{G}(\mathfrak{p}, \mathfrak{q}; \mathfrak{s}, \mathfrak{u})}{\|(\mathfrak{s}, \mathfrak{u})\|_{\Theta^k \times Q}} \geq c \|(\mathfrak{p}, \mathfrak{q})\|_{\Theta^k \times Q}, \tag{3.51}$$

with product norm $\|(\mathfrak{p}, \mathfrak{q})\|_{\Theta^k \times Q}^2 := \|\mathfrak{p}\|_{\Theta^k}^2 + \|\mathfrak{q}\|_Q^2$. Note that $\mathcal{G}$ is defined on the product of a space with itself and is symmetric, and so only the one inf-sup condition (3.51)

needs to be verified. Proving (3.51) will be accomplished by showing that for a constant $c > 0$, for each $(\mathfrak{p}, \mathfrak{q}) \in \Theta^k \times Q$ there is $(\mathfrak{s}, \mathfrak{u}) \in \Theta^k \times Q$ such that $\mathcal{G}(\mathfrak{p}, \mathfrak{q}; \mathfrak{s}, \mathfrak{u}) \geq c\|(\mathfrak{p}, \mathfrak{q})\|^2_{\Theta^k \times Q}$, and for a $C > 0$ independent of $(\mathfrak{p}, \mathfrak{q})$,

$$C\|(\mathfrak{p}, \mathfrak{q})\|_{\Theta^k \times Q} \geq \|(\mathfrak{s}, \mathfrak{u})\|_{\Theta^k \times Q}. \tag{3.52}$$

This combined with our Poincaré-type inequality will imply well-posedness. We do this by fixing $(\mathfrak{s}, \mathfrak{u})$ as the ansatz

$$\begin{aligned} w_i &= C_1 \mu_i, \qquad & s &= C_1 \overrightarrow{\overrightarrow{\tau}} + C_2 \overrightarrow{\overrightarrow{s}}_v, \qquad & q &= C_1 p, \\ \vec{u}_i &= C_3(-c_i^k \vec{\nabla} \mu_i + \omega_i^k \vec{\nabla} p) - C_1 \vec{v}_i, \qquad & \vec{u} &= -C_1 \vec{v} + C_4(\operatorname{div} \overrightarrow{\overrightarrow{\tau}} - \vec{\nabla} p). \end{aligned} \tag{3.53}$$

Here $C_1, \ldots > 0$ are constants to be set later and $s_v \in H(\operatorname{div}; \mathbb{S})$ is chosen to satisfy $\operatorname{div} \overrightarrow{\overrightarrow{s}}_v = \vec{v}$ and $\|\overrightarrow{\overrightarrow{s}}_v\|_{H(\operatorname{div};\mathbb{S})} \leq C_\Sigma \|\vec{v}\|_0$ for a constant C_Σ independent of v (its existence is guaranteed by [4, Theorem 8.1]). It is clear that (3.52) holds. With these choices of test functions we may compute

$$\begin{aligned} \mathcal{G}(\mathfrak{p}, \mathfrak{q}; \mathfrak{s}, \mathfrak{u}) = \int_\Omega \mathcal{A} \overrightarrow{\overrightarrow{\tau}} : (C_1 \overrightarrow{\overrightarrow{\tau}} + C_2 \overrightarrow{\overrightarrow{s}}_v) \, \mathrm{d}x + C_3 \sum_i \| - c_i^k \vec{\nabla} \mu_i + \omega_i^k \vec{\nabla} p\|_0^2 \\ + C_4 \| \operatorname{div} \overrightarrow{\overrightarrow{\tau}} - \vec{\nabla} p\|_0^2 + C_2 \|\vec{v}\|_0^2 - A_k(\tilde{v}, \vec{v}; \tilde{u}, \vec{u}), \end{aligned} \tag{3.54}$$

and observe that the final term on the right may be written equivalently as

$$C_1 A_k(\tilde{v}, \vec{v}; \tilde{v}, \vec{v}) - A_k\left(\tilde{v}, \vec{v}; \{C_3(-c_i^k \vec{\nabla} \mu_i + \omega_i^k \vec{\nabla} p)\}_i, C_4(\operatorname{div} \overrightarrow{\overrightarrow{\tau}} - \vec{\nabla} p)\right). \tag{3.55}$$

With λ_κ^γ given by (4) we now choose $C_2 = \|A_k\|^2 (n+1) \lambda_\kappa^\gamma$ and assume that $C_1 \geq 2\|A_k\|^2$. Then

$$C_2 \|\vec{v}\|_0^2 + C_1 A_k(\tilde{v}, v; \tilde{v}, \vec{v}) \geq \|A_k\|^2 \lambda_\kappa^\gamma \|(\tilde{v}, \vec{v})\|_Q^2. \tag{3.56}$$

Using uniform positive definiteness of the compliance tensor, the bound on $\overrightarrow{\overrightarrow{s}}_v$, and

boundedness of the operators Λ, A_k, we can proceed to bound (3.54) from below as

$$\begin{aligned}\mathcal{G}\left(\mathfrak{p},\mathfrak{q};\mathfrak{s},\mathfrak{u}\right) \geq{}& \alpha C_1 \|\vec{\vec{\tau}}\|_0^2 + \|A_k\|^2 \lambda_\kappa^\gamma \|(\tilde{v},\vec{v})\|_Q^2 + C_3 \sum_i \| - c_i^k \vec{\nabla}\mu_i + \omega_i^k \vec{\nabla} p\|_0^2 \\ &+ C_4 \|\operatorname{div} \vec{\vec{\tau}} - \vec{\nabla} p\|_0^2 - \lambda_\kappa^\gamma (n+1) C_\Sigma \|A_k\|^2 \|\Lambda\| \|v\|_0 \|\vec{\vec{\tau}}\|_0 \\ &- \|A_k\| \|(\tilde{v},\vec{v})\|_Q \left(C_3^2 \sum_i \| - c_i^k \vec{\nabla}\mu_i + \omega_i^k \vec{\nabla} p\|_0^2 + C_4^2 \|\operatorname{div} \vec{\vec{\tau}} - \vec{\nabla} p\|_0^2 \right)^{1/2}.\end{aligned} \tag{3.57}$$

Here $\alpha > 0$ is such that $\int_\Omega \mathcal{A}\vec{\vec{\tau}} : \vec{\vec{\tau}} \, \mathrm{d}x \geq \alpha \|\vec{\vec{\tau}}\|_0^2$ for all $\vec{\vec{\tau}} \in L^2(\Omega;\mathbb{S})$. The desired inequality may now be derived by judiciously selecting the constants C_1, C_3, C_4 (typically by choosing $C_1 \gg C_2 \gg \max(C_3, C_4)$) and using the weighted Young inequality. For concreteness, constants we might pick are

$$C_1 = \left(\frac{\lambda_\kappa^\gamma C_\Sigma^2 \|\Lambda\|^2 (n+1)^2}{\alpha} + 2 \right) \|A_k\|^2, \qquad C_3 = C_4 = \lambda_\kappa^\gamma. \tag{3.58}$$

With this choice and our Poincaré-type inequality from Lemma 3, combined with the inequality (3.52) we may derive

$$\begin{aligned}\mathcal{G}\left(\mathfrak{p},\mathfrak{q};\mathfrak{s},\mathfrak{u}\right) &\geq 2\alpha \|A_k\|^2 \|\vec{\vec{\tau}}\|_0^2 + \frac{\lambda_\kappa^\gamma}{6} \|A_k\|^2 \|(\tilde{v},\vec{v})\|_Q^2 \\ &\quad + \frac{\lambda_\kappa^\gamma}{4} \left(\sum_i \| - c_i^k \vec{\nabla}\mu_i + \omega_i^k \vec{\nabla} p\|_0^2 + \|\operatorname{div} \vec{\vec{\tau}} - \vec{\nabla} p\|_0^2 \right) \\ &\gtrsim |\mathfrak{p}|_{\Theta^k}^2 + \|\mathfrak{q}\|_Q^2 \gtrsim \|(\mathfrak{p},\mathfrak{q})\|_{\Theta^k \times Q}^2 \gtrsim \|(\mathfrak{p},\mathfrak{q})\|_{\Theta^k \times Q} \|(\mathfrak{s},\mathfrak{u})\|_{\Theta^k \times Q},\end{aligned} \tag{3.59}$$

which is the statement of the Babuška condition (3.51). □

3.4 Discretization and numerical experiments

We now assume that Ω is polytopal, and admits a quasi-uniform triangulation $\mathcal{T}_h$ with simplicial elements of maximal diameter h. Denote conforming finite element spaces

for the discrete solution tuple by

$$\begin{aligned}\underbrace{(X_h^n \times \Sigma_h \times P_h)}_{=:\,\Theta_h^k} \times \underbrace{(W_h^n \times V_h)}_{=:\,Q_h} \\ \subset \underbrace{(L_0^2(\Omega)^n \times L^2(\Omega;\mathbb{S}) \times L_0^2(\Omega))}_{\supset\,\Theta^k} \times \underbrace{(L^2(\Omega;\mathbb{R}^d)^n \times L^2(\Omega;\mathbb{R}^d))}_{=\,Q}.\end{aligned} \tag{3.60}$$

Here Θ_h^k is independent of k as a set, but inherits an iteration-dependent norm described below; Q_h inherits the norm of Q. Our discretized linear problem after $k \geq 0$ nonlinear iterations therefore reads: seek $((\tilde{\mu}_h, \overset{\rightrightarrows}{\tau}_h, p_h), (\tilde{v}_h, \vec{v}_h)) \in \Theta_h^k \times Q_h$ such that

$$\begin{aligned}\Lambda(\tilde{\mu}_h, \overset{\rightrightarrows}{\tau}_h, p_h; \tilde{w}_h, \overset{\rightrightarrows}{s}_h, q_h) + B_{k,h}(\tilde{w}_h, \overset{\rightrightarrows}{s}_h, q_h; \tilde{v}_h, \vec{v}_h) &= \ell_{k,h}^1(\tilde{w}_h, \overset{\rightrightarrows}{s}_h, q_h) \forall (\tilde{w}_h, \overset{\rightrightarrows}{s}_h, q_h) \in \Theta_h^k, \\ B_{k,h}(\tilde{\mu}_h, \overset{\rightrightarrows}{\tau}_h, p_h; \tilde{u}_h, \vec{u}_h) - A_{k,h}(\tilde{v}_h, \vec{v}_h; \tilde{u}_h, \vec{u}_h) &= \ell_{k,h}^2(\tilde{u}_h, \vec{u}_h) \qquad \forall (\tilde{u}_h, \vec{u}_h) \in Q_h,\end{aligned} \tag{3.61}$$

where $A_{k,h}, B_{k,h}$ are obtained from A_k, B_k, and $\ell_{k,h}^1, \ell_{k,h}^2$ from ℓ_k^1, ℓ_k^2, respectively, by replacing the discretely computed concentrations c_i^k and inverse density $(\rho^k)^{-1}$ with discrete approximations; we use these to define a norm $\|\cdot\|_{\Theta_h^k}$ for Θ_h^k in analogy to (3.30).

3.4.1 Structure-preservation and well-posedness

We have already argued the need for pressure regularity greater than L^2. We therefore employ the continuous Lagrange element of degree $t \geq 1$, $P_h = \mathrm{CG}_t(\mathcal{T}_h)$, for the pressure. From the diffusion driving forces (1.35a), it appears natural to take the chemical potential space X_h to be CG elements of at least the same degree $r \geq t$, $X_h = \mathrm{CG}_r(\mathcal{T}_h)$.

The mass-average velocity constraint (1.29) suggests that the species velocity space be contained in the space used for convective velocity, $W_h \subset V_h$. For the Stokes subsystem, it is desirable that the pair $(\Sigma_h \times P_h, V_h)$ be inf-sup compatible, for which it is sufficient to have that the full divergence $(\overset{\rightrightarrows}{\tau}, p) \mapsto \operatorname{div} \overset{\rightrightarrows}{\tau} - \vec{\nabla} p$ is surjective onto V_h. By the regularity choice (3.9) for the pressure, it is thus natural to apply div-conforming tensor elements to discretize the viscous stress. By the decomposition (3.2), symmetry of the viscous stress is equivalent to the conservation of angular momentum; for now, we consider exactly symmetric stress elements (such as the Arnold–Winther [6] and Arnold–Awanou–Winther elements [5]) since this obviates the need for a symmetry-

enforcing Lagrange multiplier which would add a further field to our $(2n+3)$-field formulation.

However, if one would like to repeat at the discrete level the proof of Theorem 5, it is necessary for $\operatorname{div} : \Sigma_h \to V_h$ to be surjective, allowing us to construct the discrete analogue of the tensor field s_v in the ansatz (3.53). This is stronger than surjectivity of $(\tau, p) \mapsto \operatorname{div}\tau - \vec{\nabla}p, \Sigma_h \times P_h \to V_h$, but in practice is equivalent because many appropriate choices of Σ_h are designed to discretize the *full* Cauchy stress. Furthermore, the discrete analogue of the constant C_Σ (and hence the resulting inf-sup constant) will *a priori* depend on h; it is therefore necessary to assume that such s_v can be constructed stably.

Assumption 2. *There exists C^Σ independent of h such that for each $u_h \in V_h$ and for the unique $s_h \in \Sigma_h / \ker(\operatorname{div})$ with $\operatorname{div} s_h = u_h$, there holds $\|s_h\|_{H(\operatorname{div};\mathbb{S})} \leq C^\Sigma \|u_h\|_0$.*

This is true for (for example) stress elements discretizing an elasticity complex which admits bounded commuting projections to the subcomplex, as is for example the case for the Arnold–Winther [6] and Arnold–Awanou–Winther elements [5]. The other relations are summarised below,[4]

$$\begin{array}{ccc} \underset{\substack{\text{chemical}\\\text{potential}}}{X_h} & & \underset{\substack{\text{species}\\\text{velocity}}}{W_h} \\ \pi_2 \uparrow & & \downarrow \subset \\ \underset{\text{stress}\times\text{pressure}}{\Sigma_h \times P_h} & \xrightarrow{(\tau,p)\mapsto \operatorname{div}\tau} & \underset{\substack{\text{convective}\\\text{velocity}}}{V_h} \end{array} \tag{3.62}$$

where $\twoheadrightarrow$ indicates surjectivity. The bottom row corresponds to the final segment of a discrete stress elasticity complex, with stress space refined for Stokes flow due to the decomposition (3.2). We will need the conditions of Lemma 3 to hold exactly in the discretization. This will in general require that we approximate the concentrations, c_i^k, and *density reciprocal*, $(\rho^k)^{-1}$, in specific discrete function spaces. The interpolation of these terms will be denoted by $c_{i,h}^k$ and $\rho_h^{k,-1}$, respectively.

Finally, to show well-posedness of the discrete problem, we require two additional conditions which do not fit neatly onto (3.62).

Assumption 3. *The operator given by*

$$\mathrm{d}_h^{i,k}(w_h, q_h) \coloneqq -c_{i,h}^k \vec{\nabla} w_h + \omega_{i,h}^k \vec{\nabla} q_h, \tag{3.63}$$

[4]Here π_i denotes projection onto the i^{th} component, i.e. we require $P_h \subset X_h$.

where $\omega_{i,h}^k \coloneqq \overline{m}_i c_{i,h}^k \rho_h^{k,-1}$*, is well-defined as a map* $\mathrm{d}_h^{i,k} : X_h \times P_h \to W_h$*, i.e., it takes values in* W_h*.*

Assumption 4. *We have* $P_h\mathbb{I} \subset \Sigma_h$*, i.e.* $p_h\mathbb{I} \in \Sigma_h \, \forall \, p_h \in P_h$*.*

Remark 10. *Note that Lemma 3 required taking the gradient of* ρ^{-1}*, and so* $\rho_h^{k,-1}$ *should at least be a continuous piecewise linear function. In order to minimize the polynomial degree for* W_h *arising from Assumption 3, it is advantageous to interpolate* $c_{i,h}^k$ *onto the space* DG_0*. These coefficients do not affect the accuracy of the discretization, only the quality of the linearization, and nonlinear convergence appears robust regardless of this approximation.*

Remark 11. *Assumption 4 implies that* $\operatorname{div} : \Sigma_h \to V_h$ *is surjective, allowing us to construct the discrete analogue of the tensor field* $\overset{\rightrightarrows}{s}_v$ *in the ansatz* (3.53)*. This is stronger than surjectivity of* $(\overset{\rightrightarrows}{\tau}, p) \mapsto \operatorname{div} \overset{\rightrightarrows}{\tau} - \vec{\nabla} p, \Sigma_h \times P_h \to V_h$*, as in* (3.62)*, but in practice is equivalent.*

Theorem 6. *Under Assumptions 3 and 4 and the relations specified in* (3.62)*, there exists a unique solution* $((\tilde{\mu}_h, \overset{\rightrightarrows}{\tau}_h, p_h), (\tilde{v}_h, \vec{v}_h)) \in \Theta_h^k \times Q_h$ *to the system* (3.61)*.*

Proof. Due to the structural conditions demanded in the Assumptions, by inspection the choices of test functions (3.53) are valid. As a consequence we may completely replicate the argument presented in the infinite-dimensional case and derive the analogue of condition (3.51), which is sufficient to show the problem is well-posed. □

3.4.2 Error estimates

Following [155, Theorem 2], for fixed k we infer the abstract error estimate

$$\|(\underline{\tilde{\mu}}^{k+1}, \underline{\overset{\rightrightarrows}{\tau}}^{k+1}, \underline{p}^{k+1}) - (\tilde{\mu}_h, \overset{\rightrightarrows}{\tau}_h, p_h)\|_{\Theta_h^k} + \|(\underline{\tilde{v}}^{k+1}, \underline{\vec{v}}^{k+1}) - (\tilde{v}_h, \vec{v}_h)\|_Q \lesssim \mathbb{E}_{\Theta_h^k} + \mathbb{E}_{Q_h}, \quad (3.64)$$

where

$$\begin{aligned} \mathbb{E}_{\Theta_h^k} &\coloneqq \inf_{(\tilde{w}_h, \overset{\rightrightarrows}{s}_h, q_h) \in \Theta_h^k} \|(\underline{\tilde{\mu}}^{k+1}, \underline{\overset{\rightrightarrows}{\tau}}^{k+1}, \underline{p}^{k+1}) - (\tilde{w}_h, \overset{\rightrightarrows}{s}_h, q_h)\|_{\Theta_h^k}, \\ \mathbb{E}_{Q_h} &\coloneqq \inf_{(\underline{\tilde{u}}_h, \underline{\vec{u}}_h) \in Q_h} \|(\underline{\tilde{v}}^{k+1}, \underline{\vec{v}}^{k+1}) - (\tilde{u}_h, \vec{u}_h)\|_Q. \end{aligned} \quad (3.65)$$

Here the tuple $((\underline{\tilde{\mu}}^{k+1}, \underline{\overset{\rightrightarrows}{\tau}}^{k+1}, \underline{p}^{k+1}), (\underline{\tilde{v}}^{k+1}, \underline{\vec{v}}^{k+1}))$ is defined as the exact solution to (3.33) but with $B_k, A_k, \ell_k^1, \ell_k^2$ replaced with $B_{k,h}, A_{k,h}, \ell_{k,h}^1, \ell_{k,h}^2$, respectively—that is, the solution of the system (3.33) with the estimates of the concentrations and inverse density replaced by $c_{i,h}^k$ and $\rho_h^{k,-1}$, respectively.

To derive a practical error estimate, we will need to bound the quantities $\mathbb{E}_{\Theta_h^k}$ and $\mathbb{E}_{Q_h}$ by interpolation estimates specific to the choice of finite element spaces, by estimating $\|\cdot\|_{\Theta_h^k}, \|\cdot\|_Q$ in terms of standard Sobolev norms. To this end we can readily check that

$$\begin{aligned}
\mathbb{E}_{\Theta_h^k} &\lesssim \max\left(1, \sum_i \|c_{i,h}^k\|_{L^\infty(\Omega)}\right) \inf_{\tilde{w}_h \in X_h^n} \|\underline{\tilde{\mu}}^{k+1} - \tilde{w}_h\|_1 \\
&\quad + \max\left(1, \sum_i \|\omega_{i,h}^k\|_{L^\infty(\Omega)}\right) \inf_{q_h \in P_h} \|\underline{p}^{k+1} - q_h\|_1 + \inf_{\vec{\vec{s}}_h \in \Sigma_h} \|\underline{\vec{\vec{\tau}}}^{k+1} - \vec{\vec{s}}_h\|_{H(\mathrm{div};\mathbb{S})}, \\
\mathbb{E}_{Q_h} &\leq \inf_{\tilde{v}_h \in W_h^n} \|\underline{\tilde{v}}^{k+1} - \tilde{u}_h\|_0 + \inf_{\vec{u}_h \in V_h} \|\underline{\vec{v}}^{k+1} - \vec{u}_h\|_0.
\end{aligned} \tag{3.66}$$

3.4.3 Examples of suitable finite elements

Having derived abstract error estimates, we now consider two simple combinations of finite elements satisfying the structural conditions (3.62) and Assumptions 3 and 4.

The design and implementation of stress elements which exactly enforce symmetry and div-conformity is notoriously difficult; in 2D, one choice of such elements is the conforming Arnold–Winther element [6], recently incorporated into the Firedrake finite element library [9, 129]. In the lowest-order case we denote this element by AW_3^c. Specifying

$$X_h = P_h = \mathrm{CG}_1(\mathcal{T}_h) \cap L_0^2(\Omega), \tag{3.67a}$$

$$\Sigma_h = \mathrm{AW}_3^c(\mathcal{T}_h), \tag{3.67b}$$

$$W_h = V_h = \mathrm{DG}_1(\mathcal{T}_h; \mathbb{R}^d), \tag{3.67c}$$

and further assuming that the discretely computed c_i^k and $(\rho^k)^{-1}$ have been interpolated into DG_0 and CG_1, respectively, then this discretization satisfies the structural properties (3.62) and Assumptions 3 and 4, hence we deduce the error estimate (3.64).

Let $\Pi_h^{\mathrm{CG}_1} : H^2(\Omega) \to \mathrm{CG}^1(\mathcal{T}_h), \Pi_h^{\mathrm{AW}_3^c} : H^1(\Omega;\mathbb{S}) \to \mathrm{AW}_3^c(\mathcal{T}_h)$, and $\Pi_h^{\mathrm{DG}_1^d} : H^1(\Omega;\mathbb{R}^d) \to \mathrm{DG}_1(\mathcal{T}_h;\mathbb{R}^d)$ be the associated interpolation operators. We then have the following estimates under sufficient regularity assumptions (for details we refer

to [6][18, p. 72][96, Ch. 3]):

$$\|\tilde{\mu} - \Pi_h^{\mathrm{CG}_1}\tilde{\mu}\|_1 \lesssim h|\tilde{\mu}|_2, \tag{3.68a}$$

$$\|p - \Pi_h^{\mathrm{CG}_1}p\|_1 \lesssim h|p|_2, \tag{3.68b}$$

$$\|\vec{\vec{\tau}} - \Pi_h^{\mathrm{AW}_3^c}\vec{\vec{\tau}}\|_0 + h\|\operatorname{div}(\vec{\vec{\tau}} - \Pi_h^{\mathrm{AW}_3^c}\vec{\vec{\tau}})\|_0 \lesssim h^2|\vec{\vec{\tau}}|_2, \tag{3.68c}$$

$$\|(\tilde{v}, \vec{v}) - \Pi_h^{\mathrm{DG}_1^d}(\tilde{v}, \vec{v})\|_Q \lesssim h^2|(\tilde{v}, \vec{v})|_1, \tag{3.68d}$$

where $\Pi_h^{\mathrm{CG}_1}, \Pi_h^{\mathrm{DG}_1^d}$ have been applied component-wise. Using these estimates for the interpolation operators and the error estimate (3.64), we can derive the error bound

$$\|(\underline{\tilde{\mu}}^{k+1}, \underline{\vec{\vec{\tau}}}^{k+1}, \underline{p}^{k+1}) - (\tilde{\mu}_h, \vec{\vec{\tau}}_h, p_h)\|_{\Theta_h^k} + \|(\underline{\tilde{v}}^{k+1}, \underline{\vec{v}}^{k+1}) - (\tilde{v}_h, \vec{v}_h)\|_Q \lesssim h. \tag{3.69}$$

We will see in practice that the order of convergence for several fields is actually higher, but the error of the species velocities and the driving forces is $\mathcal{O}(h)$.

A second class of finite elements may be found by replacing (3.67a) with

$$X_h = \mathrm{CG}_2(\mathcal{T}_h) \cap L_0^2(\Omega), P_h = \mathrm{CG}_1(\mathcal{T}_h) \cap L_0^2(\Omega), \tag{3.70}$$

and leaving the others unchanged. Again the structural conditions are validated if c_i^k and $(\rho^k)^{-1}$ are interpolated into DG_0 and CG_1, respectively. A similar error analysis again confers an error bound of $\mathcal{O}(h)$, though shortly we will see that this is actually higher in practice.

Remark 12. *These estimates bound the error between the discrete solutions at iteration $k+1$, $((\tilde{\mu}_h, \vec{\vec{\tau}}_h, p_h), (\tilde{v}_h, \vec{v}_h))$ and the continuous solution of the nonlinear scheme $((\underline{\tilde{\mu}}^{k+1}, \underline{\vec{\vec{\tau}}}^{k+1}, \underline{p}^{k+1}), (\underline{\tilde{v}}^{k+1}, \underline{\vec{v}}^{k+1}))$ with the same (discrete) coefficients. In principle this is incomplete, as ideally we would derive error estimates against the continuous solution $((\tilde{\mu}^{k+1}, \vec{\vec{\tau}}^{k+1}, p^{k+1}), (\tilde{v}^{k+1}, \vec{v}^{k+1}))$ at iteration $k+1$ with the exact (continuous) coefficients. Estimates on such consistency errors were analyzed for a simpler system in Chapter 2 and some rationale was provided as to why in practice this is not an issue, based on the formal order of the consistency error being strictly less than the discretization error. We expect a similar (if laborious) analysis could be performed here. In general the consistency errors are expected to be $\mathcal{O}(h^2)$, which will be borne out in the numerical examples.*

Remark 13. *We emphasize that we have aimed to identify appropriate structural conditions between finite element spaces in order to preserve desirable properties of the SOSM system—in particular, conditions which allow mimicry of well-posedness proofs from the infinite-dimensional problem—rather than to advocate specifically for the elements used here. We expect it is possible to use Lagrange multipliers to weakly enforce the symmetry of the viscous stress, which would allow for the choice of higher polynomial degrees.*

The system matrix of our discrete linearized system (3.61) has symmetric perturbed saddle point structure, and although indefinite, is such that both the blocks $\Lambda, A_{k,h}$ are symmetric positive semidefinite. These matrix properties hold independently of the particular material considered. We expect that this structure should be conducive to the development of fast preconditioners.

3.4.4 Validation with manufactured solutions

We now verify our scheme, implemented in Firedrake [129]. Firedrake currently only supports symmetry-enforcing stress elements in 2D, and we thus restrict ourselves to the case $d = 2$. Throughout these experiments we chose the penalty parameter $\gamma = 0.1$, and the linear systems were solved using the sparse LU factorization of MUMPS [1] via PETSc [12].

To validate our error estimates, we construct a manufactured solution for an ideal gas on the unit square $\Omega = (0, 1)^2$. If $RT = 1$, the diffusion coefficients are given by $\mathscr{D}_{ij} = D_i D_j$ for $D_j > 0$, and $g : \mathbb{R}^2 \to \mathbb{R}$ is smooth, then one can check that an analytical solution to the OSM subsystem (3.4) is given by

$$c_i = \exp\left(\frac{g}{D_i}\right), \quad \vec{v}_i = D_i \vec{\nabla} g, \tag{3.71}$$

which together implicitly define every other quantity (for given shear and bulk viscosities) apart from the chemical potentials. We compute the latter by inverting the ideal gas relation (1.16) with $p^{\ominus} = \fint_\Omega p \, \mathrm{d}x, \mu_i^{\ominus} = \fint_\Omega c_i \, \mathrm{d}x \; \forall i$. The molar mass of each species was set to 1, and ζ, η to 0.1. The initial guesses for the concentrations $\tilde{c}^0$ were set as $c_i^0 = \fint_\Omega c_i \, \mathrm{d}x$, i.e. as the average of the exact concentrations.

We used $D_i = \frac{1}{2} + \frac{i}{4}, i = 1, 2, 3$, and $g(x, y) = \frac{xy}{5}(1-x)(1-y)$ to generate Figure 3.1, the log-log error plot for the overall algorithm, which demonstrates the negligible effect of the consistency error induced by the discrete interpolations $c_{i,h}^k, \rho_h^{k,-1}$, and verifies the error estimate (3.69).

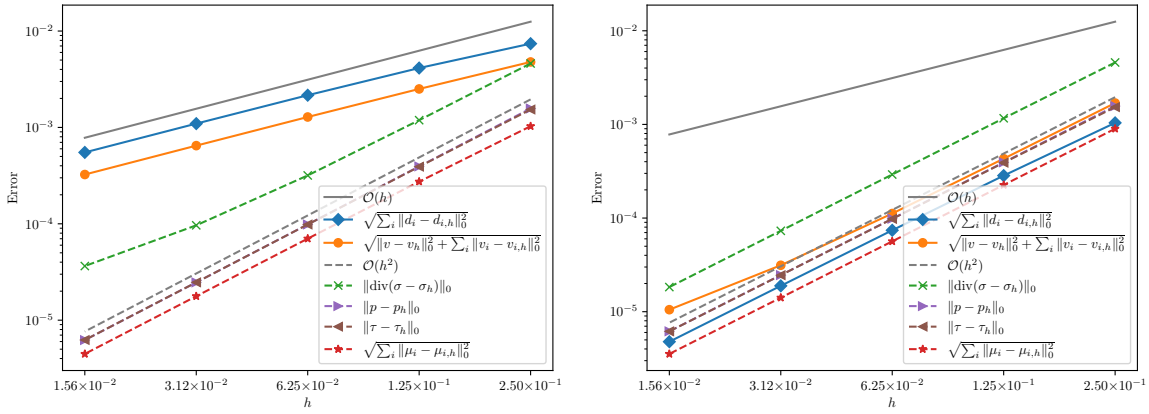

Figure 3.1: Error plots for two finite element families: (3.67) (left), and (3.70) (right).

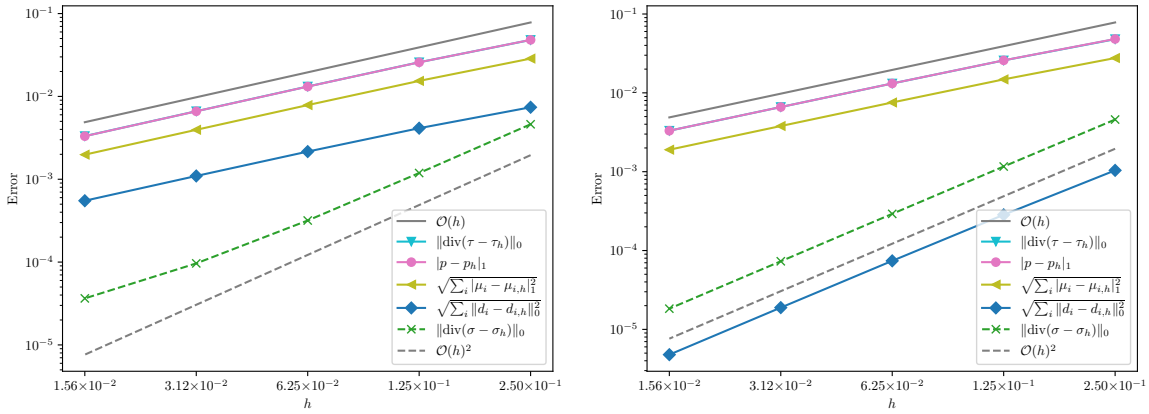

Figure 3.2: Higher-order convergence in L^2 of the divergence of the full Cauchy stress, and driving forces for two finite element families: (3.67) (left), and (3.70) (right).

The tolerance in the outer solver was 10^{-7} in the ℓ^2 norm, and took 7 nonlinear iterations on the coarsest mesh of 4×4, to 9 iterations on finest mesh of 32×32. We have denoted in fig. 3.1 $d_{i,h}$ as the discrete driving force defined by eq. (3.63) at the final iteration, and $\sigma_h \coloneqq \tau_h - p_h \mathbb{I}$. Note that we observe $\mathcal{O}(h^2)$ convergence in the L^2 norms of the chemical potential, stress, and pressure, similar to [146]; this suggests that the error estimates could be improved, for example by duality arguments.

Due to our construction of the 'linearized' function spaces (3.29), it is the norm $\|\cdot\|_{\Theta_h^k}$ with respect to which we have proved convergence of the solution tuple. It is natural to wonder whether this is an artefact of our constructed function spaces. To answer this, we measure convergence of the chemical potential gradients $\vec{\nabla}\mu_i$, pressure gradient $\vec{\nabla}p$, and divergence $\mathrm{div}\,\overrightarrow{\overrightarrow{\tau}}$ of the non-equilibrium stress to their true values, compared to the convergence of the nonlinear diffusion driving forces and the divergence of the full Cauchy stress. For the former quantities, there is *a priori* no reason to expect any convergence.

Remarkably, we observe in Figure 3.2 that not only do the components $\vec{\nabla}\mu_i, \vec{\nabla}p, \operatorname{div} \vec{\vec{\tau}}$ converge, but in fact there is convergence of the nonlinear diffusion driving forces and of the divergence of the full Cauchy stress, and at a rate one order higher than these individual components; this suggests that, rather than being a mathematical artefact of our formulation, the conditions defining the Θ^k space capture the underlying thermodynamic quantities of interest. This also provides circumstantial evidence towards the physical relevance of our nonlinear formulation in Definition 1.

3.4.5 Benzene-cyclohexane mixture

Cyclohexane (C_6H_6) is important in the petrochemical industry as it is used to synthesize a variety of products, such as nylon. It is primarily produced through the dehydrogenation of benzene (C_6H_{12}), resulting in a benzene-cyclohexane mixture. Separation of cyclohexane from this mixture is difficult due to their similar vaporization temperatures [149]. Since liquid mixtures of these components are important in the chemical industry, most of the required thermodynamic and dynamical property data are readily available in the literature. Because it provides a tractable non-ideal example for which a complete set of material properties is known, we consider here a microfluidic chamber in which Stokes flows of benzene and cyclohexane mix.

The required transport parameters (measured at 298.15 K) may be found in Guevara-Carrion et al. [74]. We can observe from these data that the Stefan–Maxwell diffusivity and the shear viscosity are both approximately constant with respect to composition and pressure, and will be approximated as $\mathscr{D}_{12} = 2.1 \times 10^{-9}$ m^2/s and 6×10^{-4} Pa$\cdot$s, respectively. Lacking accurate data for the bulk viscosities of either benzene or cyclohexane, we set them to be essentially zero, choosing $\zeta = 10^{-7}$ Pa $\cdot$ s. (Numerical experiments confirmed that a value of this order has no discernible impact on the output of the simulation.) The molar masses used in the simulation are 0.078 kg$\cdot$mol^{-1} for benzene and 0.084 kg $\cdot$ mol^{-1} for cyclohexane. The ambient pressure was taken as $p^{\ominus} = 10^5$ Pa.

Although benzene and cyclohexane are fully miscible, they form a non-ideal solution. Information relating the chemical potentials to the mole fractions is therefore required. This is accomplished using a Margules model [71] for activity coefficients, the parameters of which were reported by Tasić et al. [139]. This well-known model parameterizes activity coefficients in terms of a minimal set of functions which maintain thermodynamic rigour.

To aid convergence, we use an under-relaxation scheme with respect to the concentrations in our nonlinear solver, with a relaxation parameter of 0.1. That is, we update

the concentration as $c_i^{*,k+1}$ where

$$c_i^{*,k+1} = 0.9c_i^k + 0.1c_i^{k+1}. \tag{3.72}$$

This is necessary due to stiffness of the problem, which owes to the fact that the mixtures are essentially fully separated at the inlets to the apparatus.

To calculate the total concentration of the mixture we use

$$c_{\mathrm{T}} = \frac{c_{\mathrm{C_6H_6}}^{\mathrm{ref}} c_{\mathrm{C_6H_{12}}}^{\mathrm{ref}}}{y_{\mathrm{C_6H_6}} c_{\mathrm{C_6H_{12}}}^{\mathrm{ref}} + y_{\mathrm{C_6H_{12}}} c_{\mathrm{C_6H_6}}^{\mathrm{ref}}}, \tag{3.73}$$

where c_-^{ref} denotes the concentration (inverse molar volume) of the pure species at 10^5 Pa and 298.15 K, approximately 9.20 $\mathrm{mol\,L^{-1}}$ and 11.23 $\mathrm{mol\,L^{-1}}$ for benzene and cyclohexane, respectively. Equation (3.73) is derived from (1.18) under the assumption that the partial molar volumes of the two components are independent of the solution's composition.

We consider a two-dimensional pipe configuration where two inlets converge into a single outlet. At the top inlet, pure benzene enters and at the bottom pure cyclohexane, at speeds $v_{\mathrm{C_6H_{12}}}^{\mathrm{ref}}$ and $v_{\mathrm{C_6H_6}}^{\mathrm{ref}}$, respectively. Rather than symmetrize these speeds, superior mixing results are obtained by symmetrizing the molar fluxes at the inlets. In other words, we impose the condition

$$c_{\mathrm{C_6H_6}}^{\mathrm{ref}} v_{\mathrm{C_6H_6}}^{\mathrm{ref}} = c_{\mathrm{C_6H_{12}}}^{\mathrm{ref}} v_{\mathrm{C_6H_{12}}}^{\mathrm{ref}}. \tag{3.74}$$

We will specify that $v_{\mathrm{C_6H_{12}}}$ enters at a speed of $4\mu\mathrm{m\,s^{-1}}$. This prescribes an inlet speed for benzene of approximately $3.28\mu\mathrm{m\ s^{-1}}$. A parabolic profile across each inlet and outlet is imposed, as this is consistent with the no-slip condition and the characteristics of a plane Poiseuille flow.

Results for the fields computed by the simulation are visualized in Figures 3.3 and 3.4. We observe that the pressure profile is smooth, despite the nonconvex domain. We also note that, although the mass-average velocity exhibits rather simple predictable behaviour, the flow fields of the individual species are significantly more complex, and that these three flow profiles are cleanly distinguished. We see that both species develop convective rolls—behaviour markedly different from the convective velocity.

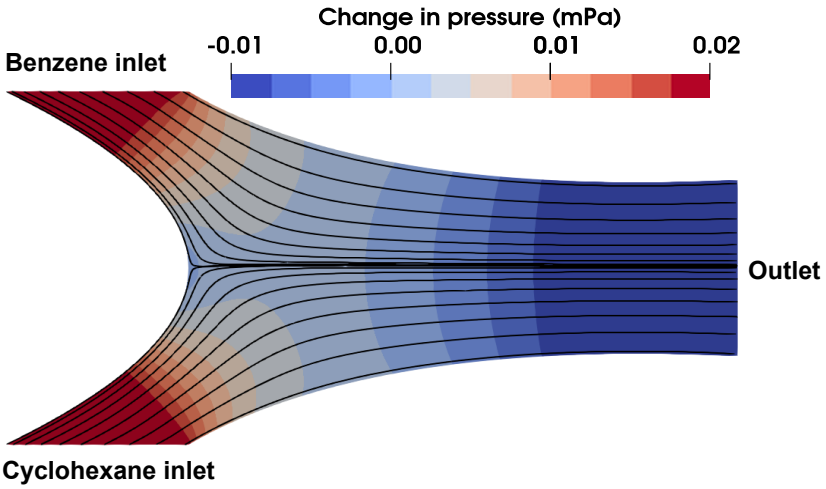

Figure 3.3: Plot of change in pressure in the mixing chamber, with streamlines computed from the mass-average velocity.

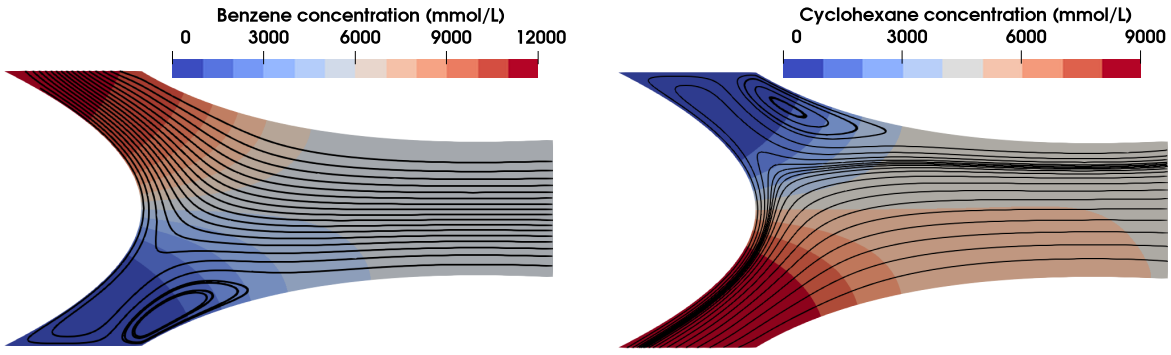

Figure 3.4: Concentrations of benzene (left) and cyclohexane (right), with streamlines computed from their velocities.

3.4.6 Code availability

For reproducibility, the exact software versions used to generate the numerical results in this paper are archived in `https://zenodo.org/record/7017917` [159]; the code, and scripts for the associated plots, are available at `https://bitbucket.org/FAznaran/sosm-numerics/`. Our implementation employs a nondimensionalization of the SOSM system.

3.5 Conclusion

We have successfully extended the framework of Chapter 2, to include pressure and convection. Similar to the results of Chapter we have cast the problem into variational form and proposed a linearization. Well-posedness of the linearized system was then shown. A discretization of this system, relying on specified structural conditions of the finite element families, was proved to satisfy convergence estimates. This was then validated numerically through a manufactured solution and the simulation of benzene and cyclohexane mixing.

A key piece analysis laid on the construction of the novel function space Θ^k. The necessity of this rather unorthodox space is reflective of the difficultly of the problem, in no small part due to varying density. The relevance of this space was demonstrated in Figure 3.2.

Standard Galerkin approximations are known become unstable in the regime of high Péclet numbers [137], and our proposed method is no exception. Therefore, in contrast to the previous chapter where we were able to develop a highly effective solver for the pure diffusion problem, further techniques are undoubtedly needed to make the solver presented here viable for problems in which convection dominates diffusion. However we anticipate this to augment the formulation and discretization proposed here.

Chapter 4

Thermodiffusion

The basis of this chapter is the original paper [145].

In the previous chapters we have analyzed the Onsager–Stefan–Maxwell equations in the non-ideal case with convection. Our finite element methods were then illustrated with a variety of numerical examples. However, heat transfer is ubiquitous and naturally we wish to extend our framework to the anisothermal case.

This is not straightforward however as the transport equations for thermodiffusion in force-explicit form have not been constructed in the literature. In this chapter we consolidate the theory of thermodiffusion by constructing the *anisothermal* transport matrix in terms of known quantities.

This chapter then faces a considerably different task than the previous ones; rather than focus on a variational formulation and its consequences, our objective is to unify the major continuum-scale theories of thermodiffusion, and to deploy the elementary principles of irreversible thermodynamics to produce accurate and robust numerical methods. As a practical matter, the unification effort reveals how to interconvert property sets measured under different paradigms.

The new proposed constitutive scheme — the Onsager–Stefan–Maxwell thermodiffusion equations — simplifies analysis and numerics by essentially treating heat as a pseudo-species. Our new anisothermal Onsager–Stefan–Maxwell transport-coefficient matrix is symmetric, and the second law of thermodynamics imbues it with simple spectral characteristics. The noteworthy consequence of phrasing the equations in this form, is that we may import our finite element methods previously developed to model heat transfer.

In addition this provides a natural route by which binary-system properties can be extrapolated to simulate multicomponent systems. For 10 noble-gas pairs, we tabu-

late the properties needed to simulate binary thermodiffusion with any of the popular theories and in addition detail how to extrapolate these properties to simulate n-ary systems. We demonstrate the applicability of the Onsager–Stefan–Maxwell framework by simulating steady, three dimensional thermodiffusion in a ternary noble-gas mixture (without convection).

Moreover in this chapter we also consider the general inversion process which facilitates the unique formulation of flux-explicit transport equations relative to any choice of convective reference velocity.

4.1 Approaches to thermodiffusion

The typical routes taken when creating thermodiffusion models are: derivation by methods of irreversible thermodynamics; derivation from kinetic theory; and intuitive formulation by extending Fick's law and Fourier's law. Each of these choices may have particular benefits and disadvantages with regard to physical rigour, ease of parameterization, and computational simplicity. Our task of reconciling these different perspectives begins with summarizing the available theories.

Considering first the framework of linear irreversible thermodynamics, we have the general anisothermal entropy production [83] (without viscous dissipation)

$$T\dot{s} = -\vec{\nabla}\ln T \cdot \vec{q}' + \sum_{i=1}^{n} \vec{d}_i \cdot \vec{v}_i. \tag{4.1}$$

Here $\vec{q}'$ denotes the irreversible heat flux, with units $\mathrm{J\,m^{-2}\,s^{-1}}$.

To ensure consistency of units among the fluxes in the dissipation functional, we define the *thermal velocity* $\vec{v}_0$ as

$$\vec{v}_0 = \frac{\vec{q}'}{\rho \hat{C}_p T}, \tag{4.2}$$

where $\hat{C}_p$ is the phase's specific constant-pressure heat capacity, in $\mathrm{J\,kg^{-1}\,K^{-1}}$ (or $\mathrm{m^2\,s^{-2}\,K^{-1}}$). This necessitates that the conjugate *thermal driving force* $\vec{d}_0$ be

$$\vec{d}_0 = -\rho \hat{C}_p \vec{\nabla} T, \tag{4.3}$$

simplified with the identity $T\vec{\nabla}\ln T = \vec{\nabla}T$. By construction, $\vec{v}_0$ and $\vec{d}_0$ have units that match the quantities $\vec{v}_i$ and $\vec{d}_i$ defined earlier. Henceforth we call members of the collection $\{\vec{d}_i\}_{i=0}^n$ *thermodiffusion driving forces*, and those of $\{\vec{v}_i\}_{i=0}^n$ *thermodiffusive*

velocities; we reserve the terms *diffusion driving forces* and *species velocities* to refer to the smaller collections $\{\vec{d}_i\}_{i=1}^n$ and $\{\vec{v}_i\}_{i=1}^n$, respectively. A phase containing n species affords $n+1$ thermodiffusive driving forces and $n+1$ thermodiffusive velocities.

Noting that $\vec{v}_0$ and $\vec{v}_i$ are each of the same tensor order, the laws of linear irreversible thermodynamics discussed in the introduction imply an anisothermal extension of (1.36a) of the following form

$$\vec{d}_0 = \widetilde{M}_{00}\vec{v}_0 + \sum_{j=1}^{n} \widetilde{M}_{0j}\vec{v}_j \tag{4.4}$$

$$\vec{d}_i = \widetilde{M}_{i0}\vec{v}_0 + \sum_{j=1}^{n} \widetilde{M}_{ij}\vec{v}_j, \tag{4.5}$$

where the second equation holds for each $i \in \{1, ..., n\}$.[1] These relationships, which we name the *Onsager–Stefan–Maxwell thermodiffusion equations*, introduce the Onsager drag coefficients $\widetilde{M}_{ij}$, a set of material properties with units $\mathrm{J\,s\,m^{-5}}$ (i.e., force per volume per velocity) that parameterizes how the thermodiffusive velocities map into the thermodiffusive driving forces. Note that equations (4.4) and (4.5) have not been written as compactly as possible because in later discussion it will sometimes be convenient to consider the equation for the thermal force $\vec{d}_0$ separately, and to keep the coefficients whose second index equals 0 out of the sums.

It is often useful to think of the set of all Onsager drag coefficients as being arrayed within an $(n+1) \times (n+1)$ matrix $\widetilde{\mathbf{M}}$ whose row and column indices range across the integers from 0 to n, which we will call the *anisothermal transport matrix*. Onsager asserts that with a proper choice of velocities and driving forces based in the energy dissipation, such as equation (4.1), the reciprocal relation among the transport coefficients is expressed by symmetry of $\widetilde{\mathbf{M}}$ [121]. This symmetry has practical implications for the spectral structure of the thermodiffusion problem.

The general diffusion driving forces within a non-isobaric, anisothermal, multicomponent fluid are [69, 83]

$$\vec{d}_i = -c_i \left(\vec{\nabla}\mu_i + \overline{S}_i \vec{\nabla} T - \frac{\overline{m}_i}{\rho} \vec{\nabla} p \right) \tag{4.6}$$

where the indices range from 1 to n. Thus practical implementation of laws (4.4) and (4.5) is possible if the thermodynamic state variables are known functions of $\{c_i\}_{i=1}^n$,

[1] We have continued the assumption that the material is isotropic and therefore the entries of $\widetilde{M}$ can be represented as scalars.

T, and p. Determining these state variables is sufficiently involved, however, that it is uncommon for experimentalists to perform measurements sufficient to specify the transport matrix $\widetilde{\mathbf{M}}$ for condensed phases.

4.1.1 The kinetic theory of gases

Chapman–Enskog theory [35] leads to a set of thermodiffusion transport laws whose structure differs from laws (4.4)-(4.5). Through the Chapman–Enskog perturbation of the Boltzmann equation for a multicomponent gas, Hirschfelder et al. [83] derived the so-called *generalized Stefan–Maxwell equations*, which we recall from chapter 1 as

$$\vec{d}_i - \sum_{j=1}^{n} \frac{RTc_ic_j}{\mathscr{D}_{ij}c_{\mathrm{T}}} \left(\frac{D_i^T}{\rho_i} - \frac{D_j^T}{\rho_j} \right) \vec{\nabla} \ln T = \sum_{j=1}^{n} \frac{RTc_ic_j}{\mathscr{D}_{ij}c_{\mathrm{T}}} \left(\vec{v}_i - \vec{v}_j \right) \tag{4.7}$$

for $i \in \{1, ..., n\}$. Here ρ_i denotes the mass density of species i; $\rho_i = c_i\overline{m}_i$. Equation (4.7) introduces another set of transport properties, namely, the coefficients of thermal diffusion D_i^T.

As pointed out by Newman [113], the parameters D_i^T have units of viscosity (*i.e.* $\mathrm{Pa\,s}$, or $\mathrm{J\,s\,m^{-3}}$, or $\mathrm{kg\,m^{-1}\,s^{-1}}$), which is unconventional for a diffusion coefficient. To retain dimensional consistency and simplify notation in the sequel, we therefore define

$$\mathscr{D}_i^T = \frac{D_i^T}{\rho_i}, \tag{4.8}$$

which we call the *Soret diffusivity* of species i. The Soret diffusivity $\mathscr{D}_i^T$ has typical units, $\mathrm{m^2\,s^{-1}}$. For isothermal multicomponent diffusion, we recall that the Stefan–Maxwell equations can be understood in terms of Onsager's transport equations by identifying the entries M_{ij} of the isothermal transport matrix $\mathbf{M}$ as

$$M_{ij} = \begin{cases} -\frac{RTc_ic_j}{\mathscr{D}_{ij}c_{\mathrm{T}}} & \text{if } i \neq j \\ \sum_{k\neq i}^{n} \frac{RTc_ic_k}{\mathscr{D}_{ik}c_{\mathrm{T}}} & \text{if } i = j \end{cases} \tag{4.9}$$

and Onsager reciprocity therefore implies symmetry of the coefficients $\mathscr{D}_{ij}$.

This partially brings the constitutive formulation (4.7) into harmony with (4.4)-(4.5). However identity (5.2) fails to carry over to the anisothermal case because the generalized Stefan–Maxwell equations (4.7) mix driving forces and fluxes, which may

also violate the conditions required to ensure a symmetric Onsager reciprocal relation [37, 111]. Specifically, equation (4.7) contains no thermal velocity on the right; on the left, it also mixes the thermal driving force with a diffusion driving force. Therefore $\widetilde{\mathbf{M}} \neq \mathbf{M}$, even if comparison is restricted to the submatrix with $1 \leq i, j \leq n$, as we shall see in section 4.2.

4.1.2 Multicomponent Fick's law

Many transport analyses begin in a more *ad hoc* fashion, by postulating flux-explicit forms of the transport laws with the structure of Fick's law [16, 45, 140]. For a general multicomponent mixture this results in expressions for the excess molar flux of species i, $\vec{J}_i$, of the form

$$\vec{J}_i = -\widetilde{D}_{i0}\vec{\nabla}T - \sum_{j=1}^{n} \widetilde{D}_{ij}\vec{\nabla}c_j \tag{4.10}$$

for $i \in \{1, ..., n\}$. To close this thermodiffusion model, Fickian laws from equation (4.10) must be augmented by a complementary extension of Fourier's law of heat conduction, written as

$$\vec{q}' = -\widetilde{D}_{00}\vec{\nabla}T - \sum_{j=1}^{n} \widetilde{D}_{0j}\vec{\nabla}c_j, \tag{4.11}$$

which expresses the irreversible heat flux.

Clearly the entries of the $(n+1) \times (n+1)$ Fickian thermodiffusion matrix $\widetilde{\mathbf{D}}$ have inconsistent units. In the multicomponent generalization of Fick's law, equation (4.10), the transport coefficients $\widetilde{D}_{ij}$ that accompany concentration gradients can be seen as traditional diffusivities, in $\mathrm{m^2\,s^{-1}}$; the coefficients of thermal diffusion $\widetilde{D}_{i0}$ have units $\mathrm{mol\,m^{-2}\,s^{-1}\,K^{-1}}$. In the generalization of Fourier's law from equation (4.11), $\widetilde{D}_{00}$ is an effective thermal conductivity, in $\mathrm{J\,m^{-1}\,s^{-1}\,K^{-1}}$, but the other $\widetilde{D}_{0j}$ are Dufour coefficients, in $\mathrm{J\,m^2\,s^{-1}\,mol^{-1}}$. These discrepancies emphasize that the reciprocal relation here is obscure; it cannot simply be a symmetry of the $\widetilde{\mathbf{D}}$ matrix.

A few paths have been proposed to connect the Onsager–Stefan–Maxwell equations (4.4)-(4.5) with relations in the Fickian forms of equations (4.10)-(4.11). Despite their linearity, transformation between force-explicit and flux-explicit constitutive formulations requires more than a simple inversion of the transport matrix. As pointed out by Helfand [79], inversion is thwarted by the fact that a Gibbs–Duhem relation constrains the diffusion driving forces. When $\vec{d}_i$ is defined with equation (4.6), the Gibbs–Duhem

equation requires that

$$\sum_{i=1}^{n} \vec{d}_i = 0, \tag{4.12}$$

which further implies singularity of the isothermal transport matrix $\mathbf{M}$ as discussed in the introduction and Chapter 2. As we will see, however, a pseudo-inversion process is enabled by considering kinematic constraints implied by the invariance of diffusion phenomena with respect to the velocity that drives convection.

Flux-law inversions implicitly based on the mass-average velocity were addressed by Curtiss and Bird [40] and Fong et al. [62]. Inversions with respect to other reference velocities have been implemented by Helfand [79] and Newman [116]. Even when applied in isothermal cases, however, these derivation procedures are somewhat impromptu. The Curtiss–Bird approach to inversion, which produces the most well known flux-explicit model for thermodiffusion, was only taken up to quaternary mixtures.

4.2 Properties of the anisothermal transport matrix

First we set out to reconcile the generalized Stefan–Maxwell equations (4.7) with the Onsager–Stefan–Maxwell thermodiffusion equations (4.4)-(4.5). We then discuss how the second law of thermodynamics and the principle of convection invariance impose further structure beyond simple symmetry of the anisothermal transport matrix $\widetilde{\mathbf{M}}$.

4.2.1 Construction and connection to kinetic theory

One can move toward the form of the generalized Stefan–Maxwell equations (4.7) by isolating $\vec{v}_0$ from equation (4.4) and substituting the result into equation (4.5). Regrouping terms and rearranging yields

$$\vec{d}_i + \frac{\widetilde{M}_{0i}\rho\hat{C}_p T}{\widetilde{M}_{00}}\vec{\nabla}\ln T = \sum_{j=1}^{n}\left(\widetilde{M}_{ij} - \frac{\widetilde{M}_{0i}\widetilde{M}_{0j}}{\widetilde{M}_{00}}\right)\vec{v}_j. \tag{4.13}$$

Agreement of the left side with (4.7) requires that

$$\frac{\widetilde{M}_{0i}\rho\hat{C}_p T}{\widetilde{M}_{00}} = -\sum_{j=1}^{n} \frac{RTc_i c_j}{c_{\mathrm{T}}\mathscr{D}_{ij}} \left(\mathscr{D}_i^T - \mathscr{D}_j^T\right). \tag{4.14}$$

Insertion of (5.2), followed by the simplification $\sum_{j=1}^{n} M_{ij} = 0$ implied by the Gibbs–Duhem equation (4.12) and the Onsager reciprocal relation, produces

$$\widetilde{M}_{0i} = -\frac{\widetilde{M}_{00}}{\rho\hat{C}_p T} \sum_{j=1}^{n} M_{ij}\mathscr{D}_j^T. \tag{4.15}$$

Similarly, agreement of the right side of (4.13) with (4.7) demands for all $1 \leq i, j \leq n$ that

$$\widetilde{M}_{ij} = M_{ij} + \frac{\widetilde{M}_{0i}\widetilde{M}_{0j}}{\widetilde{M}_{00}}, \tag{4.16}$$

where M_{ij} relates to Stefan–Maxwell diffusivities through (5.2). These conclusions can be summarized by writing the anisothermal transport matrix in block form, as

$$\widetilde{\mathbf{M}} = \begin{bmatrix} \widetilde{M}_{00} & \widetilde{\mathbf{m}}_0^{\top} \\ \widetilde{\mathbf{m}}_0 & \mathbf{M} + \dfrac{\widetilde{\mathbf{m}}_0\widetilde{\mathbf{m}}_0^{\top}}{\widetilde{M}_{00}} \end{bmatrix}, \tag{4.17}$$

in which the column matrix $\widetilde{\mathbf{m}}_0 = [\widetilde{M}_{0i}]_n^{i=1}$ contains entries $\widetilde{M}_{0i}$ defined by (4.15), superscript $\top$ indicates the matrix transpose, and the first row's entries follow from the reciprocal relation $\widetilde{\mathbf{M}} = \widetilde{\mathbf{M}}^{\top}$. This construction affirms that the generalized Stefan–Maxwell equations (4.7) derived from kinetic theory are compatible with the Onsager–Stefan–Maxwell thermodiffusion laws (4.4)-(4.5) from irreversible thermodynamics.

Despite the mixing of fluxes with driving forces in the generalized Stefan–Maxwell equations, one can show that their structure is consistent with the reciprocal relation $\widetilde{\mathbf{M}} = \widetilde{\mathbf{M}}^{\top}$. Substituting matrix (4.14) into (4.17), using flux law (4.4), then returning to the original thermal flux and driving force with (4.2)-(4.3), yields

$$\vec{q}' = -\frac{\rho^2\hat{C}_\rho^2 T}{\widetilde{M}_{00}}\vec{\nabla}T - \sum_{i,j=1}^{n} \frac{RTc_i c_j}{c_{\mathrm{T}}\mathscr{D}_{ij}} \left(\mathscr{D}_i^T - \mathscr{D}_j^T\right)\vec{v}_j. \tag{4.18}$$

This precisely matches the expression for irreversible heat flux provided by Hirschfelder, Curtiss, and Bird [83], although they define the coefficient of $-\vec{\nabla}T$ as the thermal

conductivity. For now we retain the symbol $\widetilde{M}_{00}$, leaving a detailed discussion of heat conduction to section 4.3.5.

4.2.2 Entropy generation and spectral structure

A benefit of casting the generalized Stefan–Maxwell equations into the Onsager–Stefan–Maxwell form is the structure inherited by the transport matrix $\widetilde{\mathbf{M}}$. Given constitutive laws (4.4) and (4.5), the entropy production due to thermodiffusion is equivalent to

$$T\dot{s} = \sum_{i,j=0}^{n} \vec{v_i} \cdot \widetilde{M}_{ij} \vec{v_j}. \tag{4.19}$$

The second law of thermodynamics requires that $\dot{s} \geq 0$ for every collection of thermodiffusive velocities, so the matrix $\widetilde{\mathbf{M}}$ must be positive semidefinite, as well as symmetric.

Direct calculation shows a connection between the spectral structures of the isothermal and anisothermal transport matrices, $\mathbf{M}$ and $\widetilde{\mathbf{M}}$, respectively. Insertion of (4.17) into (4.19), algebraic rearrangement of terms involving the symmetry of $\widetilde{\mathbf{M}}$, and elimination of $\vec{v}_0$ with (4.4) show that

$$T\dot{s} = \frac{1}{\widetilde{M}_{00}} \left\| \vec{d}_0 \right\|^2 + \sum_{i,j=1}^{n} \vec{v}_i \cdot M_{ij} \vec{v}_j, \tag{4.20}$$

in which $\|\vec{u}\|^2 = \vec{u} \cdot \vec{u}$ for any vector $\vec{u}$. Positive semidefiniteness of the anisothermal matrix $\widetilde{\mathbf{M}}$ is thus implied by positive semidefiniteness of isothermal matrix $\mathbf{M}$, so long as the Onsager drag coefficient $\widetilde{M}_{00}$ is positive.

It was discussed in the introduction how the isothermal transport matrix has a single null eigenvalue corresponding to the eigenvector $\mathbf{1} = [1, 1, ..., 1]^\top \in \mathbb{R}^n$, necessary to enforce the Gibbs–Duhem equation and to distinguish diffusion from convection. A similar conclusion about spectral structure can be drawn for the anisothermal transport matrix. One can use (4.15) to show that the sum over rows 1 through n of the first ($j = 0$) column of $\widetilde{\mathbf{M}}$ satisfies

$$\sum_{i=1}^{n} \widetilde{M}_{i0} = \sum_{i,j=1}^{n} M_{ij} \mathscr{D}_j^T = 0. \tag{4.21}$$

Put another way, this says the column matrix $\mathbf{1}$ is orthogonal to the previously defined column matrix $\widetilde{\mathbf{m}}_0$, so that $\mathbf{1}^\top \widetilde{\mathbf{m}}_0 = 0$. Consequently, the block matrix from (4.17)

must satisfy the matrix equation

$$\begin{bmatrix} \widetilde{M}_{00} & \widetilde{\mathbf{m}}_0^\top \\ \widetilde{\mathbf{m}}_0 & \mathbf{M} + \dfrac{\widetilde{\mathbf{m}}_0 \widetilde{\mathbf{m}}_0^\top}{\widetilde{M}_{00}} \end{bmatrix} \begin{bmatrix} 0 \\ \mathbf{1} \end{bmatrix} = 0 \cdot \begin{bmatrix} 0 \\ \mathbf{1} \end{bmatrix}, \tag{4.22}$$

demonstrating that the column matrix $[\ 0 \quad \mathbf{1}^\top\ ]^\top$ is a null eigenvector of the anisothermal transport matrix. Like the isothermal case, this spectral structure of $\widetilde{\mathbf{M}}$ ensures the enforcement of Gibbs–Duhem relation (4.12).

4.3 Inverting the constitutive laws

Many practitioners find it desirable to implement a flux-explicit (or velocity-explicit) transport formulation. As mentioned before, the transformation of force-explicit laws to a flux-explicit form is not entirely straightforward: since the isothermal transport matrix satisfies $\mathbf{M1} = 0\mathbf{1} = \mathbf{0}$, where $\mathbf{0}$ indicates a column of zeroes, it is singular, and consequently (1.36a) cannot be inverted directly. To resolve this issue it is necessary to consider how the flux-explicit laws behave with regard to the reference velocity selected to describe convection. Once the process of choosing a reference velocity is formalized, a kinematic relation derived from that choice can be exploited to develop a unique inverted formulation of the force-explicit transport laws.

4.3.1 Convective reference velocities

Convection is fundamentally anchored in species fluxes: a valid choice of convective velocity must always be a linear combination of the species velocities. Newman made the simplest choice, employing the k^{th} species' velocity $\vec{v}_k$ as a reference for convection [116]. Other common reference velocities include the mole-average velocity $\vec{v}^c$ employed by Waldmann and Van Der Valk [147, 150],

$$\vec{v}^c = \frac{1}{c_{\mathrm{T}}} \sum_{j=1}^{n} c_j \vec{v}_j, \tag{4.23}$$

and the mass-average velocity $\vec{v}^{\rho}$ which we have used in previous chapters, defined as

$$\vec{v}^{\rho} = \frac{1}{\rho} \sum_{j=1}^{n} \rho_j \vec{v}_j. \tag{4.24}$$

In previous chapters we have denoted the mass-average velocity as simply $\vec{v}$. In this chapter add the superscript ρ to emphasize this choice over other options for convective reference velocities.

In Newman's inversion process [116], after species k is selected as the reference for convection, it is shown that the isothermal transport matrix $\mathbf{M}$ can be truncated by deleting its k^{th} row and column without loss of information. This first minor matrix is nonsingular and can be inverted directly. Helfand considered isothermal, isobaric multicomponent diffusion [79]; when writing the Onsager–Stefan–Maxwell laws, he transformed the driving forces and selected a convective velocity to ensure that the null eigenvector of the flux-explicit transport-coefficient matrix coincided with that of the force-explicit matrix, enabling a Moore–Penrose pseudo-inversion. Hirschfelder et al. [83] and Curtiss and Bird [40] extensively manipulate the generalized Stefan–Maxwell equations to derive velocity-explicit thermodiffusion laws; the rather convoluted process they lay out is summarized in Bird, Stewart, and Lightfoot's book [16]. More recently Bothe et al. [21] compared the isothermal Stefan–Maxwell equations with a generalized form of Fick's law and showed equivalent properties such as positivity preservation between the two approaches.

Depending on the context, different reference velocities may be desirable in flux-explicit constitutive laws [16, 41]. Here we write a general reference velocity as $\vec{v}^{\psi}$, following Goyal and Monroe [69]. To create a convective velocity, one selects a collection of thermodynamic extensive quantities per unit volume $\{\psi_i\}_{i=1}^{n}$, whose total volumetric amount ψ_{T} is defined as

$$\psi_{\mathrm{T}} = \sum_{i=1}^{n} \psi_i = \mathbf{1}^{\top} \boldsymbol{\psi}, \tag{4.25}$$

in which the rightmost expression introduces the column vector $\boldsymbol{\psi} = [\psi_i]_n^{i=1}$. Note that the quantities ψ_i are not limited to choices with these precise physical interpretations; the only necessary restrictions on $\boldsymbol{\psi}$ are that it is real and that $\psi_{\mathrm{T}} \neq 0$ to avoid degeneracy.

The ψ-average velocity, $\vec{v}^{\psi}$, is defined as

$$\vec{v}^{\psi} = \frac{1}{\psi_{\mathrm{T}}} \sum_{j=1}^{n} \psi_j \vec{v}_j. \tag{4.26}$$

To further define the excess velocity of species i relative to the ψ-average velocity, $\vec{v}_i^{\psi}$, take

$$\vec{v}_i^{\psi} = \vec{v}_i - \vec{v}^{\psi}. \tag{4.27}$$

By design, the collection of these excess velocities satisfies a kinematic relation

$$\sum_{j=1}^{n} \psi_j \vec{v}_j^{\psi} = 0. \tag{4.28}$$

In the language of linear algebra, this says that the space of excess species velocities is orthogonal to $\boldsymbol{\psi}$. Thus we may also refer to $\boldsymbol{\psi}$ itself as the kinematic relation associated with convective velocity $\vec{v}^{\psi}$, because it defines the orthogonal subspace of the species velocities in which the set of excess species velocities must reside.

4.3.2 Inversion of the isothermal transport matrix

Invariance of the isothermal transport matrix $\mathbf{M}$ with respect to the choice of convective velocity requires that

$$\vec{d}_i = \sum_{j=1}^{n} M_{ij} \vec{v}_j = \sum_{j=1}^{n} M_{ij} \vec{v}_j^{\psi} \tag{4.29}$$

for any valid kinematic relation $\boldsymbol{\psi}$. Bearing in mind (4.28), one can augment the transport matrix and write (4.29) equivalently as

$$\vec{d}_i = \sum_{j=1}^{n} M_{ij} \vec{v}_j^{\psi} + \gamma \psi_i \sum_{j=1}^{n} \psi_j \vec{v}_j^{\psi} = \sum_{j=1}^{n} M_{ij}^{\psi,\gamma} \vec{v}_j^{\psi} \tag{4.30}$$

for any $\gamma > 0$. Again on the right we have used the *augmented transport matrix*. However this time it is with respect to a general kinematic relation $\boldsymbol{\psi}$ and is defined as

$$M_{ij}^{\psi,\gamma} = M_{ij} + \gamma \psi_i \psi_j, \quad \text{or} \quad \mathbf{M}^{\psi}(\gamma) = \mathbf{M} + \gamma \boldsymbol{\psi} \boldsymbol{\psi}^{\top}. \tag{4.31}$$

Significantly, the augmented transport matrix $\mathbf{M}^{\psi,\gamma}$ is positive definite, as proved

in Chapter 2. Upon inversion one finds that the excess velocity of i is

$$\vec{v}_i^{\,\psi} = \sum_{j=1}^{n} \left[\mathbf{M}^{\psi,\gamma}\right]^{-1}_{ij} \vec{d}_j, \tag{4.32}$$

the desired flux-explicit form of the transport equations. In its present state this formulation is not satisfactory, however. First, the 'penalty term' involving γ is artificial. Second, and of deeper physical importance, the kinematic relation from (4.28) is not obviously enforced for every collection of driving forces.

An unambiguous formulation of inverted transport laws is found by defining

$$\mathbf{L}^{\psi} = \lim_{\gamma\to\infty} \left[\mathbf{M}^{\psi,\gamma}\right]^{-1}. \tag{4.33}$$

This limit exists for any valid choice of $\mathbf{M}$ and $\boldsymbol{\psi}$. Indeed,

$$\left[\mathbf{M}^{\psi,\gamma}\right]^{-1} = \mathbf{L}^{\psi} + \mathscr{O}(\gamma^{-1}), \tag{4.34}$$

and the unique matrix $\mathbf{L}^{\psi}$, which we call the *Onsager diffusivity matrix* relative to the ψ-average velocity, is symmetric whenever $\mathbf{M}$ is. This argument is substantiated in A.1, which also provides two algebraic formulas useful to compute $\mathbf{L}^{\psi}$ from $\mathbf{M}$ without resorting to a limit process.

Since (4.32) holds for any nonzero γ, one can derive the flux-explicit form of the transport laws by calculating the limit of (4.32) as $\gamma \to \infty$, giving

$$\vec{v}_i^{\,\psi} = \sum_{j=1}^{n} L^{\psi}_{ij} \vec{d}_j \tag{4.35}$$

as a consequence of the asymptotic behavior in (4.34). The matrix $\mathbf{L}^{\psi}$ so formed also satisfies

$$\sum_{j=1}^{n} L^{\psi}_{ij} \psi_j = 0, \tag{4.36}$$

that is to say, the kinematic relation $\boldsymbol{\psi}$ is a null eigenvector of $\mathbf{L}^{\psi}$. Analogous to the spectral structure of $\mathbf{M}$ enforcing the Gibbs–Duhem equation, this spectral structure of $\mathbf{L}^{\psi}$ enforces the kinematic constraint (4.28).

The procedure outlined above encompasses all methods currently used to invert isothermal Onsager–Stefan–Maxwell equations. Newman's inverse, relative to $\vec{v}_k$, is

produced by choosing a kinematic relation such that $\psi_i = \delta_{ik}$, where δ_{ij} is the Kronecker delta. Given the diffusion driving forces in (4.6), which make $\mathbf{1}$ the null eigenvector of $\mathbf{M}$, Helfand's inverse is formed by taking $\boldsymbol{\psi} = \mathbf{1}$, an unorthodox choice where the arithmetic mean of the species velocities drives convection. Curtiss and Bird's inverse derives from the kinematic relation for the mass-average velocity, $\psi_i = \rho_i$. Crucially, the need for kinematic relations here indicates that one cannot consider a generic matrix $\mathbf{L}$ in a flux-explicit thermodiffusion model. Instead there is a class of equally valid Onsager diffusivity matrices, from which one is determined by specifying a convective velocity.

Sometimes it may be of interest to calculate $\mathbf{M}$ given an $\mathbf{L}^{\psi}$, as discussed by Monroe and Newman in a specific case [111]. This can be accomplished generally by augmenting the singular matrix $\mathbf{L}^{\psi}$ to make

$$\mathbf{L}^{\psi,\gamma} = \mathbf{L}^{\psi} + \gamma \mathbf{1}\mathbf{1}^{\top}, \tag{4.37}$$

again with $\gamma > 0$. Then, similar to the process given above, one can pass into a limit to get

$$\mathbf{M} = \lim_{\gamma \to \infty} \left[\mathbf{L}^{\psi,\gamma}\right]^{-1}. \tag{4.38}$$

The $\mathbf{M}$ form may be preferable when reporting experimental measurements, since it is independent of the convective velocity used for data processing; the $\mathbf{L}^{\psi}$ form, however, provides alternative routes for physical interpretation. Nevertheless, one should bear in mind that although there exist many legitimate $\mathbf{L}^{\psi}$ matrices, there is just one valid choice of $\mathbf{M}$ for a proper set of diffusion driving forces.

4.3.3 Inversion of the anisothermal transport matrix

Problems posed by the convection invariance of $\mathbf{M}$ carry over into the anisothermal transport matrix $\widetilde{\mathbf{M}}$: the null eigenvector $\begin{bmatrix} 0 & \mathbf{1}^{\top} \end{bmatrix}^{\top}$ induced by convection invariance implies that $\widetilde{\mathbf{M}}$ cannot be directly inverted. It is, however, straightforward to adapt the pseudo-inversion procedure developed earlier to the anisothermal case.

Thermal properties in the generalized Stefan–Maxwell equations merit some additional discussion here. Observe that only differences between Soret diffusivities appear in equation (4.7). Since the physical content of that equation is invariant to a variable change where the same scalar is added to every Soret diffusivity, it follows that the collection $\left\{\mathscr{D}_i^T\right\}_{i=1}^n$ must be linearly dependent. To quantify Soret diffusivities in isolation, one must adopt an additional constraint to close this degree of freedom. Newman

circumvented the ambiguity by defining a new property,

$$\mathscr{A}_{ij} = \frac{D_i^T}{\rho_i} - \frac{D_j^T}{\rho_j} = \mathscr{D}_i^T - \mathscr{D}_j^T, \tag{4.39}$$

which we call the *Newman–Soret diffusivity*. As well as having units $\mathrm{m}^2\,\mathrm{s}^{-1}$, the fact that $\mathscr{A}_{ii} = 0$ ensures that the nontrivial $\mathscr{A}_{ij}$ are linearly independent for a given j. Newman further asserts that these diffusivities are more approximately constant with respect to composition in binary systems [113]. Newman's choice of symbol emphasizes antisymmetry in the indices, that is, that $\mathscr{A}_{ji} = -\mathscr{A}_{ij}$.

It is standard to enforce a kinematic relation to close the degree of freedom when specifying the coefficients of thermal diffusion. Here we impose the general constraint

$$\sum_{j=1}^{n} \psi_j \mathscr{D}_j^T = 0, \tag{4.40}$$

which is agnostic to the choice of convective velocity. Given any complete set of $\mathscr{A}_{ij}$ with j fixed, the identities $\mathscr{A}_{kl} = \mathscr{A}_{kj} - \mathscr{A}_{lj}$ and $\mathscr{A}_{lk} = -\mathscr{A}_{kl}$ fill out the whole matrix of Newman–Soret diffusivities. Thus, any particular Soret diffusivity can be computed with the formula

$$\mathscr{D}_i^T = \frac{1}{\psi_{\mathrm{T}}} \sum_{k=1}^{n} \psi_k \mathscr{A}_{ik}, \tag{4.41}$$

so long as one row or column of the Newman–Soret matrix is known. Given the kinematic relation $\boldsymbol{\psi}$, (4.39) and (4.41) establish a bijective map between the Soret diffusivities and the Newman–Soret matrix.

In their implementation of Chapman–Enskog theory, Hirschfelder et al. state [83] that

$$\sum_{i=1}^{n} D_i^T = 0. \tag{4.42}$$

This implies that the properties D_i^T/ρ_i satisfy a kinematic relation $\psi_i = \rho_i$; the Soret diffusivities stand relative to the mass-average velocity. Brenner argued that some constitutive laws are more appropriately formulated with respect the volume-average velocity, however [25]. Rather than advocating one view or the other, we adopt Newman–Soret diffusivities here, which emphasizes that thermal diffusion can be fully parameterized without choosing a reference velocity for convection.

One can write a new equivalent of (4.15) in terms of the augmented transport

matrix $\mathbf{M}^{\psi,\gamma}$ from (4.31), as

$$\widetilde{M}_{0i}^{\psi,\gamma} = -\frac{\widetilde{M}_{00}}{\rho\hat{C}_p T}\sum_{j=1}^{n} M_{ij}^{\psi,\gamma}\mathscr{D}_j^T. \tag{4.43}$$

These coefficients can be assembled into an augmented column matrix $\widetilde{\mathbf{m}}_0^{\psi,\gamma} = [\widetilde{M}_{0i}^{\psi,\gamma}]_n^{i=1}$. The constraint stated in (4.40) is natural because it implies that

$$\widetilde{\mathbf{m}}_0^{\psi,\gamma} = \widetilde{\mathbf{m}}_0 \tag{4.44}$$

for any $\gamma > 0$. Thus augmentation of the anisothermal transport matrix has no impact on the thermal entries of $\widetilde{\mathbf{M}}$.

The anisothermal transport matrix augmented by kinematic relation $\boldsymbol{\psi}$ is defined as

$$\widetilde{\mathbf{M}}^{\psi,\gamma} = \begin{bmatrix} \widetilde{M}_{00} & \widetilde{\mathbf{m}}_0^\top \\ \widetilde{\mathbf{m}}_0 & \mathbf{M}^{\psi,\gamma} + \frac{\widetilde{\mathbf{m}}_0\widetilde{\mathbf{m}}_0^\top}{\widetilde{M}_{00}} \end{bmatrix}, \tag{4.45}$$

in which only the lower-right block depends on the penalty factor γ. The inverse of this augmented matrix is partially calculable through Schur's complement In block form,

$$\left[\widetilde{\mathbf{M}}^{\psi,\gamma}\right]^{-1} = \begin{bmatrix} \frac{1}{\widetilde{M}_{00}} + \frac{\widetilde{\mathbf{m}}_0^\top\left[\mathbf{M}^{\psi,\gamma}\right]^{-1}\widetilde{\mathbf{m}}_0}{\widetilde{M}_{00}^2} & -\frac{\widetilde{\mathbf{m}}_0^\top\left[\mathbf{M}^{\psi,\gamma}\right]^{-1}}{\widetilde{M}_{00}} \\ -\frac{\left[\mathbf{M}^{\psi,\gamma}\right]^{-1}\widetilde{\mathbf{m}}_0}{\widetilde{M}_{00}} & \left[\mathbf{M}^{\psi,\gamma}\right]^{-1} \end{bmatrix}. \tag{4.46}$$

Interestingly, the only matrix inversion needed to carry out this computation is that of the augmented isothermal transport matrix.

It is straightforward to rephrase (4.43) in a form that computes Soret diffusivities from the Onsager drag coefficients. The construction

$$\left[\mathscr{D}_i^T\right]_n^{i=1} = -\frac{\rho\hat{C}_p T}{\widetilde{M}_{00}}\left[\mathbf{M}^{\psi,\gamma}\right]^{-1}\widetilde{\mathbf{m}}_0 \tag{4.47}$$

retrieves a column of Soret diffusivities constrained by (4.40). With (4.47), one can define for $i \in \{1, ..., n\}$ that

$$\widetilde{L}_{0i}^{\psi} = \frac{\mathscr{D}_i^T}{\rho\hat{C}_p T}, \tag{4.48}$$

and introduce a column $\widetilde{\mathbf{l}}_0^{\psi} = [\widetilde{L}_{0i}^{\psi}]_n^{i=1}$. (The superscript ψ on these quantities empha-

sizes kinematic relationship (4.40), i.e. that $\boldsymbol{\psi}^\top \widetilde{\mathbf{l}}_0^\psi = 0$.) Then

$$\widetilde{\mathbf{l}}_0^\psi = -\frac{\left[\mathbf{M}^{\psi,\gamma}\right]^{-1} \widetilde{\mathbf{m}}_0}{\widetilde{M}_{00}} \tag{4.49}$$

for any $\gamma > 0$ (indeed, $\widetilde{\mathbf{l}}_0^\psi$ is independent of γ), and the inverse augmented transport matrix transforms to

$$\left[\widetilde{\mathbf{M}}^{\psi,\gamma}\right]^{-1} = \begin{bmatrix} \frac{1}{\widetilde{M}_{00}}\left(1 - \widetilde{\mathbf{m}}_0^\top \widetilde{\mathbf{l}}_0^\psi\right) & \left(\widetilde{\mathbf{l}}_0^\psi\right)^\top \\ \widetilde{\mathbf{l}}_0^\psi & \left[\mathbf{M}^{\psi,\gamma}\right]^{-1} \end{bmatrix}. \tag{4.50}$$

Finally, the unique inverse of the anisothermal transport matrix $\widetilde{\mathbf{M}}$ with respect to convective velocity $\vec{v}^\psi$ is found by taking the limit of equation (4.50) as $\gamma \to \infty$. This produces the *Onsager thermodiffusivity matrix*

$$\widetilde{\mathbf{L}}^\psi = \begin{bmatrix} \widetilde{M}_{00}^{-1}\left(1 - \widetilde{\mathbf{m}}_0^\top \widetilde{\mathbf{l}}_0^\psi\right) & \left(\widetilde{\mathbf{l}}_0^\psi\right)^\top \\ \widetilde{\mathbf{l}}_0^\psi & \mathbf{L}^\psi \end{bmatrix}, \tag{4.51}$$

a symmetric matrix with null eigenvector $\begin{bmatrix} 0 & \boldsymbol{\psi}^\top \end{bmatrix}^\top$.

4.3.4 Onsager–Fick–Fourier laws

Equation (4.51) gives rise to a velocity-explicit form of the anisothermal flux laws similar to the isothermal (4.35). A thermodynamically consistent form of the generalized Fick's law is given by

$$\vec{v}_i^\psi = \sum_{j=0}^{n} \widetilde{L}_{ij}^\psi \vec{d}_j. \tag{4.52}$$

Here it should be understood that $\vec{v}_0^\psi = \vec{v}_0$, because the thermal velocity $\vec{v}_0$ is not included in the kinematic constraint from (4.28). Unlike the intuitive extension of Fick's law involving transport matrix $\widetilde{\mathbf{D}}$, the derivation of $\widetilde{\mathbf{L}}^\psi$ from the Onsager–Stefan–Maxwell thermodiffusion equations ensures that the coefficient matrix in (4.52) has consistent units, as well as being symmetric positive semidefinite and satisfying a kinematic constraint.

Equation (4.52) substantiates a thermodynamically consistent set of generalized Fourier–Fick thermodiffusion laws as follows. After inserting (4.2), (4.3), and (4.48)

into (4.52), and defining the excess flux of species i relative to the ψ-average velocity as

$$\vec{J}_i^{\psi} = c_i \vec{v}_i^{\psi}, \tag{4.53}$$

one obtains flux-explicit constitutive equations

$$\vec{q}' = -\rho^2 \hat{C}_p^2 T \widetilde{L}_{00}^{\psi} \vec{\nabla} T + \sum_{j=1}^{n} \mathscr{D}_j^T \vec{d}_j, \tag{4.54}$$

$$\vec{J}_i^{\psi} = -c_i \mathscr{D}_i^T \vec{\nabla} \ln T + \sum_{j=1}^{n} c_i \widetilde{L}_{ij}^{\psi} \vec{d}_j, \tag{4.55}$$

for $i \in \{1, ..., n\}$. Equation (4.54) is analogous to Fourier's law, with extra terms describing the Dufour effect; (4.55) generalize Fick's law, with an additional term for the Soret effect. These equations satisfy Onsager's principles of irreversible thermodynamics, in that they involve all the proper fluxes and driving forces that appear in the dissipation functional, as well as including a positive-semidefinite transport matrix that satisfies a symmetric reciprocal relation and has a single null eigenvector to enforce convection invariance. To emphasize their thermodynamic rigour, we henceforth call (4.54) and (4.55) the *Onsager–Fick–Fourier equations*.

4.3.5 Perspectives on thermal conductivity

To elucidate simple heat conduction, it is worth returning to the dissipation functional (4.1). Insertion of (4.2) and (4.3) produces the compact expression

$$T\dot{s} = \sum_{i=0}^{n} \vec{d}_i \cdot \vec{v}_i. \tag{4.56}$$

Putting the Onsager–Stefan–Maxwell thermodiffusion laws (4.4)-(4.5) into (4.56) produces (4.20), which shows that the dissipation associated with temperature gradients when the species velocities vanish is proportional to $1/\widetilde{M}_{00}$. Past analyzes have asserted on this basis that $\widetilde{M}_{00}$ should be inversely proportional to the thermal conductivity [45, 134]; in that case force-explicit equation (4.4) reduces to Fourier's law of heat conduction in the absence of relative species velocities.

Alternatively, inserting the Onsager–Fick–Fourier equations (4.52) into (4.56) and

applying the Gibbs–Duhem relation (4.12) leads to

$$T\dot{s} = \sum_{i,j=0}^{n} \vec{d}_i \cdot \widetilde{L}_{ij}^{\psi} \vec{d}_j, \tag{4.57}$$

showing that the dissipation associated with temperature gradients in the absence of diffusion driving forces is proportional to $\widetilde{L}_{00}$. One could alternatively argue that thermal conductivity should be the coefficient of $-\vec{\nabla}T$ in equation (4.54), so that it reduces to Fourier's law in the absence of diffusion driving forces.

Newman pointed out that these two perspectives on thermal conductivity are mutually exclusive [113]. Indeed, after inserting the definitions of $\widetilde{\mathbf{m}}_0$ and $\widetilde{\mathbf{l}}_0^{\psi}$ into (4.54) and applying an identity similar to the one presented in (1.50), one finds that

$$\widetilde{L}_{00}^{\psi} = \frac{1}{\widetilde{M}_{00}} + \frac{R}{2\rho^2 \hat{C}_p^2 T} \sum_{i,j=1}^{n} \frac{c_i c_j \mathscr{A}_{ij}^2}{c_{\mathrm{T}} \mathscr{D}_{ij}}, \tag{4.58}$$

so the thermal conductivity cannot be proportional to both $1/\widetilde{M}_{00}$ and $\widetilde{L}_{00}$ simultaneously. Note that we have included Newman–Soret diffusivities to emphasize that this relationship is independent of the convective velocity, addressing another concern raised by Newman [113].

The appropriate definition of thermal conductivity is decided by adopting a standard approach to its experimental measurement. Thermal conductivity in fluids is typically measured by inducing a temperature gradient across a one-dimensional cell with closed ends, enforcing no-molar-flux boundary conditions. When such an apparatus reaches a steady state, the differential material balances demand that species velocities vanish throughout the cell, as well as at its ends. For this experiment, (4.4) is appropriate, and it reduces to Fourier's law if

$$k = \frac{\rho^2 \hat{C}_p^2 T}{\widetilde{M}_{00}} \tag{4.59}$$

defines the thermal conductivity k. The dissipation functional from equation (4.20) requires that $k \geq 0$.

One consequence of this definition of k is that the generalized Fourier's law contains temperature-gradient-driven heat flux in addition to $-k\vec{\nabla}T$. The extra contribution, which Bird, Stewart, and Lightfoot call the *Dufour flux* [16], can be quantified by inserting (4.58) and (4.59) into (4.54). One practical problem the experimental definition

of k raises is that thermodynamic consistency demands *a priori* knowledge of the Soret diffusivities when applying the Onsager–Fick–Fourier laws.

Our choice of thermal conductivity also has implications for thermodynamic stability. Since the second law of thermodynamics requires that $k \geq 0$, the condition that dissipation must be positive in (4.58) without diffusion driving forces places a lower bound on $\widetilde{L}_{00}^{\psi}$, namely

$$\widetilde{L}_{00}^{\psi} \geq \frac{R}{2\rho^2 \hat{C}_p^2 T} \sum_{i,j=1}^{n} \frac{c_i c_j \mathscr{A}_{ij}^2}{c_{\mathrm{T}} \mathscr{D}_{ij}}. \tag{4.60}$$

Here inclusion of the Newman–Soret diffusivity emphasizes this condition's convection invariance.

4.4 Properties and balances for viscous fluids

Thermodiffusion is simulated by solving a system of differential balance equations that govern the transient spatial distributions of temperature and composition. As well as necessitating a parameterization of the transport coefficients that make up $\widetilde{\mathbf{M}}$ or $\widetilde{\mathbf{L}}^{\psi}$, closure of this system requires various equilibrium material properties. Generally these parameters are not constants, but rather state functions dependent on local temperature, pressure, and composition. A key advantage of the irreversible thermodynamics methodology is that every equilibrium state function ultimately derives from the system's free energy.

4.4.1 Diffusion driving forces

Since molar Gibbs energy depends on temperature, pressure, and composition, all of the material properties depend locally on these basis variables, as well. Thus, elementary thermodynamic dependences imply that each diffusion driving force in a viscous fluid depends on the natural basis variables T, p, and $\{y_i\}_{i=1}^{n}$ as

$$\vec{d}_i = -RTc_{\mathrm{T}} \sum_{j=1}^{n} \chi_{ij} \vec{\nabla} y_i + c_i \left(\frac{\overline{m}_i}{\rho} - \overline{V}_i \right) \vec{\nabla} p, \tag{4.61}$$

where $\overline{V}_i$ is the partial molar volume of species i and χ_{ij} quantifies how the change in chemical activity of species i varies with the mole fraction of species j (i.e., c_j/c_{T}) at fixed T and p. Notably, the temperature-gradient term in the original definition of $\vec{d}_i$, (4.6), cancels out when chemical-potential gradients are expanded over the natural

basis. Terms involving composition gradients in (4.61) express the forces that drive mass diffusion; the remaining term drives pressure diffusion.

Entries within the $n \times n$ activity-gradient matrix $\boldsymbol{\chi}$ must adhere to many constraints. When mixing is thermodynamically ideal, $\boldsymbol{\chi} = \mathbf{I}$, where $\mathbf{I}$ is the identity matrix. Therefore, one conventionally lets $\boldsymbol{\chi} = \mathbf{I} + \boldsymbol{\Gamma}$, such that the $n \times n$ matrix $\boldsymbol{\Gamma}$ represents deviations from ideal mixing behaviour under isothermal, isobaric conditions; Gibbs–Duhem relationships suggest that $\mathbf{1}^\top \boldsymbol{\Gamma} = \mathbf{0}^\top$. A constraint that $\boldsymbol{\Gamma}\mathbf{1} = \mathbf{0}$ ensures that nonphysical composition changes lie in the nullspace of $\boldsymbol{\Gamma}$. Finally, although $\boldsymbol{\Gamma}$ is not generally symmetric, Maxwell relations still reduce its number of independent entries to $n\,(n-1)\,/2$, one for each distinct pair of species.

4.4.2 Balance equations

Every multicomponent mass-transport process is governed by a set of species material balances,[2]

$$\frac{Dc_i}{Dt} = -\vec{\nabla} \cdot (c_i \vec{v}_i^{\,\rho}) - c_i \vec{\nabla} \cdot \vec{v}^{\,\rho} \tag{4.62}$$

for $i \in \{1, ..., n\}$. Here the operator

$$\frac{D}{Dt} = \frac{\partial}{\partial t} + \vec{v}^{\,\rho} \cdot \vec{\nabla} \tag{4.63}$$

represents the substantial derivative with respect to the mass-average velocity.

Thermodynamic considerations reveal that the material balances imply a connection between changes of temperature and pressure. A state equation for the volume derives directly from the Euler equation for the Gibbs energy, by differentiation with respect to pressure. The molar volume, $1/c_\mathrm{T}$, is an intensive equilibrium property and consequently depends generally on T, p, and at most $n-1$ species fractions [69]. Thus the local concentrations satisfy

$$\sum_{i=1}^{n} \overline{V}_i c_i = 1, \tag{4.64}$$

in which the partial molar volumes depend on the same basis variables as c_T. Since $\phi_i = \overline{V}_i c_i$ represents the volume fraction occupied by species i within a phase, this can

[2] Generally, the material balances can be augmented by generation terms, for example, to account for the formation or consumption of species by homogeneous chemical reactions. Such phenomena, which produce commensurate generation terms in the thermal energy balance as well, are neglected here for simplicity.

be seen as a rather trivial statement, that species volume fractions sum to unity. But it also establishes the Gibbs phase rule, a more substantive physical conclusion.

Equation (4.64) leads to the Gibbs phase rule as follows. A substantial derivative of (4.64) combines with the Gibbs–Duhem relation derived from the extensivity of volume [69] to give

$$\frac{Dp}{Dt} = K\alpha_V \frac{DT}{Dt} + K\sum_{i=1}^{n} \overline{V}_i \frac{Dc_i}{Dt}, \tag{4.65}$$

where K is the bulk modulus (inverse isothermal compressibility) and α_V is the volumetric coefficient of thermal expansion, introduced in equations (1.14) and (1.15). Therefore, in an n-ary single phase, one of the intensive natural variables T, p, $\{c_i\}_{i=1}^{n}$ necessarily depends on the others.

To close the governing system's degree of freedom associated with temperature, a balance of thermal energy is added alongside the material balances. In any nonreactive single-phase viscous fluid, this heat balance is [69]

$$\begin{aligned}\rho\hat{C}_p \frac{DT}{Dt} = &-\vec{\nabla}\cdot\vec{q}' - \sum_{i=1}^{n} c_i \vec{v}_i^{\,\rho}\cdot\vec{\nabla}\overline{H}_i + T\alpha_V \frac{Dp}{Dt} \\ &+ \left(\overset{\rightrightarrows}{\tau} - \sum_{i=1}^{n} c_i \overline{m}_i \vec{v}_i^{\,\rho}\vec{v}_i^{\,\rho}\right) : \vec{\nabla}\vec{v}^{\,\rho},\end{aligned} \tag{4.66}$$

in which $\overline{H}_i$ is the partial molar enthalpy of species i and $\overset{\rightrightarrows}{\tau}$ is deformation stress, the latter following Bird, Stewart, and Lightfoot's sign convention [16]. The terms on the right of equation (4.66) respectively quantify local heat accumulation from: net influx of irreversible heat; excess enthalpy convection due to diffusion; externally imposed compressive power; and viscous friction.

4.4.3 Species enthalpies

The heat balance apparently introduces a new set of properties — the partial molar enthalpies — but much of the information they contain is embedded in quantities that have already been defined. In light of the standard Legendre transformation $\mu_i = \overline{H}_i - T\overline{S}_i$, the definition of the diffusion driving force and (4.61) give

$$\vec{\nabla}\overline{H}_i = \overline{V}_i\vec{\nabla}p + \frac{RTc_{\mathrm{T}}}{c_i}\sum_{j=1}^{n}\chi_{ij}\vec{\nabla}y_j + T\vec{\nabla}\overline{S}_i. \tag{4.67}$$

Also, $\overline{S}_i$ connects to the chemical potential through a Maxwell relation, so the last term depends on existing parameters. One ultimately finds [145]

$$\vec{\nabla}\overline{H}_i = \overline{C}_{p,i}\vec{\nabla}T + \left[1 - \left(\frac{\partial \ln \overline{V}_i}{\partial \ln T}\right)_p\right]\overline{V}_i\vec{\nabla}p \tag{4.68}$$

$$-\frac{RTc_{\mathrm{T}}}{c_i}\sum_{j=1}^{n}\left(\frac{\partial \chi_{ij}}{\partial \ln T}\right)_p \vec{\nabla}\left(\frac{c_j}{c_{\mathrm{T}}}\right), \tag{4.69}$$

in which $\overline{C}_{p,i}$ represents the partial molar constant-pressure heat capacity of species i.

Substituting material balances (4.62) into (4.65) shows that the time derivative of pressure in (4.66) depends only on spatial derivatives and the time derivative of temperature. Insertion of (4.69) then yields an explicit equation for the time evolution of temperature as a function of the instantaneous spatial distributions of temperature, pressure, composition, the set of excess species velocities $\{\vec{v}_i^{\,\rho}\}_{i=1}^n$, and the mass-average velocity $\vec{v}^{\,\rho}$. Since the Euler equation for entropy implies that

$$\rho\hat{C}_p = \sum_{i=1}^{n} c_i\overline{C}_{p,i}, \tag{4.70}$$

this heat balance is fully parameterized by specifying the temperature, pressure, and composition dependences of α_V, K, $\{\overline{C}_{p,i}\}_{i=1}^n$, $\{\overline{V}_i\}_{i=1}^n$, the molar masses $\{\overline{m}_i\}_{i=1}^n$, and the $n(n-1)/2$ independent state functions that underpin $\boldsymbol{\chi}$.

4.5 Thermodiffusion in monatomic-gas mixtures

Numerous measurements have been made to quantify thermodiffusion in binary noble-gas mixtures. To put this body of experimental data in context, we first lay out equilibrium properties and the thermal balance equation for multicomponent gas mixtures. We subsequently discuss the physical assumptions that underpin experimental data processing, and tabulate the measured thermodiffusion properties for various noble-gas pairs.

4.5.1 Equilibrium properties

Here we restrict the development to ideal mixtures of monatomic gases, for which a substantial amount of experimental data is available. The equilibrium material prop-

erties take simpler forms in this case, greatly simplifying both the diffusion driving forces and the energy balance.

As well as satisfying $\boldsymbol{\chi} = \mathbf{I}$, an ideal gas is defined in part by the condition that $\overline{V}_i = RT/p$ for all i. Thus (4.64) yields

$$c_{\mathrm{T}} = \frac{p}{RT}, \tag{4.71}$$

a relationship which can be used to demonstrate that $K = p$ and $\alpha_V = 1/T$, both independent of composition. Also, this form of the partial molar volumes reduces (4.69) to

$$\vec{\nabla}\overline{H}_i = \overline{C}_{p,i}\vec{\nabla}T. \tag{4.72}$$

Generally the ideal-gas state is also defined by a condition that each species' partial molar heat capacity $\overline{C}_{p,i}$ in a gas mixture equals the molar heat capacity of the pure species in isolation.

In an ideal gas, the driving diffusion force of species i reduces (4.61) to

$$\vec{d}_i = -p\vec{\nabla}y_i + (\omega_i - y_i)\,\vec{\nabla}p, \tag{4.73}$$

where we have eliminated c_{T} with state equation (4.71). Thus the driving force for pressure diffusion is proportional to the difference between the molar mass of species i and the number-average molar mass of the mixture, $\rho/c_{\mathrm{T}} = \sum_{i=1}^{n} \overline{m}_i y_i$. For isobaric gas thermodiffusion, the condition that $\vec{\nabla}p = \vec{0}$ simplifies diffusion driving forces (4.73) to

$$\vec{d}_i = -p\vec{\nabla}y_i. \tag{4.74}$$

The equilibrium thermal properties simplify even more if all the species comprising an ideal gas are assumed to be monatomic. In a monatomic ideal gas, $\overline{C}_{p,i} = \frac{5}{2}R$ for each i. Through (4.70), the volumetric heat capacity of a monatomic ideal-gas mixture is therefore $\rho\hat{C}_p = \frac{5}{2}c_{\mathrm{T}}R$, independent of composition.

4.5.2 Thermodiffusion property measurements

Experiments to parameterize thermodiffusion typically employ binary gas mixtures. The measurement is performed in an apparatus designed to be one-dimensional spatially, which is subjected to a temperature difference across its ends. Designating one

end of the apparatus by a and the other by b, experimentalists record the steady-state value of the parameter

$$\alpha_{12} = \frac{\ln\left(y_2^b/y_1^b\right) - \ln\left(y_2^a/y_1^a\right)}{\ln T^b/T^a}, \tag{4.75}$$

known as the thermal diffusion factor [73]. Conventionally, index 1 is assigned to the heavier of the two species.

An expression relating α_{12} to transport properties derives naturally from the Onsager–Stefan–Maxwell laws. In a steady state, the condition $\vec{v}^\rho = 0$ simplifies material balances (4.62) dramatically, to

$$0 = -\vec{\nabla} \cdot (c_i \vec{v}_i^{\,\rho}) \tag{4.76}$$

for each species i. In a one-dimensional apparatus with closed ends, these balances imply that $\vec{v}_i = \vec{0}$ for every species i. Thus the force-explicit flux law (4.4) can be used to eliminate $\vec{v}_0$ from (4.5), showing that

$$\vec{d}_i = \frac{\widetilde{M}_{i0}}{\widetilde{M}_{00}} \vec{d}_0 \tag{4.77}$$

for each species $i = 1, \ldots, n$. Substitution of driving forces (4.3) and (4.74) into (4.77), followed by simplification with equation of state (4.71) and rearrangement based on the fact that $y_2 = 1 - y_1$, gives

$$\vec{\nabla} \ln\left(\frac{y_2}{y_1}\right) = \frac{\mathscr{A}_{12}}{\mathscr{D}_{12}} \vec{\nabla} \ln T \tag{4.78}$$

for an isobaric binary mixture of monatomic gases in a closed, one-dimensional apparatus subjected to a steady temperature polarization. Integration from end a to end b yields

$$\alpha_{12} = \frac{\mathscr{A}_{12}}{\mathscr{D}_{12}}, \tag{4.79}$$

assuming that the ratio $\mathscr{A}_{12}/\mathscr{D}_{12}$ is constant with respect to temperature and composition. Thus the thermal diffusion factor relates directly to the Newman–Soret coefficient and the Stefan–Maxwell diffusivity.

Table 4.1 presents the binary diffusion coefficients and thermal diffusion factors for various pairs of noble gases. In the first-order approximation of the Chapman–Enskog expansion, the terms $p\mathscr{D}_{12}$ and α_{12} are independent of pressure [83]. Hence the reported values are nominally valid for a range of pressures. Binary diffusion coeffi-

Gas pair	$p\mathscr{D}_{12}$ (atm cm^{2}s^{-1})	α_{12} (unitless)
Ne - He	1.1079	0.3432
Ar - He	0.7560	0.3984
Kr - He	0.6553	0.4279
Xe - He	0.5611	0.4250
Ar - Ne	0.3250	0.1741
Kr - Ne	0.2647	0.2710
Xe - Ne	0.2231	0.2951
Kr - Ar	0.1398	0.0705
Kr - Ar	0.1144	0.0803
Xe - Kr	0.0745	0.0262

Table 4.1: Thermodiffusion transport coefficients measured for noble-gas pairs at $T = 300$ K as reported by Mason and Marrero [101] and Taylor [141]. In all cases data were gathered from experimental systems which comprise uniform equimolar mixtures when relaxed to isothermal equilibrium.

Gas	k (W cm^{-1} K^{-1})
He	15.66
Ne	4.98
Ar	1.78
Kr	0.95
Xe	0.55

Table 4.2: Thermal conductivities k for pure noble gases at 300 K at atmospheric pressure and average isotopic composition [89].

cients were computed with the least-squares equations compiled in the comprehensive review by Mason and Marrero [101]. The thermal separation factors were taken from temperature-dependent least-squares correlations reported by Taylor [141].

Many additional measurements of thermal gas-mixture separation exist in the literature. The reported data cover hydrogen/noble-gas mixtures [54], mixtures of hydrogen isotopes [72], halogen/noble-gas mixtures [55, 104], and gas mixtures that include methane [53].

Complete specification of the thermodiffusion transport matrix requires a value for the thermal conductivity. Thermal conductivities of pure noble gases are reported in Table 4.2, taken from the survey of Kestin et al. [89]. Note that Helium is understood to be at its average isotopic composition. Even simulating binary systems leads to

complications because the thermal conductivity is a strong function of composition; for example, the thermal conductivities of xenon and helium differ by well over an order of magnitude. Thus it is necessary to incorporate a mixing rule for thermal conductivities, a topic for which there is a significant body of literature. Options include the Wassijewa model [153] based on the kinetic theory of gases, the empirical Kennard mixing rule [88], and the Mason–Saxena mixing rule [102]. Recently, an accurate and easily-implemented mixing rule based on equivalent-circuit analysis was proposed by Udoetok [143].

4.6 Numerical computation

Practical modelling of thermodiffusion has been impeded by the difficulty of numerical implementation. On one hand, deriving Onsager–Fick–Fourier laws for multicomponent mixtures is a complex procedure, and, as we have illustrated, the parameterization of the Onsager thermodiffusivity matrix $\widetilde{\mathbf{L}}^{\psi}$ depends strongly on the choice of reference velocity. On the other hand, in the generalized Stefan–Maxwell equations (4.7), the mixture of fluxes and driving forces apparently yields no useful mathematical structure to facilitate numerical algorithms.

In Chapter 2 we formulated a finite element method effect for the Stefan–Maxwell equations, that is the isobaric, isothermal diffusion equations for an ideal gas mixture. Having now formulated the equations for thermodiffusion in a force explicit form, we can see that heat may be treated as a pseudospecies and it is straightforward to transfer the algorithm in chapter 2 to the anisothermal case as the structure is almost entirely inherited. In particular we use the augmented anisothermal matrix (4.43) instead of the augmented transport matrix, we include the thermal driving force and velocity, and add the thermal balance equation (4.66).

In general the complication when extending to the anisothermal case is the balance equation, which possesses addition terms describing heat generation within the medium. For a steady-state isobaric monatomic gas mixture with no mass-average velocity this simplifies to

$$-\vec{\nabla}q' = \sum_{j=1}^{n} \frac{5}{2} R c_i v_i \cdot \vec{\nabla} T. \tag{4.80}$$

It is anticipated that the framework developed in Chapter 3 may also be transferred over to include convection. Specifically there is little difficultly in transferring the discretization detailed in Chapter (3) on the premise that heat acts as another species. However it should be noted that when we add convection, prudent consideration of the

choice of linearisation remains as future work. Indeed the general form of the driving forces, which now include a temperature gradient, make the analysis considerably more involved, and it is not immediately obvious how to extend the theorems from Chapter (3).

4.6.1 Extension of binary data

The Onsager–Stefan–Maxwell equations allow a natural extrapolation of isothermal property data from binary systems to multicomponent systems. Reasoning physically that species/species drag is dominated by pairwise interactions to a first approximation, one can use diffusion coefficients $\mathscr{D}_{ij}$ measured from binary systems directly in simulations with more than two species. A similar process cannot be used to infer the set of Newman–Soret diffusivities $\mathscr{A}_{ij}$ from binary measurements, however, as a consequence of the structure required by (4.39). Producing a consistent form of the multicomponent Newman–Soret matrix requires that the binary data be regularized to ensure kinematic consistency. A.2 presents a regularization process underpinned by the method of least squares.

4.6.2 Steady thermodiffusion in a ternary noble-gas mixture

Here we consider steady, three-dimensional thermodiffusion in an isobaric ternary mixture of noble gases. In this situation, flux laws (4.4)-(4.5) for species $i \in \{0,1,2,3\}$ are written in compact form as

$$\vec{d}_i = \sum_{j=0}^{3} \widetilde{M}_{ij}\vec{v}_j, \tag{4.81}$$

where it is understood that $\vec{d}_0 = -\frac{5}{2}c_{\mathrm{T}}R\vec{\nabla}T$ and $\vec{v}_0 = \vec{q}'/(\frac{5}{2}c_{\mathrm{T}}RT)$. To close the model we adopt the condition $\vec{v}^{\,\rho} = 0$, which simplifies the material balances to the form of (4.76) for each $i \in \{1,2,3\}$. For a monatomic-gas mixture, the steady-state heat balance simplifies to

$$0 = -\frac{5}{2}\vec{\nabla}\cdot(c_{\mathrm{T}}RT\vec{v}_0), \tag{4.82}$$

and (4.73) describes the diffusion driving forces.

4.6.3 Example

We adapt the numerical method from Chapter 2 by simulating the separation of an equimolar ternary gas mixture of helium, argon and krypton in a three dimensional

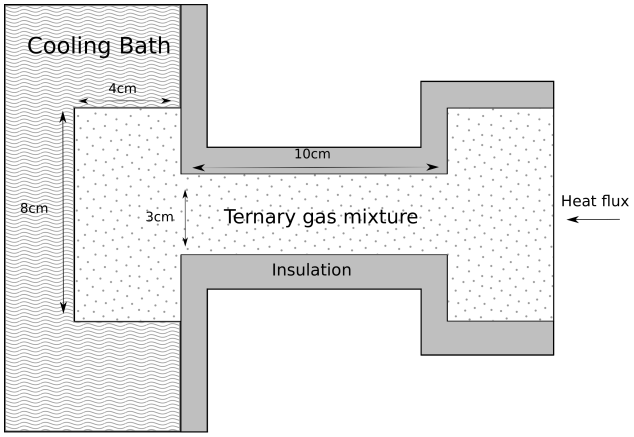

Figure 4.1: Schematic diagram of the separation chamber. The figure shows a cross section of the axially symmetric device.

separation chamber. The conceptual schematic for this numerical experiment is shown in Figure 4.1.

Values of binary Stefan–Maxwell coefficients $\mathscr{D}_{ij}$ were taken from Table 4.1. Newman–Soret coefficients $\mathscr{A}_{ij}$ computed using binary data for α_{12} are tabulated in Table 4.3, and the regularized Newman–Soret matrix used for simulations is presented in Table 4.4. Thermal conductivities for each pure component were taken from Table 4.2; to evaluate the thermal conductivity of the mixture, the mixing rule proposed by Udoetok [143] was employed. This mixing rule was chosen due to its good balance between accuracy and simplicity, the latter of which is key because conductivity must be computed dynamically from the local composition and temperature at each quadrature point in the domain. The exact molar masses used for the simulation were $4.00\,\mathrm{g\,mol^{-1}}$, $39.95\,\mathrm{g\,mol^{-1}}$, and $83.80\,\mathrm{g\,mol^{-1}}$ for helium, argon, and krypton, respectively.

The simulation was performed with Firedrake software [129], using the MUMPS direct linear solver [1, 2] via PETSc [12, 13]. The mesh of the geometry was constructed using the Gmsh software [65]. Each linear system had 3,895,568 degrees of freedom and convergence was achieved in 11 non-linear iterations. The exact scripts used to produce each numerical experiment can be found at `https://bitbucket.org/vanbrunt/consolidated-thermodiffusion-repository` along with the mesh used for the separation chamber. The exact software versions used to produce the results in this chapter, along with instructions for installation, have been archived on Zenodo [158].

For the experiment, the cooling bath was maintained at 300 K, a condition reflected in the simulation by imposing Dirichlet boundary conditions specifying the wall temperatures of the left chamber. To drive the temperature gradient, an evenly-distributed fixed heat flux was fed normally into the rightmost face of the device. The remaining boundary conditions were set as homogeneous Neumann conditions to reflect the

$\mathscr{A}_{ij}$ from binary measurements			
	He	Ar	Kr
He	0	−0.3012	−0.2804
Ar	0.3012	0	−0.0099
Kr	0.2804	0.0099	0

Table 4.3: Newman–Soret diffusivities computed using the experimental data from binary systems summarized in Table 4.1 and (4.79).

Inferred $\mathscr{A}_{ij}$ entries			
	He	Ar	Kr
He	0	−0.2910	−0.2906
Ar	0.2910	0	0.004
Kr	0.2906	−0.004	0

Table 4.4: Table of regularized Newman–Soret diffusivities for a He–Ar–Kr mixture, determined from the data in Table 4.3 with the procedure detailed in A.2.

presence of insulation and gas-impermeable walls. Last, it was assumed that the total molar amounts of each gas are constants of the closed system. The constant total amount of material in the separation chamber, n_{T}, necessarily satisfies

$$\int_V c_{\mathrm{T}} dV = n_{\mathrm{T}}, \tag{4.83}$$

where V indicates the chamber volume. Through equation of state (4.71), this implies that

$$p = \frac{R n_{\mathrm{T}}}{\int_V 1/T dV}, \tag{4.84}$$

which was used to determine a self-consistent steady-state pressure from the temperature distribution. For simulations, n_{T} was chosen to be consistent with an average total concentration given by equation (4.71) with $p = 1\,\mathrm{atm}$ and $T = 300\,\mathrm{K}$.

A heat input of 135 W induces a temperature difference of approximately 100 K across the separation chamber, as can be seen from Figure 4.2 alongside arrows that indicate the direction and magnitude of local irreversible heat flux. The separation of helium effected by the temperature gradient is plotted in Figure 4.3. As expected, helium, the lightest component, tends to build up towards the hotter end [78]; a 7.5% separation of helium is induced by the heat flux. The steady-state separation of krypton

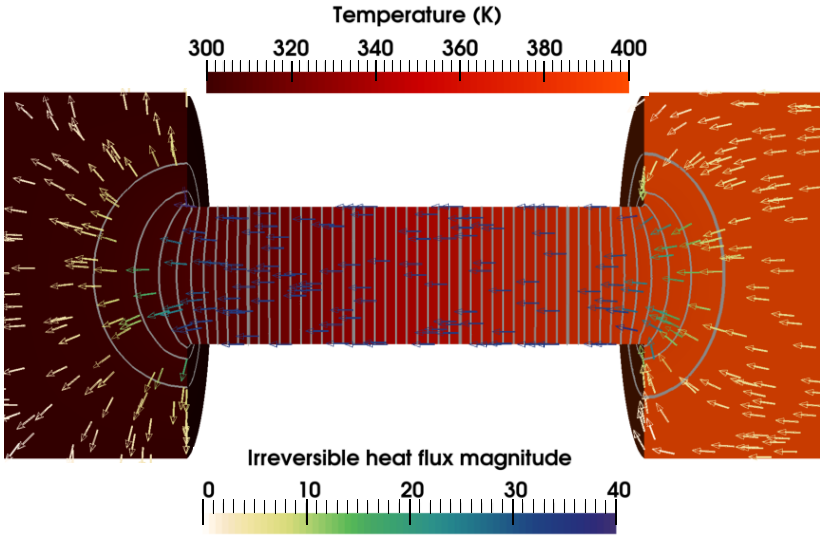

Figure 4.2: Temperature profile within the separation chamber. Arrows indicate the irreversible-heat-flux ($\mathrm{W\,cm^{-2}}$) vector field.

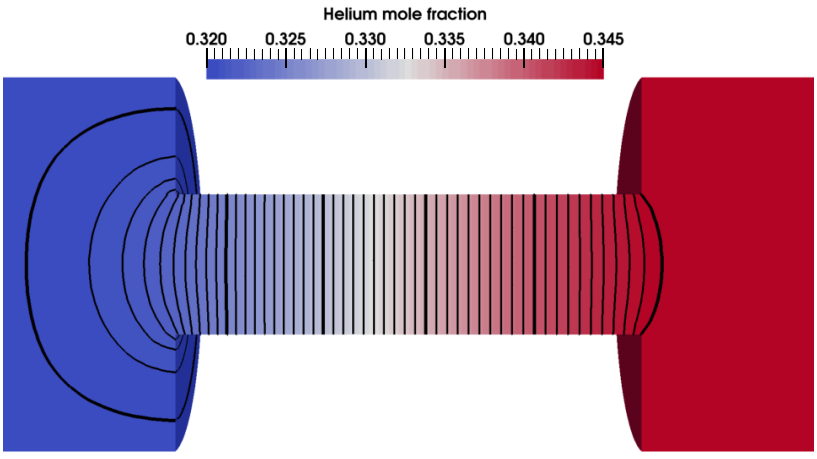

Figure 4.3: Mole fraction profile of helium.

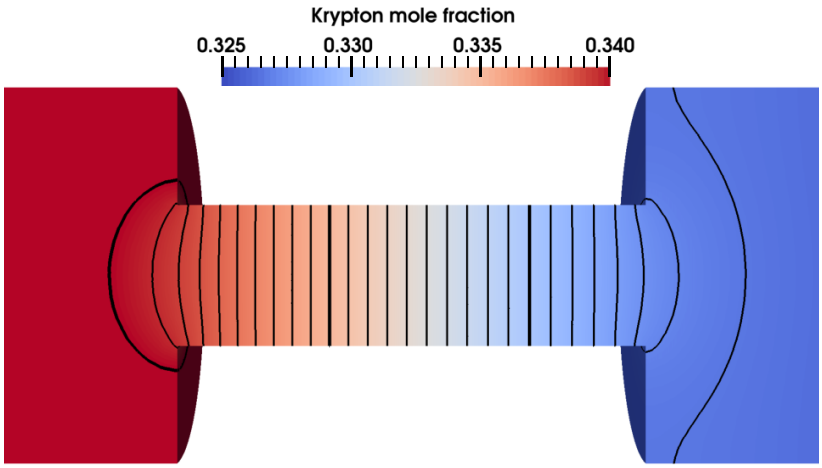

Figure 4.4: Mole fraction profile of krypton.

induced by the heat flux is shown in Figure 4.4. Krypton tends to move towards the cooler end, but the separation is only about 4.5%.

This numerical example demonstrates the potential of the Onsager–Stefan–Maxwell framework for modelling thermodiffusion in multispecies phases with three-dimensional geometries. From this perspective, one can investigate a rich variety of phenomena for a number of practical applications. To the best of the author's knowledge, no other multidimensional simulations of thermodiffusion have been performed using the linear irreversible thermodynamics approach.

4.7 Conclusion

A unified framework for modelling fluid thermodiffusion was presented. The new force-explicit Onsager–Stefan–Maxwell formulation was shown to be compatible with the generalized Stefan–Maxwell equations implied by kinetic theory, as well as the commonly employed flux-explicit Onsager–Fick–Fourier constitutive laws. A general method for inverting isothermal transport laws to obtain velocity-explicit forms from force-explicit forms, and vice versa, was proposed, and shown to encompass the disparate prior approaches to flux-law inversion proposed by Newman, Helfand, and Curtiss and Bird. The general inversion process was further extended to cover anisothermal situations, proving equivalence of the various constitutive formulations.

The Onsager–Stefan–Maxwell thermodiffusion equations involve an anisothermal transport matrix that proves to have a simple spectral structure. It was shown how to infer entries of multicomponent transport matrices given binary measurements, allowing for straightforward practical implementation of the theory. Further mathematical

relationships necessary to implement a thermodiffusion model, such as balance equations and expressions of the driving forces in terms of natural thermodynamic basis variables, were provided for thermodynamically non-ideal viscous fluids and ideal gases. Finally, an effective and novel numerical method to simulate thermodiffusion was deployed, in which heat was treated as a pseudospecies. Multidimensional simulations of steady thermodiffusion in a ternary noble-gas mixture demonstrated the effectiveness of the proposed approach.

Although the numerical methodology was shown to be sound, the absence of convection (i.e., a zero mass-average velocity) is generally not a valid physical assumption. Addressing this issue requires consideration of a local momentum balance alongside the balances of material and heat. Future work is needed to confront the full dynamics of convective thermodiffusion from the irreversible-thermodynamics perspective, and to appropriately analyze the resulting set of partial differential equations in variational form as was done in Chapters 2 and 3.

Chapter 5

Structural electroneutrality in the Onsager–Stefan–Maxwell models with charged species

5.1 Introduction

The growing impetus for improved electrochemical energy storage makes it vital to understand ion transport. The term *concentrated solution theory* [114, 116] refers to multicomponent transport (as described in the previous chapters) applied to model electrolytic materials on the continuum scale. One of the most popular implementations of concentrated solution theory is Doyle, Fuller and Newman's landmark physics-based model of the dual-insertion lithium-ion battery. This relies on a model of a binary liquid solution, comprising a simple salt dissolved in a neutral solvent, typically $LiPF_6$ in ethyl methyl carbonate (EMC) or propylene carbonate (PC) [49, 51]. It derives from the Onsager–Stefan–Maxwell transport laws [83, 116], written for n species in an isothermal, isobaric common phase as [1]

$$-\vec{\nabla}\mu_i = \sum_{j=1}^{n} M_{ij}^{\mathbf{c}} \vec{N}_j, \tag{5.1}$$

[1] Throughout this chapter we will express the Onsager–Stefan–Maxwell equations in terms of fluxes $N_i = c_i v_i$ and chemical potentials rather than driving forces. Primarily this is due to these being the more natural variables for identifying voltage and current.

Here we have written a transport matrix $\mathbf{M}^{\mathbf{c}}$, closely related to $\mathbf{M}$ from previous sections, whose entries are

$$M_{ij}^{\mathbf{c}} = \begin{cases} -\dfrac{RT}{c_{\mathrm{T}}\mathscr{D}_{ij}} & \text{if } i \neq j \\ \dfrac{RT}{c_{\mathrm{T}}}\displaystyle\sum_{k\neq i}^{n}\frac{c_k}{\mathscr{D}_{ik}c_j} & \text{if } i = j. \end{cases} \tag{5.2}$$

This matrix is also symmetric positive semidefinite with a null eigenvalue corresponding to the vector $\mathbf{c} = [c_1, c_2, ..., c_n]^\top$.

An important practicality emerges when considering transport in liquids such as electrolytic solutions, which conduct electricity via the motion of ions. If mobile species in a fluid carry charge, their thermal motion will screen any local charge imbalances on a length scale comparable to the Debye length (typically of the order of 1 nm) [46]. Thus, if volume elements in a simulation have characteristic size much larger than the Debye length, the local excess charge density ρ_{e} can be assumed to vanish locally, that is,

$$\rho_e = F\sum_{j=1}^{n} z_j c_j = 0, \tag{5.3}$$

where F is Faraday's constant and z_i is the equivalent charge of species i. Local electroneutrality is foundational to concentrated solution theory and has been assumed nearly ubiquitously in its applications.

Adopting the local electroneutrality approximation simplifies transport models by allowing one charged-species concentration to be eliminated from the governing equations, both reducing the complexity of thermodynamic parametrization and streamlining calculations. Electroneutrality makes concentrated-solution theory hard to reconcile with the Onsager–Stefan–Maxwell theory for nonelectrolytes, however, because the additional algebraic constraint imposed by equation (5.3) appears to induce an overdetermination within equations (5.1). Indeed for fluids wholly made up of uncharged species, the Onsager–Stefan–Maxwell equations, when combined with an equation that establishes a convective velocity, have been shown in Chapters 2-3 to constitute a closed model.

Newman and colleagues carefully circumvented the issues raised by electroneutrality when formulating their models of binary electrolytes and ternary salt mixtures [114, 115, 125]. The importance of separating terms into neutral and non-neutral contributions was emphasized in their analyses. In particular, individual ion concen-

trations were lumped into salt concentrations; species fluxes were expressed in terms of salt chemical potentials and current density; and terms associated with charge density and charge convection were explicitly neglected.

Possible applications of electroneutral Onsager–Stefan–Maxwell theory readily exceed the scope of the few cases that have been considered to date. For example, aqueous vanadium flow batteries—a system comprising at least eight distinct species—have recently been modelled [38, 39], but it is not immediately clear how that framework can be extended to account for side reactions, additives, or contaminants. At the same time, the increased demand for electrochemical transport simulations raises the need for a general, numerically robust model formulation.

This chapter generalizes Newman's particular implementations of electroneutral concentrated-solution theory for binary solutions and salt melts. We introduce a structure-preserving transformation that maps the free energies of individual charged species into those of uncharged combinations of species, assembling species electrochemical potentials into a basis set of component chemical potentials and a single quantity interpretable as an electric potential. The same transformation regroups charged-species fluxes into component fluxes and current density. As well as reconciling the electroneutrality approximation with the fundamental equations of linear irreversible thermodynamics in a structure-preserving way, the theory produces a general set of transference numbers and an ionic conductivity that match definitions given by Newman, as well as leading to a naturally symmetric set of component diffusivities. The transformation preserves the spectral structure of $\mathbf{M}$, making the equations amenable to numerical methods developed in previous chapters.

5.2 Construction of a salt–charge basis

Our key mathematical concepts are linear transformations and inner products, typically represented by matrix operations. These tools are used to develop a change of composition basis from one that lists charged-species molarities into one that lists neutral-salt molarities alongside charge density. Instead of beginning with species concentrations, however, the new composition basis is identified by grouping species electrochemical potentials into new quantities that represent electrically neutral combinations of species. For any given electrolytic material, one can establish a minimal set of such combinations by positing a set of independent hypothetical chemical reactions that we call *fundamental equilibria*, which leave uncharged species alone or bring

charged species together to form neutral salts. We refer to products of the fundamental equilibria as *components*, rather than species.

Every electrochemical system is globally electroneutral at equilibrium and every electrochemical reaction necessarily balances both charge and atoms between its reactants and products. Moreover, any physically realizable electrolytic solution must contain at least two countercharged species. It follows that the n species comprising any electrolyte combine to form at most $n-1$ distinct uncharged components. We call the elementary structure that establishes the species charges and a minimal set of hypothetical reactions that neutralize them a *salt–charge basis*.

It is helpful to illustrate with an example. Consider a solution of Na^+, Cl^-, Mg^{2+} and SO_4^{2-} in water (H_2O). Among these five species, one can write $5-1=4$ independent reactions to form electrically neutral entities. First write a trivial equilibrium between the naturally uncharged water molecule and itself, and then write three equilibria among distinct countercharged pairs of ions:

$$H_2O \leftrightharpoons H_2O \tag{5.4}$$

$$Na^+ + Cl^- \leftrightharpoons NaCl \tag{5.5}$$

$$Mg^{2+} + 2Cl^- \leftrightharpoons MgCl_2 \tag{5.6}$$

$$2Na^+ + SO_4^{2-} \leftrightharpoons Na_2SO_4. \tag{5.7}$$

Along with the list of species charges $\{0, 1, -1, 2, -2\}$, these fundamental equilibria define a salt–charge basis for this five-species aqueous solution.

The choice of reactions to form a salt–charge basis is not generally unique, but any neutral component not defined can always be recovered by writing additional reactions involving products formed by the selected fundamental equilibria. In the example system, observe that one can create the fourth possible simple binary salt, $MgSO_4$, via the recombination reaction

$$MgCl_2 + Na_2SO_4 \leftrightharpoons 2NaCl + MgSO_4. \tag{5.8}$$

Thus any thermodynamic property of $MgSO_4$ in this system — such as its chemical potential, partial molar volume, or partial molar entropy — is determined by properties of dissolved NaCl, Na_2SO_4, and $MgCl_2$. The energetics of any multi-ion salt with higher

formula-unit stoichiometry also follows from the fundamental equilibria. Consider

$$\mathrm{MgCl_2} + \mathrm{Na_2SO_4} \leftrightharpoons \mathrm{NaCl} + \mathrm{MgNaClSO_4},$$

which forms the more complex salt $\mathrm{MgNaClSO_4}$ from all four available ions.

The formal procedure for creating a salt–charge basis generalizes the preceding example. Start by placing the species in an ordered list, wherein each species' position assigns its numerical index. List all uncharged species first, and charged species afterward. For consistency with prior approaches, ensure that the nth and $(n-1)$th species have opposite charges [70, 108]. Then let $\mathbf{z} = [z_1, ..., z_n]^\top$ be a column matrix comprising the species equivalent charges in their assigned order and suppose there are $n_c < n-1$ charged species. The ordering ensures that entries $z_1, ..., z_{n-n_\mathrm{c}}$ of $\mathbf{z}$ equal zero, entries $z_{n-n_\mathrm{c}+1}, ..., z_n$ of $\mathbf{z}$ are nonzero, and $z_n/z_{n-1} < 0$. In the example above, we have $\mathbf{z}^\top = [0, 1, -1, 2, -2]^\top$.

Next, write a set of $n-1$ fundamental equilibria involving the species, beginning with $n - n_\mathrm{c}$ trivial equilibria for the naturally uncharged species, and following with $n_\mathrm{c} - 1$ linearly independent association equilibria, within which countercharged pairs of charged species react to form simple binary salts. Here 'simple' means that the reactant stoichiometric coefficients are coprime positive integers. Let column matrix $\boldsymbol{\nu}_i = [\nu_{i1}, \nu_{i2}, ..., \nu_{in}]^\top$ contain the stoichiometric coefficients ν_{ij} of reactant species j in the ith fundamental equilibrium. For example in the equilibria (5.7), which is the dissociation of $\mathrm{Na_2SO_4}$, these are 2 for $\mathrm{Na^+}$ and 1 for $\mathrm{SO_4{}^{2-}}$. For uncharged species $i = 1, ..., n - n_\mathrm{c}$, stoichiometric column $\boldsymbol{\nu}_i$ will be the ith column of the identity matrix, notated henceforth as $\mathbf{i}_i$. For $i = n - n_\mathrm{c} + 1, ..., n-1$, $\boldsymbol{\nu}_i$ has two positive-integer entries, corresponding to the stoichiometric coefficients of species in a formula unit of the simple binary salt they form. The restriction to simple salts ensures that the total number of ions in each formula unit is minimal.

The Guggenheim condition requires that ion stoichiometry within a formula unit of salt always balances charge [76]. In terms of reactant stoichiometry in the ith fundamental equilibrium, the condition is expressed as

$$\boldsymbol{\nu}_i^\top \mathbf{z} = 0, \tag{5.9}$$

where superscript $\top$ indicates the matrix transpose. Note that this condition also holds for every trivial fundamental equilibrium based on an uncharged reactant.

It is useful to view equation (5.9) as a statement about a matrix inner product, namely: the Guggenheim condition requires that each column $\boldsymbol{\nu}_i$ is orthogonal to $\mathbf{z}$. Since the set of stoichiometric columns is also linearly independent by construction, the reactant stoichiometries from the $n-1$ fundamental equilibria establish an $(n-1)$-dimensional linear space orthogonal to the span of $\mathbf{z}$. Moreover, the n-tuple $\{\boldsymbol{\nu}_1, ..., \boldsymbol{\nu}_{n-1}, \mathbf{z}\}$ is linearly independent, and consequently forms a basis for the entire n-dimensional composition space. This set of column vectors formally represents the chosen salt–charge basis.

5.3 The chemical potential in a salt–charge basis

The selection of a salt–charge basis enables the construction of a linear transformation that maps the n_c charged-species electrochemical potentials into $n_\mathrm{c} - 1$ chemical potentials of neutral salts, leaving a single additional combination of electrochemical potentials to describe charge. The transformation is represented by an $n \times n$ matrix $\mathbf{Z}$,

$$\mathbf{Z} = \begin{bmatrix} \boldsymbol{\nu}_1^\top \\ \vdots \\ \boldsymbol{\nu}_{n-1}^\top \\ \mathbf{z}^\top / \|\mathbf{z}\| \end{bmatrix}, \tag{5.10}$$

in which $\|\mathbf{v}\| = \sqrt{\mathbf{v}^\top \mathbf{v}}$ for any column $\mathbf{v}$. Its rows are linearly independent, so $\mathbf{Z}$ is invertible. Each of the first $n-1$ rows is orthogonal to the last (nth) row, and each of the first $n - n_\mathrm{c}$ rows, which correspond to uncharged species, is orthogonal to every other row. Internal rows corresponding to salts, that is, rows $i = n - n_\mathrm{c} + 1, ..., n-1$ of $\mathbf{Z}$, are not mutually orthogonal in general.

The transformation $\mathbf{Z}$ combines species electrochemical potentials into component chemical potentials as follows. Let the column matrix $\boldsymbol{\mu} = [\mu_1, ..., \mu_n]^\top$ contain the species electrochemical potentials in order. Then multiplication by $\mathbf{Z}$ maps $\boldsymbol{\mu}$ into new coordinates $\boldsymbol{\mu}_Z$ that stand over the chosen salt–charge basis. In the form of a matrix equation, $\boldsymbol{\mu}_Z$ is defined as

$$\boldsymbol{\mu}_Z = \mathbf{Z}\boldsymbol{\mu}. \tag{5.11}$$

The first $n-1$ rows of $\boldsymbol{\mu}_Z$ so formed comprise the chemical potentials of a minimal number of neutral components, with the ith row representing the chemical potential of the product formed by the ith fundamental equilibrium used to define a salt–charge

basis. In our running example, the chemical potential of the salt Na_2SO_4 would be $\mu_{Na_2SO_4} = 2\mu_{Na} + \mu_{SO_4}$, which reflects the equilibrium in (5.7). The last row of (5.11) quantifies all of the information in the set of species electrochemical potentials associated with reversible processes that do not conserve charge. It is convenient to subdivide $\boldsymbol{\mu}_Z$, as

$$\boldsymbol{\mu}_Z = \begin{bmatrix} \boldsymbol{\mu}_\nu \\ \mu_z \end{bmatrix}, \tag{5.12}$$

where the $(n-1)$-dimensional column $\boldsymbol{\mu}_\nu$ contains the $n-1$ component chemical potentials. More explicitly, if $\boldsymbol{\nu}_i$ has a single nonzero entry, $\mu_{\nu,i} = (\boldsymbol{\mu}_\nu)_i = \boldsymbol{\nu}_i^\top \boldsymbol{\mu}$ reproduces the chemical potential expected for a naturally uncharged species; otherwise $\mu_{\nu,i}$ forms a salt chemical potential by the same process outlined by Newman and Thomas–Alyea [116]. As we shall see later, the remaining quantity, μ_z, leads naturally to a definition of solution voltage.

5.4 Concentration and flux in a salt–charge basis

The transformation to a salt–charge basis embodied by $\mathbf{Z}$ can be exploited to form quantities which describe the amounts and motion of uncharged components. Natural definitions of component concentrations and component fluxes arise heuristically from an invariance argument.

We assert as a physical principle that the elementary laws from thermodynamics and irreversible thermodynamics must retain their structures when expressed in terms of components, rather than species. In equilibrium thermodynamics, this is asserting that the change of basis does not change the energy of the system. Here the essential thermodynamic relation is the Euler equation,

$$\tilde{G} = \sum_{i=1}^{n} \mu_i c_i, \tag{5.13}$$

for which $\tilde{G}$ is the volumetric Gibbs free energy in terms of species molarities. The essential relation from irreversible thermodynamics is the dissipation function, written at a point within an isothermal, isobaric single phase as

$$T\dot{s} = \sum_{i=1}^{n} \vec{N}_i \cdot \left(-\vec{\nabla}\mu_i\right), \tag{5.14}$$

which relates local energy loss $T\dot{s}$ to the species fluxes.

Natural composition variables over a salt–charge basis are identified by requiring $\tilde{G}$ to retain its structure whether written in terms of species or components. In that case, the matrix relationship

$$\tilde{G} = \boldsymbol{\mu}^\top \mathbf{c} = \boldsymbol{\mu}_Z^\top \mathbf{c}_Z \tag{5.15}$$

defines the column matrix $\mathbf{c}_Z$ that lists component concentrations in the chosen salt–charge basis. Since $\mathbf{Z}$ is nonsingular, it follows from definition (5.11) that

$$\mathbf{c}_Z = \mathbf{Z}^{-\top} \mathbf{c}, \tag{5.16}$$

where superscript $-\top$ indicates the inverse transpose.

It is illuminating to introduce Faraday's law. Faraday's law for charge combines with equation (5.16) to show that excess charge density can be expressed in two ways,

$$\rho_\mathrm{e} = F \sum_{i=1}^{n} z_i c_i = F \mathbf{z}^\top \mathbf{c} = F \left(\mathbf{Z}\mathbf{z} \right)^\top \mathbf{c}_Z, \tag{5.17}$$

in which the distributive property of the matrix transpose was used to rearrange the last equality. Since the first $n-1$ rows of $\mathbf{Z}$ are orthogonal to $\mathbf{z}^\top$, $\mathbf{Z}\mathbf{z} = \|\mathbf{z}\| \, \mathbf{i}_n$ by equation (5.10), and consequently equation (5.17) implies that

$$\left(\mathbf{c}_Z \right)_n = \frac{\rho_\mathrm{e}}{F \, \|\mathbf{z}\|}, \tag{5.18}$$

i.e., the last entry of $\mathbf{c}_Z$ quantifies excess charge density. Thus $\mathbf{c}_Z$ naturally partitions into a column that represents an ordered set of $n-1$ neutral *component concentrations*, written as $\mathbf{c}_\nu$, followed by an entry expressing the excess charge in molar units,

$$\mathbf{c}_Z = \begin{bmatrix} \mathbf{c}_\nu \\ \dfrac{\rho_\mathrm{e}}{F \, \|\mathbf{z}\|} \end{bmatrix}. \tag{5.19}$$

Entry $c_{\nu,i} = \left(\mathbf{c}_\nu \right)_i$ of the component concentrations $\mathbf{c}_\nu$ represents the molarity of the product formed by the ith fundamental equilibrium.

Flux descriptors over a salt–charge basis are created by demanding that the structure of the energy dissipation $T\dot{s}$ is preserved. Assemble the species fluxes into a

column $\vec{\mathbf{n}} = [\vec{N}_1, ..., \vec{N}_n]^\top$. Structure preservation requires that

$$T\dot{s} = \vec{\mathbf{n}}^\top \cdot \left(-\vec{\nabla}\boldsymbol{\mu}\right) = \vec{\mathbf{n}}_Z^\top \cdot \left(-\vec{\nabla}\boldsymbol{\mu}_Z\right), \tag{5.20}$$

where the column $\vec{\mathbf{n}}_Z$ lists fluxes in salt–charge basis $\mathbf{Z}$. (The notation $\vec{\nabla}\mathbf{u}$ indicates a column matrix whose ith entry is the vector $\vec{\nabla}u_i$, where u_i is the ith entry of $\mathbf{u}$.) The transformation from $\vec{\mathbf{n}}$ into $\vec{\mathbf{n}}_Z$ therefore must be

$$\vec{\mathbf{n}}_Z = \mathbf{Z}^{-\top}\vec{\mathbf{n}}, \tag{5.21}$$

identical to the mapping that sends species concentrations into component concentrations.

Faraday's law — this time, for current — also provides detail about the new fluxes $\vec{\mathbf{n}}_Z$. In matrix form, Faraday's law casts current density $\vec{i}$ in terms of species fluxes as

$$\vec{i} = F\mathbf{z}^\top\vec{\mathbf{n}} = F\left(\mathbf{Z}\mathbf{z}\right)^\top\vec{\mathbf{n}}_Z. \tag{5.22}$$

Again, the fact that $\mathbf{Z}\mathbf{z} = \|\mathbf{z}\|\,\mathbf{i}_n$ comes into play, yielding

$$\left(\vec{\mathbf{n}}_Z\right)_n = \frac{\vec{i}}{F\,\|\mathbf{z}\|}. \tag{5.23}$$

Thus the last entry of $\vec{\mathbf{n}}_Z$ represents a renormalized current density. It is again natural to partition $\vec{\mathbf{n}}_Z$, as

$$\vec{\mathbf{n}}_Z = \left[\begin{array}{c} \vec{\mathbf{n}}_\nu \\ \hline \dfrac{\vec{i}}{F\,\|\mathbf{z}\|} \end{array}\right], \tag{5.24}$$

in which $\vec{\mathbf{n}}_\nu$ is an $(n-1)$-dimensional column matrix representing the set of *total component fluxes*.

Other fundamental thermodynamic laws also readily transform. For example, prior definitions imply

$$\sum_{i=1}^{n} c_i\vec{\nabla}\mu_i = \mathbf{c}^\top\vec{\nabla}\boldsymbol{\mu} = \mathbf{c}_Z^\top\vec{\nabla}\boldsymbol{\mu}_Z = \vec{0}, \tag{5.25}$$

so the change to a salt–charge basis retains a structurally identical isothermal, isobaric Gibbs–Duhem equation.

One can also cast the total species concentration c_T in terms of the component

concentrations. Letting $\mathbf{1}$ stand for a column matrix whose entries are all '1', one has that

$$c_{\mathrm{T}} = \sum_{i=1}^{n} c_i = \mathbf{1}^{\top}\mathbf{c} = \boldsymbol{\nu}_Z^{\top}\mathbf{c}_Z, \tag{5.26}$$

in which the column matrix $\boldsymbol{\nu}_Z$, defined as

$$\boldsymbol{\nu}_Z = \mathbf{Z1} = \begin{bmatrix} \boldsymbol{\nu} \\ \hline \dfrac{\mathbf{z}^{\top}\mathbf{1}}{\|\mathbf{z}\|} \end{bmatrix}, \tag{5.27}$$

summarizes information about net reactant stoichiometry in the fundamental equilibria. The second equality here indicates that the stoichiometric column $\boldsymbol{\nu}_Z$ also partitions into $(n-1)$ entries $\boldsymbol{\nu}$ that describe components and a final entry associated with charge. When component $i < n$ derives from a naturally uncharged species, the corresponding entry of $\boldsymbol{\nu}$, that is, ν_i, is 1; when component $i < n$ is a salt, ν_i is the total number of ions in its formula unit.

Molar concentrations are convenient for stating the thermodynamic laws, but they make characterization efforts error-prone because molarity varies with temperature and pressure at fixed composition. It is useful to introduce two alternative composition descriptors, called the *species fractions* $\mathbf{y}$ and *component fractions* $\mathbf{y}_Z$, and defined as

$$\mathbf{y} = \frac{1}{c_{\mathrm{T}}}\mathbf{c} \quad \text{and} \quad \mathbf{y}_Z = \frac{1}{c_{\mathrm{T}}}\mathbf{c}_Z, \tag{5.28}$$

respectively. These afford the fundamental properties that

$$\mathbf{1}^{\top}\mathbf{y} = 1 \quad \text{and} \quad \boldsymbol{\nu}_Z^{\top}\mathbf{y}_Z = 1, \tag{5.29}$$

and are independent of temperature or pressure.

5.5 Governing equations in a salt–charge basis

Since the component concentrations and component fluxes in a salt–charge basis come from $\mathbf{c}$ and $\vec{\mathbf{n}}$ through the same linear transformation, the move to a salt–charge basis preserves the structure of material balances. In the absence of homogenous reactions,

all the species continuity equations are summarized in matrix form as

$$\frac{\partial \mathbf{c}}{\partial t} = -\vec{\nabla} \cdot \vec{\mathbf{n}}. \tag{5.30}$$

(Given any column $\vec{\mathbf{v}}$, the operation $\vec{\nabla} \cdot \vec{\mathbf{v}}$ forms a column matrix whose ith entry is the scalar $\vec{\nabla} \cdot \vec{v}_i$.) Multiplication by $\mathbf{Z}^{-\top}$ and use of equations (5.16) and (5.21) yields

$$\frac{\partial \mathbf{c}_Z}{\partial t} = -\vec{\nabla} \cdot \vec{\mathbf{n}}_Z, \tag{5.31}$$

confirming structure preservation. Bringing in the decompositions from equations (5.19) and (5.24), one can alternatively express equation (5.31) as a set of $n-1$ component mole balances,

$$\frac{\partial \mathbf{c}_\nu}{\partial t} = -\vec{\nabla} \cdot \vec{\mathbf{n}}_\nu, \tag{5.32}$$

along with the single equation

$$\frac{\partial \rho_\mathrm{e}}{\partial t} = -\vec{\nabla} \cdot \vec{i}, \tag{5.33}$$

which establishes charge continuity. Note that any model governed by species material balances which also incorporates Faraday's law is compatible with Maxwellian electrodynamics, because Maxwell's equations imply a charge-continuity relationship identical to equation (5.33) [86].

Because the transformations that form $\mathbf{c}_Z$ and $\vec{\mathbf{n}}_Z$ preserve the structure of the dissipation function, they also preserve the structure of the Onsager–Stefan–Maxwell constitutive laws. Equation (5.1) takes the matrix form

$$-\vec{\nabla}\boldsymbol{\mu} = \mathbf{M}^{\mathbf{c}}\vec{\mathbf{n}}. \tag{5.34}$$

Equations (5.11) and (5.21) show that this transforms to

$$-\vec{\nabla}\boldsymbol{\mu}_Z = \mathbf{M}_Z\vec{\mathbf{n}}_Z \tag{5.35}$$

over a salt–charge basis. The transport matrix $\mathbf{M}_Z$ in the salt–charge representation of the Onsager–Stefan–Maxwell laws relates to the matrix $\mathbf{M}$ from equation (5.2) through

$$\mathbf{M}_Z = \mathbf{Z}\mathbf{M}^{\mathbf{c}}\mathbf{Z}^\top, \tag{5.36}$$

a congruence transformation. It follows from this congruence that $\mathbf{M}^{\mathbf{c}}$ is symmetric if and only if $\mathbf{M}_Z$ is symmetric, so that the Onsager–Stefan–Maxwell transport coefficients retain symmetry when expressed over a salt–charge basis. Sylvester's law of inertia implies further that the signatures and ranks of $\mathbf{M}^{\mathbf{c}}$ and $\mathbf{M}_Z$ equate. As mentioned before, the non-dissipative nature of convection implies that $\mathbf{M}^{\mathbf{c}}$ affords $\mathbf{c}$ as its sole null eigenvector; in light of congruence relation (5.36) and Sylvester's law, this implies that $\mathbf{c}_Z$ is the sole null eigenvector of $\mathbf{M}_Z$.

Thus, transformation to a salt–charge basis preserves the structure of the differential balance equations as well as all spectral properties of the Onsager–Stefan–Maxwell equations. Both $\mathbf{M}^{\mathbf{c}}$ and $\mathbf{M}_Z$ are symmetric matrices, and each affords a single null eigenvector. Although the null spaces of $\mathbf{M}^{\mathbf{c}}$ and $\mathbf{M}_Z$ generally differ, each matrix affords just one null eigenvector ($\mathbf{c}$ and $\mathbf{c}_Z$, respectively). The nonzero eigenvalues of $\mathbf{M}^{\mathbf{c}}$ generally differ in magnitude from those of $\mathbf{M}_Z$, but both sets are all positive.

5.6 The salt–charge potential

It is prudent to introduce a thermodynamic potential with units of voltage to quantify electrical energy and power. To put electricity in a thermodynamic context, however, one must acknowledge an essential limitation on how electrochemical equilibria are parametrized.

When proposing the electrochemical potential concept, Guggenheim introduced constitutive laws

$$\mu_i = RT \ln a_i + F z_i \Phi, \tag{5.37}$$

in which a_i represents the chemical activity of species i and Φ is an electric potential in the solution phase [75, 76, 116]. Observing that the equilibrium compositions of practical macroscopic systems cannot be adjusted along paths that violate global electroneutrality, Guggenheim noted that the partitioning of electrochemical potentials into chemical and electrical parts is necessarily ambiguous. Therefore a model of electrolyte energetics must never depend on the chemical activity of a single charged species in isolation [76]. To cast this notion formally, define a non-neutral free-energy contribution μ_z, written in terms of Guggenheim's species activities and solution potential as

$$\mu_z = \frac{1}{\|\mathbf{z}\|} \sum_{i=1}^{n} z_i \mu_i = \frac{RT}{\|\mathbf{z}\|} \sum_{i=1}^{n} z_i \ln a_i + F \|\mathbf{z}\| \Phi. \tag{5.38}$$

Guggenheim's principle states that no macroscopic experiment can discern the term that involves the solution potential Φ in this expression from those involving the species activities a_i [75].

Rather than using the solution potential Φ, we instead employ a quantity we call the *salt–charge potential* Φ_z, defined as

$$\Phi_z = \frac{\mu_z}{F \left\| \mathbf{z} \right\|}. \tag{5.39}$$

Guggenheim's principle requires that no experiment can distinguish chemical and electrical contributions to Φ_z. Despite this ambiguity, one can still understand the salt–charge potential Φ_z as a type of electrical potential. Inserting decompositions (5.12) and (5.19), then introducing definition (5.39) recasts the Euler equation for $\tilde{G}$ as

$$\tilde{G} = \boldsymbol{\mu}_\nu^\top \mathbf{c}_\nu + \Phi_z \rho_\mathrm{e}. \tag{5.40}$$

Here, the $\Phi_z \rho_\mathrm{e}$ term apparently quantifies excess coulomb energy, that is, the available energy associated with imbalanced charge. Similarly, inserting decompositions (5.12) and (5.24) restates the dissipation as

$$T\dot{s} = \vec{\mathbf{n}}_\nu^\top \cdot \left(-\vec{\nabla} \boldsymbol{\mu}_\nu \right) + \vec{i} \cdot \left(-\vec{\nabla} \Phi_z \right). \tag{5.41}$$

The $-\vec{i} \cdot \vec{\nabla} \Phi_z$ term is the local ohmic loss — the rate of energy dissipation associated with electrical current flow. Observe that local electroneutrality makes the coulomb term disappear from $\tilde{G}$, but leaves the ohmic term in $T\dot{s}$.

Although the species material balances summarized in equation (5.30) imply charge-continuity equation (5.33), and are therefore compatible with Maxwell's equations, equilibrium thermodynamics cannot provide insight into the Maxwellian electric field, because Guggenheim's principle mandates that it is impossible to determine experimentally whether or not $-\vec{\nabla} \Phi_z$ is a purely electrical quantity.

Still, the energy density and dissipative power associated with salt–charge potential (and its gradient) have unambiguous meanings, because the coulomb term in $\tilde{G}$ and ohmic term in $T\dot{s}$ do not vary with the choice of components. Whereas one can only speak of 'a' salt–charge basis since $\mathbf{Z}$ is not always unique, one may refer to 'the' salt–charge potential, which is unique for a given set of equivalent charges $\mathbf{z}$.

5.7 Thermodynamic factors in a salt–charge basis

To implement a simulation of any transport system, one requires constitutive relationships that express how thermodynamic potentials depend on the concentrations of extensive properties. The particular mapping that sends composition gradients into electrochemical-potential gradients in isothermal, isobaric situations is expressed by a matrix of equilibrium properties commonly referred to as *thermodynamic factors*, introduced in the last chapter as $\boldsymbol{\chi}$.

For an isothermal, isobaric, n-species mass-transport system, the thermodynamic factors depend parametrically on $\frac{1}{2}n\,(n-1)$ composition-dependent state functions — one state function for every pair of species [70, 110, 145]. In their discussion of Onsager reciprocal relations for multicomponent diffusion, Monroe and Newman introduced an $(n-1)\times(n-1)$ matrix of dimensionless Darken factors $\mathbf{Q}$ [109], defined such that

$$\operatorname{diag}(\mathbf{y})\,\vec{\nabla}\boldsymbol{\mu} = RT\boldsymbol{\chi}\vec{\nabla}\mathbf{y} = RT\begin{bmatrix}\mathbf{I}_{n-1}\\ -\mathbf{1}^{\top}\end{bmatrix}\mathbf{Q}\begin{bmatrix}\mathbf{I}_{n-1} & \mathbf{o}\end{bmatrix}^{\top}\vec{\nabla}\mathbf{y}, \tag{5.42}$$

where $\mathbf{I}_{n-1}$ indicates the $(n-1)\times(n-1)$ identity matrix, $\mathbf{o}$ represents a column of zeroes, and the linear operator $\operatorname{diag}(\mathbf{v})$ forms column matrix $\mathbf{v}$ into a diagonal square matrix whose ith diagonal entry is v_i.[2] Each entry Q_{ij} of $\mathbf{Q}$ represents the thermodynamic derivative of the (log) activity of species i with respect to the particle fraction of species $j<n$, leaving temperature, pressure, and all particle fractions save those of species j and n fixed. In terms of Guggenheim's species activities,

$$Q_{ij} = y_i\left(\frac{\partial\ln a_i}{\partial y_j}\right)_{T,p,y_{k\neq j,n}} = \delta_{ij} + y_i\left(\frac{\partial\ln\lambda_i}{\partial y_j}\right)_{T,p,y_{k\neq j,n}}, \tag{5.43}$$

in which δ_{ij} represents the Kronecker delta. Species n must generally be left free to vary when differentiating with composition because the sum of particle fractions is always constrained such that $\mathbf{1}^{\top}\mathbf{y}=1$. The expression in terms of the activity coefficient of species i, λ_i, emphasizes that $\mathbf{Q}=\mathbf{I}_{n-1}$ for an ideal solution.

Although the simplicity of $\mathbf{Q}$ in the ideal case is useful, Maxwell relations among these Darken factors in non-ideal situations are obscure. It is sometimes convenient to

[2] Generally $\operatorname{diag}(\mathbf{a})\,\mathbf{b} = \operatorname{diag}(\mathbf{b})\,\mathbf{a}$; both products form a column $\mathbf{c}$ with entries $c_i = a_i b_i$. Also $\mathbf{1}^{\top}\operatorname{diag}(\mathbf{a}) = \mathbf{a}^{\top}$ and $\operatorname{diag}(\mathbf{a})\mathbf{1} = \mathbf{a}$. The notation $\operatorname{diag}(\mathbf{a})^{-1}$ indicates the diagonal matrix whose ith entry is $1/a_i$, such that $\operatorname{diag}(\mathbf{a})^{-1}\,\mathbf{a} = \mathbf{1}$.

work instead with the $(n-1) \times (n-1)$ Hessian matrix $\mathbf{K}$,

$$K_{ij} = \frac{\partial^2}{\partial y_i \partial y_j} \left(\frac{\tilde{G}}{RTc_{\mathrm{T}}} \right)_{T,p,y_{k \neq i,j,n}}, \tag{5.44}$$

for which Maxwell relations imply that $\mathbf{K} = \mathbf{K}^\top$ [110]. Thermodynamic stability demands that $\mathbf{K}$ is positive semidefinite [70]. The Darken factors $\mathbf{Q}$ depend on $\mathbf{K}$ through

$$\mathbf{Q} = \mathbf{Y}^{-1}\mathbf{K}, \tag{5.45}$$

where the definition

$$\mathbf{Y}^{-1} = \begin{bmatrix} \mathbf{I}_{n-1} & \mathbf{o} \end{bmatrix} \left(\operatorname{diag}(\mathbf{y}) - \mathbf{y}\mathbf{y}^\top \right) \begin{bmatrix} \mathbf{I}_{n-1} \\ \mathbf{o}^\top \end{bmatrix} \tag{5.46}$$

puts in matrix form the $(n-1) \times (n-1)$ inverse composition matrix $\mathbf{Y}^{-1}$ employed by Monroe and Newman [111]. Substituting equations (5.45) and (5.46) into equation (5.42) and algebraically simplifying the result gives

$$\vec{\nabla}\boldsymbol{\mu} = RT \left(\mathbf{I} - \mathbf{1}\mathbf{y}^\top \right) \begin{bmatrix} \mathbf{K} & \mathbf{o} \\ \mathbf{o}^\top & 0 \end{bmatrix} \vec{\nabla}\mathbf{y}, \tag{5.47}$$

which shows how the isothermal, isobaric composition dependence of $\vec{\nabla}\boldsymbol{\mu}$ is parametrized by the $\frac{1}{2}n(n-1)$ independent entries of $\mathbf{K}$. Observe that the block matrix here has a nullspace spanned by the null eigenvector $\mathbf{i}_n$, which reflects the fact that gradients $\vec{\nabla}y_n$ have no independent effect on species electrochemical potentials.

Some of the benefits of the Darken matrix $\mathbf{Q}$ can be brought into the analysis of equations expressed in terms of $\mathbf{K}$. The composition Hessian separates into two parts,

$$\mathbf{K} = \mathbf{Y} + \Delta\mathbf{K}, \tag{5.48}$$

such that $\mathbf{Y}$ accounts for derivatives of ideal mixing free energy and $\Delta\mathbf{K}$ expresses the

Hessian of excess free energy. The composition matrix $\mathbf{Y}$ here is written explicitly as

$$\mathbf{Y} = \left[\begin{array}{cc} \mathbf{I}_{n-1} & \mathbf{o} \end{array} \right] \left(\operatorname{diag}(\mathbf{y})^{-1} + \frac{\mathbf{1}\mathbf{1}^{\top}}{\mathbf{i}_n^{\top}\mathbf{y}} \right) \left[\begin{array}{c} \mathbf{I}_{n-1} \\ \mathbf{o}^{\top} \end{array} \right]. \tag{5.49}$$

Upon substitution into equation (5.47), algebraic simplification yields an equivalent alternative form,

$$\begin{aligned} \vec{\nabla}\boldsymbol{\mu} = {} & RT \operatorname{diag}(\mathbf{y})^{-1} \vec{\nabla}\mathbf{y} \\ & + RT \left(\mathbf{I} - \mathbf{1}\mathbf{y}^{\top} \right) \left[\begin{array}{cc} \Delta\mathbf{K} & \mathbf{o} \\ \mathbf{o}^{\top} & 0 \end{array} \right] \vec{\nabla}\mathbf{y}, \end{aligned} \tag{5.50}$$

in which the $(n-1) \times (n-1)$ matrix $\Delta\mathbf{K}$ is symmetric, and vanishes when mixing is ideal.

The nonideal term in equation (5.50) translates readily into a salt–charge basis. Use the congruence relationship

$$\Delta\mathbf{K}_Z = \mathbf{Z} \left[\begin{array}{cc} \Delta\mathbf{K} & \mathbf{o} \\ \mathbf{o}^{\top} & 0 \end{array} \right] \mathbf{Z}^{\top} \tag{5.51}$$

to define a transformed excess Hessian $\Delta\mathbf{K}_Z$. All n^2 entries of this symmetric matrix are generally nonzero. The nullspace of $\Delta\mathbf{K}_Z$ has a minimum dimension of 1, because $\mathbf{Z}^{-\top}\mathbf{i}_n$ is always a null eigenvector. Multiplying equation (5.50) through by $\mathbf{Z}$ and inserting $\Delta\mathbf{K}_Z$, one finds

$$\begin{aligned} \vec{\nabla}\boldsymbol{\mu}_Z = {} & RT\mathbf{Z} \operatorname{diag}(\mathbf{y})^{-1} \vec{\nabla}\mathbf{y} \\ & + RT \left(\mathbf{I} - \boldsymbol{\nu}_Z \mathbf{y}_Z^{\top} \right) \Delta\mathbf{K}_Z \vec{\nabla}\mathbf{y}_Z \end{aligned} \tag{5.52}$$

after using equations (5.11), (5.16), and (5.29) to simplify. The assertion that species potentials depend on independent particle fractions necessitates that component chemical potentials have this structure.

It is noteworthy that the ideal part of the component chemical-potential gradients in equation (5.52) involves entries of the salt–charge transformation $\mathbf{Z}$ as prefactors: the

ideal mixing free energy associated with a salt scales linearly with its ion stoichiometry, rather than logarithmically. Also, multiplication of equation (5.52) from the left by $\mathbf{c}_Z^\top = c_\mathrm{T}\mathbf{y}_Z^\top$ verifies that the Gibbs–Duhem equation is satisfied by constitutive laws (5.52) for any choice of the symmetric excess Hessian matrix $\Delta\mathbf{K}_Z$.

Although equation (5.52) is formally correct, the parameters within $\Delta\mathbf{K}_Z$ are not all measurable. In particular, as discussed after equation (5.38), adherence to Guggenheim's principle demands that the coefficients of $\vec{\nabla}\mathbf{y}_Z$ on the right side of the equation for $\vec{\nabla}\mu_z$ should remain ambiguous because they cannot be disentangled with equilibrium experiments. Therefore it is appropriate to discard this component of the expansion in equation (5.52).

Notation is simplified by defining an $n\times(n-1)$ matrix $\mathbf{N}$, whose columns represent the reactant stoichiometry in the fundamental equilibria:

$$\mathbf{N} = \left[\begin{array}{ccc} \boldsymbol{\nu}_1 & \dots & \boldsymbol{\nu}_{n-1} \end{array}\right], \quad \text{so} \quad \mathbf{Z} = \left[\begin{array}{c} \mathbf{N}^\top \\ \hline \mathbf{z}^\top \\ \hline \|\mathbf{z}\| \end{array}\right]. \tag{5.53}$$

Bringing this quantity in, and noting that $\boldsymbol{\nu} = \mathbf{N}^\top\mathbf{1}$, the general expression

$$\begin{aligned} \vec{\nabla}\boldsymbol{\mu}_\nu =& RT\mathbf{N}^\top \operatorname{diag}(\mathbf{y})^{-1}\vec{\nabla}\mathbf{y} \\ &+ RT\left(\left[\begin{array}{cc} \mathbf{I}_{n-1} & \mathbf{o} \end{array}\right] - \boldsymbol{\nu}\mathbf{y}_Z^\top\right)\Delta\mathbf{K}_Z\vec{\nabla}\mathbf{y}_Z \end{aligned} \tag{5.54}$$

expresses the portion of the expansion that remains after striking the last row of matrix equation (5.52). In the next section, this form of the component chemical-potential gradients will facilitate analyzing how properties are constrained under the electroneutrality approximation.

5.8 Structural implications of electroneutrality

Imposing local electroneutrality on the Onsager–Stefan–Maxwell transport model impacts both the variables involved and the parameters that quantify material properties. The constraint separately impacts the thermodynamic and dynamical aspects of the general theory.

5.8.1 Electroneutral composition

The simplest consequence of electroneutrality is that it limits the available composition space, because one charged-species concentration becomes linearly dependent on the others. It is useful to establish some relationships that demonstrate the effect of this constraint.

When excess charge density vanishes everywhere, the n-dimensional column of species concentrations $\mathbf{c}$ becomes limited to a set of locally electroneutral species concentrations, which we notate as $\mathbf{c}^0$. Necessarily, any solution compositions in the space that $\mathbf{c}^0$ occupies must be instantiable by assembling neutral components and dissociating them into their constituent species. This idea can be put in mathematical terms by leveraging a salt–charge basis. Over such a basis $\mathbf{c}^0$ is determined by the mapping

$$\mathbf{c}^0 = \mathbf{Z}^\top \begin{bmatrix} \mathbf{c}_\nu \\ 0 \end{bmatrix} = \mathbf{N}\mathbf{c}_\nu, \tag{5.55}$$

which results from equations (5.16) and (5.19) when $\rho_\mathrm{e} = 0$. Thus the first $(n-1)$ columns of $\mathbf{Z}^\top$ (that is, the columns of $\mathbf{N}$) serve as a basis for the subspace occupied by $\mathbf{c}^0$, and the $(n-1)$-dimensional column of electroneutral component concentrations $\mathbf{c}_\nu$ expresses the coordinates of a given $\mathbf{c}^0$ over this basis. Electroneutrality constrains the total concentration's domain in a similar way. The electroneutral total concentration, c_T^0, depends on $\mathbf{c}_\nu$ as

$$c_\mathrm{T}^0 = \mathbf{1}^\top \mathbf{c}^0 = \boldsymbol{\nu}_Z^\top \begin{bmatrix} \mathbf{c}_\nu \\ 0 \end{bmatrix} = \boldsymbol{\nu}^\top \mathbf{c}_\nu, \tag{5.56}$$

simplified with the definition of $\boldsymbol{\nu}$ from equation (5.27).

Some additional physical principles outside thermodynamics restrict the range of neutral compositions. Since negative species molarities are meaningless, every entry of $\mathbf{c}^0$ must be non-negative. Because mass transport has no meaning in the absence of species, c_T^0 is strictly positive. These inequalities place bounds on the entries of the component-composition column $\mathbf{c}_\nu$.

The restrictions on $\mathbf{c}^0$ and c_T^0 also imply that every entry of the electroneutral species fractions, $\mathbf{y}^0$, defined as

$$\mathbf{y}^0 = \frac{1}{c_\mathrm{T}^0}\mathbf{c}^0 = \mathbf{Z}^\top \begin{bmatrix} \mathbf{y}_\nu \\ 0 \end{bmatrix} = \mathbf{N}\mathbf{y}_\nu, \tag{5.57}$$

must be strictly non-negative. Under electroneutrality this object retains the property that $\mathbf{1}^\top \mathbf{y}^0 = 1$, established by equation (5.29). Furthermore, the condition

$$\boldsymbol{\nu}^\top \mathbf{y}_\nu = 1 \qquad \text{(electroneutral)} \tag{5.58}$$

constrains component fractions under electroneutrality.

Note that requiring $\mathbf{c}^0$ or $\mathbf{y}^0$ to have non-negative entries does not ensure that every component concentration within $\mathbf{c}_\nu$ (or $\mathbf{y}_\nu$) is non-negative. Over a salt–charge basis, negative component concentrations can occur when the choice of products in the fundamental equilibria is not unique. Consider the solution of Na^+, Cl^-, Mg^{2+} and SO_4^{2-} in H_2O from section 5.2 by way of example. The electroneutral composition space for this solution reaches extremes corresponding to four distinct binary electrolytes: aqueous NaCl with a trace amount of $MgSO_4$; aqueous $MgCl_2$ with trace Na_2SO_4; aqueous Na_2SO_4 with trace $MgCl_2$; and aqueous $MgSO_4$ with trace NaCl. Suppose the neutral salts for a salt–charge basis are chosen to be NaCl, $MgCl_2$, and Na_2SO_4, as in section 5.2. In the laboratory, these salts cannot be mixed with water to produce, say, 1 M aqueous $MgSO_4$. To formulate 1 M $MgSO_4$ with the given precursor salts, one would have to add Na_2SO_4 to supply the sulfate, add $MgCl_2$ to introduce magnesium, and then utilize a separation process (e.g., precipitation, heterogeneous extraction, etc.) to remove NaCl. Thus, aqueous 1 M $MgSO_4$ is represented by a $\mathbf{c}_\nu$ column with entries for 1 M Na_2SO_4, 1 M $MgCl_2$, and -2 M NaCl. Although the NaCl molarity is negative, that of every ion remains non-negative. Since $MgSO_4$ can be formed by recombination reaction (5.8), its chemical potential depends unambiguously on those of Na_2SO_4, $MgCl_2$, and NaCl. The negative concentration just indicates that NaCl is a product of a recombination reaction, rather than a reactant.

5.8.2 Component activity coefficients

Electroneutrality has ramifications for Guggenheim's constitutive framework. Definition (5.37) can be rewritten in terms of species activity coefficients λ_i^0 as

$$\begin{aligned} \mu_i^0 &= \mu_i^\ominus + RT \ln\left(\lambda_i^0 y_i^0\right) + z_i F \Phi, \qquad \text{or} \\ \boldsymbol{\mu}^0 &= \boldsymbol{\mu}^\ominus + RT \ln\left(\mathbf{y}^0\right) + RT \ln\left(\boldsymbol{\lambda}^0\right) + F\Phi \mathbf{z}, \end{aligned} \tag{5.59}$$

where the composition-independent parameters $\mu_i^\ominus$ that make up the n-dimensional column $\boldsymbol{\mu}^\ominus$ quantify species electrochemical potentials in a secondary reference state,

and $\ln(\mathbf{v})$ represents a column matrix wherein each entry is the natural logarithm of the corresponding entry of $\mathbf{v}$. Thermodynamic consistency mandates that every activity coefficient comprising $\boldsymbol{\lambda}^0$ is positive. Since $(\mathbf{c}^0)^\top \mathbf{z} = 0$ by design, these constitutive laws meet the requirement that

$$\tilde{G} = \left(\mathbf{c}^0\right)^\top \boldsymbol{\mu}^0 = \mathbf{c}_\nu^\top \boldsymbol{\mu}_\nu^0 \tag{5.60}$$

as a consequence of equations (5.11) and (5.55).

Constitutive laws for component chemical potentials that are consistent with Guggenheim's formulation are identified by using the second equality in equation (5.60), which implies

$$\left(\mathbf{c}^0\right)^\top \mathbf{Z}^{-1} \left(\mathbf{Z}\boldsymbol{\mu}^0 - \boldsymbol{\mu}_Z^0\right) = 0. \tag{5.61}$$

Insertion of equations (5.53) and (5.59) into equation (5.61), followed by partitioning of $\boldsymbol{\mu}_Z^0$ with equation (5.12), application of the relation $\mathbf{Z}\mathbf{z} = \|\mathbf{z}\|\,\mathbf{i}_n$, and substitution of Φ in favor of Φ_z^0 with equations (5.38) and (5.39), reveals that Guggenheim's laws are consistent with component chemical potentials constituted by equations of the form

$$\mu_{\nu,k}^0 = \mu_{\nu,k}^\ominus + RT \sum_{m=1}^{n} \nu_{km} \ln y_m^0 + RT\nu_k \ln \lambda_{\nu,k}^0, \tag{5.62}$$

wherein $\mu_{\nu,k}^\ominus(T,p)$ is the chemical potential of component k in the reference state and ν_k is the kth entry of the column $\boldsymbol{\nu}$ that quantifies total component stoichiometry. The parameter $\lambda_{\nu,k}^0$ is called the *mean molar activity coefficient* of component k.

All of the component chemical-potential constitutive laws can therefore be summarized by a matrix equation,

$$\boldsymbol{\mu}_\nu^0 = \boldsymbol{\mu}_\nu^\ominus + \boldsymbol{\mu}_\nu^{0,\text{ideal}} + RT\,\text{diag}(\boldsymbol{\nu}) \ln \boldsymbol{\lambda}_\nu^0, \tag{5.63}$$

wherein the term

$$\boldsymbol{\mu}_\nu^{0,\text{ideal}} = RT\mathbf{N}^\top \ln \mathbf{y}^0 \tag{5.64}$$

accounts for the part of a component's chemical potential attributable to ideal mixing, and the reference chemical potentials and mean molar activity coefficients of each component make up the $(n-1)$-dimensional columns $\boldsymbol{\mu}_\nu^\ominus$ and $\boldsymbol{\lambda}_\nu^0$, respectively: the

expression

$$\boldsymbol{\mu}_{\nu}^{\ominus} = \mathbf{N}^{\top}\boldsymbol{\mu}^{\ominus}, \quad \text{or} \quad \mu_{\nu,k}^{\ominus} = \sum_{m=1}^{n} \nu_{km}\mu_{m}^{\ominus}, \tag{5.65}$$

where $k \in \{1, ..., n-1\}$, shows how reactant stoichiometries in the fundamental equilibria relate the reference potentials of components and species, and

$$\begin{aligned} \ln \boldsymbol{\lambda}_{\nu}^{0} &= \operatorname{diag}(\boldsymbol{\nu})^{-1}\mathbf{N}^{\top} \ln \boldsymbol{\lambda}^{0}, \quad \text{or} \\ \ln \lambda_{\nu,k}^{0} &= \sum_{m=1}^{n} \frac{\nu_{km}}{\nu_{k}} \ln \lambda_{m}^{0}, \end{aligned} \tag{5.66}$$

puts the mean molar component activity coefficients in terms of species activity coefficients. Note that the versions of equations (5.65) and (5.66) written in terms of summations identify with definitions stated by Guggenheim [76] and Newman [116].

5.8.3 Electroneutral thermodynamic factors

Applying electroneutrality to equations (5.25) and (5.40) reveals equilibrium energetics to be independent of Φ_{z}^{0}. The electroneutral Euler and Gibbs–Duhem equations,

$$\tilde{G} = \left(\boldsymbol{\mu}_{\nu}^{0}\right)^{\top}\mathbf{c}_{\nu} \tag{5.67}$$

and

$$\mathbf{c}_{\nu}^{\top}\vec{\nabla}\boldsymbol{\mu}_{\nu}^{0} = \vec{0}, \tag{5.68}$$

respectively, imply that isothermal, isobaric component chemical potentials have the functionality $\boldsymbol{\mu}_{\nu}^{0} = \boldsymbol{\mu}_{\nu}^{0}(\mathbf{c}_{\nu})$, or, equivalently, $\boldsymbol{\mu}_{\nu}^{0}(\mathbf{y}_{\nu})$.[3] The mean molar activity coefficients in electroneutral constitutive laws (5.63) thus depend only on $\mathbf{y}_{\nu}$ at constant temperature and pressure.

These facts come together with the discussion of Darken factors from section 5.7 to establish Maxwell relations and component thermodynamic factors for the electroneu-

[3]The implication $\boldsymbol{\mu}_{\nu}^{0}(\mathbf{c}_{\nu}) \implies \boldsymbol{\mu}_{\nu}^{0}(\mathbf{y}_{\nu})$ relies on the fact that total concentration depends only on the species particle fractions at fixed temperature and pressure. This is justified by Euler equation (5.13) because the molar Gibbs energy $\overline{G} = \tilde{G}/c_{\mathrm{T}}$ must produce the molar volume $1/c_{\mathrm{T}}$ through the derivative $(\partial\overline{G}/\partial p)_{T,y_i} = 1/c_{\mathrm{T}}$.

tral Onsager–Stefan–Maxwell diffusion driving forces. Let

$$\Lambda^0_{\nu,ij} = \nu_i \left(\frac{\partial \ln \lambda^0_{\nu,i}}{\partial y_{\nu,j}} \right)_{T,p,y_{\nu,k\neq j,n-1}} \tag{5.69}$$

represent the partial derivative of the mean molar activity coefficient of component i with respect to the fraction of component j, leaving all of the $n-1$ component fractions save the jth and $(n-1)$th fixed. In light of Gibbs–Duhem equation (5.68), the component chemical-potential gradients can be expanded as

$$\begin{aligned} \vec{\nabla}\boldsymbol{\mu}^0_\nu =& \vec{\nabla}\boldsymbol{\mu}^{0,\text{ideal}}_\nu \\ &+ RT\left(\mathbf{I}_{n-1} - \boldsymbol{\nu}\mathbf{y}_\nu^\top\right) \begin{bmatrix} \boldsymbol{\Lambda}^0_\nu & \mathbf{o} \\ \mathbf{o}^\top & 0 \end{bmatrix} \vec{\nabla}\mathbf{y}_\nu, \end{aligned} \tag{5.70}$$

in which $\boldsymbol{\Lambda}^0_\nu$ is an $(n-2)\times(n-2)$ matrix of electroneutral component Darken factors, and

$$\begin{aligned} \vec{\nabla}\boldsymbol{\mu}^{0,\text{ideal}}_\nu &= RT\mathbf{N}^\top \operatorname{diag}\left(\mathbf{y}^0\right)^{-1} \vec{\nabla}\mathbf{y}^0 \\ &= RT\mathbf{N}^\top \operatorname{diag}\left(\mathbf{N}\mathbf{y}_\nu\right)^{-1} \mathbf{N}\vec{\nabla}\mathbf{y}_\nu \end{aligned} \tag{5.71}$$

expresses the gradient of the ideal contribution to every component chemical potential.

Equation (5.70) contains $(n-2)^2$ excess component Darken factors $\Lambda^0_{\nu,ij}$, but these are not all independent because of Maxwell relations, whose structure can be understood by revisiting the electroneutral form of equation (5.54). After insertion of equation (5.71) and simplification with equation (5.57), equation (5.54) becomes

$$\vec{\nabla}\boldsymbol{\mu}^0_\nu = \vec{\nabla}\boldsymbol{\mu}^{0,\text{ideal}}_\nu + RT\left(\mathbf{I}_{n-1} - \boldsymbol{\nu}\mathbf{y}_\nu^\top\right)\Delta\mathbf{K}^0_\nu\vec{\nabla}\mathbf{y}_\nu, \tag{5.72}$$

in which the $(n-1)\times(n-1)$ matrix $\Delta\mathbf{K}^0_\nu$ is formed by striking the nth row and nth column of $\Delta\mathbf{K}^0_Z$,

$$\Delta\mathbf{K}^0_\nu = \begin{bmatrix} \mathbf{I}_{n-1} & \mathbf{o} \end{bmatrix} \Delta\mathbf{K}^0_Z \begin{bmatrix} \mathbf{I}_{n-1} \\ \mathbf{o}^\top \end{bmatrix}, \tag{5.73}$$

and is consequently symmetric. Equating the right sides of equations (5.70) and (5.72)

shows that

$$\left(\mathbf{I}_{n-1} - \boldsymbol{\nu}\mathbf{y}_\nu^\top\right) \begin{bmatrix} \boldsymbol{\Lambda}_\nu^0 & \mathbf{o} \\ \mathbf{o}^\top & 0 \end{bmatrix} = \left(\mathbf{I}_{n-1} - \boldsymbol{\nu}\mathbf{y}_\nu^\top\right) \Delta\mathbf{K}_\nu^0, \tag{5.74}$$

which relates the thermodynamic factors that make up $\boldsymbol{\Lambda}_\nu^0$ to the truncated excess Hessian $\Delta\mathbf{K}_\nu^0$. Compatibility of the species and component perspectives thus demands that the last column of $\Delta\mathbf{K}_\nu^0$ lies in the nullspace of $\left(\mathbf{I}_{n-1} - \boldsymbol{\nu}\mathbf{y}_\nu^\top\right)$, that is, it must be proportional to $\boldsymbol{\nu}$. (Guggenheim's principle demands that the constant of proportionality cannot be determined, however.) The last row of $\Delta\mathbf{K}_\nu^0$ is therefore proportional to $\boldsymbol{\nu}^\top$, as required by the Hessian's symmetry. Multiplication through by $\mathbf{y}_\nu^\top$ additionally verifies that the last row of equation (5.74) is linearly dependent, since Gibbs–Duhem relations constrain both sides of the equality in the same way.

In short, the last row of equation (5.74) is redundant, and the last column, trivial. Discarding these, isolating the truncated Hessian that remains by exploiting a Sherman–Morrison formula, and further rearranging demonstrates that for all $i \neq j$, the Maxwell relations

$$\nu_i \left(\frac{\partial \ln \lambda_{\nu,i}^0}{\partial y_{\nu,j}}\right)_{T,p,y_{\nu,k\neq j,n-1}} = \nu_j \left(\frac{\partial \ln \lambda_{\nu,j}^0}{\partial y_{\nu,i}}\right)_{T,p,y_{\nu,k\neq i,n-1}} \tag{5.75}$$

hold; the matrix $\boldsymbol{\Lambda}_\nu^0$ is symmetric. This substantiates the claim that $\frac{1}{2}(n-1)(n-2)$ properties, which quantify isothermal, isobaric gradients of $n-1$ component chemical potentials, parametrize the mixing free energy of any n-ary electroneutral electrolyte.

Henceforth, we will write the electroneutral gradients of component chemical potentials in the more compact form

$$\vec{\nabla}\boldsymbol{\mu}_\nu^0 = RT\mathbf{X}_\nu^0\vec{\nabla}\mathbf{y}_\nu, \tag{5.76}$$

where the $(n-1)\times(n-1)$ matrix of electroneutral thermodynamic factors $\mathbf{X}_\nu^0$ is defined as

$$\begin{aligned} \mathbf{X}_\nu^0 =& \mathbf{N}^\top \operatorname{diag}\left(\mathbf{N}\mathbf{y}_\nu\right)^{-1}\mathbf{N} \\ &+ \left(\mathbf{I}_{n-1} - \boldsymbol{\nu}\mathbf{y}_\nu^\top\right) \begin{bmatrix} \boldsymbol{\Lambda}_\nu^0 & \mathbf{o} \\ \mathbf{o}^\top & 0 \end{bmatrix}, \end{aligned} \tag{5.77}$$

wherein $\mathbf{\Lambda}_\nu^0 = (\mathbf{\Lambda}_\nu^0)^\top$, and equation (5.69) establishes how independent entries in $\mathbf{\Lambda}_\nu^0$ can be measured experimentally.

5.8.4 Electroneutrality and dynamics

Applying electroneutrality to the dynamical governing equations (that is the OSM equations and the continuity equations) is simpler than electroneutral thermodynamics. When excess charge density vanishes, there is no change to the $(n-1)$-dimensional component material balance equation (5.32) that was produced by moving to a salt–charge basis. Charge continuity, embodied by equation (5.33), does simplify slightly, to

$$\vec{\nabla} \cdot \vec{i} = 0, \qquad \text{(electroneutral)} \tag{5.78}$$

which expresses Kirchhoff's law of the node.

Entries in the Onsager transport matrix from equation (5.2) change their structure under electroneutrality. The transport matrix $\mathbf{M}^{\mathbf{c}^0}$ that relates species fluxes to species driving forces in the electroneutral case has entries

$$M_{ij}^{\mathbf{c}^0} = \begin{cases} -\dfrac{RT}{c_{\mathrm{T}}^0 \mathscr{D}_{ij}} & \text{if } i \neq j \\ \dfrac{RT}{c_{\mathrm{T}}^0} \displaystyle\sum_{k \neq i}^{n} \dfrac{c_k^0}{\mathscr{D}_{ik} c_j^0} & \text{if } i = j, \end{cases} \tag{5.79}$$

in which the neutral composition descriptors $\mathbf{c}^0$ and c_{T}^0 are given in terms of the component concentrations $\mathbf{c}_\nu$ by equations (5.55) and (5.56), respectively. Although the n species concentrations here depend only on $n-1$ component concentrations from a salt–charge basis, the effect is relatively minor because the constraint does not affect the rank of $\mathbf{M}^{\mathbf{c}^0}$.

When the whole set of Onsager–Stefan–Maxwell equations is sent into a salt–charge basis, the transport coefficients that appear after applying electroneutrality follow from congruence relation (5.36):

$$\mathbf{M}_Z^0 = \mathbf{Z}\mathbf{M}^{\mathbf{c}^0}\mathbf{Z}^\top = \begin{bmatrix} \mathbf{M}_\nu & \mathbf{m}_z \\ \mathbf{m}_z^\top & M_{zz} \end{bmatrix}. \tag{5.80}$$

The second equality here defines sub-blocks that will be useful for expressing other

macroscopic transport properties in terms of the electroneutral Onsager drag coefficients over a salt–charge basis, $\mathbf{M}_Z^0$. Sub-block $\mathbf{M}_\nu$ is an $(n-1) \times (n-1)$ square matrix, $\mathbf{m}_z$, an $(n-1)$-dimensional column matrix, and M_{zz}, a scalar.

Recall from section 5.5 that the change to a salt–charge basis implies $\mathbf{c}_Z$ is the sole null eigenvector of $\mathbf{M}_Z$. After electroneutrality is adopted, the column $\mathbf{c}_Z^0$, defined as

$$\mathbf{c}_Z^0 = \begin{bmatrix} \mathbf{c}_\nu \\ 0 \end{bmatrix}, \tag{5.81}$$

is a null eigenvector of $\mathbf{M}_Z^0$. This in turn implies that

$$\mathbf{M}_\nu \mathbf{c}_\nu = \mathbf{o}, \tag{5.82}$$

which is to say, the column of component concentrations is a null eigenvector of the symmetric sub-block $\mathbf{M}_\nu$, and also that

$$\mathbf{m}_z^\top \mathbf{c}_\nu = 0, \tag{5.83}$$

so that the column $\mathbf{m}_z$ is orthogonal to the component concentrations.

Once the transport matrix from equation (5.80) has been incorporated, the Onsager–Stefan–Maxwell equations over a salt–charge basis from equation (5.35) become

$$-\begin{bmatrix} \vec{\nabla}\boldsymbol{\mu}_\nu^0 \\ F\,\|\mathbf{z}\|\,\vec{\nabla}\Phi_z^0 \end{bmatrix} = \begin{bmatrix} \mathbf{M}_\nu & \mathbf{m}_z \\ \mathbf{m}_z^\top & M_{zz} \end{bmatrix} \begin{bmatrix} \vec{\mathbf{n}}_\nu \\ \dfrac{\vec{i}}{F\,\|\mathbf{z}\|} \end{bmatrix} \tag{5.84}$$

after local electroneutrality is assumed. The transport matrix here is symmetric positive semidefinite and affords the single null eigenvector $\mathbf{c}_Z^0$, preserving the spectral structure of the species flux laws. Bear in mind that the component chemical potential gradients $\vec{\nabla}\boldsymbol{\mu}_\nu^0$ are parametrized by a set of thermodynamic factors $\mathbf{X}_\nu^0$ dependent on $\mathbf{y}_\nu$ and a matrix of material parameters through equations (5.77), in turn constrained by the symmetry of the excess property matrix $\boldsymbol{\Lambda}_\nu^0$. Henceforth we call equation (5.84), with $\vec{\nabla}\boldsymbol{\mu}_\nu^0$ parametrized by equations (5.76) and (5.77), the *electroneutral Onsager–Stefan–Maxwell equations*.

5.9 Flux-explicit formulation

Typical constitutive frameworks for electrolytic transport, including the standard concentrated-solution theory and the Nernst–Planck equations, are written in flux-explicit forms. Laws giving component flux and current density in terms of the gradients of composition and voltage can be derived from force-explicit Onsager–Stefan–Maxwell equations with the inversion process of detailed in Chapter 4. Flux-explicit constitutive laws for diffusion must generally be expressed in terms of excess species fluxes, so the inversion necessitates choosing a bulk velocity to associate with the rate of convection.

Compatibility with the familiar mass continuity equation is ensured by adopting the mass-average (barycentric) velocity as the reference for convection, as implemented in Chapter 3. To incorporate mass into the governing framework, let $\overline{m}_i$ represent the molar mass of species i, and assemble the set of these masses into an n-dimensional column $\overline{\mathbf{m}}$. The mass density ρ of a multi-species solution is generally given by

$$\rho = \sum_{i=1}^{n} \overline{m}_i c_i = \overline{\mathbf{m}}^\top \mathbf{c}. \tag{5.85}$$

Further let ψ_i represent a weighting factor with units of inverse molarity (or, equivalently, molar volume),

$$\psi_i = \frac{\overline{m}_i}{\rho}, \qquad \text{or} \qquad \boldsymbol{\psi} = \frac{\overline{\mathbf{m}}}{\rho}, \tag{5.86}$$

where the second relationship summarizes the definition for all i by introducing an n-dimensional column matrix $\boldsymbol{\psi}$ with entries ψ_i. Note that equation (5.85) implies a general constraint among the weighting factors,

$$\boldsymbol{\psi}^\top \mathbf{c} = 1, \tag{5.87}$$

that is, the species mass fractions $\psi_i c_i$ sum to unity. The mass-average velocity $\vec{v}$, and excess molar fluxes $\vec{\mathbf{j}}$ are then given by

$$\vec{v} = \boldsymbol{\psi}^\top \vec{\mathbf{n}} \qquad \vec{\mathbf{j}} = \vec{\mathbf{n}} - \vec{v}\,\mathbf{c}. \tag{5.88}$$

where the latter equation introduces the n-dimensional column $\vec{\mathbf{j}}$ whose entries are each of the $\vec{J}_i = \vec{N}_i - c_i \vec{v}$ in sequence. In light of equations (5.87), multiplication of equation

(5.88) through by $\boldsymbol{\psi}^\top$ reveals

$$\boldsymbol{\psi}^\top \vec{\mathbf{j}} = \vec{0}, \tag{5.89}$$

the kinematic relation among the excess species fluxes (4.28).

Electroneutrality affects density and the kinematic relation in different ways. Application of electroneutrality to equation (5.85) and insertion of equation (5.55) show that density is a function of $n-1$ component concentrations,

$$\rho^0 = \overline{\mathbf{m}}^\top \mathbf{c}^0 = \overline{\mathbf{m}}_\nu^\top \mathbf{c}_\nu, \tag{5.90}$$

in which $\overline{\mathbf{m}}_\nu = \mathbf{N}^\top \overline{\mathbf{m}}$ is an $(n-1)$-dimensional column comprising the component molar masses. Excess species fluxes then transform into the salt–charge basis as

$$\vec{\mathbf{j}}_Z = \mathbf{Z}^{-\top} \vec{\mathbf{j}} = \begin{bmatrix} \vec{\mathbf{j}}_\nu \\ \dfrac{\vec{i} - \rho_\mathrm{e} \vec{v}}{F \left\| \mathbf{z} \right\|} \end{bmatrix} \tag{5.91}$$

because $\rho_\mathrm{e} = F \mathbf{z}^\top \mathbf{c}$. Imposing local electroneutrality on $\vec{\mathbf{j}}_Z$ here reveals that the current density is independent of convection. Under electroneutrality the last entry of $\vec{\mathbf{j}}_Z^0$ does not vanish, however, and consequently the dimensionality of the domain of excess fluxes does not reduce in the same way that the domain of ρ^0 reduced.

Defining $\boldsymbol{\psi}_Z = \mathbf{Z}\boldsymbol{\psi}$, one can change basis to write the kinematic relation as

$$\boldsymbol{\psi}_Z^\top \vec{\mathbf{j}}_Z = \vec{0}, \tag{5.92}$$

showing that the column of component fluxes is orthogonal to $\boldsymbol{\psi}_Z^\top$. Electroneutral species fluxes $\vec{\mathbf{j}}^0$ depend on the component excess fluxes over a salt–charge basis, $\vec{\mathbf{j}}_\nu$, as

$$\vec{\mathbf{j}}^0 = \mathbf{Z}^\top \vec{\mathbf{j}}_Z^0 = \mathbf{N} \vec{\mathbf{j}}_\nu + \frac{\vec{i}}{F \left\| \mathbf{z} \right\|} \cdot \frac{\mathbf{z}}{\left\| \mathbf{z} \right\|}, \tag{5.93}$$

a form that necessarily includes the current, as well as the excess component fluxes.

Through equation (5.91), the electroneutral Onsager–Stefan–Maxwell equations (5.84) become

$$- \begin{bmatrix} \vec{\nabla} \boldsymbol{\mu}_\nu^0 \\ F \left\| \mathbf{z} \right\| \vec{\nabla} \Phi_z^0 \end{bmatrix} = \begin{bmatrix} \mathbf{M}_\nu & \mathbf{m}_z \\ \mathbf{m}_z^\top & M_{zz} \end{bmatrix} \begin{bmatrix} \vec{\mathbf{j}}_\nu \\ \dfrac{\vec{i}}{F \left\| \mathbf{z} \right\|} \end{bmatrix} \tag{5.94}$$

in terms of the excess component fluxes $\vec{\mathbf{j}}_\nu$. The inversion process developed in Chapter 4 is implemented by forming a matrix $\mathbf{L}_Z^0$ with null eigenvector $\boldsymbol{\psi}_Z$ from $\mathbf{M}_Z^0$, either through the limit process

$$\mathbf{L}_Z^0 = \lim_{\gamma \to 0} \left(\mathbf{M}_Z^0 + \frac{\boldsymbol{\psi}_Z \boldsymbol{\psi}_Z^\top}{\gamma} \right)^{-1} \tag{5.95}$$

or from the algebraic equation

$$\mathbf{L}_Z^0 = \left(\mathbf{M}_Z^0 + \gamma \boldsymbol{\psi}_Z \boldsymbol{\psi}_Z^\top \right)^{-1} - \frac{\mathbf{c}_Z^0 \left(\mathbf{c}_Z^0 \right)^\top}{\gamma}, \tag{5.96}$$

which yields the same result for any nonzero value of the augmentation parameter γ. After partitioning $\mathbf{L}_Z^0$ into the block form

$$\mathbf{L}_Z^0 = \begin{bmatrix} \mathbf{L}_\nu & \mathbf{l}_z \\ \mathbf{l}_z^\top & L_{zz} \end{bmatrix}, \tag{5.97}$$

one can immediately write

$$\begin{bmatrix} \vec{\mathbf{j}}_\nu \\ \hline \dfrac{\vec{i}}{F \left\| \mathbf{z} \right\|} \end{bmatrix} = - \begin{bmatrix} \mathbf{L}_\nu & \mathbf{l}_z \\ \mathbf{l}_z^\top & L_{zz} \end{bmatrix} \begin{bmatrix} \vec{\nabla} \boldsymbol{\mu}_\nu^0 \\ \hline F \left\| \mathbf{z} \right\| \vec{\nabla} \Phi_z^0 \end{bmatrix}, \tag{5.98}$$

the flux-explicit form of the electroneutral Onsager transport laws with respect to a salt–charge basis.

5.10 Conductivity, diffusion, and migration

Transport properties that arise in concentrated-solution theory can be expressed for general multicomponent systems by leveraging the electroneutral Onsager transport laws. First and foremost, the last row of equation (5.98) establishes the MacInnes equation, a current–voltage relation that can be viewed as a modified form of Ohm's law accounting for concentration overpotential. First, identifying the ionic conductivity

κ^0 as[4]

$$\kappa^0 = F^2 \left\|\mathbf{z}\right\|^2 L_{zz}. \tag{5.99}$$

Then further letting an $(n-1)$-entry column $\boldsymbol{\xi}$ represent a set of what we will call *component migration coefficients*, defined by

$$\boldsymbol{\xi} = \frac{1}{L_{zz}} \mathbf{l}_z, \tag{5.100}$$

the MacInnes equation can be written as

$$\vec{i} = -\kappa^0 \vec{\nabla} \Phi_z^0 - \frac{\kappa^0 \boldsymbol{\xi}^\top \vec{\nabla} \boldsymbol{\mu}_\nu^0}{F \left\|\mathbf{z}\right\|} \tag{5.101}$$

in terms of the salt–charge potential and the component chemical potentials.

Values of the migration coefficients must be constrained to ensure that $\boldsymbol{\psi}_Z$ is a null eigenvector of $\mathbf{L}_Z^0$. By partitioning $\boldsymbol{\psi}_Z$ into two parts $\boldsymbol{\psi}_\nu$ and ψ_z such that

$$\boldsymbol{\psi}_Z = \begin{bmatrix} \mathbf{N}^\top \boldsymbol{\psi} \\ \dfrac{\mathbf{z}^\top \boldsymbol{\psi}}{\left\|\mathbf{z}\right\|} \end{bmatrix} = \begin{bmatrix} \boldsymbol{\psi}_\nu \\ \psi_z \end{bmatrix}, \tag{5.102}$$

one can write

$$\boldsymbol{\psi}_\nu^\top \boldsymbol{\xi} = -\psi_z \tag{5.103}$$

to phrase the constraint on migration coefficients entirely in terms of the species charges and molar masses.

Newman writes transport laws in a partially inverted form, where the gradient of electric potential is replaced with current density [116]. Parameters that express information about component diffusivities can be identified through this form as follows. Eliminate $\vec{\nabla} \Phi_z^0$ from the electroneutral Onsager transport laws for the excess component fluxes $\vec{\mathbf{j}}_\nu$ given by equation (5.97). Let the symmetric matrix

$$\overline{\mathbf{L}}_\nu = \frac{RT}{c_{\mathrm{T}}^0} \left(\mathbf{L}_\nu - \frac{\kappa^0 \boldsymbol{\xi} \boldsymbol{\xi}^\top}{F^2 \left\|\mathbf{z}\right\|^2} \right) \tag{5.104}$$

define the set of thermodynamic component diffusivities relative to the mass-average

[4] A definition which can be shown to match Newman's [116, equation (12.42)]. As Newman notes further, this is independent of convective velocity.

velocity, $\overline{\mathbf{L}}_\nu$. Then the laws for excess component fluxes become

$$\vec{\mathbf{j}}_\nu = -\frac{c_{\mathrm{T}}^0 \overline{\mathbf{L}}_\nu}{RT} \vec{\nabla} \boldsymbol{\mu}_\nu^0 + \boldsymbol{\xi} \frac{\vec{i}}{F \left\| \mathbf{z} \right\|}, \tag{5.105}$$

in which $\overline{\mathbf{L}}_\nu$ has the standard units of area per time.

Constitutive laws within concentrated-solution theory are generally put in terms of species fluxes, rather than component fluxes. Such laws can be written using the ionic conductivity, migration coefficients, and the component diffusivity matrix by leveraging equation (5.93). Insertion of equations (5.105) yields

$$\vec{\mathbf{j}}^0 = -\frac{\mathbf{N} \overline{\mathbf{L}}_\nu c_{\mathrm{T}}^0}{RT} \vec{\nabla} \boldsymbol{\mu}_\nu^0 + \left(\mathbf{N} \boldsymbol{\xi} + \frac{\mathbf{z}}{\left\| \mathbf{z} \right\|} \right) \frac{\vec{i}}{F \left\| \mathbf{z} \right\|}, \tag{5.106}$$

an expression useful for understanding the spectral structure of the thermodynamic component diffusivities. Inserting these transport laws into kinematic relation (5.89), introducing $\boldsymbol{\psi}_\nu$ and ψ_z with equation (5.102), and applying equation (5.103) show that

$$-\frac{c_{\mathrm{T}}^0 \boldsymbol{\psi}_\nu^\top \overline{\mathbf{L}}_\nu}{RT} \vec{\nabla} \boldsymbol{\mu}_\nu^0 = \vec{0}, \tag{5.107}$$

for any $\vec{\nabla} \boldsymbol{\mu}_\nu^0$. Thus, because $\overline{\mathbf{L}}_\nu$ is symmetric, it must afford $\boldsymbol{\psi}_\nu$ as a null eigenvector: $\overline{\mathbf{L}}_\nu \boldsymbol{\psi}_\nu = \mathbf{o}$.

Note that in the absence of current density, equation (5.105) reduces to a generalized Fick's law that expresses component excess fluxes solely in terms of the symmetric component-diffusivity matrix $\overline{\mathbf{L}}_\nu$ and without contributions from migration. Miller deployed transport laws of this form in his experimental tests of the Onsager reciprocal relations [106], which confirmed symmetry of the matrix $\overline{\mathbf{L}}_\nu$.

A property count is helpful here. The $(n-1) \times (n-1)$ component-diffusivity matrix $\overline{\mathbf{L}}_\nu$ is symmetric, reducing its number of independent entries by $\frac{1}{2}(n-1)(n-2)$, and affords $\boldsymbol{\psi}_\nu$ as a null eigenvector, adding $(n-1)$ additional constraints; this leaves $\frac{1}{2}(n-1)(n-2)$ of its entries independently specifiable. The $(n-1)$-dimensional column $\boldsymbol{\xi}$ is constrained by species molar masses and equivalent charges by equation (5.103), leaving $(n-2)$ independent migration coefficients. Finally, equation (5.99) defines a single ionic conductivity. Summing up, the symmetric, positive-semidefinite

flux-explicit Onsager matrix with respect to the salt–charge basis breaks down as

$$\mathbf{L}_Z^0 = \frac{c_{\mathrm{T}}^0}{RT}\begin{bmatrix} \overline{\mathbf{L}}_\nu & \mathbf{o} \\ \mathbf{o}^\top & 0 \end{bmatrix} + \frac{\kappa^0}{F^2\left\|\mathbf{z}\right\|^2}\begin{bmatrix} \boldsymbol{\xi}\boldsymbol{\xi}^\top & \boldsymbol{\xi} \\ \boldsymbol{\xi}^\top & 1 \end{bmatrix}, \tag{5.108}$$

in which $\overline{\mathbf{L}}_\nu \boldsymbol{\psi}_\nu = \mathbf{o}$ and $\boldsymbol{\psi}_\nu^\top \boldsymbol{\xi} + \psi_z = 0$, with $\boldsymbol{\psi}_\nu$ and ψ_z defined in terms of stoichiometry in the fundamental equilibria, species molar masses, and species charges through equations (5.86) and (5.102), and consequently depends on $\frac{1}{2}n(n-1)$ independent transport coefficients. This equals the number of Stefan–Maxwell diffusivities that underpin the original transport matrix $\mathbf{M}^0$.

Recently molecular-dynamics techniques have been deployed to measure the Onsager diffusion matrix $\mathbf{L}$, which sits relative to the mass-average velocity and appears in the electroneutral inverted form of equation (5.34) [62],[5]

$$\vec{\mathbf{j}}^0 = -\mathbf{L}^0 \vec{\nabla}\boldsymbol{\mu}^0. \tag{5.109}$$

The transport properties that make up $\mathbf{L}^0$ relate to $\mathbf{M}^0$ directly through

$$\mathbf{M}^0 = \lim_{\gamma \to 0}\left[\mathbf{L}^0 + \frac{\mathbf{c}^0\left(\mathbf{c}^0\right)^\top}{\gamma}\right]^{-1}, \tag{5.110}$$

which is the inversion in limit form as in Chapter 4. The congruence transformation

$$\mathbf{L}_Z^0 = \mathbf{Z}^{-\top}\mathbf{L}^0\mathbf{Z}^{-1} \tag{5.111}$$

also relates the naive Onsager matrix directly to the component diffusivities, migration coefficients, and ionic conductivity over a salt–charge basis through equation (5.108).

5.11 Alternative convective velocities

Up to now we have adopted a convention of defining $\mathbf{L}_Z^0$ and $\vec{\mathbf{j}}$ relative to the mass-average velocity, but it is straightforward to change the kinematic constraint that defines the convective reference velocity in equation (5.88) to any other $\boldsymbol{\psi}'$ satisfying

[5] A molecular dynamics simulation can be described with equation (5.109) if the simulated control volume conserves charge and has characteristic dimensions much larger than the Debye length.

equation (5.87). (For example, letting $\boldsymbol{\psi}' = \mathbf{1}/c_{\mathrm{T}}$ defines the mole-average velocity.) The conversion of the set of excess molar fluxes relative to the mass-average velocity, composed of $\vec{J}_i$, to excess fluxes relative to another velocity, composed of $\vec{J}_i^{\psi'}$, is accomplished by the projection operator

$$\vec{\mathbf{j}}^{\psi'} = \left(\mathbf{I} - \mathbf{c}\boldsymbol{\psi}'^{\top}\right)\vec{\mathbf{j}}. \tag{5.112}$$

Observe that a similar projection can be used to move from excess fluxes that satisfy kinematic relation $\boldsymbol{\psi}'$ back to fluxes in excess of convection at the mass-average reference velocity, through

$$\vec{\mathbf{j}} = \left(\mathbf{I} - \mathbf{c}\boldsymbol{\psi}^{\top}\right)\vec{\mathbf{j}}^{\psi'}. \tag{5.113}$$

Transformation (5.112) can be expressed in terms of excess fluxes over a salt–charge basis as

$$\vec{\mathbf{j}}_Z^{\psi'} = \left[\mathbf{I} - \mathbf{c}_Z(\boldsymbol{\psi}'_Z)^{\top}\right]\vec{\mathbf{j}}_Z, \tag{5.114}$$

where $\boldsymbol{\psi}'_Z = \mathbf{Z}\boldsymbol{\psi}'$.

With an alternative kinematic relation in hand, one can exploit equation (5.95) or (5.96), with $\boldsymbol{\psi}'_Z$ in place of $\boldsymbol{\psi}_Z$, to identify the flux-explicit electroneutral transport relations relative to $\boldsymbol{\psi}'$ as

$$\vec{\mathbf{j}}_Z^{0,\psi'} = -\mathbf{L}_Z^{0,\psi'}\vec{\nabla}\boldsymbol{\mu}_Z^0, \tag{5.115}$$

in which

$$\mathbf{L}_Z^{0,\psi'} = \left[\mathbf{I} - \mathbf{c}_Z^0(\boldsymbol{\psi}'_Z)^{\top}\right]\mathbf{L}_Z^0\left[\mathbf{I} - \boldsymbol{\psi}'_Z(\mathbf{c}_Z^0)^{\top}\right] \tag{5.116}$$

establishes a congruence between $\mathbf{L}_Z^{0,\psi'}$ and $\mathbf{L}_Z^0$. One can also compute $\mathbf{L}_Z^{0,\psi'}$ directly from $\mathbf{M}_Z^0$, using

$$\mathbf{L}_Z^{0,\psi'} = \lim_{\gamma\to 0}\left(\mathbf{M}_Z^0 + \frac{\boldsymbol{\psi}_Z\boldsymbol{\psi}_Z^{\top}}{\gamma}\right)^{-1}, \tag{5.117}$$

which is analogous to equation (5.95). In this new reference frame for the excess fluxes, diffusivities and migration coefficients can be identified by partitioning $\mathbf{L}_Z^{0,\psi'}$ as

$$\begin{aligned}\mathbf{L}_Z^{0,\psi'} =& \frac{c_{\mathrm{T}}^0}{RT}\begin{bmatrix}\overline{\mathbf{L}}_{\nu}^{\psi'} & \mathbf{o}\\ \mathbf{o}^{\top} & 0\end{bmatrix}\\ &+ \frac{\kappa^0}{F^2\left\|\mathbf{z}\right\|^2}\begin{bmatrix}\boldsymbol{\xi}^{\psi'}\left(\boldsymbol{\xi}^{\psi'}\right)^{\top} & \boldsymbol{\xi}^{\psi'}\\ \left(\boldsymbol{\xi}^{\psi'}\right)^{\top} & 1\end{bmatrix},\end{aligned} \tag{5.118}$$

similar to how $\mathbf{L}_Z^0$ is partitioned in equation (5.108). Note that the second matrix on the right is proportional to the outer product of $[\boldsymbol{\xi}^{\psi'}, 1]^\top$, and is consequently positive semidefinite in general.

One can write excess component fluxes relative to the alternative convective velocity and with respect to the salt–charge basis as

$$\vec{\mathbf{j}}_\nu^{\,\psi'} = -\frac{c_{\mathrm{T}}^0 \overline{\mathbf{L}}_\nu^{\psi'}}{RT} \vec{\nabla} \boldsymbol{\mu}_\nu^0 + \boldsymbol{\xi}^{\psi'} \frac{\vec{i}}{F \left\| \mathbf{z} \right\|}, \tag{5.119}$$

which derives from equation (5.105). Here, the component diffusivities relative to the average velocity determined by $\boldsymbol{\psi}'$ are defined as

$$\overline{\mathbf{L}}_\nu^{\psi'} = \left[\mathbf{I}_{n-1} - \mathbf{c}_\nu (\boldsymbol{\psi}'_\nu)^\top \right] \overline{\mathbf{L}}_\nu \left[\mathbf{I}_{n-1} - \boldsymbol{\psi}'_\nu (\mathbf{c}_\nu)^\top \right], \tag{5.120}$$

and

$$\boldsymbol{\xi}^{\psi'} = \left[\mathbf{I}_{n-1} - \mathbf{c}_\nu (\boldsymbol{\psi}'_\nu)^\top \right] \boldsymbol{\xi} - \psi'_z \mathbf{c}_\nu \tag{5.121}$$

defines migration coefficients in the new frame. Similar to the projection in equation (5.113), one can create transformations that change the reference frame from velocity ${\boldsymbol{\psi}'}^\top \vec{\mathbf{n}}$ back to the mass-average velocity by replacing $\boldsymbol{\psi}'_\nu$ with $\boldsymbol{\psi}_\nu$ and ψ'_z with ψ_z in equations (5.120) and (5.121), as well as swapping $\overline{\mathbf{L}}_\nu^{\psi'}$ with $\overline{\mathbf{L}}_\nu$ and $\boldsymbol{\xi}^{\psi'}$ with $\boldsymbol{\xi}$.

In Newman's implementations of concentrated-solution theory [116], one of the species velocities — say, that of species m — is used as the convective reference. Thus the coefficients that Newman identifies in the flux-explicit equations follow from taking $\boldsymbol{\psi}'_Z = \mathbf{Z}\mathbf{i}_m / c_m^0$ in equation (5.116). This produces species flux laws in the form

$$\vec{\mathbf{j}}^{0,\psi'} = -\frac{c_{\mathrm{T}}^0 \mathbf{N} \overline{\mathbf{L}}_\nu^{\psi'}}{RT} \vec{\nabla} \boldsymbol{\mu}_\nu^0 + \left(\mathbf{N} \boldsymbol{\xi}^{\psi'} + \frac{\mathbf{z}}{\left\| \mathbf{z} \right\|} \right) \frac{\vec{i}}{F \left\| \mathbf{z} \right\|}. \tag{5.122}$$

Newman's development also produces a slightly different MacInnes equation,

$$\vec{i} = -\kappa^0 \vec{\nabla} \Phi_z^0 - \frac{\kappa^0}{F \left\| \mathbf{z} \right\|} \left(\boldsymbol{\xi}^{\psi'} \right)^\top \vec{\nabla} \boldsymbol{\mu}_\nu^0, \tag{5.123}$$

wherein the migration coefficients are constrained by kinematic relation $\boldsymbol{\psi}'$, but κ^0 remains unaffected because its value is independent of the choice of convective velocity.

Note that the embedding of an arbitrary reference velocity in flux-explicit transport matrices (e.g., $\mathbf{L}$) makes properties derived from them somewhat ambiguous. When

tabulating transport parameters, it may be preferable to work with the electroneutral transport matrix $\mathbf{M}_Z^0$, which conveys frame-invariant information. The computation of $\mathbf{M}_\nu$ can be accomplished readily given a flux-explicit form; in fact, one can use the procedure of Chapter 4 and a block inversion identity to show that

$$\mathbf{M}_\nu = \frac{RT}{c_{\mathrm{T}}^0} \lim_{\gamma \to 0} \left(\overline{\mathbf{L}}_\nu^{\psi'} + \frac{\mathbf{c}_\nu \mathbf{c}_\nu^\top}{\gamma} \right)^{-1}, \tag{5.124}$$

and also that

$$\mathbf{m}_z = \mathbf{M}_\nu \boldsymbol{\xi}^{\psi'} \quad \text{and} \quad M_{zz} = \frac{F^2 \|\mathbf{z}\|^2}{\kappa^0} + (\boldsymbol{\xi}^{\psi'})^\top \mathbf{M}_\nu \boldsymbol{\xi}^{\psi'} \tag{5.125}$$

for any $\boldsymbol{\psi}'$, elucidating the structure within $\mathbf{M}_Z^0$ through equation (5.80). Despite its basis on a transport matrix $\mathbf{L}_Z^{0,\psi'}$, it should be emphasized that $\mathbf{M}_Z^0$ enjoys uniqueness and is independent of the convective velocity. Notably, the submatrix $\mathbf{M}_\nu$ depends only on the diffusion coefficients. and the only matrix inversion that needs to be performed is that in equation (5.124). The entries of $\mathbf{m}_z$ are zero in the absence of migration, and M_{zz} matches the electric resistivity plus a quadratic correction.

5.12 Transference numbers

Equations (5.101) and (5.106) provide a pair of constitutive equations similar, but not identical, to the familiar equations from concentrated-solution theory and Nernst–Planck dilute-solution theory. To achieve complete agreement one must consider how migration coefficients relate to the transference numbers more familiar from electrochemistry [14, 98, 116]. Let the transference number of species i relative to the mass-average velocity be t_i. These can be formed into an n-dimensional column matrix $\mathbf{t}$, related to the migration coefficients as

$$\mathbf{t} = \frac{\operatorname{diag}(\mathbf{z})}{\|\mathbf{z}\|} \left(\mathbf{N}\boldsymbol{\xi} + \frac{\mathbf{z}}{\|\mathbf{z}\|} \right). \tag{5.126}$$

Multiplication of this result through by $\mathbf{1}^\top$ shows that $\mathbf{1}^\top \mathbf{t} = 1$, that is, transference numbers sum to unity. Note that even in the case of vanishing migration coefficients, the right side of equation (5.126) is non-zero, and the transference numbers become a partition of unity weighted by the species charge. The migration coefficients deviate from this standard.

Sometimes it is desirable to change the reference velocity relative to which transference is expressed. Incorporating the alternative migration coefficient from equation (5.121) into equation (5.126) shows that

$$\mathbf{t}^{\psi'} = \frac{\operatorname{diag}(\mathbf{z})}{\|\mathbf{z}\|}\left(\mathbf{N}\boldsymbol{\xi}^{\psi'} + \frac{\mathbf{z}}{\|\mathbf{z}\|}\right) \tag{5.127}$$

yields the set of species transference numbers relative to the reference velocity established by kinematic relation $\boldsymbol{\psi}'$. These also afford the property that $\mathbf{1}^{\top}\mathbf{t}^{\psi'} = 1$.

Because $\operatorname{diag}(\mathbf{z})$ appears on the right of equation (5.126), t_i vanishes for all i such that $z_i = 0$. Thus, transference numbers as traditionally defined only have meaning for charged species. Importantly, specifying a set of independent transference numbers does not generally suffice to specify the Onsager transport matrix. Newman addresses this point by using transference numbers for uncharged species expressed as ratios t_i/z_i, noting that the ratio is finite for any species i with $z_i = 0$ [116]. Indeed, one can see with equation (5.126) that t_i/z_i can be written under the assumption that $t_i \propto z_i$ as

$$\frac{t_i}{z_i} = \frac{1}{\|\mathbf{z}\|}\left(\mathbf{N}\boldsymbol{\xi} + \frac{\mathbf{z}}{\|\mathbf{z}\|}\right)_i, \tag{5.128}$$

in which the right side is generally nonzero for any i.

Rather than taxing ourselves by ignoring apparent divisions by zero when transference numbers are involved, we propose that it is simpler to think of transport in terms of migration coefficients, which are defined unambiguously in terms of Onsager coefficients for species with and without charge, as fundamental. The nontrivial transference numbers that make up $\mathbf{t}$ are subsidiary quantities that have a useful physical interpretation, but do not have as much essential content. Note that the distinction between $\mathbf{t}$ and $\boldsymbol{\xi}$ becomes particularly important for electrolytes containing multiple uncharged species, such as the cosolvent blends commonly used in lithium-ion-battery electrolytes [144, 156], fuel-cell membranes susceptible to gas crossover [154], or electrolytes for lithium–air batteries [107].

5.13 Component diffusion coefficients

Although the component diffusivity matrices $\overline{\mathbf{L}}_{\nu}$ and $\overline{\mathbf{L}}_{\nu}^{\psi'}$ have units of area per time, their dependence on the convective velocity obfuscates their connection to energy dissipation. Newman addresses this issue by identifying combinations of Stefan–Maxwell

coefficients that quantify the frame-invariant part of the dissipation that arises from component interdiffusion [116, 125]. The process Newman uses to identify thermodynamic component diffusivities within binary solutions can be generalized to situations with more components as follows.

Instead of defining coefficients as entries of the diffusivity matrix $\overline{\mathbf{L}}_\nu$, a more natural set of component diffusivities is defined by revisiting the Stefan–Maxwell form. Physically, one expects that in situations where electroneutrality is maintained and the current density vanishes uniformly, the mass-transport model describing an n-species electrolytic system should be no different than the model describing a corresponding $(n-1)$-species nonelectrolytic transport system in which every uncharged species is taken to be a component of the original n-ary electrolyte. This equivalence suggests that $\mathbf{M}_\nu$ possesses the structure

$$\frac{c_{\mathrm{T}}^0}{RT}\mathbf{M}_{\nu_{ij}} = \begin{cases} -\dfrac{\nu_i\nu_j}{\mathfrak{D}_{ij}} & \text{if } i \neq j \\ \displaystyle\sum_{k\neq i}^{n-1} \frac{\nu_i\nu_k c_{\nu,k}}{\mathfrak{D}_{ik}c_{\nu,j}} & \text{if } i = j \end{cases}, \tag{5.129}$$

which defines an alternative set of binary diffusion coefficients $\mathfrak{D}_{ij}$ that describe drag interactions between components i and j as they move relative to each other. Here, the diffusivities that parametrize current-free, electroneutral component–component interactions are defined analogously to how species–species interactions are defined in equation (5.2), with a minor stoichiometric correction to account for the fact that component i within a salt–charge basis is actually made up of ν_i species through the fundamental equilibria. We shall distinguish component diffusion coefficients from Stefan–Maxwell coefficients by writing them in Fraktur font, rather than a script font.

Intrinsic properties of the Onsager matrix $\mathbf{M}_Z$ demand that the coefficients defined by equation (5.129) are symmetric in their indices, $\mathfrak{D}_{ij} = \mathfrak{D}_{ji}$, and that $\mathfrak{D}_{ii}$ is undefined for all i. Hence equation (5.129) defines $\frac{1}{2}(n-1)(n-2)$ independent diffusion coefficients — one for each pair of components. Matrix $\mathbf{M}_\nu$ must be positive semidefinite, a property guaranteed if each $\mathfrak{D}_{ij}$ is positive, and by construction it affords $\mathbf{c}_\nu$ as a null eigenvector. Furthermore, a block inversion identity shows that equations (5.117) and (5.118) imply

$$\overline{\mathbf{L}}_\nu^{\psi'} = \lim_{\gamma\to 0}\left(\frac{c_{\mathrm{T}}^0}{RT}\mathbf{M}_\nu + \frac{\boldsymbol{\psi}'_\nu{\boldsymbol{\psi}'_\nu}^\top}{\gamma}\right)^{-1}, \tag{5.130}$$

an inverted form of equation (5.124). Thus, $\overline{\mathbf{L}}_\nu^{\psi'}$, the portion of the Onsager diffusivity

matrix for electroneutral components over a salt–charge basis limited to situations where current density vanishes uniformly, relates directly to the pseudoinverse of $\mathbf{M}_\nu$.

When casting $\overline{\mathbf{L}}_\nu$ in terms of component diffusivities $\mathfrak{D}_{ij}$ with definition (5.129) and inversion formula (5.130), it is necessary to assume that every entry of $\mathbf{c}_\nu$ is nonzero almost everywhere. This must be borne in mind when considering systems where products of the fundamental equilibria are not unique. The situation described in section 5.2, where two binary salts without a common ion are dissolved into an uncharged solvent, provides a simple example. That system can pass locally through compositions where a component concentration vanishes, but all of the ions have non-negative concentrations, as described in the discussion at the end of section 5.8.1. This state nominally induces singular behavior in one of the diagonal entries defined in equation (5.129). Observe, however, that the component diffusivities $\mathfrak{D}_{ij}$ are defined solely in terms of the off-diagonal entries of $\mathfrak{M}_{ij}$. Therefore, although must take care when applying inversion formula (5.130), the diffusion coefficients $\mathfrak{D}_{ij}$ remain well posed across the range of available $\mathbf{c}_\nu$.

5.14 Reference electrodes

Despite the ambiguity in Φ_z^0 demanded by Guggenheim's principle, the salt–charge potential can be related directly to an experimentally measurable voltage by introducing the concept of a reference electrode. A heterogeneous half-reaction suitable for use within a reference electrode can be generally expressed as

$$\sum_{i=1}^{n} s_i \mathrm{X}_i^{z_i} + \sum_j s'_j \mathrm{Y}_j \leftrightharpoons n_{\mathrm{e}^-} \mathrm{e}^-, \tag{5.131}$$

in which $\mathrm{X}_i^{z_i}$ is the chemical symbol of species i, Y_j is the symbol of uncharged entity j that forms in an immediately adjacent phase, e^- denotes electrons, the integer s_i is the stoichiometric coefficient of species i in the half-reaction, integer s'_i is the stoichiometric coefficient of Y_j, and the positive integer n_{e^-} is the number of electrons involved. Since half-reactions balance charge, the set $\{s_i\}_{i=1}^n$ must generally satisfy

$$\sum_{i=1}^{n} s_i z_i = \mathbf{s}^\top \mathbf{z} = n_{\mathrm{e}^-} z_{\mathrm{e}^-}, \tag{5.132}$$

where z_{e^-} is the equivalent charge of electrons. (If a half-reaction is written as a reduction, then s_i or s_i' is negative when species i is a reactant and positive when it is a product.) Note that the matrix form in the middle of this expression indicates that by definition, the half-reaction stoichiometry column $\mathbf{s}$ is not orthogonal to $\mathbf{z}$.

The oxidation potential $\Phi^{\ominus}$ associated with reference-electrode reaction (5.131) is defined such that

$$n_{\mathrm{e}^-} F z_{\mathrm{e}^-} \vec{\nabla}\Phi^{\ominus} = \sum_{i=1}^{n} s_i \vec{\nabla}\mu_i. \tag{5.133}$$

After defining $\mathbf{s}_Z = \mathbf{Z}^{-\top}\mathbf{s} = [\mathbf{s}_\nu, s_z]^\top$ and assuming an electroneutral state, this is written equivalently as

$$n_{\mathrm{e}^-} F z_{\mathrm{e}^-} \vec{\nabla}\Phi^{\ominus} = \mathbf{s}_Z^\top \vec{\nabla}\boldsymbol{\mu}_Z^0 = \mathbf{s}_\nu^\top \vec{\nabla}\boldsymbol{\mu}_\nu^0 + s_z F \left\|\mathbf{z}\right\| \vec{\nabla}\Phi_z^0, \tag{5.134}$$

and since

$$\mathbf{s}^\top \mathbf{z} = \mathbf{s}_Z^\top \mathbf{Z}\mathbf{z} = \left\|\mathbf{z}\right\| s_z = n_{\mathrm{e}^-} z_{\mathrm{e}^-}, \tag{5.135}$$

it follows that

$$\vec{\nabla}\Phi^{\ominus} = \frac{\mathbf{s}_\nu^\top \vec{\nabla}\boldsymbol{\mu}_\nu^0}{n_{\mathrm{e}^-} F z_{\mathrm{e}^-}} + \vec{\nabla}\Phi_z^0, \tag{5.136}$$

a relation that allows the voltage of a given reference electrode to be inferred after one has computed the component and salt-charge potentials. Note that at uniform temperature, pressure, and composition,

$$\left(\vec{\nabla}\Phi^{\ominus}\right)_{T,p,\mathbf{y}_\nu} = \left(\vec{\nabla}\Phi_z^0\right)_{T,p,\mathbf{y}_\nu} \tag{5.137}$$

for any reference-electrode half-reaction, showing the intrinsic utility of the salt–charge potential.

5.15 Examples

5.15.1 The binary electrolyte

The model of a binary electrolytic solution — a liquid comprising a single simple salt dissolved in a single uncharged solvent — is the simplest and most common implementation of concentrated solution theory. Newman's identification of transport laws for this system begins by adopting Onsager–Stefan–Maxwell equations (5.1) with the

transport coefficients defined in equation (5.2). He uses these in combination with the electroneutrality approximation (5.3), Guggenheim condition (5.9) for the salt, and Faraday's law (5.22) to derive species flux laws in the form of equation (5.122) and a MacInnes equation in the form of equation (5.123), casting both in terms of properties relative to the solvent velocity. The development involves apparently ad hoc manipulation of the transport equations to obtain compact forms of the flux-explicit laws.

Newman's process can be formalized with a salt–charge basis under electroneutrality. Let 0, +, and − distinguish the solvent, cation, and anion species, respectively, and subscripts $0, \mathrm{e}$ denote the solvent and salt components. Set the stoichiometric coefficients for the reactants in the fundamental equilibrium forming the salt as

$$\nu_+ = -\frac{\nu z_-}{z_+ - z_-}, \qquad \nu_- = \frac{\nu z_+}{z_+ - z_-}, \tag{5.138}$$

and note that $\nu = \nu_+ + \nu_-$. This framing demonstrates that $z_+\nu_+ + z_-\nu_- = 0$ more directly, and will produce results more obviously consistent with Newman [50]. The products of the fundamental equilibria for this system are unique, so the salt–charge basis is unique up to ordering of the ions. We let the salt–charge transformation $\mathbf{Z}$ take the form

$$\mathbf{Z} = \begin{bmatrix} 1 & 0 & 0 \\ 0 & -\frac{\nu z_-}{z_+ - z_-} & \frac{\nu z_+}{z_+ - z_-} \\ 0 & \frac{z_+}{\|\mathbf{z}\|} & \frac{z_-}{\|\mathbf{z}\|} \end{bmatrix}, \tag{5.139}$$

in which $\|\mathbf{z}\| = \sqrt{z_+^2 + z_-^2}$ because $z_0 = 0$. Given this transformation, one can write the set of species concentrations in the neutral state, $\mathbf{c}^0$, as a parametric function of the component concentrations c_0 and c_e through equation (5.55),

$$\begin{bmatrix} c_0^0 \\ c_+^0 \\ c_-^0 \end{bmatrix} = \mathbf{Z}^\top \begin{bmatrix} c_0 \\ c_\mathrm{e} \\ 0 \end{bmatrix} = \begin{bmatrix} c_0 \\ -\frac{z_-\nu}{z_+ - z_-} \cdot c_\mathrm{e} \\ \frac{z_+\nu}{z_+ - z_-} \cdot c_\mathrm{e} \end{bmatrix}. \tag{5.140}$$

The electroneutral component chemical potentials can be written using equations (5.76)

and (5.77), which together with the relation $y_0 = 1 - \nu y_\mathrm{e}$ show that

$$\vec{\nabla}\begin{bmatrix} \mu_0^0 \\ \mu_\mathrm{e}^0 \end{bmatrix} = RT \begin{bmatrix} X_{00}^0 & X_{0\mathrm{e}}^0 \\ X_{\mathrm{e}0}^0 & X_{\mathrm{ee}}^0 \end{bmatrix} \vec{\nabla}\begin{bmatrix} y_0 \\ y_\mathrm{e} \end{bmatrix}$$
$$= \frac{RT\left(1 + \Lambda_{00}\nu y_\mathrm{e} y_0\right)}{y_\mathrm{e} y_0} \begin{bmatrix} -y_\mathrm{e} \\ y_0 \end{bmatrix} \nu\vec{\nabla} y_\mathrm{e}, \tag{5.141}$$

parametrized by the single excess activity-coefficient derivative function $\Lambda_{00}\left(y_\mathrm{e}\right)$.

Using the salt–charge transformation from equation (5.139) in equation (5.80) shows that

$$\mathbf{M}_\nu = \frac{\nu RT\left(z_+ \mathscr{D}_{0+} - z_- \mathscr{D}_{0-}\right)}{c_\mathrm{T}\left(z_+ - z_-\right)\mathscr{D}_{0+}\mathscr{D}_{0-}} \begin{bmatrix} \dfrac{c_\mathrm{e}}{c_0} & -1 \\ -1 & \dfrac{c_0}{c_\mathrm{e}} \end{bmatrix}, \tag{5.142}$$

$$\mathbf{m}_z = \frac{RT\left(z_+ \mathscr{D}_{0-} + z_- \mathscr{D}_{0+}\right)}{c_\mathrm{T}\left\|\mathbf{z}\right\|^2 \mathscr{D}_{0+}\mathscr{D}_{0-}} \begin{bmatrix} -1 \\ \dfrac{c_0}{c_\mathrm{e}} \end{bmatrix}, \quad \text{and} \tag{5.143}$$

$$M_{zz} = -\frac{RT\|\mathbf{z}\|^2}{c_\mathrm{T} z_+ z_-}\left[\frac{1}{\mathscr{D}_{+-}} + \frac{\left(z_+ - z_-\right)\left(z_+^3 \mathscr{D}_{0-} + z_-^3 \mathscr{D}_{0+}\right)c_0}{\|\mathbf{z}\|^4 \mathscr{D}_{0+}\mathscr{D}_{0-}\nu c_\mathrm{e}}\right]. \tag{5.144}$$

Since the $\mathbf{M}_Z^0$ matrix is invariant with respect to the choice of convective velocity, these expressions can be used in equation (5.84) or (5.94), or even alternative versions of equation (5.94) in which the set of excess component fluxes relative to the mass-average velocity, $\vec{\mathbf{j}}_Z^0$, is replaced with a set relative to some other velocity, $\vec{\mathbf{j}}_Z^{0,\psi'}$.

Newman's concentrated solution theory uses flux-explicit forms of the transport laws. Following Newman, we refer the excess fluxes to the solvent velocity (i.e., $\vec{N}_0/c_0$) by taking

$$\boldsymbol{\psi}'_Z = \frac{\mathbf{Z}}{c_0^0}\begin{bmatrix} 1 \\ 0 \\ 0 \end{bmatrix} = \frac{1}{c_0}\begin{bmatrix} 1 \\ 0 \\ 0 \end{bmatrix} \tag{5.145}$$

in equation (5.114). This changes the dynamical variables to a set of electroneutral

excess species fluxes

$$\vec{\mathbf{j}}_Z^{0,0} = \begin{bmatrix} 0 \\ \vec{J}_{\mathrm{e}}^{0,0} \\ \dfrac{\vec{i}}{F\,\|\mathbf{z}\|} \end{bmatrix} \tag{5.146}$$

whose first member is trivial, and whose second describes the excess salt flux relative to the solvent velocity.

With matrix $\mathbf{M}_Z^0$ built up of the sub-blocks defined by equations (5.142) through (5.144), the transport matrix $\mathbf{L}_Z^0$ for the flux-explicit transport laws can be computed directly using equation (5.96). The ionic conductivity follows from the entry in the last row and column of $\mathbf{L}_Z^0$ through equation (5.99), yielding

$$\kappa^0 = -\frac{c_{\mathrm{T}} F^2 z_+ z_-}{RT} \left[\frac{1}{\mathscr{D}_{+-}} + \frac{c_0\,(z_+ - z_-)}{\nu c_{\mathrm{e}}\,(z_+ \mathscr{D}_{0+} - z_- \mathscr{D}_{0-})} \right]^{-1}, \tag{5.147}$$

whence the last column (or last row) of $\mathbf{L}_Z^0$ can be inserted into equation (5.100), after which equation (5.121) produces

$$\boldsymbol{\xi}^0 = \begin{bmatrix} \xi_0^0 \\ \xi_{\mathrm{e}}^0 \end{bmatrix} = \begin{bmatrix} 0 \\ -\dfrac{(z_+ - z_-)\,(z_- \mathscr{D}_{0+} + z_+ \mathscr{D}_{0-})}{\|\mathbf{z}\|\,\nu\,(z_+ \mathscr{D}_{0+} - z_- \mathscr{D}_{0-})} \end{bmatrix}, \tag{5.148}$$

the component migration coefficients relative to the solvent velocity. Migration coefficients can be used to compute transference numbers with equation (5.127), yielding

$$\mathbf{t}^0 = \begin{bmatrix} t_0^0 \\ t_+^0 \\ t_-^0 \end{bmatrix} = \begin{bmatrix} 0 \\ \frac{z_+ \mathscr{D}_{0+}}{z_+ \mathscr{D}_{0+} - z_- \mathscr{D}_{0-}} \\ -\frac{z_- \mathscr{D}_{0-}}{z_+ \mathscr{D}_{0+} - z_- \mathscr{D}_{0-}} \end{bmatrix}. \tag{5.149}$$

The transference number t_0^0 vanishes necessarily because the solvent species is uncharged, conveniently matching the solvent component's null migration coefficient. For binary electrolytes, no information is lost by using transference numbers in place of migration coefficients.

A third flux-explicit transport property, $\mathfrak{D}$, is related to the Stefan–Maxwell coefficients upon comparison of the computed expression (5.142) with (5.129). This shows

that

$$\mathfrak{D} = \frac{(z_+ - z_-)\,\mathscr{D}_{0+}\mathscr{D}_{0-}}{z_+\mathscr{D}_{0+} - z_-\mathscr{D}_{0-}} \tag{5.150}$$

defines the thermodynamic diffusivity of salt in solvent.

Equations (5.147), (5.148), and (5.150) establish three macroscopic transport properties that parametrize equations (5.122) and (5.123) in terms of Stefan–Maxwell diffusivities. Notably, equations (5.147), (5.149), and (5.150) respectively match the definition of ionic conductivity in Newman's equation 12.23, cation transference number relative to the solvent velocity in Newman's 12.11, and thermodynamic diffusivity in Newman's 12.10 [116].

Given $\boldsymbol{\xi}$ and $\mathbf{L}_Z^0$, the component diffusivities relative to the mass-average velocity, $\overline{\mathbf{L}}_\nu$, are given by equation (5.108), producing

$$\overline{\mathbf{L}}_\nu^0 = \begin{bmatrix} 0 & 0 \\ 0 & \dfrac{c_\mathrm{e}\,(z_+ - z_-)\,\mathscr{D}_{0+}\mathscr{D}_{0-}}{\nu c_0\,(z_+\mathscr{D}_{0+} - z_-\mathscr{D}_{0-})} \end{bmatrix} \tag{5.151}$$

after changing the reference velocity to that of the solvent with equation (5.120).

Since transport properties are often measured by postulating flux-explicit constitutive laws, it is useful to take an alternative approach in which kinematically and thermodynamically consistent flux-explicit transport equations are written a priori, and then work in the opposite direction to establish how the component Onsager–Stefan–Maxwell matrix $\mathbf{M}_Z^0$ depends on the posited properties. This route enables the incorporation of macroscopic transport properties into numerical solvers that exploit the spectral structure of force-explicit forms, such as those presented Chapter 2 and 3.

For the binary electrolyte, $\mathbf{i}_0$ (the first column of the identity matrix) sits in the nullspace of the symmetric matrix $\overline{\mathbf{L}}_\nu^0$, and consequently the matrix only has one nonzero entry (in the second row and second column),

$$\overline{\mathbf{L}}_\nu^0 = \begin{bmatrix} 0 & 0 \\ 0 & \mathscr{L} \end{bmatrix} = \begin{bmatrix} 0 & 0 \\ 0 & \dfrac{c_\mathrm{e}\mathfrak{D}}{\nu c_0} \end{bmatrix}, \tag{5.152}$$

in which the single Onsager diffusivity of salt relative to the solvent velocity, $\mathscr{L}$, is expressed in terms of a thermodynamic diffusivity $\mathfrak{D}$ by applying inversion formula (5.130) to definition (5.129). Similarly, $\mathbf{i}_0$ is orthogonal to $\boldsymbol{\xi}^0$, which therefore also

must have just one nonzero entry,

$$\boldsymbol{\xi}^0 = \begin{bmatrix} 0 \\ \xi \end{bmatrix}, \tag{5.153}$$

where ξ stands for the salt migration coefficient relative to the solvent velocity. This property relates to the cation transference number relative to solvent as

$$\xi = -\frac{(z_+ - z_-)\left[\left(1 - t_+^0\right) z_+^2 - z_-^2 t_+^0\right]}{\nu z_+ z_- \|\mathbf{z}\|} \tag{5.154}$$

through equation (5.127).

The known structures of $\overline{\mathbf{L}}_\nu^0$ and $\boldsymbol{\xi}^0$ allow species flux laws relative to the solvent velocity to be written directly in the form of equation (5.122). Bringing in equations (5.138), (5.149), and (5.152), one finds

$$\vec{J}_0^0 = 0, \tag{5.155}$$

$$\vec{J}_+^0 = -\frac{\mathfrak{D} c_{\mathrm{T}}^0}{RT} \frac{\nu_+ c_{\mathrm{e}}}{\nu c_0} \vec{\nabla} \mu_{\mathrm{e}}^0 + \frac{t_+^0 \vec{i}}{F z_+}, \tag{5.156}$$

$$\vec{J}_-^0 = -\frac{\mathfrak{D} c_{\mathrm{T}}^0}{RT} \frac{\nu_- c_{\mathrm{e}}}{\nu c_0} \vec{\nabla} \mu_{\mathrm{e}}^0 + \frac{\left(1 - t_+^0\right) \vec{i}}{F z_-}. \tag{5.157}$$

Flux laws (5.156) and (5.157) match Newman's equations 12.8 and 12.9, respectively [116]. A discussion describing the similarity and differences of these flux explicit laws to the Nernst–Planck theory (1.53) may be found in [116].

Finally, posit an ionic conductivity κ^0 to write an electroneutral MacInnes equation in the form of (5.123), as

$$\frac{\vec{i}}{\kappa^0} = -\vec{\nabla} \Phi_z^0 - \frac{(z_+ - z_-)}{\nu F z_+ z_-} \left(\frac{z_+^2}{z_+^2 + z_-^2} - t_+^0 \right) \vec{\nabla} \mu_{\mathrm{e}}^0, \tag{5.158}$$

which depends on the salt–charge potential. Introducing a reference-electrode potential

with equation (5.136) gives

$$\begin{aligned}\frac{\vec{i}}{\kappa^0} =& -\vec{\nabla}\Phi^{\ominus} + \frac{s_0\vec{\nabla}\mu_0^0}{n_{\mathrm{e}^-}Fz_{\mathrm{e}^-}} \\ &+ \frac{z_+ - z_-}{n_{\mathrm{e}^-}Fz_{\mathrm{e}^-}\nu}\left[t_+^0\frac{s_-}{z_+} - \left(1-t_+^0\right)\frac{s_+}{z_-}\right]\vec{\nabla}\mu_{\mathrm{e}}^0,\end{aligned} \tag{5.159}$$

in harmony with Newman's equation 12.27 [116].

Given κ^0, as well as $\overline{\mathbf{L}}_\nu^0$ and $\boldsymbol{\xi}^0$ matrices in the forms from equations (5.152) and (5.153), one can use relationships (5.124) and (5.125) to construct the $\mathbf{M}_Z^0$ matrix needed to implement the electroneutral Onsager–Stefan–Maxwell equations. Performing the calculation, one finds

$$\mathbf{M}_\nu = \frac{RT}{c_{\mathrm{T}}^0\mathfrak{D}}\begin{bmatrix} \frac{\nu c_{\mathrm{e}}}{c_0} & -\nu \\ -\nu & \frac{\nu c_0}{c_{\mathrm{e}}}\end{bmatrix}, \tag{5.160}$$

$$\mathbf{m}_z = \frac{\nu RT\xi}{c_{\mathrm{T}}^0\mathfrak{D}}\begin{bmatrix} 1 \\ -\frac{c_0}{c_{\mathrm{e}}}\end{bmatrix}, \tag{5.161}$$

and

$$M_{zz} = \frac{F^2\left\|\mathbf{z}\right\|^2}{\kappa^0} + \frac{\nu RTc_0\xi^2}{c_{\mathrm{T}}^0c_{\mathrm{e}}\mathfrak{D}}. \tag{5.162}$$

One can also elucidate the Stefan–Maxwell coefficients, by inverting the congruence transformation in equation (5.80): $\mathbf{M}^{\mathfrak{c}^0} = \mathbf{Z}^{-1}\mathbf{M}_Z^0\mathbf{Z}^{-\top}$. Off-diagonal entries of $\mathbf{M}^0$ relate to $\mathscr{D}_{ij}$ values through equation (5.2). Introduce t_+^0 in favor of ξ via equation (5.154) to show that

$$\begin{aligned}\frac{1}{\mathscr{D}_{0+}} =& -\frac{\left(1-t_+^0\right)\left(z_+ - z_-\right)}{z_-\mathfrak{D}}, \\ \frac{1}{\mathscr{D}_{0-}} =& \frac{t_+^0\left(z_+ - z_-\right)}{z_+\mathfrak{D}}, \\ \frac{1}{\mathscr{D}_{+-}} =& -\frac{F^2z_+z_-c_{\mathrm{T}}^0}{RT\kappa^0} + \frac{t_+^0(1-t_+^0)\left(z_+ - z_-\right)^2c_0}{\nu\mathfrak{D}z_+z_-c_{\mathrm{e}}},\end{aligned} \tag{5.163}$$

consistent with Newman's equations 14.1–14.3.

5.15.2 The molten salt

Pollard and Newman applied concentrated solution theory [125] to the other possible liquid electrolyte with three species: a molten solution of two simple salts that share a common ion. For, example a molten mixture of the ions Na^+, Al^{3+} and Cl^- finds uses in sodium-nickel-chloride batteries [138]. From transport laws based in the Onsager–Stefan–Maxwell equations, they ultimately developed flux-explicit laws in the form of equation (5.122) and a MacInnes equation in the form of equation (5.123).

Here we apply the salt–charge framework to obtain transport laws consistent with Pollard and Newman's results. The flux laws we formulate will not precisely identify with the Pollard–Newman equations, however. Whereas they used the common ion's velocity as the reference for convection, we instead use the velocity of one of the salts. This alternative convention creates component flux laws that involve a single chemical-potential gradient directly, rather than requiring additional use of the Gibbs–Duhem equation to eliminate a dependent driving force.

Let the charges of the three species comprising the binary molten salt be $\mathbf{z} = [z_1, z_2, z_3]^\top$. We assume that the third species is counter-charged to the first two, and denote the sign of its charge by $\pm$. Again, the choice of products of the fundamental equilibria is unique; we label the simple salts formed from these three species with indices corresponding to the similarly charged ion that distinguishes them: e_1 and e_2. The stoichiometric coefficients of the ions within these salts are written in terms of the species charges and total formula-unit stoichiometries ν_{e_1} and ν_{e_2} as

$$\nu_1^{\mathrm{e}_1} = -\frac{\nu_{\mathrm{e}_1} z_3}{z_1 - z_3}, \qquad \nu_3^{\mathrm{e}_1} = \frac{\nu_{\mathrm{e}_1} z_1}{z_1 - z_3}, \tag{5.164}$$

$$\nu_2^{\mathrm{e}_2} = -\frac{\nu_{\mathrm{e}_2} z_3}{z_2 - z_3}, \qquad \nu_3^{\mathrm{e}_2} = \frac{\nu_{\mathrm{e}_2} z_2}{z_2 - z_3}, \tag{5.165}$$

so that $\nu_{\mathrm{e}_1} = \nu_1^{\mathrm{e}_1} + \nu_3^{\mathrm{e}_1}$ and $\nu_{\mathrm{e}_2} = \nu_2^{\mathrm{e}_2} + \nu_3^{\mathrm{e}_2}$. The matrix $\mathbf{Z}$ that represents the salt–charge basis is unique up to ordering of the ions. We choose to write it as

$$\mathbf{Z} = \begin{bmatrix} \nu_1^{\mathrm{e}_1} & 0 & \nu_3^{\mathrm{e}_1} \\ 0 & \nu_2^{\mathrm{e}_2} & \nu_3^{\mathrm{e}_2} \\ \frac{z_1}{\|\mathbf{z}\|} & \frac{z_2}{\|\mathbf{z}\|} & \frac{z_3}{\|\mathbf{z}\|} \end{bmatrix}, \tag{5.166}$$

where $\|\mathbf{z}\| = \sqrt{z_1^2 + z_2^2 + z_3^2}$, bearing in mind that the reactant stoichiometric coefficients from the fundamental equilibria satisfy equations (5.164) and (5.165).

With salt–charge transformation (5.166), the electroneutral species concentrations $\mathbf{c}^0$ are cast in terms of component concentrations c_{e_1} and c_{e_2} through equation (5.55), as

$$\begin{bmatrix} c_1^0 \\ c_2^0 \\ c_3^0 \end{bmatrix} = \mathbf{Z}^\top \begin{bmatrix} c_{\mathrm{e}_1} \\ c_{\mathrm{e}_2} \\ 0 \end{bmatrix} = \begin{bmatrix} -\frac{\nu_{\mathrm{e}_1} z_3}{z_1 - z_3} c_{\mathrm{e}_1} \\ -\frac{\nu_{\mathrm{e}_2} z_3}{z_2 - z_3} c_{\mathrm{e}_2} \\ \nu_1^{\mathrm{e}_1} c_{\mathrm{e}_1} + \nu_2^{\mathrm{e}_2} c_{\mathrm{e}_2} \end{bmatrix}. \tag{5.167}$$

The electroneutral component chemical potentials can then be written using equations (5.76) and (5.77). Together with the relation $\nu_{\mathrm{e}_2} y_{\mathrm{e}_2} = 1 - \nu_{\mathrm{e}_1} y_{\mathrm{e}_1}$, these show that

$$\begin{aligned} \vec{\nabla} \begin{bmatrix} \mu_{\mathrm{e}_1}^0 \\ \mu_{\mathrm{e}_2}^0 \end{bmatrix} &= RT \begin{bmatrix} X_{\mathrm{e}_1\mathrm{e}_1}^0 & X_{\mathrm{e}_1\mathrm{e}_2}^0 \\ X_{\mathrm{e}_2\mathrm{e}_2}^0 & X_{\mathrm{e}_2\mathrm{e}_2}^0 \end{bmatrix} \vec{\nabla} \begin{bmatrix} y_{\mathrm{e}_1} \\ y_{\mathrm{e}_2} \end{bmatrix} \\ &= RT \begin{bmatrix} \frac{\nu_1^{\mathrm{e}_1}}{y_{\mathrm{e}_1}} + \frac{(\nu_3^{\mathrm{e}_1})^2}{\nu_3^{\mathrm{e}_1} y_{\mathrm{e}_1} + \nu_3^{\mathrm{e}_2} y_{\mathrm{e}_2}} & \frac{\nu_3^{\mathrm{e}_1} \nu_3^{\mathrm{e}_2}}{\nu_3^{\mathrm{e}_1} y_{\mathrm{e}_1} + \nu_3^{\mathrm{e}_2} y_{\mathrm{e}_2}} \\ \frac{\nu_3^{\mathrm{e}_1} \nu_3^{\mathrm{e}_2}}{\nu_3^{\mathrm{e}_1} y_{\mathrm{e}_1} + \nu_3^{\mathrm{e}_2} y_{\mathrm{e}_2}} & \frac{\nu_2^{\mathrm{e}_2}}{y_{\mathrm{e}_2}} + \frac{(\nu_3^{\mathrm{e}_2})^2}{\nu_3^{\mathrm{e}_1} y_{\mathrm{e}_1} + \nu_3^{\mathrm{e}_2} y_{\mathrm{e}_2}} \end{bmatrix} \vec{\nabla} \begin{bmatrix} y_{\mathrm{e}_1} \\ y_{\mathrm{e}_2} \end{bmatrix} \\ &\quad + \frac{\Lambda_{\mathrm{e}_1\mathrm{e}_1} \nu_{\mathrm{e}_1} y_{\mathrm{e}_1} \nu_{\mathrm{e}_2} y_{\mathrm{e}_2}}{\nu_{\mathrm{e}_1}^2} \begin{bmatrix} -y_{\mathrm{e}_2} \\ y_{\mathrm{e}_1} \end{bmatrix} \nu_{\mathrm{e}_2} \vec{\nabla} y_{\mathrm{e}_2}, \end{aligned} \tag{5.168}$$

in which a single function $\Lambda_{\mathrm{e}_1\mathrm{e}_1}(y_{\mathrm{e}_2})$ parametrizes the gradient of either salt's mean molar activity coefficient within the solution. Observe that the ideal contribution to mixing free energy depends in a rather subtle way on the salt fractions y_{e_1} and y_{e_2}.

Rather than repeating in their entirety the development illustrated for the binary electrolyte, we leverage the structural knowledge provided by our framework to abbreviate the process. Because there are three species, there are three macroscopic transport properties $\mathfrak{D}$, ξ and κ^0. Using the structure posited in (5.129) we may write

$$\mathbf{M}_\nu = \frac{RT \nu_{\mathrm{e}_1} \nu_{\mathrm{e}_2}}{c_{\mathrm{T}}^0 \mathfrak{D}} \begin{bmatrix} \frac{c_{\mathrm{e}_2}}{c_{\mathrm{e}_1}} & -1 \\ -1 & \frac{c_{\mathrm{e}_1}}{c_{\mathrm{e}_2}} \end{bmatrix}. \tag{5.169}$$

To eliminate the chemical-potential gradient of salt 1 from the flux-explicit laws, it is convenient to choose $\boldsymbol{\psi}'$ such that $\boldsymbol{\psi}'_Z = \mathbf{i}_{\mathrm{e}_1}$ — that is, to let the convective velocity be that of the first salt (i.e., $\vec{N}_{\mathrm{e}_1}/c_{\mathrm{e}_1}$). There is a single non-trivial migration coefficient ξ

relative to this reference velocity:

$$\boldsymbol{\xi}^{\mathrm{e}_1} = \begin{bmatrix} 0 \\ \xi \end{bmatrix}. \tag{5.170}$$

Using equations (5.125) then shows that

$$\mathbf{m}_z = \frac{RT\nu_{\mathrm{e}_1}\nu_{\mathrm{e}_2}\xi}{c_{\mathrm{T}}^0\mathfrak{D}} \begin{bmatrix} -1 \\ \dfrac{c_{\mathrm{e}_1}}{c_{\mathrm{e}_2}} \end{bmatrix} \quad \text{and} \tag{5.171}$$

$$M_{zz} = \frac{F^2\|z\|^2}{\kappa^0} + \frac{RT\nu_{\mathrm{e}_1}\nu_{\mathrm{e}_2}\xi^2}{c_{\mathrm{T}}^0\mathfrak{D}}\frac{c_{\mathrm{e}_1}}{c_{\mathrm{e}_2}}. \tag{5.172}$$

Next, taking the transport matrix (5.2), performing the congruence transformation (5.36) and comparing it to the equations (5.169), (5.171), (5.172) allows identification of the three macroscopic transport properties in terms of Stefan–Maxwell coefficients. These are

$$\mathfrak{D} = \frac{c_3^0(z_1 - z_3)(z_2 - z_3)}{\left(\frac{c_3^0 z_3^2}{\mathscr{D}_{12}} + \frac{c_2^0 z_2^2}{\mathscr{D}_{13}} + \frac{c_1^0 z_1^2}{\mathscr{D}_{23}}\right)}, \tag{5.173}$$

$$\begin{aligned}\xi \cdot \tfrac{\nu_{\mathrm{e}_1}\nu_{\mathrm{e}_2}c_1^0c_3^0z_3^2}{\mathfrak{D}\nu_1^{\mathrm{e}1}} =& \tfrac{z_3^2c_3(c_1^0z_2 - c_2^0z_1)}{\mathscr{D}_{12}\|z\|} - \tfrac{z_2c_1^0c_2^0(z_1^2+z_3^2)+(c_2^0)^2z_1z_2^2}{\mathscr{D}_{13}\|z\|} \\ &+ \tfrac{(c_1^0)^2z_1^2z_2+c_1^0c_2^0z_1(z_2^2+z_3^2)}{\mathscr{D}_{23}\|z\|},\end{aligned} \tag{5.174}$$

$$\kappa^0 = \frac{F^2c_{\mathrm{T}}^0\left(\frac{z_1^2c_1^0}{\mathscr{D}_{23}} + \frac{z_2^2c_2^0}{\mathscr{D}_{13}} + \frac{z_3^2c_3^0}{\mathscr{D}_{12}}\right)}{RT\left(\frac{c_1^0}{\mathscr{D}_{12}\mathscr{D}_{13}} + \frac{c_2^0}{\mathscr{D}_{12}\mathscr{D}_{23}} + \frac{c_3^0}{\mathscr{D}_{13}\mathscr{D}_{23}}\right)}. \tag{5.175}$$

Here the conductivity is identical to Pollard and Newman's equation 33 [125]. The diffusivity defined in equation (5.173) relates to the diffusion coefficient identified in equation 9 of reference [125], which we will label $\mathscr{D}$, as

$$\mathfrak{D} = \mathscr{D}\frac{c_{\mathrm{T}}^0}{c_3^0}\frac{\nu_{\mathrm{e}_1}\nu_{\mathrm{e}_2}}{\nu_1^{\mathrm{e}_1}\nu_2^{\mathrm{e}_2}}. \tag{5.176}$$

Although the prefactor that relates our $\mathfrak{D}$ to Pollard and Newman's $\mathscr{D}$ is composition-dependent, the factor only involves the mole fraction of the common ion, which is always of order unity.

It is equally straightforward to invert this process. Similar to the binary electrolyte, entries of $\mathbf{M}^0$ may be related to the original Stefan–Maxwell diffusivities $\mathscr{D}_{ij}$ by inverting the congruence transformation in equation (5.80) and examining the off-diagonal elements in light of equation (5.79). This comparison shows that the diffusivities relate to the macroscopic properties by

$$\begin{aligned}
\frac{1}{\mathscr{D}_{12}} =& \frac{\left[c_1^0(z_1^2+z_3^2)+c_2^0 z_1 z_2\right]\left[c_2^0(z_2^2+z_3^2)+c_1^0 z_1 z_2\right]\nu_{\mathrm{e}_1}\nu_{\mathrm{e}_2}}{\mathfrak{D} c_1^0 c_2^0 \nu_1^{\mathrm{e}_1}\nu_2^{\mathrm{e}_2}\|\mathbf{z}\|^4} \\
&- \frac{\xi\nu_{\mathrm{e}_1}\nu_{\mathrm{e}_2}[c_1^0 z_1(z_1^2-z_2^2+z_3^2)-c_2^0 z_2(-z_1^2+z_2^2+z_3^2)]}{\mathfrak{D}\|\mathbf{z}\|^3 c_2^0 \nu_1^{\mathrm{e}}} \\
&- \left(\frac{F^2 c_{\mathrm{T}}^0}{RT\kappa^0} + \frac{\nu_{\mathrm{e}_1}\nu_{\mathrm{e}_2}\xi^2}{\mathfrak{D}}\frac{c_{\mathrm{e}_1}}{c_{\mathrm{e}_2}}\right)\frac{z_1 z_2}{\|\mathbf{z}\|^2}, \\
\frac{1}{\mathscr{D}_{13}} =& -\frac{z_3(c_1^0 z_2 - c_2^0 z_1)\left[c_2^0(z_2^2+z_3^2)+c_1^0 z_1 z_2\right]\nu_{\mathrm{e}_1}\nu_{\mathrm{e}_2}}{\mathfrak{D} c_1^0 c_2^0 \nu_1^{\mathrm{e}_1}\nu_2^{\mathrm{e}_2}\|\mathbf{z}\|^4} \\
&+ \frac{\xi z_3 \nu_{\mathrm{e}_1}\nu_{\mathrm{e}_2}\left[c_2^0(-z_1^2+z_2^2+z_3^2)+2c_1^0 z_1 z_2\right]}{\mathfrak{D} c_2^0 \nu_1^{\mathrm{e}_1}\|\mathbf{z}\|^3} \\
&- \left(\frac{F^2 c_{\mathrm{T}}^0}{RT\kappa^0} + \frac{\nu_{\mathrm{e}_1}\nu_{\mathrm{e}_2}\xi^2}{\mathfrak{D}}\frac{c_{\mathrm{e}_1}}{c_{\mathrm{e}_2}}\right)\frac{z_1 z_3}{\|\mathbf{z}\|^2}, \\
\frac{1}{\mathscr{D}_{23}} =& -\frac{z_3(c_2^0 z_1 - c_1^0 z_2)\left[c_2^0(z_1^2+z_3^2)+c_2^0 z_1 z_2\right]\nu_{\mathrm{e}_1}\nu_{\mathrm{e}_2}}{\mathfrak{D} c_1^0 c_2^0 \nu_1^{\mathrm{e}_1}\nu_2^{\mathrm{e}_2}\|\mathbf{z}\|^4} \\
&+ \frac{\xi z_3 \nu_{\mathrm{e}_1}\nu_{\mathrm{e}_2}\left[c_1^0(z_1^2-z_2^2+z_3^2)+2c_2^0 z_1 z_2\right]}{\mathfrak{D} c_2^0 \nu_1^{\mathrm{e}_2}\|\mathbf{z}\|^3} \\
&- \left(\frac{F^2 c_{\mathrm{T}}^0}{RT\kappa^0} + \frac{\nu_{\mathrm{e}_1}\nu_{\mathrm{e}_2}\xi^2}{\mathfrak{D}}\frac{c_{\mathrm{e}_1}}{c_{\mathrm{e}_2}}\right)\frac{z_2 z_3}{\|\mathbf{z}\|^2}.
\end{aligned} \tag{5.177}$$

Pollard and Newman do not write down these relationships, presumably because of their algebraic complexity. Stating explicit forms for the Stefan–Maxwell coefficients in terms of flux-explicit properties becomes increasingly cumbersome as the number of species (and the number of charged species) in a system increases.

With our choice of convective velocity, the matrix $\overline{\mathbf{L}}_{\nu}^{\mathrm{e}_1}$ also affords a single non-trivial entry,

$$\overline{\mathbf{L}}_{\nu}^{\mathrm{e}_1} = \begin{bmatrix} 0 & 0 \\ 0 & \dfrac{\mathfrak{D}}{\nu_{\mathrm{e}_1}\nu_{\mathrm{e}_2}}\dfrac{\nu_1^{\mathrm{e}_1} c_{\mathrm{e}_2}}{c_{\mathrm{e}_1}} \end{bmatrix} \tag{5.178}$$

After deriving transference numbers $t_1^{\mathrm{e}_1}$, $t_2^{\mathrm{e}_1}$, and $t_3^{\mathrm{e}_1}$ relative to salt 1 with equation

(5.127), the laws governing the species excess fluxes are found to be

$$\vec{J}_1^{\mathrm{e}_1} = \frac{t_1^{\mathrm{e}_1}\vec{i}}{Fz_1} \tag{5.179}$$

$$\vec{J}_2^{\mathrm{e}_1} = -\frac{c_{\mathrm{T}}^0\mathfrak{D}}{RT}\frac{\nu_1^{\mathrm{e}_1}\nu_2^{\mathrm{e}_2}c_{\mathrm{e}_2}}{\nu_{\mathrm{e}_1}\nu_{\mathrm{e}_2}c_{\mathrm{e}_1}}\vec{\nabla}\mu_{\mathrm{e}_2}^0 + \frac{t_2^{\mathrm{e}_1}\vec{i}}{Fz_2} \tag{5.180}$$

$$\vec{J}_3^{\mathrm{e}_1} = -\frac{c_{\mathrm{T}}^0\mathfrak{D}}{RT}\frac{\nu_1^{\mathrm{e}_1}\nu_3^{\mathrm{e}_2}c_{\mathrm{e}_2}}{\nu_{\mathrm{e}_1}\nu_{\mathrm{e}_2}c_{\mathrm{e}_1}}\vec{\nabla}\mu_{\mathrm{e}_2}^0 + \frac{t_3^{\mathrm{e}_1}\vec{i}}{Fz_3}. \tag{5.181}$$

Interestingly, excess flux of ion 1 relative to the velocity of salt 1 can be driven by migration, but not by diffusion. Equation (5.127) shows that all three transference numbers here are parametric functions of the single migration coefficient ξ, through

$$\begin{bmatrix} t_1^{\mathrm{e}_1} \\ t_2^{\mathrm{e}_1} \\ t_3^{\mathrm{e}_1} \end{bmatrix} = \frac{\operatorname{diag}(\mathbf{z})\,\mathbf{Z}^\top}{\|\mathbf{z}\|}\begin{bmatrix} 0 \\ \xi \\ 1 \end{bmatrix}. \tag{5.182}$$

Thus, as well as satisfying the relation $t_1^{\mathrm{e}_1} + t_2^{\mathrm{e}_1} + t_3^{\mathrm{e}_1} = 1$ that follows from the last row of this matrix equation, the species transference numbers relative to salt 1 are also constrained such that $(z_2^2 + z_3^2)t_1^{\mathrm{e}_1} + z_1^2(t_2^{\mathrm{e}_1} + t_3^{\mathrm{e}_1}) = 0$, which follows from the first row.

The reference velocity under $\boldsymbol{\xi}^{\mathrm{e}_1}$ can be changed to that of the common ion by moving through the mass-average velocity with transformation (5.121). Then one can derive the associated transference numbers, denoted t_i^3, with equation (5.127) to find Pollard and Newman's expression

$$t_2^3 = \frac{\frac{z_2}{\mathscr{D}_{13}} - \frac{z_3}{\mathscr{D}_{12}}}{\left(\frac{z_2}{\mathscr{D}_{13}} - \frac{z_3}{\mathscr{D}_{12}}\right) + \frac{z_1 c_1^0}{z_2 c_2^0}\left(\frac{z_1}{\mathscr{D}_{23}} - \frac{z_3}{\mathscr{D}_{12}}\right)}, \tag{5.183}$$

which appears in their equation 10 [125]. With a migration coefficient relative to salt 1 and the reference-electrode potential from equation (5.136), one finds a concise MacInnes equation,

$$\frac{\vec{i}}{\kappa^0} = -\vec{\nabla}\Phi^{\ominus} + \frac{s_{\mathrm{e}_1}\vec{\nabla}\mu_{\mathrm{e}_1}^0}{n_{\mathrm{e}^-}Fz_{\mathrm{e}^-}} + \left(\frac{s_{\mathrm{e}_2}}{n_{\mathrm{e}^-}Fz_{\mathrm{e}^-}} - \frac{\kappa^0\xi}{F\|\mathbf{z}\|}\right)\vec{\nabla}\mu_{\mathrm{e}_2}^0, \tag{5.184}$$

which agrees with Pollard and Newman's equation 32 [125].

5.15.3 The cosolvent electrolyte

For a final illustration of our method of developing flux laws for concentrated multicomponent electrolytes, we consider a four-species liquid solution comprising two uncharged species (which we call a cosolvent) and a single salt. Electrolytic solutions of this type are used in lithium-ion batteries, which typically use a blend of a linear and a cyclic carbonate to dissolve a simple lithium salt [156]. We let subscripts + and − describe the cation and anion, respectively, a subcript e, the salt they associate to form and the two solvents as the subscripts 0 and o. Similarly to the binary-electrolyte example, the stoichiometric coefficients for the salt satisfy equation (5.138), where ν is the total salt stoichiometry.

A salt–charge basis for the cosolvent electrolyte is embodied by the transformation matrix

$$\mathbf{Z} = \begin{bmatrix} 1 & 0 & 0 & 0 \\ 0 & 1 & 0 & 0 \\ 0 & 0 & -\frac{\nu z_-}{z_+ - z_-} & \frac{\nu z_+}{z_+ - z_-} \\ 0 & 0 & \frac{z_+}{\|\mathbf{z}\|} & \frac{z_-}{\|\mathbf{z}\|} \end{bmatrix}. \tag{5.185}$$

The species concentrations in the neutral state in terms of the composition concentrations are then

$$\begin{bmatrix} c_0^0 \\ c_\mathrm{o}^0 \\ c_+^0 \\ c_-^0 \end{bmatrix} = \mathbf{Z} \begin{bmatrix} c_0 \\ c_\mathrm{o} \\ c_\mathrm{e} \\ 0 \end{bmatrix} = \begin{bmatrix} c_0 \\ c_\mathrm{o} \\ -\frac{z_- \nu}{z_+ - z_-} \cdot c_\mathrm{e} \\ \frac{z_+ \nu}{z_+ - z_-} \cdot c_\mathrm{e} \end{bmatrix}, \tag{5.186}$$

parametric functions of the three component concentrations c_0, c_o, and c_e.

The nonideal parts of the electroneutral component chemical potentials are parametrised by a symmetric 2×2 block matrix

$$\mathbf{\Lambda} = \begin{bmatrix} \Lambda_{00} & \Lambda_{0\mathrm{o}} \\ \Lambda_{0\mathrm{o}} & \Lambda_{\mathrm{oo}}, \end{bmatrix}, \tag{5.187}$$

whose three independent entries are functions of only two of the three component fractions y_0, y_o, and y_e. Following equation (5.70), the gradients of the electroneutral

component chemical potentials are expanded as

$$\vec{\nabla}\begin{bmatrix}\mu_0^0\\ \mu_{\mathrm{o}}^0\\ \mu_{\mathrm{e}}^0\end{bmatrix} = RT\vec{\nabla}\ln\mathbf{y}_\nu + RT(\mathbf{I}_3 - \boldsymbol{\nu}\mathbf{y}_\nu^\top)\begin{bmatrix}\boldsymbol{\Lambda} & \mathbf{o}\\ \mathbf{o}^\top & 0\end{bmatrix}\vec{\nabla}\mathbf{y}_\nu, \tag{5.188}$$

where in this case $\boldsymbol{\nu} = [1, 1, \nu]^\top$ and $\mathbf{y}_\nu = [y_0, y_{\mathrm{o}}, y_{\mathrm{e}}]^\top$.

To derive force and flux explicit laws, we again use the ansatz (5.129) to write

$$\frac{c_{\mathrm{T}}^0\mathbf{M}_\nu}{RT} = \begin{bmatrix}\frac{c_{\mathrm{o}}}{c_0\mathfrak{D}_{0\mathrm{o}}} + \frac{\nu c_{\mathrm{e}}}{c_0\mathfrak{D}_{0\mathrm{e}}} & -\frac{1}{\mathfrak{D}_{0\mathrm{o}}} & -\frac{\nu}{\mathfrak{D}_{0\mathrm{e}}}\\ -\frac{1}{\mathfrak{D}_{0\mathrm{o}}} & \frac{c_1^0}{c_2^0\mathfrak{D}_{0\mathrm{o}}} + \frac{\nu c_{\mathrm{e}}}{c_{\mathrm{o}}\mathfrak{D}_{\mathrm{oe}}} & -\frac{\nu}{\mathfrak{D}_{\mathrm{oe}}}\\ -\frac{\nu}{\mathfrak{D}_{0\mathrm{e}}} & -\frac{\nu}{\mathfrak{D}_{\mathrm{oe}}} & \frac{\nu c_0}{c_{\mathrm{e}}\mathfrak{D}_{0\mathrm{e}}} + \frac{\nu c_{\mathrm{o}}}{c_{\mathrm{e}}\mathfrak{D}_{\mathrm{oe}}}\end{bmatrix}. \tag{5.189}$$

These entries straightforwardly relate to the Stefan–Maxwell coefficients through

$$\mathfrak{D}_{0\mathrm{o}} = \mathscr{D}_{0\mathrm{o}}, \tag{5.190}$$

$$\mathfrak{D}_{0\mathrm{e}} = \frac{(z_+ - z_-)\mathscr{D}_{0+}\mathscr{D}_{0-}}{\mathscr{D}_{0+}z_+ - \mathscr{D}_{0-}z_-}, \tag{5.191}$$

$$\mathfrak{D}_{\mathrm{oe}} = \frac{(z_+ - z_-)\mathscr{D}_{\mathrm{o}+}\mathscr{D}_{\mathrm{o}-}}{\mathscr{D}_{\mathrm{o}+}z_+ - \mathscr{D}_{\mathrm{o}-}z_-}. \tag{5.192}$$

Observe that the second two definitions take forms similar to equation (5.150), despite the addition of a solvent.

Taking the reference velocity to be that of the first solvent, i.e, $\boldsymbol{\psi}' = \mathbf{i}_0$, the diffusivity matrix and migration coefficients assume the forms

$$\overline{\mathbf{L}}_\nu^0 = \begin{bmatrix}0 & 0 & 0\\ 0 & \mathscr{L}_{\mathrm{o}} & \mathscr{L}_\times\\ 0 & \mathscr{L}_\times & \mathscr{L}_{\mathrm{e}}\end{bmatrix}, \quad \boldsymbol{\xi}^0 = \begin{bmatrix}0\\ \xi_{\mathrm{o}}\\ \xi_{\mathrm{e}}\end{bmatrix}. \tag{5.193}$$

The terms appearing in the diffusion matrix are understood as follows. $\mathscr{L}_{\mathrm{o}}$ denotes the

Onsager diffusivity of the second solvent relative to the velocity of the first, $\mathscr{L}_\times$ the cross-diffusivity between the second solvent and the salt in a frame moving with the first solvent, and $\mathscr{L}_\mathrm{e}$ the diffusivity of the salt relative to the first solvent's velocity. Each of these parameters is independent. The set of migration coefficients depends on two independent parameters ξ_o and ξ_e. A distinction from the previous cases is that a neutral species — the second solvent — may carry current. Thus transference numbers as typically understood do not suffice to write complete flux-explicit transport laws for this system.

By relation (5.130), the Onsager diffusivities that make up $\overline{\mathbf{L}}^0_\nu$ can be understood in terms of component diffusivities, as

$$\mathscr{L}_\mathrm{o} = \frac{c_\mathrm{o}\mathscr{D}_{0\mathrm{o}}(\mathscr{D}_{\mathrm{oe}}c_0 + \mathscr{D}_{0\mathrm{e}}c_\mathrm{o})}{c_0(\mathscr{D}_{\mathrm{oe}}c_0 + \mathscr{D}_{0\mathrm{o}}\nu c_\mathrm{e} + \mathscr{D}_{0\mathrm{e}}c_\mathrm{o})} \tag{5.194}$$

$$\mathscr{L}_\mathrm{e} = \frac{c_\mathrm{e}\mathscr{D}_{0\mathrm{e}}(\mathscr{D}_{\mathrm{oe}}c_0 + \mathscr{D}_{0\mathrm{o}}\nu c_\mathrm{e})}{c_0(\mathscr{D}_{\mathrm{oe}}c_0 + \mathscr{D}_{0\mathrm{o}}\nu c_\mathrm{e} + \mathscr{D}_{0\mathrm{e}}c_\mathrm{o})} \tag{5.195}$$

$$\mathscr{L}_\times = \frac{\mathscr{D}_{0\mathrm{o}}\mathscr{D}_{0\mathrm{e}}c_\mathrm{o}c_\mathrm{e}}{c_0(\mathscr{D}_{\mathrm{oe}}c_0 + \nu\mathscr{D}_{0\mathrm{o}}c_\mathrm{e} + \mathscr{D}_{0\mathrm{e}}c_\mathrm{o})}. \tag{5.196}$$

Each of these expressions agrees within a prefactor with the thermodynamic oxygen diffusivity, the thermodynamic electrolyte diffusivity, and the cross diffusivity reported for lithium/air-battery electrolytes by Monroe [107].

The benefits of relying on both migration coefficients and directly writing flux laws in the salt–charge basis are made most clear by this example. Equation (5.119) reads for the two-solvent case as

$$\vec{J}^0_0 = \vec{0}, \tag{5.197}$$

$$\vec{J}^0_\mathrm{o} = -\mathscr{L}_\mathrm{o}\frac{c^0_\mathrm{T}\vec{\nabla}\mu_\mathrm{o}}{RT} - \mathscr{L}_\times\frac{c^0_\mathrm{T}\vec{\nabla}\mu_\mathrm{e}}{RT} + \xi_\mathrm{o}\frac{\vec{i}}{F\|z\|} \tag{5.198}$$

$$\vec{J}^0_\mathrm{e} = -\mathscr{L}_\times\frac{c^0_\mathrm{T}\vec{\nabla}\mu_\mathrm{o}}{RT} - \mathscr{L}_\mathrm{e}\frac{c^0_\mathrm{T}\vec{\nabla}\mu_\mathrm{e}}{RT} + \xi_\mathrm{e}\frac{\vec{i}}{F\|z\|}. \tag{5.199}$$

Equations (5.197)-(5.199) are equivalent to equations 14-16 in the paper by Monroe [107]. These laws combine with the MacInnes equation for a reference electrode, written through equations (5.123) and (5.136) as

$$\vec{i} = -\kappa^0\vec{\nabla}\Phi^\ominus + \frac{\kappa^0\mathbf{s}_\nu^\top\vec{\nabla}\boldsymbol{\mu}^0_\nu}{n_{\mathrm{e}^-}Fz_{\mathrm{e}^-}} - \frac{\kappa^0{\boldsymbol{\xi}^0}^\top\vec{\nabla}\boldsymbol{\mu}^0_\nu}{F\,\|\mathbf{z}\|}, \tag{5.200}$$

to offer a complete description of isothermal, isobaric mass transport in the cosolvent electrolyte.

One could proceed as in the previous examples to elucidate how the migration coefficients, diffusivities, and conductivity relate to the Stefan–Maxwell coefficients. We refrain from doing so here, because of the substantial rise in complexity entailed in extending this process to four species. On account of the matrix inversion involved, writing out the entries within transport-property matrices becomes increasingly untenable as the number of species increases. Nevertheless, this process was implemented and found to produce relationships among parameters consistent with those reported earlier [107].

The matrix forms that connect flux-explicit and force-explicit representations of transport laws are compact and generally useful. The operations described in prior sections are readily implemented with symbolic manipulation programs for systems containing large numbers of species. Perhaps most important is that the structures of the transport coefficients that support both force-explicit and flux-explicit representations of the electroneutral transport laws are very general. As shown in these examples, structural knowledge can used to create consistent sets of thermodynamic and transport constitutive laws a priori in any representation, for electrolytes involving any number of components.

5.16 Numerical implementation: Hull cell

Numerical schemes that are developed to solve the OSM equations for transport of neutral species, and whose efficacy relies on the spectral structure of $\mathbf{M}^{\mathbf{c}}$ or $\mathbf{M}$, may be implemented on the electroneutral OSM equations. Indeed, we have discussed how Sylvester's law of inertia guarantees that the spectral structure remains essentially intact, in that $\mathbf{M}_Z^0$ is symmetric positive semidefinite with one null eigenvalue corresponding to the vector $\mathbf{c}_Z^0$.

Chapters 2 and 3 developed such schemes using finite elements. The singularity of the transport matrices was numerically resolved by the augmentation procedure (4.30). In this context specifically, for a reference velocity ψ we solve the augmented electroneutral OSM equations as

$$-\vec{\nabla}\mu_Z = \mathbf{M}_Z^{\gamma,\psi}\vec{\mathbf{n}}_Z, \tag{5.201}$$

where $\mathbf{M}_Z^{\gamma,\psi}$, defined as $\mathbf{M}_Z + \gamma \boldsymbol{\psi}_Z \boldsymbol{\psi}_Z^\top$ can be shown to be a symmetric positive definite matrix (essentially a mimicry of Lemma 1). These equations are coupled to the component balances (5.32) and (electroneutral) charge continuity (5.33).

We illustrate this by considering the numerical solution of a hull cell containing an electrolytic solution of $LiPF_6$ in EMC, an electrolyte commonly used in lithium ion batteries. The transformation matrix to the salt-charge basis we use is

$$\mathbf{Z} = \begin{bmatrix} 1 & 0 & 0 \\ 0 & 1 & 1 \\ 0 & \frac{1}{\sqrt{2}} & -\frac{1}{\sqrt{2}} \end{bmatrix}. \tag{5.202}$$

The first two rows correspond to the equilibria

$$\mathrm{EMC} \rightleftharpoons \mathrm{EMC} \quad \text{and} \quad \mathrm{Li}^+ + \mathrm{PF}_6^- \rightleftharpoons \mathrm{LiPF}_6. \tag{5.203}$$

The transport properties for this electrolyte, along with its composition dependence, has been extensively measured. The properties in [151, 152], are summarized in Table 5.1. Here the terms D, χ are defined through the relations

$$D = \mathfrak{D}\chi \tag{5.204}$$

$$\chi = 1 + \Lambda_{00}\nu y_{\mathrm{e}} y_0. \tag{5.205}$$

The relation between the migration coefficient ξ transference number, equation (5.154) reduces to

$$\xi = \frac{1 - 2t_+^0}{\sqrt{2}}. \tag{5.206}$$

The ρ term appearing in Table 5.1 is derived from a least squares fit from densiometric data contained in the supplementary information of [151, 152], and acts as the equation of state for this system.

After inferring the component diffusivity and migration coefficients from equations (5.204) and (5.206), we may use equations (5.160)-(5.162) to assemble the matrix $\mathbf{M}_Z$.

The composition of the electrolyte at rest was taken as $y_{\mathrm{e}} = 0.15$. The molar mass of EMC, $\overline{m}_0$, is 104.105 gmol^{-1} and the molar mass of $LiPF_6$, $\overline{m}_{\mathrm{e}}$, is 151.905 gmol^{-1}. A voltage difference across the anode and cathode of $\mathrm{V}^{\mathrm{an}} = 10\mathrm{mV}$ and $\mathrm{V}^{\mathrm{cath}} = 0$ was

Properties		
Term	Function	Units
κ	$\left(48.93y_{\mathrm{e}}^{3/2} - 284.8y_{\mathrm{e}}^{5/2}817.8y_{\mathrm{e}}^{4}\right)^2$	$\mathrm{S\ m^{-1}}$
D	$(4.998 - 29.96y_{\mathrm{e}} + 53.78y_{\mathrm{e}}^2) \times 10^{-10}$	$\mathrm{m^2 s^{-1}}$
χ	$1 - 18.38y_{\mathrm{e}}^{\frac{1}{2}} + 155.3y_{\mathrm{e}} - 450.6y_{\mathrm{e}}^{\frac{3}{2}} + 1506y_{\mathrm{e}}^{\frac{5}{2}}$	$-$
t_+^0	$0.4107 - 1.487y_{\mathrm{e}} + 2.547y_{\mathrm{e}}^2$	$-$
ρ	$1007.1 + 10^5 \times \left(0.0180y_{\mathrm{e}} - 0.1946y_{\mathrm{e}}^2 + 1.960y_{\mathrm{e}}^3 - 7.008y_{\mathrm{e}}^4 + 8.004y_{\mathrm{e}}^5\right)$	$\mathrm{g\ L^{-1}}$

Table 5.1: All data necessary to construct the transport matrix and the thermodynamic factor.

applied and enforced by the Robin boundary condition

$$\vec{i} \cdot n\big|_{\mathrm{an}} = -\frac{F\|\mathbf{z}\|i_0}{RT}\left(\mathrm{V}^{\mathrm{an}} - \Phi\right) \tag{5.207}$$

$$\vec{i} \cdot n\big|_{\mathrm{cath}} = -\frac{F\|\mathbf{z}\|i_0}{RT}\left(\mathrm{V}^{\mathrm{cath}} - \Phi\right) \tag{5.208}$$

for i_0 chosen large (1000 $\mathrm{A}m^{-2}$) as to ensure the condition $\Phi = \mathrm{V}^{\mathrm{an/cath}}$. We assume stripping and plating of lithium at the cathode and anode respectively. This is via the relation

$$\vec{N}_{\mathrm{Li}} \cdot n = \frac{\vec{i} \cdot n}{F\|\mathbf{z}\|}. \tag{5.209}$$

All other boundary conditions are set as homogenous Neumann boundary conditions.

The stripping and plating of lithium at the boundary as expressed in (5.209) implies a transfer of mass across the solution. It would be therefore be inconsistent to take the reference velocity as the mass-average velocity and then assume this to be zero. Instead we utilise the method of Chapter 2, but choose the reference velocity to be that of the solvent, and assume this is zero. This is also convenient due to this being the reference frame in which the transference numbers are measured. A steady–state simulation was performed with Firedrake software [129], using the MUMPS direct linear solver [1, 2] via PETSc [12, 13]. The mesh of the geometry was constructed using the Gmsh software [65]. Each linear system had 183831 degrees of freedom. The finite elements are choosen as CG^2 for component mole fractions/voltage and DG^1 for fluxes/current.

The computed current distribution from this set up is plotted in Figure 5.1. We can observe the current concentrates at the upper corner as this is closer to the anode.

This example illustrates the potential of the framework to model concentrated electrolyte with the full composition dependence, on complex geometries. Similarly we

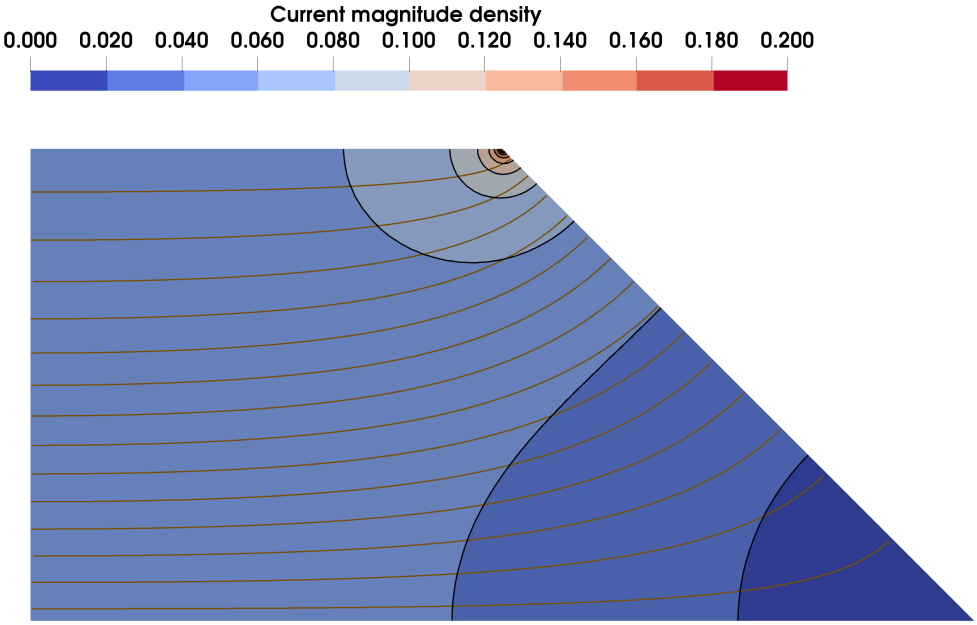

Figure 5.1: Plot of the current density (mA cm^{-2}) magnitude $|\vec{i}|$. The streamlines denote the trajectory of the current from the anode (left) to the cathode (right).

might consider modeling two solvents or transient dynamics. Given the relevant transport data, the scope of application could be extended much further.

5.17 Conclusion

We have detailed the consequences of electroneutrality on the Onsager–Stefan–Maxwell equations. The implications of electroneutrality on the chemical potential constituent laws and other thermodynamic quantities are provided. Crucially, rather than introducing an additional algebraic constraint, it was seen that by constructing the salt-charge basis, electroneutrality may be inbuilt into the equations. This allowed us to consider the electroneutral Onsager–Stefan–Maxwell equations which involve $n-1$ neutral species and voltage. The process to invert this to a flux explicit form was given and the transport properties common in concentrated solution theory, given along with several examples to substantiate the process. Taken together, this has provided a general formulation of the transport equations for an electroneutral electrolyte which retains the structure of the transport equations for neutral species. The utility of this formulation was underlined by simulating electrolyte transport in the same way we would that of neutral species.

Chapter 6

Conclusions

The thesis has developed a framework for modelling multicomponent transport. The original research upon which this thesis is based covers both novel numerical techniques based on the thermodynamic structure of the problem, and original formulations and consolidations of the theory such that it may fit under common paradigms. At every stage the practicality of this framework was demonstrated by implementing various examples.

In reality, this has only opened gates of possible applications that fall under the purview of the methodologies developed here. From here it we might apply these techniques to model a variety of battery chemistries, or to simulate a catalytic reactor. Clearly, the utility of the framework laid here in more complex and impactful examples.

The thesis lays the bulk of the foundation work for such examples, although numerical and practical challenges lie ahead. For example, it is well known that in regimes such as high Péclet numbers, finely engineered numerical techniques are needed for robustness. Nor have we introduced upon any efficient methods to solve the linear systems, likely required for practical simulations in three dimensions.

It is hoped a primary strength of this thesis will be its generality. Rather than advocating for one particular application, or one particular finite element family, or even one particular numerical formulation, it is the systematic use and preservation of the structure of linear irreversible thermodynamics and its consequences in computation that is expected to be useful. The accomplishment of this thesis lies then in providing a platform to effectively solve multicomponent transport both by developing the fundamental structure of the equations, and by way of providing a concrete numerical technique. It is hoped that the development of this platform will make for fruitful and interesting future research.

Appendix A

A.1 Inversion of transport matrices

Both the procedure that maps $\mathbf{M}$ to $\mathbf{L}^{\psi}$ for a given kinematic relation $\boldsymbol{\psi}$, and the inverse process, by which $\mathbf{L}^{\psi}$ maps to $\mathbf{M}$ given the Gibbs–Duhem relation $\mathbf{1}$, require some further justification. Here we present formulas to construct $\mathbf{L}^{\psi}$ from $\mathbf{M}$ and $\mathbf{M}$ from $\mathbf{L}^{\psi}$, as well as demonstrating that these two mappings are inverses of each other.

Given a symmetric matrix $\mathbf{R}$ with a single null eigenvector $\mathbf{r}$, and an additional column matrix $\mathbf{p}$ such that $\mathbf{p}^{\top}\mathbf{r} \neq 0$, the augmented matrix $\mathbf{R}^{p}(\gamma)$, defined as

$$\mathbf{R}^{p}(\gamma) = \mathbf{R} + \gamma \mathbf{p}\mathbf{p}^{\top}, \tag{A.1}$$

has rank one higher than $\mathbf{R}$ whenever $\gamma \neq 0$. This construction is amenable to one of the generalized Sherman–Morrison formulas derived by Baksalary et al. [11]. We employ the notation $\mathbf{A}^{\sharp}$ to represent the Moore–Penrose pseudoinverse of $\mathbf{A}$. Further note that since there is just one null eigenvector of $\mathbf{R}$, the matrix Baksalary and colleagues call $\mathbf{Q}_{\mathbf{R}^{\top}}$, which represents the orthogonal projector onto the orthogonal complement of the column space of $\mathbf{R}$, can be formed explicitly:

$$\mathbf{Q}_{\mathbf{R}^{\top}} = \frac{\mathbf{r}\mathbf{r}^{\top}}{\mathbf{r}^{\top}\mathbf{r}}. \tag{A.2}$$

Equation (2.5) from reference [11] then yields

$$\left[\mathbf{R}^{p}(\gamma)\right]^{\sharp} = \left(\mathbf{I} - \frac{\mathbf{r}\mathbf{p}^{\top}}{\mathbf{r}^{\top}\mathbf{p}}\right)\mathbf{R}^{\sharp}\left(\mathbf{I} - \frac{\mathbf{p}\mathbf{r}^{\top}}{\mathbf{r}^{\top}\mathbf{p}}\right) + \frac{1}{\gamma}\frac{\mathbf{r}\mathbf{r}^{\top}}{(\mathbf{r}^{\top}\mathbf{p})^{2}} \tag{A.3}$$

after some algebraic rearrangement.

Next define the matrix $\mathbf{P}$ such that

$$\mathbf{P} = \left(\mathbf{I} - \frac{\mathbf{r}\mathbf{p}^\top}{\mathbf{r}^\top\mathbf{p}}\right)\mathbf{R}^\sharp\left(\mathbf{I} - \frac{\mathbf{p}\mathbf{r}^\top}{\mathbf{r}^\top\mathbf{p}}\right). \tag{A.4}$$

Direct calculation shows that $\mathbf{P}$ affords $\mathbf{p}$ as a null eigenvector, explaining its notation. The matrix $\mathbf{P}$ so formed is unique because $\mathbf{R}^\sharp$ is, and the fact that symmetry of $\mathbf{R}$ implies symmetry of $\mathbf{R}^\sharp$ means $\mathbf{P} = \mathbf{P}^\top$ as well.

Since $\mathbf{R}$ has a single null eigenvector and $\mathbf{R}^p(\gamma)$ has rank one higher than $\mathbf{R}$, it follows that $\mathbf{R}^p(\gamma)$ is invertible. Therefore the pseudoinverse $[\mathbf{R}^p(\gamma)]^\sharp$ simplifies to the standard matrix inverse; equation (A.3) rearranges to give

$$\mathbf{P} = [\mathbf{R}^p(\gamma)]^{-1} - \frac{1}{\gamma}\frac{\mathbf{r}\mathbf{r}^\top}{(\mathbf{r}^\top\mathbf{p})^2}. \tag{A.5}$$

This formula for $\mathbf{P}$ is independent of the choice of nonzero γ and circumvents the computation of $\mathbf{R}^\sharp$. A trivial rearrangement of this result,

$$[\mathbf{R}^p(\gamma)]^{-1} = \mathbf{P} + \frac{1}{\gamma}\frac{\mathbf{r}\mathbf{r}^\top}{(\mathbf{r}^\top\mathbf{p})^2}, \tag{A.6}$$

substantiates the asymptotic behaviour asserted in equation (4.34). Direct calculation then shows that

$$\mathbf{P} = \lim_{\gamma\to\infty}[\mathbf{R}^p(\gamma)]^{-1}, \tag{A.7}$$

justifying the claim that the limit in equation (4.33) exists.

Finally we consider uniqueness of the mapping between $\mathbf{P}$ and $\mathbf{R}$. Suppose we have a new matrix, $\hat{\mathbf{P}}$, whose sole null eigenvector is also the previously defined column matrix $\mathbf{p}$, and let $\mathbf{r}$ continue to be the sole null eigenvector of $\mathbf{R}$. For any $\phi \neq 0$ the augmented matrix

$$\hat{\mathbf{P}}^r(\phi) = \hat{\mathbf{P}} + \phi\mathbf{r}\mathbf{r}^\top \tag{A.8}$$

is invertible with rank one higher than $\hat{\mathbf{P}}$. As before, the formula of Baksalary et al. [11] constructs a unique matrix

$$\hat{\mathbf{R}} = \left[\hat{\mathbf{P}}^r(\phi)\right]^{-1} - \frac{1}{\phi}\frac{\mathbf{p}\mathbf{p}^\top}{(\mathbf{r}^\top\mathbf{p})^2}. \tag{A.9}$$

Letting $\gamma = \phi^{-1}\left(\mathbf{r}^\top\mathbf{p}\right)^{-2}$ in equation (A.1) and using that result to eliminate the

second term on the right produces an equality which proves that $\hat{\mathbf{R}} = \mathbf{R}$ if and only if

$$\left[\hat{\mathbf{P}}^r(\phi)\right]^{-1} = \mathbf{R}^p\left(\frac{1}{\phi\left(\mathbf{r}^\top\mathbf{p}\right)^2}\right). \tag{A.10}$$

Since the matrices here are nonsingular, one can invert both sides, then insert equations (A.6) and (A.8) to show that $\hat{\mathbf{P}} = \mathbf{P}$. Thus our flux-law inversion establishes a bijective mapping between the space of matrices $\mathbf{P} = \mathbf{P}^\top$ whose nullspaces are spanned by $\mathbf{p}$ and the space of matrices $\mathbf{R} = \mathbf{R}^\top$ whose nullspaces are spanned by $\mathbf{r}$.

The transport-law inversions developed in section 4.3.2 can be implemented directly using the general equations provided here. Specifically, to get flux-explicit isothermal transport laws from the Onsager–Stefan–Maxwell formulation, take $\mathbf{r} = \mathbf{1}$, $\mathbf{p} = \boldsymbol{\psi}$, and $\mathbf{R} = \mathbf{M}$, then use equation (A.4), (A.5), or (A.7) to produce $\mathbf{P} = \mathbf{L}^\psi$. Alternatively, to retrieve force-explicit isothermal transport laws from the isothermal Onsager–Fick–Fourier formulation, let $\mathbf{r} = \boldsymbol{\psi}$, $\mathbf{p} = \mathbf{1}$, and $\mathbf{R} = \mathbf{L}^\psi$, in which case any of the same equations will produce $\mathbf{P} = \mathbf{M}$.

A.2 Construction of Soret diffusivities

For $i, j = 1, 2, ..., n$, take as given a set of Newman–Soret diffusivities $\tilde{\mathscr{A}_{ij}}$ that satisfy $\tilde{\mathscr{A}_{ij}} = -\tilde{\mathscr{A}_{ij}}$ and $\tilde{\mathscr{A}_{ii}} = 0$. Practically, these would be taken from measurements of each binary system, analogous to the construction of Table 4.3. Consistency of the modelling framework demands that a proper Newman–Soret matrix with entries $\mathscr{A}_{ij}$ be based on a set of Soret diffusivities $\mathscr{D}_i$. What constrains us from immediately identifying $\mathscr{A}_{ij}$ with $\tilde{\mathscr{A}_{ij}}$ is the fact that it is not clear that this extrapolated $\mathscr{A}_{ij}$ has the form demanded by equation (4.39) for some set of Soret diffusivities $\mathscr{D}_i^T$. For example, in a ternary mixture, equation (4.39) implies that $\mathscr{A}_{12} + \mathscr{A}_{23} = \mathscr{A}_{13}$, but inspection of the entries tabulated in Table 4.3 shows that this does not hold. Thus the data in $\tilde{\mathscr{A}_{ij}}$ require some regularization to produce $\mathscr{A}_{ij}$.

To regularize $\mathscr{A}_{ij}$, we choose its entries such that each is as close to possible to $\tilde{\mathscr{A}_{ij}}$. That is, we impose structure (4.39) on the coefficients, while minimizing the changes, according to the minimization problem

$$\min_{\mathscr{D}_i^T \in \mathbb{R}} \sum_{i,j}^{n} \left[\left(\mathscr{D}_i^T - \mathscr{D}_j^T\right) - \tilde{\mathscr{A}_{ij}}\right]^2, \tag{A.11}$$

subject to the constraint given by equation (4.40) with $\boldsymbol{\psi} = \mathbf{1}$. A direct computation shows that this minimum is obtained by setting

$$\mathscr{D}_i^T = \frac{1}{n} \sum_{j=1}^{n} \tilde{\mathscr{A}_{ij}}. \tag{A.12}$$

Note that the kinematic relation chosen for the minimization problem implicitly sets a somewhat nonphysical reference velocity for Soret diffusivities. Since $\mathscr{A}_{ij}$ is independent of the convective reference velocity, however, this mathematically convenient choice is immaterial. To enforce a constraint on $\mathscr{D}_i^T$ with another $\boldsymbol{\psi}$ in (4.40), one could simply perform a shift analogous to that stated in equation (4.27) post facto.

Bibliography

[1] P. R. Amestoy, I. S. Duff, J.-Y. L'Excellent, and J. Koster. A fully asynchronous multifrontal solver using distributed dynamic scheduling. *SIAM Journal on Matrix Analysis and Applications*, 23(1):15–41, 2001.

[2] P. R. Amestoy, A. Guermouche, J.-Y. L'Excellent, and S. Pralet. Hybrid scheduling for the parallel solution of linear systems. *Parallel Computing*, 32(2):136–156, 2006.

[3] R. Aris. *Vectors, Tensors and the Basic Equations of Fluid Mechanics*. Dover Books on Mathematics. Dover Publications, 1990.

[4] D. N. Arnold. *Finite element exterior calculus*. Number 93 in CBMS-NSF Regional Conference Series in Applied Mathematics. SIAM, Philadelphia, 2018.

[5] D. N. Arnold, G. Awanou, and R. Winther. Finite elements for symmetric tensors in three dimensions. *Mathematics of Computation*, 77(263):1229–1251, July 2008.

[6] D. N. Arnold and R. Winther. Mixed finite elements for elasticity. *Numerische Mathematik*, 92(3):401–419, 2002.

[7] A. Assyr and G. Vilmart. A priori error estimates for finite element methods with numerical quadrature for nonmonotone nonlinear elliptic problems. *Numerische Mathematik*, 121:397–431, 2012.

[8] P. Atkins and J. de Paula. *Atkins' Physical Chemistry*. Oxford University Press, 2010.

[9] F. R. A. Aznaran, P. E. Farrell, and R. C. Kirby. Transformations for Piola-mapped elements. *arXiv*, 2021.

[10] I. Babuška. Error-bounds for finite element method. *Numerische Mathematik*, 16:322–333, January 1971.

[11] J. K. Baksalary, O. M. Baksalary, and G. Trenkler. A revisitation of formulae for the Moore–Penrose inverse of modified matrices. *Linear Algebra and its Applications*, 372:207–224, 2003.

[12] S. Balay, S. Abhyankar, M. F. Adams, J. Brown, P. Brune, K. Buschelman, L. Dalcin, V. Eijkhout, W. D. Gropp, D. Karpeyev, D. Kaushik, M. G. Knepley, D. May, L. C. McInnes, R. T. Mills, T. Munson, K. Rupp, P. Sanan, B. F. Smith, S. Zampini, H. Zhang, and H. Zhang. PETSc users manual. Technical Report ANL-95/11 - Revision 3.11, 2019.

[13] S. Balay, W. D. Gropp, L. C. McInnes, and B. F. Smith. Efficient management of parallelism in object oriented numerical software libraries. In E. Arge, A. M. Bruaset, and H. P. Langtangen, editors, *Modern Software Tools in Scientific Computing*, pages 163–202. Birkhäuser Press, 1997.

[14] A. J. Bard and L. R. Faulkner. *Electrochemical Methods: Fundamentals and Applications, 2nd Edition*. John Wiley & Sons, Incorporated, 2000.

[15] G. Billet, V. Giovangigli, and G. Gassowski. Impact of volume viscosity on a shock-hydrogen-bubble interaction. *Combustion Theory and Modelling*, 12:221–248, 2008.

[16] R. B. Bird, W. E. Stewart, and E. N. Lightfoot. *Transport Phenomena*. John Wiley & Sons, New York, second edition, 2002.

[17] P. B. Bochev and R. Lehoucq. Regularization and stabilization of discrete saddle-point variational problems. *Electronic Transactions on Numerical Analysis*, 22:97–113, 2006.

[18] D. Boffi, F. Brezzi, and M. Fortin. *Mixed Finite Element Methods and Applications*. Springer Series in Computational Mathematics. Springer, Berlin Heidelberg, 2013.

[19] A. Bondesan, L. Boudin, and B. Grec. A numerical scheme for a kinetic model for mixtures in the diffusive limit using the moment method. *Numerical Methods for Partial Differential Equations*, 35(3):1184–1205, 2019.

[20] D. Bothe and W. Dreyer. Continuum thermodynamics of chemically reacting fluid mixtures. *Acta Mechanica*, 226(6):1757–1805, June 2015.

[21] D. Bothe and P. Druet. On the structure of continuum thermodynamical diffusion fluxes – A novel closure scheme and its relation to the Maxwell-Stefan and the Fick-Onsager approach. *arXiv: Mathematical Physics*, 2020.

[22] L. Boudin, D. Götz, and B. Grec. Diffusion models of multicomponent mixtures in the lung. *ESAIM: Proceedings.*, 30:90–103, 2010.

[23] A. Bousquet, X. Hu, M. Maximilian, and J. Xu. Newton solvers for drift-diffusion and electrokinetic equations. *SIAM Journal on Scientific Computing*, 40(3):B982–B1006, 2018.

[24] J. Boussinesq. *Theorie analytique de la Chaleur*. Gauthier-Villars, 1903.

[25] H. Brenner. Bi-velocity hydrodynamics. Multicomponent fluids. *International Journal of Engineering Science*, 47(9):902–929, 2009.

[26] M. Bulíček, E. Maringová, and J. Málek. On nonlinear problems of parabolic type with implicit constitutive equations involving flux. *Mathematical Models and Methods in Applied Sciences*, 31(10):2039–2090, 2021.

[27] E. Burman, A. Ern, and V. Giovangigli. Bunsen flame simulation by finite elements on adaptively refined, unstructured triangulations. *Combustion Theory and Modelling*, 8(1):65–84, 2004.

[28] C. Cancés, V. Ehrlacher, and L. Monasse. Finite volumes for the Stefan–Maxwell cross-diffusion system. 2020. arXiv:2007.09951.

[29] J. A. Carrillo, Y. Huang, and M. Schmidtchen. Zoology of a nonlocal cross-diffusion model for two species. *SIAM Journal on Applied Mathematics*, 78(2):1078–1104, 2018.

[30] C. Carstensen, J. Gedicke, and E.-J. Park. Numerical experiments for the Arnold–Winther mixed finite elements for the Stokes problem. *SIAM Journal on Scientific Computing*, 34(4):A2267–A2287, 2012.

[31] H. B. G. Casimir. On Onsager's principle of microscopic reversibility. *Reviews of Modern Physics.*, 17:343–350, Apr 1945.

[32] S. Caucao, D. Mora, and R. Oyarzúa. A priori and a posteriori error analysis of a pseudostress-based mixed formulation of the Stokes problem with varying density. *IMA Journal of Numerical Analysis*, 36(2):947–983, April 2016.

[33] D. A. Caughey and A. Jameson. Development of computational techniques for transonic flows: An historical perspective. In *Symposium Transsonicum IV, International Union of Theoretical and Applied Mechanics, (September 2-6, 2002)*, DLR Gottingen, Germany.

[34] H. K. Chang, R. C. Tai, and L. E. Farhi. Some implications of ternary diffusion in the lung. *Respiration Physiology*, 23(1):109–120, 1975.

[35] S. Chapman and T.G. Cowling. *The Mathematical Theory of Non-uniform Gases*. Cambridge University Press, third edition, 1970.

[36] P. Ciarlet, J. Huang, and J. Zou. Some observations on generalized saddle-point problems. *SIAM Journal on Matrix Analysis and Applications*, 25(1):224–236, 2003.

[37] B. D. Coleman and C. Truesdell. On the reciprocal relations of Onsager. *The Journal of Chemical Physics*, 33(1):28–31, 1960.

[38] A. R. Crothers, R. M. Darling, A. Kusoglu, C. J. Radke, M. L. Perry, and A. Z. Weber. Theory of multicomponent phenomena in cation-exchange membranes: Part III. transport in vanadium redox-flow-battery separators. *Journal of The Electrochemical Society*, 167(1):013549, jan 2020.

[39] A. R. Crothers, R. M. Darling, A. Kusoglu, C. J. Radke, and A. Z. Weber. Theory of multicomponent phenomena in cation-exchange membranes: Part II. transport model and validation. *Journal of The Electrochemical Society*, 167(1):013548, jan 2020.

[40] C. F. Curtiss and R. Byron Bird. Multicomponent diffusion. *Industrial & Engineering Chemistry Research*, 38(7):2515–2522, 1999.

[41] E.L. Cussler. *Diffusion: Mass Transfer in Fluid Systems*. Cambridge University Press, third edition, 2009.

[42] L. D. Dalcin, R. R. Paz, P. A. Kler, and A. Cosimo. Parallel distributed computing using Python. *Advances in Water Resources*, 34(9):1124–1139, 2011.

[43] L. S. Darken. Diffusion, mobility and their interrelation through free energy in binary metallic systems. *Transactions of the AIME*, 175:184–201, 1948.

[44] R. Datta and S. A. Vilekar. The continuum mechanical theory of multicomponent diffusion in fluid mixtures. *Chemical Engineering Science*, 65(22):5976–5989, 2010.

[45] S. R. de Groot and P. Mazur. *Non-Equilibrium Thermodynamics*. North-Holland, Amsterdam, 1962.

[46] P. J. W. Debye and E. Hückel. On the theory of electrolytes. I. Freezing point depression and related phenomena, *trans.* from *Physikalische Zeitschrift* 24 (1923) 185-206. In *The Collected Papers of Peter J. W. Debye*, pages 217–263. Interscience Publishers, Inc., London, 1954.

[47] K. G. Denbigh. *The Thermodynamics of the Steady State*. Methuen's monographs on chemical subjects. Methuen, 1951.

[48] J. Douglas and T. Dupont. A Galerkin Method for a Nonlinear Dirichlet Problem. *Mathematics of Computation*, 29(131):689–696, 1975.

[49] M. Doyle, T. F Fuller, and J. Newman. Modeling of galvanostatic charge and discharge of the lithium/polymer/insertion cell. *Journal of The Electrochemical Society*, 140(6):1526–1533, jun 1993.

[50] M. Doyle and J. Newman. Analysis of capacity rate data for lithium batteries using simplified models of the discharge process. *Journal of Applied Electrochemistry*, 27:846–856, 1997.

[51] M. Doyle, J. Newman, A. S. Gozdz, C. N. Schmutz, and J. M. Tarascon. Comparison of modeling predictions with experimental data from plastic lithium ion cells. *Journal of the Electrochemical Society*, 143(6):1890–1903, 1996.

[52] L. Dufour. Über die Diffusion der Gase durch poröse Wände und die sie begleitenden Temperaturveränderungen. *Annalen der Physik*, 224(3):490–492, 1873.

[53] P. J. Dunlop and C. M. Bignell. Diffusion and thermal diffusion in binary mixtures of methane with noble gases and of argon with krypton. *Physica A: Statistical Mechanics and its Applications*, 145(3):584–596, 1987.

[54] P. J. Dunlop, H. L. Robjohns, and C. M. Bignell. Diffusion and thermal diffusion in binary mixtures of hydrogen with noble gases. *The Journal of Chemical Physics*, 86(5):2922–2926, 1987.

[55] S. A. Edelstein, A. Gedeon, and P. Davidovits. Thermal diffusion of I_2 in the noble gases. *The Journal of Chemical Physics*, 56(2):825–829, 1972.

[56] H. C. Elman, D. J. Silvester, and A. J. Wathen. *Finite Elements and Fast Iterative Solvers: With Applications in Incompressible Fluid Dynamics*. Numerical Mathematics and Scientific Computation. Oxford University Press, 2 edition, 2014.

[57] A. Ern and V. Giovangigl. Thermal diffusion effects in hydrogen-air and methane-air flames. *Combustion Theory and Modelling*, 2(4):349–372, 1998.

[58] A. Ern and V. Giovangigli. *Multicomponent Transport Algorithms*. Number 24 in Lecture Notes in Artificial Intelligence. Springer-Verlag, 1994.

[59] A. Ern and V. Giovangigli. Impact of detailed multicomponent transport on planar and counterflow hydrogen/air and methane/air flames. *Combustion Science and Technology*, 149(1-6):157–181, 1999.

[60] L. C. Evans. *Partial Differential Equations*. Graduate studies in mathematics. American Mathematical Society, Providence, R.I., 2010.

[61] A. Fick. Über Diffusion. *Annalen der Physik*, 170(1):59–86, 1855.

[62] K. D. Fong, H. K. Bergstrom, B. D. McCloskey, and K. K. Mandadapu. Transport phenomena in electrolyte solutions: nonequilibrium thermodynamics and statistical mechanics. *AIChE Journal*, 66(12):e17091, 2020.

[63] M. Fortin and R. Glowinski. *Augmented Lagrangian Methods: Application to the Solution of Boundary-Value Problems*, volume 15 of *Studies in Mathematics and its Applications*. Elsevier, Amsterdam-New York, North-Holland, 1983.

[64] J. B. J. Fourier. *Théorie analytique de la chaleur*. Chez Firmin Didot, père et fils, 1822.

[65] C. Geuzaine and J. F. Remacle. Gmsh: A 3-D finite element mesh generator with built-in pre- and post-processing facilities. *International Journal for Numerical Methods in Engineering*, 79(11):1309–1331, 2009.

[66] R. Giles. *Mathematical Foundations of Thermodynamics*. International series of monographs in pure and applied mathematics. Macmillan, 1964.

[67] V. Giovangigli. Mass conservation and singular multicomponent diffusion algorithms. *IMPACT of Computing in Science and Engineering*, 2(1):73–97, 1990.

[68] V. Giovangigli. *Multicomponent Flow Modeling*. Modeling and Simulation in Science, Engineering and Technology. Birkhäuser Basel, 1999.

[69] P. Goyal and C. W. Monroe. New foundations of Newman's theory for Solid electrolytes: Thermodynamics and transient balances. *Journal of The Electrochemical Society*, 164(11):E3647–E3660, 2017.

[70] P. Goyal and C. W. Monroe. Thermodynamic factors for locally non-neutral, concentrated electrolytic fluids. *Electrochimica Acta*, 371:137638, 2021.

[71] D. W. Green and R. H. Perry. *Perry's Chemical Engineers' Handbook, Eighth Edition*. McGraw Hill Professional. McGraw-Hill Education, 2007.

[72] K. E. Grew and A. E. Humphreys. Thermal diffusion in some binary mixtures of the hydrogen isotopes. *The Journal of Chemical Physics*, 45(11):4267–4273, 1966.

[73] K. E. Grew and T. L. Ibbs. *Thermal diffusion in gases*. Cambridge University Press, 1952.

[74] G. Guevara-Carrion, T. Janzen, Y. Muñoz-Muñoz, and J. Vrabec. Mutual diffusion of binary liquid mixtures containing methanol, ethanol, acetone, benzene, cyclohexane, toluene, and carbon tetrachloride. *The Journal of Chemical Physics*, 144:124501, 2016.

[75] E. A. Guggenheim. The conceptions of electrical potential difference between two phases and the individual activities of ions. *The Journal of Physical Chemistry*, 33:842–849, 1928.

[76] E. A. Guggenheim. *Thermodynamics: An advanced treatment for chemists and physicists*. North-Holland Books. North-Holland, 1985.

[77] A. C. Guyton and J. E. Hall. *Textbook of Medical Physiology*. Guyton Physiology Series. Elsevier Saunders, 2006.

[78] B. Hafskjold, T. Ikeshoji, and K. R. Signe. On the molecular mechanism of thermal diffusion in liquids. *Molecular Physics*, 80(6):1389–1412, December 1993.

[79] E. Helfand. On inversion of the linear laws of irreversible thermodynamics. *The Journal of Chemical Physics*, 33(2):319–322, 1960.

[80] C. S. Helrich. *Modern Thermodynamics with Statistical Mechanics*. Springer Berlin Heidelberg, 2008.

[81] B. Hendrickson and R. Leland. A multilevel algorithm for partitioning graphs. In *Supercomputing '95: Proceedings of the 1995 ACM/IEEE Conference on Supercomputing*, pages 28–es, New York, NY, USA, 1995. Association for Computing Machinery.

[82] M. Herz, N. Ray, and P. Knabner. Existence and uniqueness of a global weak solution of a Darcy-Nernst-Planck-Poisson system. *GAMM-Mitteilungen*, 35:191–208, 2012.

[83] J. O. Hirschfelder, C. F. Curtiss, and R. B. Bird. *The Molecular Theory of Gases and Liquids*. John Wiley & Sons, New York, 1954.

[84] R. Hooke. *Lectures de Potentia Restitutiva, Or of Spring Explaining the Power of Springing Bodies*. Cutlerian lecture. John Martyn, 1678.

[85] W. Hundsdorfer and J.G. Verwer. *Numerical Solution of Time-Dependent Advection-Diffusion-Reaction Equations*. Springer Series in Computational Mathematics. Springer Berlin Heidelberg, 2013.

[86] J. D. Jackson. *Classical Electrodynamics*. Wiley, 2012.

[87] G. A. Jaumann. Geschlossenes System Physikalischer und chemischer Differentialgesetze. *Akademie der Wissenschaften in Wien*, 120:385–530, 1911.

[88] E. H. Kennard. *The Kinetic Theory of Gases*. McGraw, New York, 1938.

[89] J. Kestin, K. Knierim, E. A. Mason, B. Najafi, S. T. Ro, and M. Waldman. Equilibrium and transport properties of the noble gases and their mixtures at low density. *Journal of Physical and Chemical Reference Data*, 13(1):229–303, 1984.

[90] G. A. Kluitenberg. On rheology and thermodynamics of irreversible processes. *Physica*, 28(11):1173–1183, 1962.

[91] G. Kraaijeveld and J. A. Wesselingh. Negative Maxwell–Stefan diffusion coefficients. *Industrial & Engineering Chemistry Research*, 32(4):738–742, 1993.

[92] R. Krishna and J.A. Wesselingh. The Maxwell-Stefan approach to mass transfer. *Chemical Engineering Science*, 52(6):861–911, 1997.

[93] V. G. Levich. *Physicochemical Hydrodynamics*. Prentice-Hall International Series in the Physical and Chemical Engineering Sciences. Prentice-Hall, Englewood Cliffs, New Jersey, 1962.

[94] E. N. Lightfoot, E. L. Cussler, and R. L. Rettig. Applicability of the Stefan–Maxwell equations to multicomponent diffusion in liquids. *AIChE Journal*, 8(5):708–710, 1962.

[95] C. Liu, M. Metti, and J. Xu. Energetically stable discretizations for charge carrier transport and electrokinetic models. *Journal of Computational Physics*, 306:1–18, 2015.

[96] A. Logg, K.-A. Mardal, and G. N. Wells, editors. *Automated Solution of Differential Equations by the Finite Element Method: The FEniCS Book*, volume 84 of *Lecture Notes in Computational Science and Engineering*. Springer, 2012.

[97] C. Ludwig. Diffusion zwischen ungleich erwärmten Orten gleich zusammengesetzter Lösung. *Akademie der Wissenschaften in Wien*, 20:539, 1856.

[98] D. A. MacInnes. *The Principles of Electrochemistry*. Dover books on advanced mathematics. Dover, 1961.

[99] H. Manouzi and M. Farhloul. Mixed finite element analysis of a non-linear three-fields Stokes model. *IMA Journal of Numerical Analysis*, 21(1):143–164, 2001.

[100] E. Marchandise, C. Carton de Wiart, W. G Vos, C. Geuzaine, and J.F. Remacle. High-quality surface remeshing using harmonic maps — Part II: Surfaces with high genus and of large aspect ratio. *International Journal for Numerical Methods in Engineering*, 86:1303–1321, 2011.

[101] T. R. Marrero and E. A. Mason. Gaseous diffusion coefficients. *Journal of Physical and Chemical Reference Data*, 1(1):3–118, 1972.

[102] E. A. Mason and S. C. Saxena. Approximate formula for the thermal conductivity of gas mixtures. *The Physics of Fluids*, 1(5):361–369, 1958.

[103] J. C. Maxwell. IV. On the dynamical theory of gases. *Philosophical Transactions of the Royal Society of London*, 157:49–88, 1867.

[104] J. Maya and P. Davidovits. Thermal diffusion of Br_2 and Cl_2 in the noble gases. *The Journal of Chemical Physics*, 60(4):1624–1627, 1974.

[105] M. McLeod and Y. Bourgault. Mixed finite element methods for addressing multi-species diffusion using the Maxwell-Stefan equations. *Computer Methods in Applied Mechanics and Engineering*, 279:515–535, 2014.

[106] D. G. Miller. Thermodynamics of irreversible processes. The experimental verification of the Onsager reciprocal relations. *Chemical Reviews*, 60(1):15–37, 1960.

[107] C. W. Monroe. Does oxygen transport affect the cell voltages of metal/air batteries? *Journal of The Electrochemical Society*, 164:E3547–E3551, 2017.

[108] C. W. Monroe and C. Delacourt. Continuum transport laws for locally non-neutral electrolytes. *Electrochimica Acta*, 114:649–657, 2013.

[109] C. W. Monroe and J. Newman. Onsager reciprocal relations for Stefan–Maxwell diffusion. *Industrial & Engineering Chemistry Research*, 45:5361–5367, 2006.

[110] C. W. Monroe, D. R. Wheeler, and J. Newman. Nonequilibrium linear response theory: application to Onsager–Stefan–Maxwell diffusion. *Industrial & Engineering Chemistry Research*, 54(16):4460–4467, 2015.

[111] Charles W. Monroe and John Newman. Onsager's shortcut to proper forces and fluxes. *Chemical Engineering Science*, 64:4804–4809, 2009.

[112] W. Nernst. Zur Kinetik der in Lösung befindlichen Körper. *Zeitschrift für Physikalische Chemie*, 2U(1):613–637, 1888.

[113] J. Newman. Thermoelectric Effects in Electrochemical Systems. *Industrial & Engineering Chemistry Research*, 34:3208–3216, 1995.

[114] J. Newman, D. Bennion, and C. W. Tobias. Mass transfer in concentrated binary electrolytes. *Berichte der Bunsengesellschaft für physikalische Chemie*, 69(7):608–612, 1965.

[115] J. Newman and T. W. Chapman. Restricted diffusion in binary solutions. *AIChE Journal*, 19:343–348, 1973.

[116] J. Newman and K. E. Thomas-Alyea. *Electrochemical Systems*. John Wiley & Sons, Hoboken, New Jersey, 2004.

[117] I. Newton. *Philosophiae naturalis principia mathematica*. J. Societatis Regiae ac Typis J. Streater, 1687.

[118] R. A. Nicolaides. Existence, uniqueness and approximation for generalized saddle point problems. *SIAM Journal on Numerical Analysis*, 19(2):349–357, 1982.

[119] A. Oberbeck. Ueber die Wärmeleitung der Flüssigkeiten bei Berücksichtigung der Strömungen infolge von Temperaturdifferenzen. *Annalen der Physik*, 243(6):271–292, 1879.

[120] L. Onsager. Reciprocal Relations in Irreversible Processes. I. *Physical Review*, 37:405–426, 1931.

[121] L. Onsager. Reciprocal relations in irreversible processes. II. *Physical Review*, 38:2265–2279, 1931.

[122] L. Onsager. Theories and problems of liquid diffusion. *Annals of the New York Academy of Sciences*, 46(5):241–265, 1945.

[123] H. C. Öttinger. *Beyond Equilibrium Thermodynamics*. John Wiley & Sons, Ltd, 2005.

[124] M. Planck. Über die Potentialdifferenz zwischen zwei verdünnten Lösungen binärer Electrolyte. *Annalen der Physik*, 276(8):561–576, 1890.

[125] R. Pollard and J. Newman. Transport equations for a mixture of two binary molten salts in a porous electrode. *Journal of The Electrochemical Society*, 126(10):1713–1717, oct 1979.

[126] I. Prigogine. *Introduction to Thermodynamics of Irreversible Processes*. Interscience Publishers, 1961.

[127] K. Rajagopal. On implicit constitutive theories. *Applications of Mathematics*, 48:279–319, 2003.

[128] K. Rajagopal and A. Srinivasa. On the thermodynamics of fluids defined by implicit constitutive relations. *Zeitschrift für angewandte Mathematik und Physik* , 59:715–729, 2008.

[129] F. Rathgeber, D. A. Ham, L. Mitchell, M. Lange, F. Luporini, A. T. T. McRae, G. Bercea, G. R. Markall, and P. H. J. Kelly. Firedrake: Automating the Finite Element Method by Composing Abstractions. *ACM Transactions on Mathematical Software (TOMS)*, 43(3):1–27, 2017.

[130] J.F. Remacle, C. Geuzaine, G. Compère, and E. Marchandise. High-quality surface remeshing using harmonic maps. *International Journal for Numerical Methods in Engineering*, 83(4):403–425, 2010.

[131] R. Schmidt and K. Singh. Meshmixer: an interface for rapid mesh composition. In *ACM SIGGRAPH 2010 Talks*, Los Angeles, California, 2010. Association for Computing Machinery.

[132] M. Schmuck. Analysis of the Navier–Stokes–Nernst–Planck–Poisson System. *Mathematical Models and Methods in Applied Sciences*, 19:993–1014, 2009.

[133] C. Soret. Sur l'état d'équilibre que prend, au point de vue de sa concentration, une dissolution saline primitivement homogène, dont deux parties sont portées à des températures différentes. *Archives des Sciences Physiques et Naturelles de Genève*, 9(1):48–60, 1879.

[134] G. L. Standart, R. Taylor, and R. Krishna. The Maxwell-Stefan formulation of irreversible thermodynamics for simultaneous heat and mass transfer. *Chemical Engineering Communications*, 3(4-5):277–289, 1979.

[135] J. Stefan. Über das Gleichgewicht und die Bewegung, insbesondere die Diffusion von Gasgemengen. *Sitzungsberichte der Mathematisch-Naturwissenschaftlichen Classe der Kaiserlichen Akademie der Wissenschaften Wien*, 63:63–124, 1871.

[136] R. Stenberg. Some new families of finite elements for the stokes equations. *Numerische Mathematik*, 56(8):827–838, 1989.

[137] M. Stynes and D. Stynes. *Convection-Diffusion Problems*. Graduate Studies in Mathematics. American Mathematical Society, 2018.

[138] J. L. Sudworth. The sodium/nickel chloride (ZEBRA) battery. *Journal of Power Sources*, 100(1):149–163, 2001. Journal of Power Sources Volume 100.

[139] A. Tasić, B. Djordjević, D. Grozdanić, N. Afgan, and D. Malić. Vapour–liquid equilibria of the systems acetone–benzene, benzene–cyclohexane and acetone–cyclohexane at 25°C. *Chemical Engineering Science*, 33(2):189–197, 1978.

[140] R. Taylor and R. Krishna. *Multicomponent Mass Transfer*. Wiley Series in Chemical Engineering. John Wiley & Sons, 1993.

[141] W. L. Taylor. Thermal diffusion factors for the binary noble gas mixtures. *The Journal of Chemical Physics*, 72(9):4973–4981, 1980.

[142] V. Thomée. *Galerkin Finite Element Methods for Parabolic Problems*. Springer Series in Computational Mathematics. Springer Berlin Heidelberg, 2013.

[143] E. S. Udoetok. Thermal conductivity of binary mixtures of gases. *Frontiers in Heat and Mass Transfer*, 4:023008, 2013.

[144] L. O. Valøen and J. N. Reimers. Transport properties of $lipf_6$-based li-ion battery electrolytes. *Journal of The Electrochemical Society*, 152(5):A882–A891, 2005.

[145] A. J. Van-Brunt, P. E. Farrell, and C. W. Monroe. Consolidated theory of fluid thermodiffusion. *AIChE Journal*, 2021.

[146] A. J. Van-Brunt, P. E. Farrell, and C. W. Monroe. Augmented saddle point formulation of the steady-state Stefan–Maxwell diffusion problem. *IMA Journal of Numerical Analysis*, 2023.

[147] F. Van Der Valk. Thermal diffusion in ternary mixtures: I. Theory. *Physica*, 29(5):417–426, 1963.

[148] I. Villaluenga, D. M. Pesko, K. Timachova, Z. Feng, J. Newman, J. Srinivasan, and N. P. Balsara. Negative Stefan–Maxwell diffusion coefficients and complete electrochemical transport characterization of homopolymer and block copolymer electrolytes. *Journal of The Electrochemical Society*, 165(11):A2766–A2773, 2018.

[149] J. Villaluenga and A. Tabe-Mohammadi. A review on the separation of benzene/cyclohexane mixtures by pervaporation process. *Journal of Membrane Science*, 169:159–174, 2000.

[150] L. Waldmann. *Transporterscheinungen in Gasen von mittlerem Druck*, pages 295–514. Springer Berlin Heidelberg, Berlin, Heidelberg, 1958.

[151] A. A. Wang, A. B. Gunnarsdóttir, J. Fawdon, P. Mauro, C. P. Grey, and C. W. Monroe. Potentiometric MRI of a superconcentrated lithium electrolyte: Testing the irreversible thermodynamics approach. *ACS Energy Letters*, 6(9):3086–3095, 2021.

[152] Andrew A. Wang, Tianhong Hou, Minnie Karanjavala, and Charles W. Monroe. Shifting-reference concentration cells to refine composition-dependent transport characterization of binary lithium-ion electrolytes. *Electrochimica Acta*, 358:136688, 2020.

[153] A. Wassiljewa. Heat conduction in gas mixtures. *Physikalische Zeitschrift*, 13(1):737–742, 1904.

[154] A. Z. Weber. Gas-crossover and membrane-pinhole effects in polymer-electrolyte fuel cells. *Journal of the Electrochemical Society*, 155(6):B521–B531, 2008.

[155] J. Xu and L. Zikatanov. Some observations on Babuška and Brezzi theories. *Numerische Mathematik*, 94:195–202, 2003.

[156] K. Xu. Nonaqueous liquid electrolytes for lithium-based rechargeable batteries. *Chemical Reviews*, 104(10):4303–4418, 2004.

[157] Software used in 'Augmented saddle point formulation of the steady-state Stefan–Maxwell diffusion equations', 2020. https://doi.org/10.5281/zenodo.3860438.

[158] Software used in 'Consolidated theory of fluid thermodiffusion', 2021. https://doi.org/10.5281/zenodo.5651136.

[159] Software used in 'Finite element methods for multicomponent convection-diffusion', 2022. https://doi.org/10.5281/zenodo.7017917.